

Adaptive and Reconfigurable Robotic Gripper Hands with a Meso-Scale Gripping Range

Guochao Bai

Submitted for the degree of Doctor of Philosophy

Heriot-Watt University

School of Engineering and Physical Sciences

March 2018

The copyright in this thesis is owned by the author. Any quotation from the thesis or use of any of the information contained in it must acknowledge this thesis as the source of the quotation or information.

ABSTRACT

Grippers and robotic hands are essential and important end-effectors of robotic manipulators. Developing a gripper hand that can grasp a large variety of objects precisely and stably is still an aspiration even though research in this area has been carried out for several decades.

This thesis provides a development approach and a series of gripper hands which can bridge the gap between micro-gripper and macro-gripper by extending the gripping range to the mesoscopic scale (meso-scale). Reconfigurable topology and variable mobility of the design offer versatility and adaptability for the changing environment and demands. By investigating human grasping behaviours and the unique structures of human hand, a CFB-based finger joint for anthropomorphic finger is developed to mimic a human finger with a large grasping range. The centres of CFB mechanism are explored and a contact-aided CFB mechanism is developed to increase stiffness of finger joints. An integrated gripper structure comprising cross four-bar (CFB) and remote-centre-of-motion (RCM) mechanisms is developed to mimic key functionalities of human hand. Kinematics and kinetostatic analyses of the CFB mechanism for multi-mode gripping are conducted to achieve passive-adjusting motion. A novel RCM-based finger with angular, parallel and underactuated motion is invented. Kinematics and stable gripping analyses of the RCM-based multi-motion finger are also investigated. The integrated design with CFB and RCM mechanisms provides a novel concept of a multi-mode gripper that aims to tackle the challenge of changing over for various sizes of objects gripping in mesoscopic scale range.

Based on the novel designed mechanisms and design philosophy, a class of gripper hands in terms of adaptive meso-grippers, power-precision grippers and reconfigurable hands are developed. The novel features of the gripper hands are one degree of freedom (DoF), self-adaptive, reconfigurable and multi-mode. Prototypes are manufactured by 3D printing and the grasping abilities are tested to verify the design approach.

ACKNOWLEDGEMENTS

First of all, I must thank my first supervisor, Dr. Xianwen Kong, for his support, encourage and guidance in each stage of my PhD work. The completion of the work and contribution during my PhD period is due to his inspiration and his constructive suggestions. I thank Dr. Kong for providing me many opportunities to broad my minds by participating international conferences, for kindly discussing with me no matter when I knocked his office door and how busy he was. The influence and inspiration of Dr. Kong – at the beginning of topic selection, through his multi-mode idea – can be seen throughout the thesis and the final prototyping and testing. The PhD study, research and teaching at Heriot-Watt and supervision from Dr Kong provided me an opportunity to understand the differences between the West and the East in education, culture and research. These will be my greatest treasure and lifelong fantastic memory.

Equally thanks for my second supervisor Prof. James Ritchie, Dean of the University. He has introduced me to manufacturing and automotive assembly areas. He has always shared me with most valuable knowledge and helpful ideas after our meetings. I am grateful to his patience, precious time and tolerance for my errors in paper writing. I have learned a lot from his precious comments and revision.

I also express my thankfulness to Prof. Jian S Dai, my former supervisor from King's College London and Prof Will Shu, University of Strathclyde. I am grateful for receiving their selfless help and encouragement no matter when I need help.

For serving as colleagues, supporters and (sometimes) critics, I thank Dr. Ross Walker, Jieyu Wang, Nguyen Hao Le, Artem Lukianov, Dr. Peter Szabo, Tariq Chaudhary, Muhammad Farooq, etc.

I deeply thank my parents, my older brother Guoqiang Bai and my sister in law Na Zhi. Thanks for your understanding, patience and support. I am grateful to my brother and sister in law for their taking care of our parents and leaving me enough time for my career development.

Especially thank my wife, Lina Ti. With your love, accompanying, support and encouragement, I can put myself out there, taking my full energy to my research work. My mother in law also deserves special mention for her understanding and support for me and my wife.

In addition, I would also like to thank international Doctoral Training Partnership (DTP) from EPSRC for the financial support to my tuition fee and maintenance and Engineering and Physical Sciences Research Council (EPSRC), United Kingdom, for the financial support to my PhD research under Grant No. EP/K018345/1.

ACADEMIC REGISTRY
Research Thesis Submission



Name:	Guochao Bai		
School:	School of Engineering and Physical Sciences		
Version: <i>(i.e. First, Resubmission, Final)</i>	Final	Degree Sought:	PhD in Mechanical Engineering

Declaration

In accordance with the appropriate regulations I hereby submit my thesis and I declare that:

- 1) the thesis embodies the results of my own work and has been composed by myself
- 2) where appropriate, I have made acknowledgement of the work of others and have made reference to work carried out in collaboration with other persons
- 3) the thesis is the correct version of the thesis for submission and is the same version as any electronic versions submitted*.
- 4) my thesis for the award referred to, deposited in the Heriot-Watt University Library, should be made available for loan or photocopying and be available via the Institutional Repository, subject to such conditions as the Librarian may require
- 5) I understand that as a student of the University I am required to abide by the Regulations of the University and to conform to its discipline.
- 6) I confirm that the thesis has been verified against plagiarism via an approved plagiarism detection application e.g. Turnitin.

* Please note that it is the responsibility of the candidate to ensure that the correct version of the thesis is submitted.

Signature of Candidate:		Date:	08/03/2018
-------------------------	--	-------	------------

Submission

Submitted By <i>(name in capitals)</i> :	
Signature of Individual Submitting:	
Date Submitted:	

For Completion in the Student Service Centre (SSC)

Received in the SSC by <i>(name in capitals)</i> :			
Method of Submission <i>(Handed in to SSC; posted through internal/external mail):</i>			
E-thesis Submitted <i>(mandatory for final theses)</i>			
Signature:		Date:	

TABLE OF CONTENTS

ABSTRACT	1
ACKNOWLEDGEMENTS.....	2
ACADEMIC REGISTRY	3
TABLE OF CONTENTS.....	4
CHAPTER 1 – Introduction	7
1.1 Background	7
1.2 State-of-Art Robotic Hands and Applications	9
1.2.1 Robotic Grippers for Industry	9
1.2.2 Robotic Hands for Fragile Grasping	10
1.2.3 Robotic Hands for Dexterity Research.....	11
1.2.4 Prosthetic Hand	12
1.2.5 Underactuated Adaptive Hand	13
1.2.6 Micro-Nano Gripper.....	14
1.3 Project Motivation.....	15
1.3.1 Motivation Scenario.....	15
1.3.2 Key Challenges and Unmet Needs	16
1.4 Development of Robotic Gripper.....	17
1.4.1 Classifications of Gripping Configurations and Gripped Objects	17
1.4.2 Definition of Meso-Scale for Artificial Gripping.....	19
1.4.3 Design Process of Gripper Hand	20
1.5 Objectives.....	23
1.6 Thesis Outline.....	23
CHAPTER 2 – CFB-Based Anthropomorphic Finger	25
2.1 Natural Gripping Systems and Evolution.....	26
2.1.1 Classification of Bio-grippers.....	26
2.1.2 Evolution of the Human Hand	28
2.2 Articular System of Human Hand	30
2.3 Concave and Cross linkages for Biological Morphology	34
2.4 Kinematic Analysis of Contact-Aided CFB Mechanism	35
2.4.1 Fixed and Moving Centroides of CFB Mechanism	35
2.4.2 Design of Contact-Aided CFB Mechanism.....	40
2.5 Contact-Aided CFB-Based Anthropomorphic Finger.....	41
2.5.1 Gripping Analysis and Design of Finger Joints.....	41
2.5.2 Design Process of a Two-Joint Finger	42
2.5.3 Prototype and Testing	43
2.6 Summary	47
CHAPTER 3 – CFB-Based Multi-Mode Fingertip	48
3.1 Flexible Gripping in Manufacturing.....	48
3.2 Types of Planar Four-Bar Linkages.....	50
3.2.1 RRRR Mechanisms.....	51
3.2.2 Configuration Zones of RRRR Mechanisms	53
3.2.3 Basic Planar Four-Bar Mechanisms	56
3.3 Configurations Zones of CFB Mechanisms	56
3.4 Kinetic Equilibrium of a CFB Mechanism.....	61
3.5 CFB Mechanism for Multi-Mode Gripping	61
3.6 Equilibrium Analysis of a CFB Mechanism for Gripping	63
3.6.1 Simplified CFB Mechanism with Point Contact	63
3.6.2 General CFB Mechanism with Point Contact.....	65

3.6.3	General CFB Mechanism with Surface Contact.....	66
3.6.4	Summary of Multi-Mode Gripping with CFB Fingertip	67
3.7	Gripping Capabilities of a CFB Mechanism	68
3.7.1	CFB Mechanism for Passive-Adjusting Gripping	68
3.7.2	CFB Mechanism for Angular Gripping	69
3.8	Gripping Zone of CFB-Based Gripper	70
3.9	Kinetostatic Analysis of CFB-Based Fingertip	71
3.10	Gripping Force Analysis of CFB-Based Fingertip	73
3.11	Summary	80
CHAPTER 4 – RCM-Based Multi-Motion Finger		81
4.1	Kinematic Analysis of Double-Parallelogram RCM Mechanism	81
4.2	Motion Transmission of RCM-Based Fingers	85
4.2.1	Angular Motion of RCM-Based Finger	86
4.2.2	Parallel Motion of RCM-Based Finger	87
4.2.3	Underactuated Motion of RCM-Based Finger	89
4.3	Static Analysis of RCM-Based Finger	90
4.3.1	Static Analysis of RCM-Based Finger with Angular Motion	90
4.3.2	Static Analysis of RCM-Based Finger with Parallel Motion	92
4.3.3	Static Analysis of RCM-Based Finger with Underactuated Motion	93
4.4	Summary	99
CHAPTER 5 – Development and Testing of Robotic Gripper Hands.....		100
5.1	Gripper Hands with Meso-Scale Gripping	100
5.2	Development of a Meso-Gripper	102
5.2.1	Analysis of Human Grasping Behaviours	102
5.2.2	Metamorphic Gripping of the Multi-Mode Gripper	104
5.3	Dimensional Synthesis of the Meso-Gripper	105
5.3.1	Task-Based Dimensional Synthesis	105
5.3.2	Dimensional Synthesis Process	105
5.3.3	Kinematic Analysis of the Synthesized Meso-Gripper	111
5.4	Modified Multi-Mode Gripper	112
5.4.1	Modified Schematic of the Gripper	112
5.4.2	Modified RCM-Based Finger	115
5.4.3	Modified CFB-Based Fingertip	116
5.5	Actuation and Transmission	117
5.5.1	Actuation	117
5.5.2	Differential Force Transmission	118
5.6	Prototyping and Testing	120
5.6.1	Meso-Gripper	121
5.6.2	Power-Precision Gripper	124
5.6.3	Reconfigurable Hand	125
5.7	Summary	128
CHAPTER 6 – Conclusions.....		129
6.1	General Conclusions	129
6.2	Contributions	129
6.3	Future Work	130
Appendix A – Specifications of Commercial Robotic Grippers/Hands		131
Appendix B – Micro - Nano Grippers		133
Appendix C – Grasp Taxonomy		136
Appendix D – Cognate of Planar Four-bar Mechanisms and Their Extensions ..		140
D.1	Coupler-Point Curves and Cognate Mechanisms	140

D.2 Extension of Translation-Body Six-Bar Mechanisms	141
D.3 Extension of Cognate Six-Bar Mechanisms	143
D.4 Cognate Four- and Six-Bar Mechanisms of Basic Four-Bar Mechanisms.....	144
Appendix E – Cognate of Straight-Line Mechanisms and Their Extensions.....	149
E.1 Straight-Line Mechanisms	150
E.2 Cognate and Transformation-Body Mechanisms of the Straight-Line Mechanisms 153	
E.3 Correlation of Straight-Line Mechanisms and Their Cognates.....	160
Appendix F – Synthesis of Multi-RCM Mechanism	161
F.1 Analysis of a Mechanism with Multiple Remote Centres.....	161
F.2 Synthesis Procedure of a Multi-RCM Mechanism.....	163
F.3 Synthesis Example of Two-RCM Mechanism	164
Appendix G – Implementation of Cognate Mechanisms by Software	167
LIST OF PUBLICATIONS.....	172
REFERENCES.....	173

CHAPTER 1 – Introduction

1.1 Background

With the development of robots, the price of utilisation is becoming cheaper than before. Robots work in hostile, complex and dirty environments to replace humans in arduous and repetitive tasks at high speed to reduce labour costs and to ensure consistent quality control of process, such as agriculture, textile industry and logistics storage. For both hazardous environment and rapid production change, research on reconfigurable, adaptive, affordable mechanisms is a necessary new direction.

A survey identified six grand challenges for manufacturers that present gaps between current practices and the vision of manufacturing in 2020 [1]:

Grand Challenge 1. Achieve concurrency in all operations.

Grand Challenge 2. Integrate human and technical resources to enhance workforce performance and satisfaction.

Grand Challenge 3. “Instantaneously” transform information gathered from a vast array of diverse sources into useful knowledge for making effective decisions.

Grand Challenge 4. Reduce production waste and product environmental impact to “near zero”.

Grand Challenge 5. **Reconfigure manufacturing** enterprises rapidly responding to changing needs and opportunities.

Grand Challenge 6. Develop innovative manufacturing processes and products with a focus on decreasing dimensional scale.

Reconfigurable topology and variable mobility of manufacturing offer versatility, adaptability and low cost for the changing environment and demand. Currently, manufacturing technology is expected to be much more flexible than it was several decades ago. Because product life cycles are counted in months for some products in consumer electronics industry, i.e. mobile phones. The handling process of work pieces in manufacturing is often underrated as simple or even trivial technologically in fixed manufacturing line. Handling is considered to be secondary to technical solutions in the manufacturing process. The time necessary for manufacturing is separated into machine time and handling time (see Figure 1.1). Manufacturing planning aims to synchronize handling time and machine time in order to reduce cycle time and optimize machine time or minimise handling time and to move as many work pieces as possible per time unit [2].

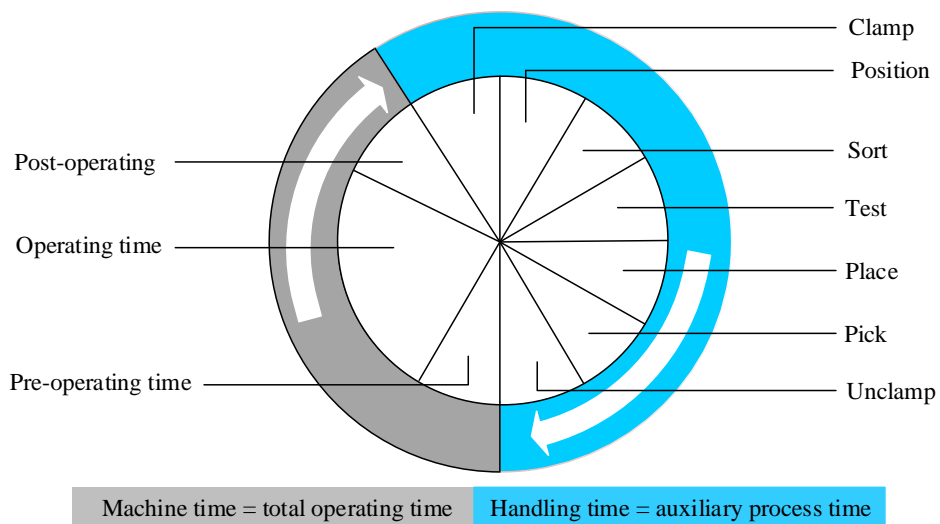


Figure 1.1. Machine time/ handling time [2]

The gripping task is mainly influenced by the work piece, its features and status, i.e. shapes, displacement, orientation. The moving task is determined by combination of gripper and work piece, as shown in Figure 1.2.

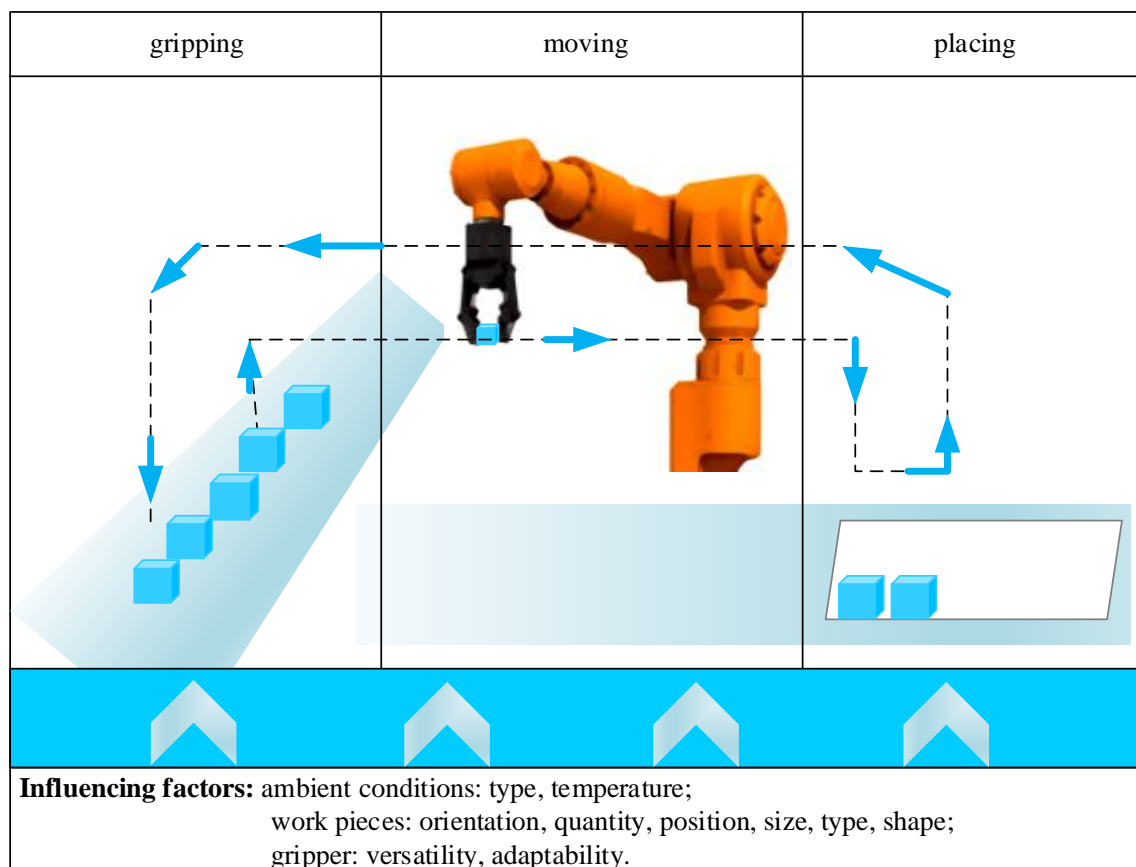


Figure 1.2. Phases of a handling process and its ambient conditions

Versatility provides the capability to manage a defined range of tasks in a manufacturing process. **Adaptability** means that the transfer from one work process to the next within a manufacturing system accrues less time and cost. From the analysis of versatility and adaptability, a robot is able to perform a task adequately only when it is assigned proper tooling, adequate methods of grasping and associated work pieces. If the shape of the object to be handled varies for each task then the gripper must also be changed, thus versatility is required. In proportion to its size in a manufacturing system, a gripper provides a definitive contribution to the practical success of an automated and/or robotized solution, therefore the **innovative design** of the gripper is of fundamental importance. Generally speaking, the design of a gripper must take into account several aspects of the system together with the peculiarities of the given application or a multi-task activity.

Hazardous environments and rapid production change need manufacturing systems that can rapidly and frequently adapt in the field of manufacturing processes. This is recognized as operational flexibility and requires a quick reaction to any change in production. Manufacturing systems must enable product process innovation and variety by providing cost effective flexibility and adaptability to environment variations and changes.

1.2 State-of-Art Robotic Hands and Applications

A robotic hand is an important and much desired component for a robot to communicate and contact flexibly and adaptively with the ambient environment. The competence of human hand, with millions of years' evolution, is one of the central advantages that humans possess. Therefore, providing this human hand like functionality to improve the capabilities of robots is an essential goal. The following section reviews technologies on robotic hands including industrial hands, dexterous hands, prosthetic hands, underactuated-adaptive hands and micro-nano hands. Reviewing the forms and functions of these different types of hand can provide research inspirations for the design of adaptive and reconfigurable end-effectors for miniaturized product assembly.

1.2.1 Robotic Grippers for Industry

Early work in manipulator design focused on the development of mechanisms and human hand-like grippers of different types. Research into the kinematic synthesis of industrial gripper design used versatile mathematical approaches to provide variants of mechanisms for a range of grasping applications [3, 4, 5, 6, 7, 8, 9 and 10]. A two-fingered gripper corresponds to the minimum number of fingers and minimum complexity of a hand. Most industrial grippers are actuated by linear actuators.

However, two actuators can be useful when the finger can operate independently with symmetric or unsymmetrical behaviours. Typical grippers used in industry comprising linkage mechanisms are shown in Figure 1.3. Detailed specifications can be found in **Appendix A**. This type of gripper is simple and durable, some of which can produce very a high gripping force. However, their capabilities as simple claws on their industrial applications are limited to simple pick-and-place functions.



Figure 1.3. Industrial gripper

1.2.2 Robotic Hands for Fragile Grasping

For flexible or fragile object grasping the use of compliant material, vacuum or magnetic grippers are preferable. Either a magnetic field [11] or a vacuum [12, 13] is applied as the surface of the gripper in contact with the object. However, any errors in placement of the object will be reflected at the destination. Therefore, these grippers cannot be used for high accuracy applications. Recently, some compliant, vacuum or magnetic grippers exist as shown in Figure 1.4. The vacuum gripping system in Figure 1.4(a) is equipped with suction cups for objects. Figure 1.4(b) shows a magnetic gripper which can only grip magnetic substances. Figure 1.4(c) is a rubber ball jammed with small granular materials. It conforms to the object's natural contours by jamming transition. Figure 1.4(d) shows flexible fingers with Fin Ray structures. Figure 1.4(e) is an octopus-inspired soft gripper with two rows of suction cups on the inside of the silicone tentacle. The last one, in Figure 1.4(f), is a gripper with electroadhesion process

which uses electrodes to generate positive and negative charges on a surface. The gripping system induces charges in its own surface as well when it touches its target object.



(a) Vacuum gripper
by Schmalz



(b) Magnetic gripper
by Pascal



(c) Versaball gripper
by Empire Robotics



(d) Multi Choice Gripper
by Festo



(e) Octopus Gripper
by Festo



(f) Electrodehesion Gripper
by Grabit

Figure 1.4. Latest gripper with vacuum and magnetic features.

1.2.3 Robotic Hands for Dexterity Research

Dexterous hands always have at least 3 fingers and multiple degrees of freedom. They achieve features like quick response and accurate grasp. Renowned dexterous hands include the Stanford/JPL hand [14], UTAH/MIT hand [15], Southampton hand [16], DLR series hand [17], Robonaut hand [18], Shadow series hand [19], UB series hand [20], Cyber Hand [21], Gifu series hand [22, 23], BH series hand [24], DLR/HIT series hand [25], Metamorphic hand [26], see Figure 1.5. However, these types of robotic hands have dozens of actuators, control is quite complicated and the costs are usually very high, even though they have the ability to manipulate complex objects.

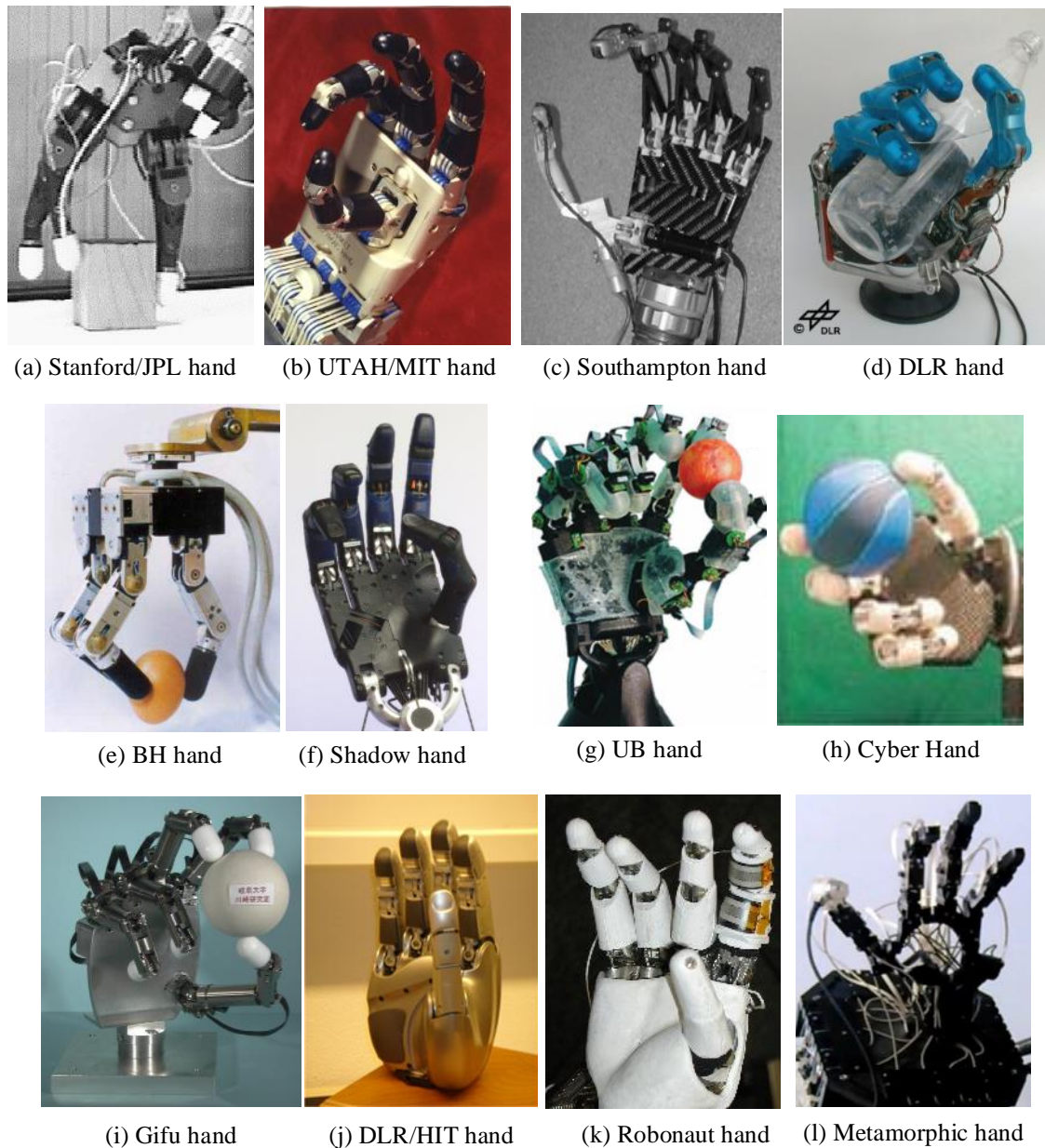


Figure 1.5. Dexterous hands.

1.2.4 Prosthetic Hand

Prosthetic hands are developed for cosmetic, utilitarian and functional applications. Sometimes such a hand can also be called an anthropomorphic prosthetic hand or upper-limb prostheses, which interfaces with the arm of an amputee. The development of a prostheses is much more difficult compared to dexterous hands with major limiting factors such as weight, power, size constraints and control. Prosthetic hands have been well developed, taking advantage of the latest technological advances over the last two decades. However, even the state-of-art hands still lack durability, functionality, cosmetic and affordability. Figure 1.6 shows the latest commercial prosthetic hands.



Figure 1.6. Commercial myoelectric prosthetic hands.

1.2.5 Underactuated Adaptive Hand

An adaptive approach used is to develop clever hardware with passive elements such as springs that automatically envelope objects without any sensor feedback. An underactuated hand refers to a hand with less actuators than degrees of freedom [27]. As a consequence of these advantages, under-actuation and self-adaption are widely accepted and many underactuated hands have been developed with anthropomorphic graspings. Many of self-adaptive hands can grasp objects with different sizes and shapes. The underactuated hands with adaptive characteristics including the Laval hand [28, 29], TBM hand [30], Manus-Hand [31], LARM hand [32], GCUA hand [33, 34], SDM hand [35], i-HY hand [36], Meka H₂ hand [37], Velo hand [38], Kinova hand [39], Barrett hand [40], etc (Figure 1.7). The Robotiq hand [41] developed based on Laval hand is widely used because it can grasp a wide variety of objects with a very simple control structure. The last four gripper hands [42, 43, 44, 45] developed in this thesis aims to merge the gap between micro and macro gripping ranges. Their functionalities mimic the human hand and works in adaptive or reconfigurable configures with various gripping modes. This type of hand provides numerous advantages in terms of cost, size, weight, and mechanical/electrical complexity while offering a large range of shape-adaptive grasping. Therefore, more and more hands of this type exist. One drawback of underactuated hands is might be human-like dexterity for manipulation which relies more on mobility or actuators of the hand.

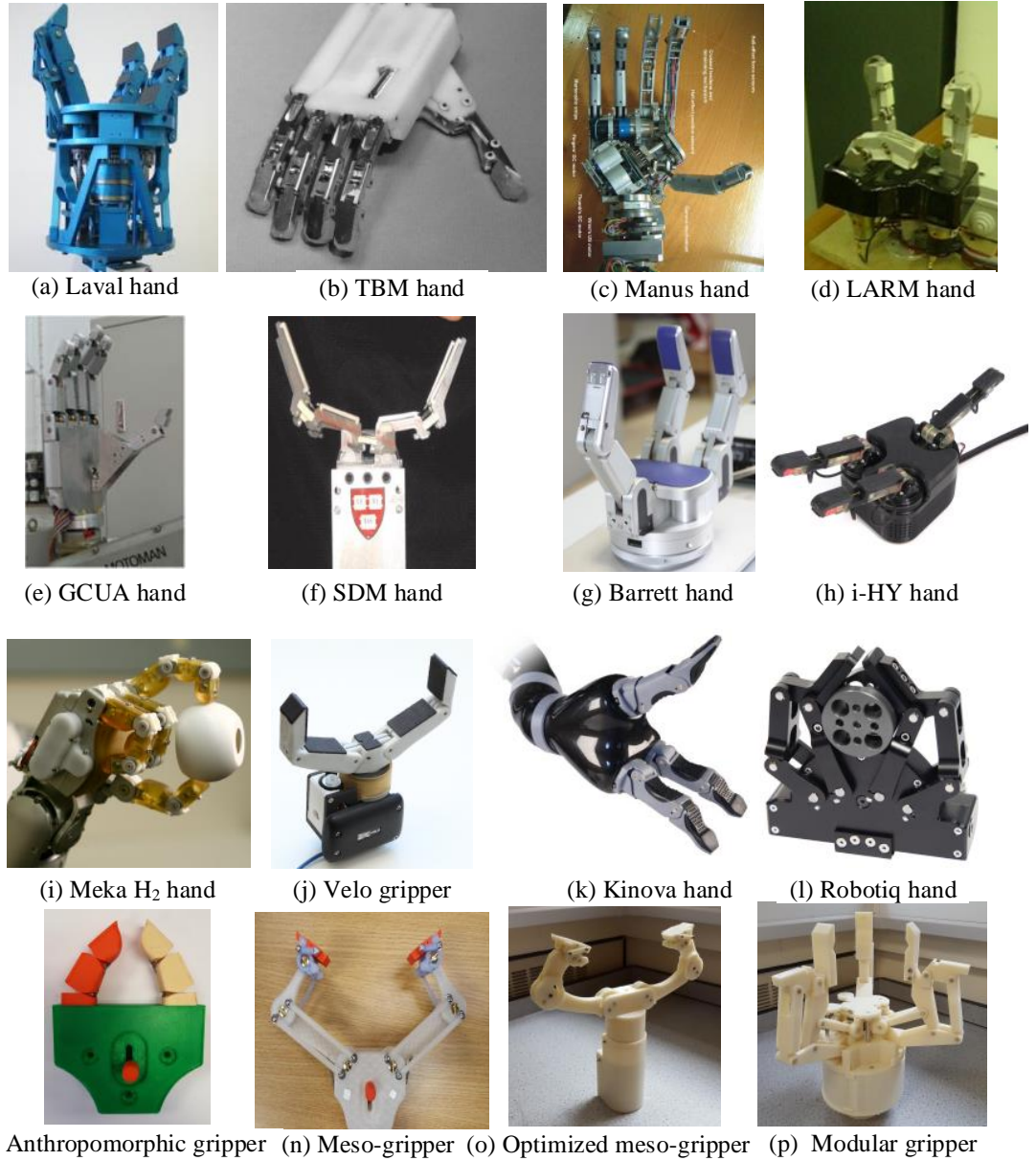


Figure 1.7. Underactuated adaptive hands

1.2.6 Micro-Nano Gripper

Nowadays high precision positioning systems involve many applications from micro-assembly to medical instruments. In the past few years, micro-assembly technology has advanced greatly. Such a system generally consists of two parts: an end effector and a position system [46]. For micro-grippers, there are three requirements: grasp, force and sense. In some applications, it is possible to handle or manipulate very small objects, such as living cells or semiconductor electronics. The order of magnitude may be micro- or nano-scale. The approaches for dealing with these small objects are in terms of precision control systems and miniature structures. The latter have been developed very much in the past few years because of the advantages of delicate force and

accuracy control. All these are possible thanks to the development of theoretical research on compliant mechanisms and fabrication methods, such as silicon processing, photolithographic techniques, X-ray lithographic and wire electro-discharge. Four engineering issues need to be addressed in building micro-robotic systems: the power source, the propulsion method, control integrated with sensing and communications with the macro-world [47]. A list of micro-nano grippers is given in **Appendix B**. There are two-fingered micro-hand [48], electroadhesive microgripper [49], compliant microgrippers [50, 51, 52, 53, 54, 55], electrostatic/gecko-like adhesive gripper [56], microrobotic tentacles [57], colloidal asters [58] and self-folding gripper [59].

Research on robotic grippers/hands is a very large area in robotics. According to the types and applications of grippers/hands, the flexibility, adaptability and economic efficiency of the hand should be the most primary characteristics considered before development.

1.3 Project Motivation

The demand for digital multimedia products has been growing rapidly. With the focus shifting to 3C (computing, consumer electronics & communications) and IA (Information application) related products, there are two major production problems in 3C electronics industry production: a shortage of skilled labour and a need for design flexibility. Robots can help factories to optimize production, improve product quality and lower operating costs which in turn increases factory profits. According to survey [60], the use of robots and automation can reduce the number of works by a 30% with a 15%-20% growth in work-based salaries. Then the corporate profits for factory are beneficial for the growing costs. Currently customised manufacturing needs more human fabrication rather than machine automation. Because low production volumes mean that it is uneconomical to automate process with skilled factory operators. However, this greatly increases the cost and lead time for fabrication. Therefore, versatile, adaptive and low-cost gripper hands should be developed to meet the flexible manufacturing process and miniaturized product assembly. .

1.3.1 Motivation Scenario

Today, the perfect model for technology as an end-effector in automation is still a constant challenge to engineering. In the early stages, a gripper had to adapt to robot capacities before standardized components were set in motion for reliable factory production. After this universal grippers were developed for grasping most of the different sizes or shapes in unconstructed ambient. Even though many hands or grippers were developed during the past decades, gripper hands with a mesoscopic-scale range

(meso-scale for short) with mm to macroscopic-scale range (macro-scale for short) with tens of mm haven't been available for product assembly. Most of the assemblies working on the smartphone or in consumer electronics are within this range. So the research and development on this requirement is necessary to reduce industry cost.

The gripper required for the product assembly shown in Figure 1.8 has manipulation ranges as follows: from 1mm with few grams payload to 55 mm with 1kg payload; a large gripper force range from 1N to 33N.

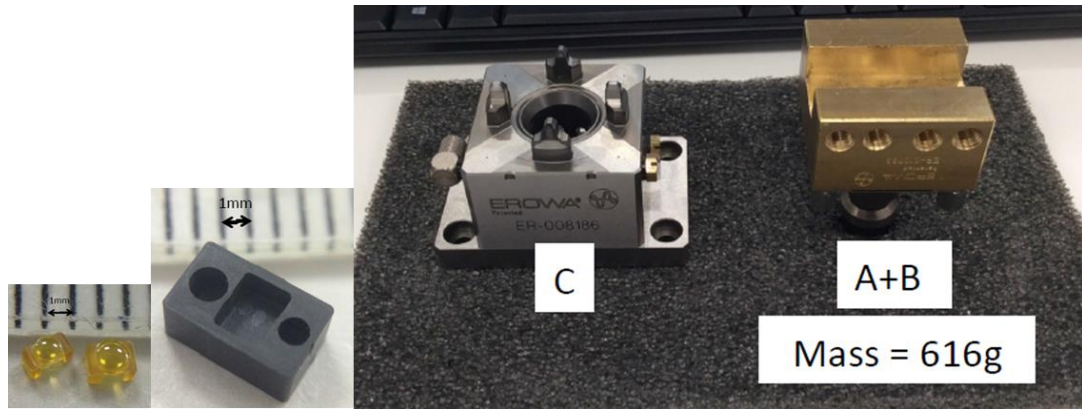


Figure 1.8. Practical requirement of product assembly

According to the commercial literature, there is currently no one that can achieve this range, see **Appendix A**. Therefore, a novel mechanical design for this application, incorporating a hand, should be researched. A flexible, adaptive and reliable structure of the finger should be considered by using mathematical and modelling software. To match up with the finger design, the transmission mechanism and the control system should be modified according to previous commercial products or researched hands.

1.3.2 Key Challenges and Unmet Needs

Robotic grippers or multi-fingered hands are a wide-ranging subject in robotics research. Each robot possesses one or more manipulators in order to handle material panels of various shapes, sizes and weight and unstructured functions such as agriculture [61], surgical devices [62], textile facilities [63] and industrial assemblies [64]. The critical issues facing manufacturers and the assembly industry are three foci: versatility, adaptability and low cost. Therefore the future research foci should be:

1. Mimicking natural grasps, especially the human hand, to develop gripping schemes in which the functionality of the gripper should be identified by considering the structure design.

2. Mechanical grippers which have a simplified structure and redundant degree of freedom for large scale of dimensions.

3. Making a manipulator without the complexities of hardware and software to accommodate variously uncertain grasping tasks in unstructured ambient with the characteristics of reliability, low cost and high speed;

4. Taking the advantages of intelligent mechanisms, electronics, software and cyber-physical systems to fit the future modularity of smart factories.

1.4 Development of Robotic Gripper

To develop a robotic gripper for optimum gripping, several aspects need to be considered. The knowledge of gripped objects needs to be known before grasping and can also be used for the optimisation of grasping configurations. This information will affect the development of the structural and functional features of gripping systems. This section provides some investigations, a definition and a design process for a gripper hand.

1.4.1 Classifications of Gripping Configurations and Gripped Objects

The systematic way of classification shows that the two main directions of grasping (power and precision) have different functions in grasping. Power grip is a type of force grip which focuses on security and stability of prehension while precision grip emphasises dexterity. Currently, the understanding of human grasping objects, such as kinematic implications, limitations and patterns, is also important in many domains ranging from gripper design, interaction, rehabilitation, manufacturing and so on. In human-computer interaction design, how to adjust grasping postures to task demands is more important than understanding the posture itself [65, 66, 67]. The guiding interaction needs for haptic feedback are increasingly important in this area [68]. Prosthetic hands are often designed to have a set of grasp types to complete a practical grasping environment [69]. Based on the two concepts of power and precision grips introduced by Napier, a classification of configurations of human hand has been introduced by [70, 71, 72, 73]. Based on the previous grasp taxonomies, a grasp taxonomy containing 33 types was provided in [74]. Further work considering the grasping range that a human commonly uses is shown in [75] with some of grasp taxonomies shown in **Appendix C**.

The objects subject to gripping can vary in shape, size and weight, etc. as shown in Figure 1.9.

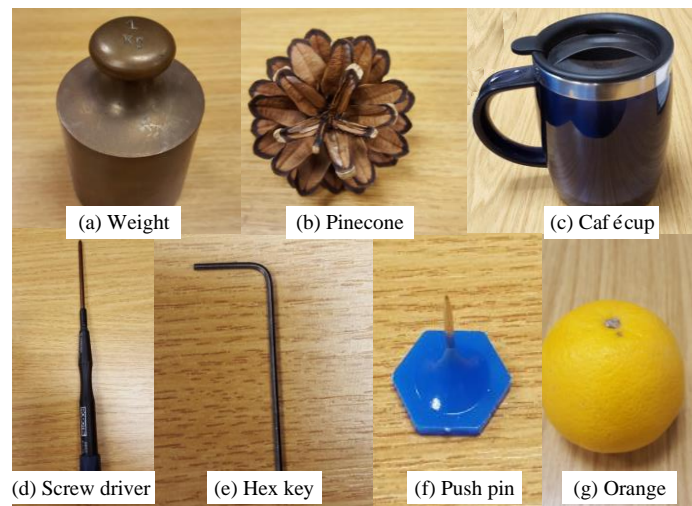


Figure 1.9. Gripped objects.

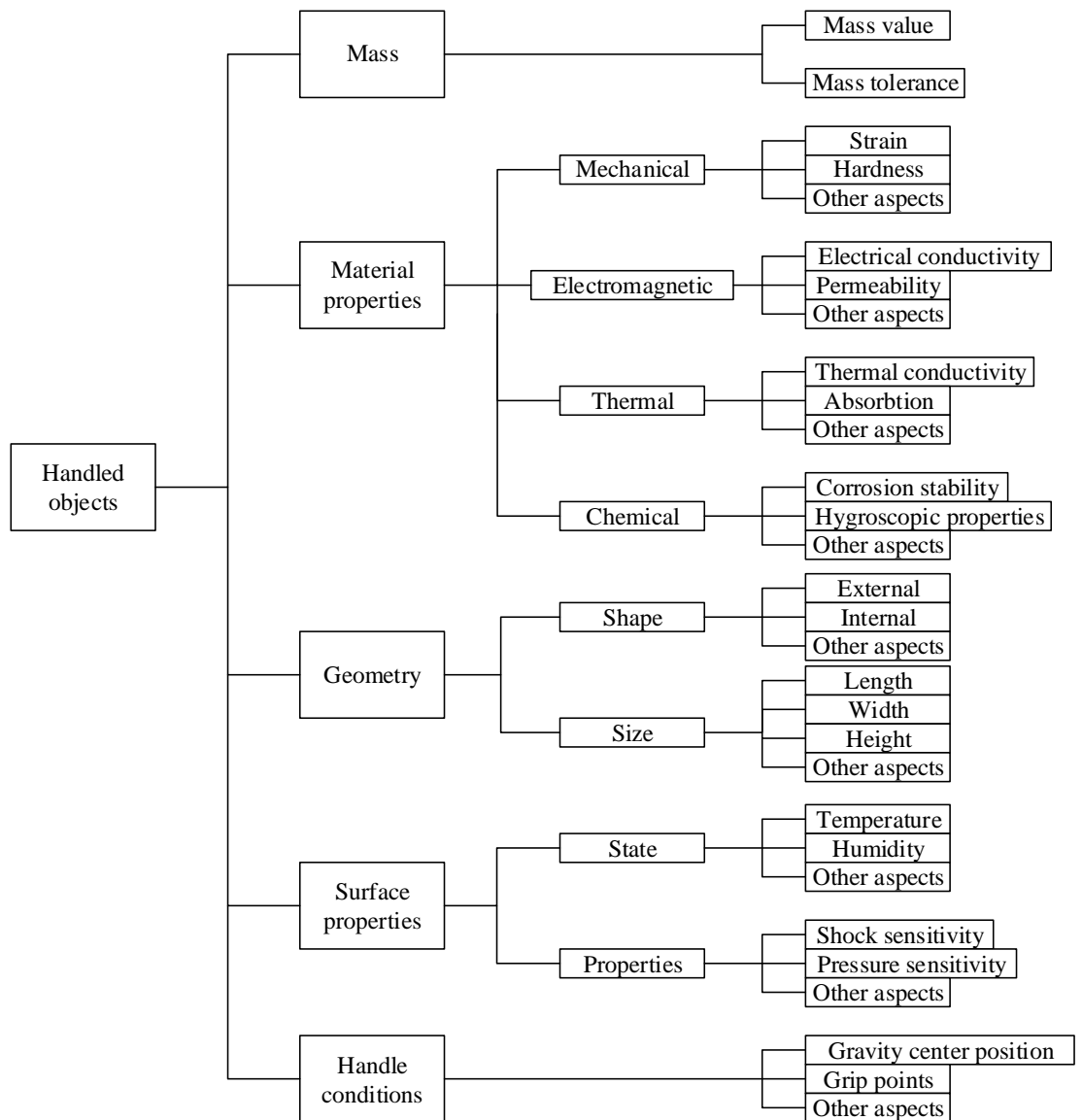


Figure 1.10. Properties of gripping objects.

Studies show that the identification of parts is based on the visibly geometrical features with the manner of grippings strongly influenced by the piece geometry and surface roughness [76]. As shown in Figure 1.10, the mass of the object affects the applied gripping force. The material properties may interfere with the gripping force measurement and gripping preparation for the ambient environment. The geometrical properties in terms of shape and size require changeable fingertips or gripping configurations. The surface function of the object depends on its coefficient of friction during gripping and how to increase this for stable gripping. For different objects gripping, the centre of gravity and stable gripping position can also be considered. This requires the gripper to have adaptive, changeable and reconfigurable capabilities for these various gripping requirements.

1.4.2 Definition of Meso-Scale for Artificial Gripping

According to the analysis of human grasping behaviours during a wide range of unstructured tasks by Yale GRAB lab [77]: 55% of the gripped objects have at least one dimension larger than 15cm; 92% of objects have a mass of 500g or less; 96% of grasp locations are 7cm or less in width; 94% of the instances subject to grasp the smallest dimension. Therefore, in general, domestic grasping is quite different from industry applications. There are some rules to follow if a robotic gripper is developed for these tasks for which a classification of artificial gripping is necessary.

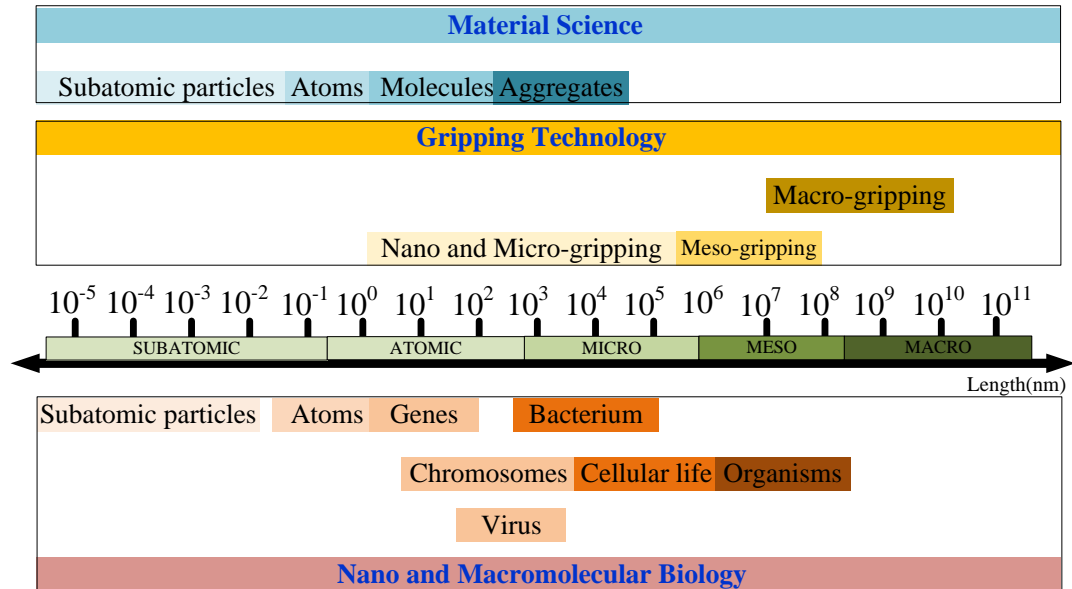


Figure 1.11 Schematic comparison of the length scales in material science, gripping technology and molecular biology

Generally speaking, the meso-scale comprises different length scales in different research areas. A comparison of the relevant length scales in material science and molecular biology shows that the mesoscopic length is 10^6 - 10^8 nm (1-100mm) [78].

However, some specifically designed micro-grippers handle objects up to 500 μ m; therefore the minimum gripping size of a meso-gripper has been defined in this work as 500 μ m. A meso-gripper bridges the gap between micro-grippers and macro-grippers by extending the macro-gripping range, preferably without switching grippers for industrial assembly. Therefore in Figure 1.11, a definition of the working gripping dimension range of meso-grippers is set at 0.5 to 100mm, based on typical requirements for the assembly of multimedia products and human hand grasping behaviours.

1.4.3 Design Process of Gripper Hand

A mechanical system or machine generally consists of a power source and associated mechanisms to transform forces and motion into desired forces and motion by the controlled use of power. A mechanism is assembled by moving components such as cams, gears, belts and linkages as well as friction devices such as brakes and clutches and structural components such as frames, bearing and springs. The linkage can consist of bars or links as well as joints which refer to lower pairs (revolute and prismatic joints) [79].

The gripper acts as a bridge between a robotic arm and the world around it. The design of a gripper should reflect its role and match up the functions to the tasks in the real world. Therefore, the ideal gripper should be synthesized by considering three considerations: the ability of arm, gripped object and manufacturing tasks some of which have been mentioned previously.

The design of such a task requires an in-depth knowledge of several interrelated subjects including: gripper design, gripper control and grasp configurations [80]. Even four decades ago, researchers emphasized the importance of versatility. A number of robot grippers were developed and tested. They were classified and separated as grippers with stiff fingers, grippers with spring or flexible fingers, vacuum grippers, magnetic grippers, grippers with sensors and miscellaneous grippers [10]. The control for a gripper includes force and position control, stiffness control and compliant motion control. The grasp configurations, referring to grasping plans, derive several approaches such as theoretical computational approaches and experimental approaches.

At the initial design stage, mechanism types and actuation methods have to be considered in priority. The design depends on the grasping task along with consideration of lightness, small dimensions, rigidity, multi-task capability, simplicity, reliability and lack of maintenance. These design characteristics can be achieved by considering specific end effectors or grippers.

A mechanical gripper is an end-effector that uses mechanical fingers actuated by a mechanism to grasp an object (Figure 1.12). There are two main methods of constraining a part in a gripper:

1. Physical construction of parts within fingers where the finger encloses the part to some extent and thereby changing the contact surface of finger to be an approximate shape of the part geometry.
2. Holding the part by friction between fingers and work pieces. The finger must apply a force that is sufficient for friction to retain the part against gravity. For the friction method, the gripper must be designed to exert a force that depends on the weight of part, the coefficient of friction of fingertip and acceleration of placing.

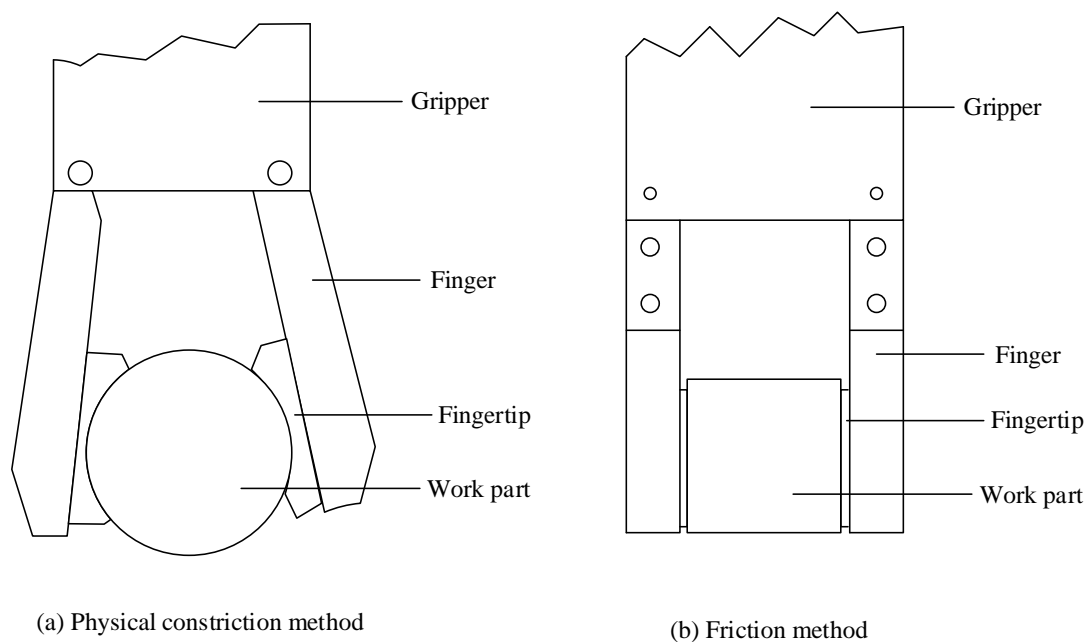


Figure 1.12. Two methods of constraining part in gripper

Angular and parallel mechanical grippers are categorized by the output kinematics transferred from their drives. A simple mechanical gripper always has two types of finger movement: pivoting/angular movement and linear/translational movement. To achieve these, five drive methods are considered: 1). linkage actuation; 2). gear and rack actuation; 3). cam actuation; 4). screw actuation; 5). pulley actuation. In some cases rotary drive movements need to be transferred into linear output movements. The input movements of drives transferred to the output movements of fingers are linear or rotary, respectively. It depends on the types needed and the transfer mechanisms between them [2], see Table 1.1.

Table 1.1 Comparison of input and output movements of different drive types [2].

			Output movement			
			Linear		Rotary	
Input movement	Linear	Sheer grinding drive				
		Tendon drive				
		Fork lever drive				
		Clip lever drive				
		Wedge drive with rocker switch				
		Elbow lever drive				
	Rotary	Curve tongue drive				
		Anchor drive				
		thread spindle drive				
		Excenter drive				

1.5 Objectives

The main objective of the thesis is to develop a robotic gripper/hand with adaptive and reconfigurable characteristics, low-cost, accurate grasping position and payload and grasping ranges greater than any product on current market.

The objective of this research is to present a design methodology for robotic gripper design. To develop low-cost and adaptable hybrid manipulators for miniaturized product assembly, related advances should be investigated, such as disassembly-free reconfigurable manipulators [81], deployable and scalable systems [82], high-precision compliant motion systems [83] and adaptive grippers [84]. A theoretical framework on the design of a deployable/scalable and adaptive fixtures of adaptive hybrid manipulators will be established.

To obtain one gripper with a large size range and a hybrid mechanism containing mechanisms with multiple motion modes should be researched. The inspiration studied from nature provides excellent ideas for novel designs. Bio-inspired systems are much more complex than conventional mechanical engineering. Numerical methods will be applied in the study. Research will be done via a process of hypothesis and verification, including steps such as model, simulation and experimental measurements. According to this process, new mechanisms inspired by biological structures will be obtained.

It is hoped that the innovative design methodology and process presented in this thesis will provide some inspiration to adaptive robot design engineers and pave a way to develop new artificially intelligent devices by considering mechanical intelligence [85].

1.6 Thesis Outline

This thesis provides a development process of adaptive and reconfigurable gripper hands based on cross-four-bar (CFB) and remote-centre-of-motion (RCM) mechanisms. The main objective is to design and research a class of robotic gripper hands which are capable of grasping a large variety of objects with meso-scale range.

This chapter has shown different categories of gripper hands for various applications. Reviewing these different types has provided research inspiration for the design of adaptive and reconfigurable end effectors for meso-scale gripping. Chapter 2 investigates the human anatomy and human grasping behaviours. RCM linkage is adopted for mimicking finger joints. A two-fingered anthropomorphic hand is also developed to verify its functionality. Chapter 3 focuses on fingertip development. A multi-mode fingertip based on CFB linkage is discussed. The multi-mode gripping capability relates to the inherent characteristics by kinematic and kinetostatic analysis. Chapter 4 refers to a novel finger design based on RCM mechanism. According to

analysis of geometrical characteristics and motion of the RCM mechanism, it is the best choice as a finger with angular, parallel and underactuated modes. Static analysis and grasping stability analyses are also conducted. Chapter 5 outlines the development and testing of three types of adaptive or reconfigurable gripper hands. The general actuation, grasping system, transmission mechanisms and their selection are also considered. Chapter 6 concludes the thesis with an evaluation of the design and discusses future works.

The thesis focuses more on novel mechanisms development and analysis for grasping solutions rather than the detailed design of a system, i.e. stress analysis of synthesized mechanism, dimensional optimization, etc. Therefore, the main body of the work neither contains details of element design and calculations carried out during the design process nor includes standard element selection, such as bearing, springs, actuators and control boards. Some works refer to open source, such as coding for stepper motor control and the shape deposition manufacturing approach.

CHAPTER 2 – CFB-Based Anthropomorphic Finger

Investigating anthropomorphic robotic hands aids the understanding of the human hand and vice versa. The grasping and manipulation abilities of current robotic hands are far less dexterous than the human hand, even though significant progress has been made in the past four decades [86, 87, 88]. The design considerations include the numbers of fingers, joints, degrees-of-freedom (DOFs), the range of motion for each joint, the speed of movement and the force generation capability [89]. The design of a versatile and robust robotic hand that has similar dexterity to the human hands is, an undisputedly, a challenging task.

Several biological features of a finger of the human hand are difficult to mimic [90]. They include: (1) the unique shape of bones at the joints; (2) the joint capsule formed by ligaments to limit the range of joint motion; (3) cartilage and synovial fluid low-friction contact; (4) non-linear interactions between tendons and bones to dynamically determine the finger motion.

In a human hand, the anatomical structure and nervous system make significant contributions to its versatility and adaptability. Anatomical studies show that finger joints have a complex structure formed by non-symmetric surfaces and usually produce much more complex movement than a simple revolute motion. Most existing robotic hands are connected with revolute joints between phalanges in order to achieve the required DOFs and kinematic characteristics, e.g. hinges, gimbals, cables, gears or belts. Compliant materials have been recently used as joints. Xu proposed one type of Metacarpophalangeal (MCP) joint whose biomechanics and dynamic properties are close to human counterparts [91]. The artificial joint is composed of a ball joint, crocheted ligaments and a silicon rubber sleeve which is distinctive to the other finger joints.

Many robotic hands are driven by gears [92, 93] or tendons [94]. There are also ultrasonic motor [95] and air muscle [96] types. The function of these drive approaches is to make the trajectory of a fingertip similar to the typical human trajectory when reaching and grasping objects.

In this chapter, a novel type of anthropomorphic finger based on an RCM linkage is proposed. Unlike most current finger designs, this finger has characteristics, such as mimicking, nonlinear joints, fingernails and soft fingertips. This chapter is organized as follows. Firstly, the natural gripping system is investigated and the classification of the bio-gripper and the evolution of human hand presented. Then the articular system of the human hand is introduced referring to bones and joints. The physical parameters of the

finger skeleton and the approximate limits of joints' motions are summarized. The simplest four-bar linkages for biological morphology are then investigated, followed by the kinematics of a cross four-bar (CFB) linkage. The motion of the cross four-bar (CFB) mechanism is then studied. Fixed and moving centrodes of the mechanism are also derived for building and identifying contact surfaces. The human joint is then mimicked using contact-aided CFB mechanism which can also be used for mimicking a prosthetic knee. Based on the structure of the human hand articular system, a two-joint thumb finger is developed. The proposed development process and associated design approach are able to mimic any type of joint. Finally, a two-fingered robotic hand prototype is built considering functional artificial fingers including 3D printed fingernails and soft fingertips. This is consequently tested for grasping of a large range of objects to verify its performance.

2.1 Natural Gripping Systems and Evolution

2.1.1 Classification of Bio-grippers

In nature, there is a large variety of gripping systems, which is one source of inspiration for new knowledge and future technologies. A biogripping system generally consists of bioenergy as power source, the brain as processor, neural cells as sensors and hands/claws as end-effectors, all of which makes a closed loop for stable gripping, a diagram of which is as shown in Figure 2.1.

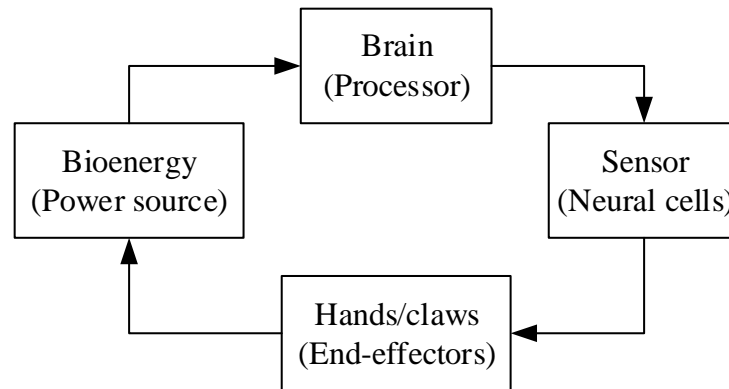










Figure 2.1. Diagram of a natural gripping system

The end-effector performs grasping and partial sensing functions based on specific structures and actuation methods. This is an important part of a biosystem and acts as a interface between the mainbody and its surroundings (Table 2.1). Depending on the grasping manner, natural gripping can be classified as coverage, jagged and fingered. From wrapping to fingered, gripping features an evolutionary process. For example, a typical coverage grip is used by an octopus, which lives in an aquatic environment. The

jagged grip generally appears in amphibious or terrestrial environments and is utilized by crabs, some birds and mammals. The most advanced fingered grip is the human hand; of course all the primates are fingered.

Table 2.1. Classification of grips according to gripping manner.

Coverage	Octopus	
	Reptiles	
	Elephant	
Jagged	Shrimps & Crabs	
	Some Birds	
	Mammals	
Fingered	Some Birds	
	Primates	

2.1.2 Evolution of the Human Hand

The human hand is a sophisticated mechanism, the product of millions of years of evolution; versatile in its functionality and essential for humans to interact with the world. Major evolutionary transformational steps include the formation of a five-fingered structure with opposable thumb, the development of flat nails from claws and increased sensitivity of a palm (inner hand) surface [97].

Why mimic the human hand to solve grasping problems in robotics?

Charles Darwin's theory of evolution may answer this question. Life, a process of natural selection, is a self-improving process which reinvents itself to solve problems in the natural world. These improvements and the natural selection process have accumulated over hundreds of millions of years in plants and animals. The "hand" is the key differentiator between humans and other species.

As the famed surgeon Frederick Wood-Jones said: "The difference between the hand of a man and the hand of a monkey lies not so much in the movements which the arrangement of muscles, bones and joints make possible...but in the purposive volitional movements which under ordinary circumstances the animal habitually exercises."

The primate hands family tree shows the differences between these hands and why the human hand should be researched other than the other species (Figure 2.2).

The human hands and the other primate hands share many general characteristics; however, each primate sub-family has its unique characteristics. Almost all primates have retained five digits on the hand and foot. All, to different degrees, possess prehensile (grasping) hands and all (except humans) prehensile feet. Lemurs, for example, lack the functional duality of the hands of most apes and Old World monkeys (catarrhines). The hands of catarrhines (Old World monkeys and apes) show a larger range of precise manipulative activity than those of other primates. New World monkeys show a considerable advance over primitive primates in tactile sensitivity but they possess less functionally effective hands in prehensile terms than Old World monkeys.

Duality in hand function has been described in terms of precision and power grips which were proposed by John Napier organized the movements of the hand on an anatomical basis [98]. Precision and power grips can be represented by a throwing grip and clubbing, see Figure 2.3. The throwing and clubbing grips yield reproductive advantages for millions of years and drove natural selection to transform the ancestral

ape hand into the human hand [99]. A fully opposable thumb gives the human hand a power grip (left) and a precision grip (right).

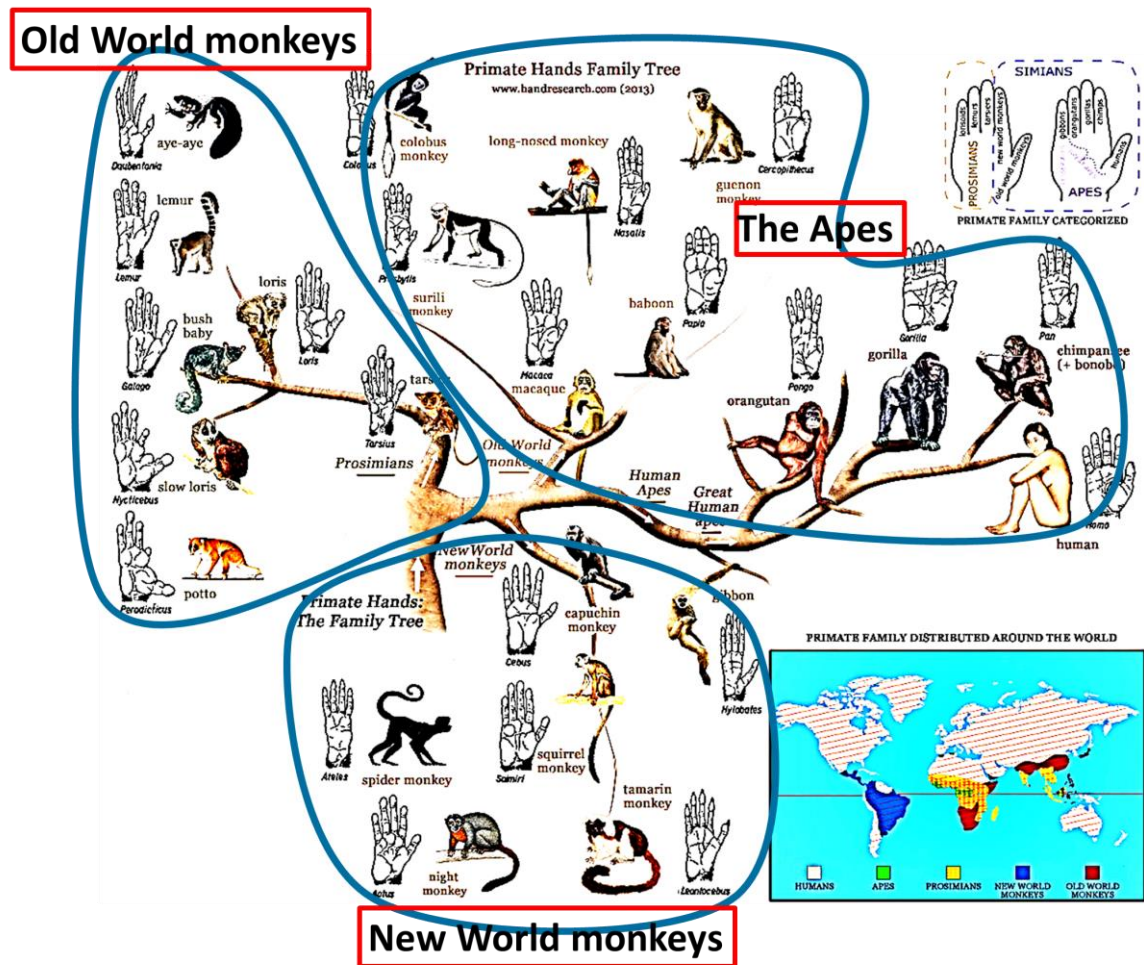


Figure 2.2. The Primate Hands Family Tree (The hands drawn inside the picture originate from A. H. Schultz, *The Life of Primates*, Universe Books, 1969; (<http://www.handresearch.com/news/primatology-palm-reading-primate-hands-family-tree.htm>))

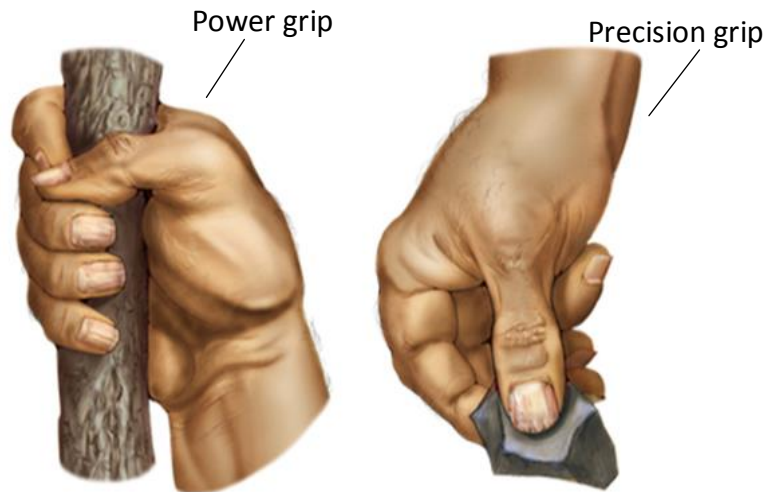


Figure 2.3. Power and precision grips.

2.2 Articular System of Human Hand

In order to mimic the human hand for grasping objects, its articular system is investigated. The skeletal structure of the hand is comprised of 27 bones (8 form the wrist, 5 are found in the palm, and 14 constitute finger phalanges). More than 30 muscles in the hand and forearm actuate the hand commanded via signals from three major nerves, radial, median and ulnar, as well as more than 20 identified muscular branches. Accurate models of the human finger have been proposed based on anatomical studies [100, 101]. The bone and articular structure of human hand are two key components to be imitated because their structures and relative movements have essential effects when grasping objects. Human bones and articulations are now briefly introduced. The DoF and range of motion of each joint are summarized in literature [102, 103].

The following subscripts are used: I for the thumb, II for the index, III for the middle, IV for the ring, and V for the small finger. Three types of hand bones, carpals, metacarpals and phalanges are shown in Figure 2.4. The names of joints are defined according to hand bones, such as carpalmetacarpal joint (CMC) which locates between carpal and metacarpal. Hand fingers are separated into the proximal, middle and distal phalanges, excepting thumb finger which has only two phalanges.

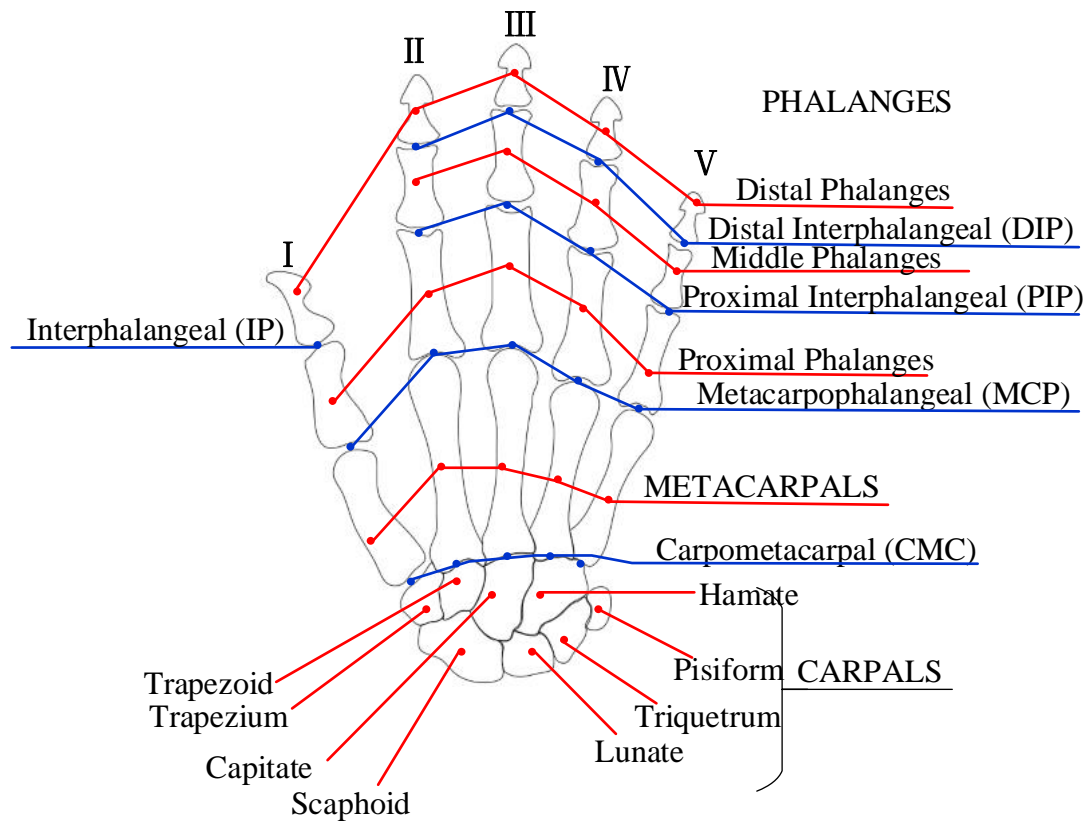


Figure 2.4. Bones and joints (left hand anterior view).

The definition of each finger movement passing over the dotted line in terms of extension/flexion, abduction/adduction and hyper-extension is shown in Figure 2.5. Extension: angle between the finger and the palm increased to straight; flexion: angle between finger and palm decreased to limited position; hyper-extension: finger extended over the straight line respect with palm; abduction: fingers moving away from midline; adduction: fingers moving towards the midline.

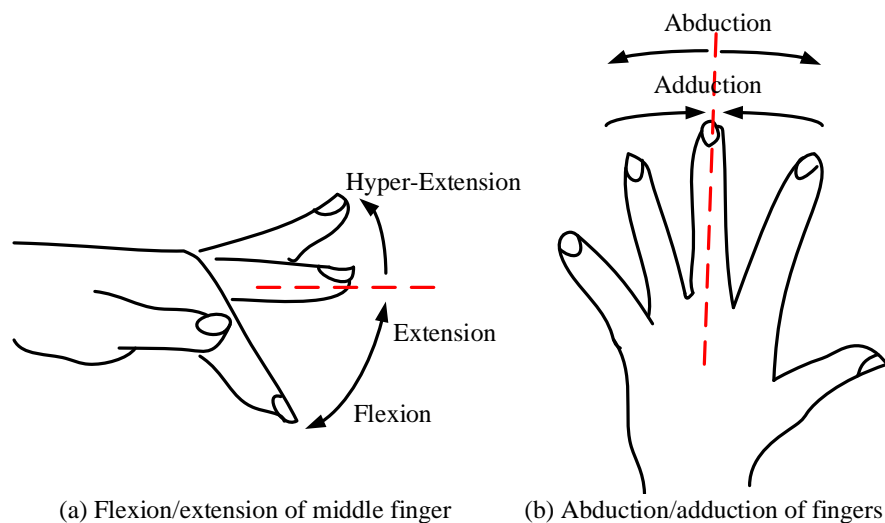


Figure 2.5. Flexion/extension of middle finger and abduction/adduction of fingers [104].

Fingers play an important role in grasping and manipulation. Investigations of ranges of movement of human fingers and the general lengths of their phalanges provide us the objectives for mimicking human finger. These physical parameters are shown in Table 2.2 and Table 2.3.

Table 2.2. Ranges of movement of the finger joints (H refers to hyper extension) [104].

Fingers	Joints	Action	Ranges(in degree)
Thumb	CMC	Adduction/Abduction	0(contact)/60
		Extension/Flexion	25/35
	MCP	Adduction/Abduction	0/60
		Extension/Flexion	10H/55
	IP	Extension/Flexion	15H/80
Index	MCP	Adduction/Abduction	13/42
		Extension/Flexion	0/80
	PIP	Extension/Flexion	0/100
	DIP	Extension/Flexion	10H/90
Middle	MCP	Adduction/Abduction	8/35
		Extension/Flexion	0/80
	PIP	Extension/Flexion	0/100
	DIP	Extension/Flexion	10H/90
Ring	MCP	Adduction/Abduction	14/20
		Extension/Flexion	0/80
	PIP	Extension/Flexion	0/100
	DIP	Extension/Flexion	20H/90
Small	MCP	Adduction/Abduction	19/33
		Extension/Flexion	0/80
	PIP	Extension/Flexion	0/100
	DIP	Extension/Flexion	30H/90

Table 2.3. Range lengths of the finger skeleton.

Phalanges	Length(in mm)
Proximal phalanges	38-55
Middle phalanges	24-35
Distal phalanges	22-30

Figure 2.6 shows human thumb and index finger during tip-to-tip and pad-to-pad precision grips. The figure shows the anatomy of the thumb distal phalanx and its relationship with soft structures related to manipulation: a huge proximopalmar fossa (orange) is associated with a palmarly protruding ridge (red) for insertion of the flexor pollicis longus; a compartmentalized digital pulp to accommodate the shape of the object being manipulated is reflected in the presence of an unguis fossa (green) associated with the large and mobile proximal pulp and as a wide apical tuberosity (blue) associated with the smaller and less mobile distal pulp; and finally, the unguis spines (yellow), where the collateral intraosseous ligaments sustain the nail bed insert [105]. Humans prefer tip-to-tip and pad-to-pad grips as shown: More than 92% and 65% respectively in which the tips of the thumb and the index finger make contact [106].

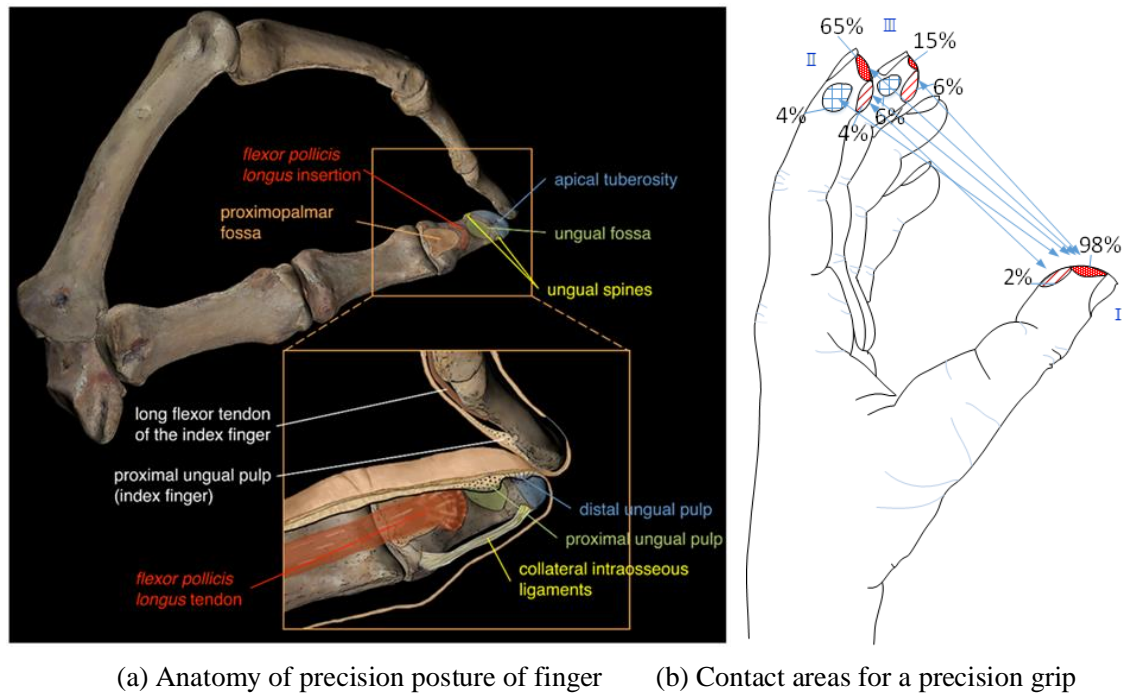


Figure 2.6. Human tip-to-tip and pad-to-pad grips configuration and contact areas for a precision grip.

Other research on human grasping behaviours shows that, during a wide range of unstructured tasks, 92% of objects have a mass of 500g or less; implying that a high payload capacity may be unnecessary to accomplish a large subset of human grasping behaviour [107]. In order to grasp 90% of the objects in the data set the way a human does, a hand should be able to grasp objects up to 7cm wide and up to a mass of 700g. Furthermore, it has been shown that the human has a clear tendency to grasp the

smallest dimension of an object. These results can translate directly to performance specifications for a robotic hand in terms of maximum grip aperture and payload capacity for handling a suitable percentage of common objects in human environments. These results come from the Yale human grasping dataset [107] which analyses human grasping behaviours during a wide range of unstructured tasks.

2.3 Concave and Cross linkages for Biological Morphology

In last two sections, natural grasping systems, especially human grasping systems, were investigated. As the most adaptable and versatile gripping system, human hand gripping was analysed in terms of gripping behaviours and anatomy. In the following sections, mimicking human hand grasping will be presented. Before that, some examples are provided which relate to biological mimicking using basic linkages.

Biological applications of the cross-four-bar (CFB) mechanism have been presented in the human knee joint. For example, a four-bar linkage system was shown in [108] to replicate the polycentric motion of the knee that occurs during passive knee flexion-extension. A CFB mechanism was proposed in [109] for the knee design of bipedal robot. An artificial foldable hinged wing based on two CFB linkages was developed to mimic the behaviours of the beetle's hind wing [110]. Applications on robotic hands for motion imitation also existed in [111, 112, 113]. As depicted in a lateral view in Figure 2.7, the anterior and posterior cruciate ligaments connecting the upper femur and the lower tibia cross each other. AB and CD represent the femur and tibia while BC and AD represent two ligaments. The ideal configuration allows the femur to roll on the tibia without friction. The contact-aided CFB mechanism is a better option to design artificial knee joint prosthetics than pin joint.

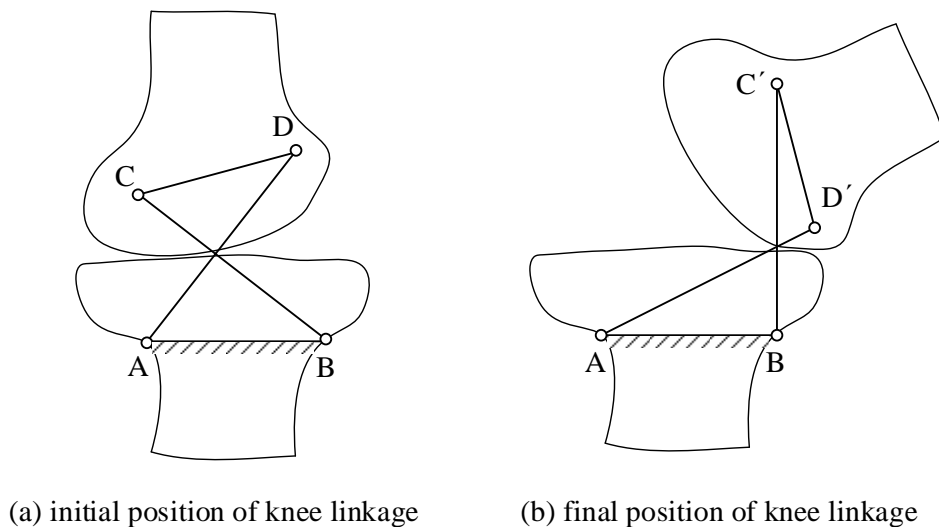


Figure 2.7. CFB mechanism in human knee joint.

There is a large amount of research on convex four-bar linkages aiming to produce a desired output motion for a specific input motion by kinematic analysis and synthesis. Concave linkages are little mentioned by scholars. Research shows that concave and cross four-bar (CFB) linkages play important role in animals' skeleton systems [114].

Biological linkages are widely distributed in animals, such as the following two examples which refer to concave four-bar linkages. Revolute joints are rare in biological systems and movement ranges are small due to mechanical constraints. Figure 2.8(a) shows a mantis shrimp's strike which generates extremely rapid speed and high force [115]. Morphological analysis shows that a concave four-bar linkage is the main kinematic component which amplifies rotation in the system. Figure 2.8(b) is another concave isosceles four-bar linkage in teleost fish [116]. Force-amplification occurs when the hyoid bars are close to the in-line position. In this mechanism, a weak input can produce a very large output force.

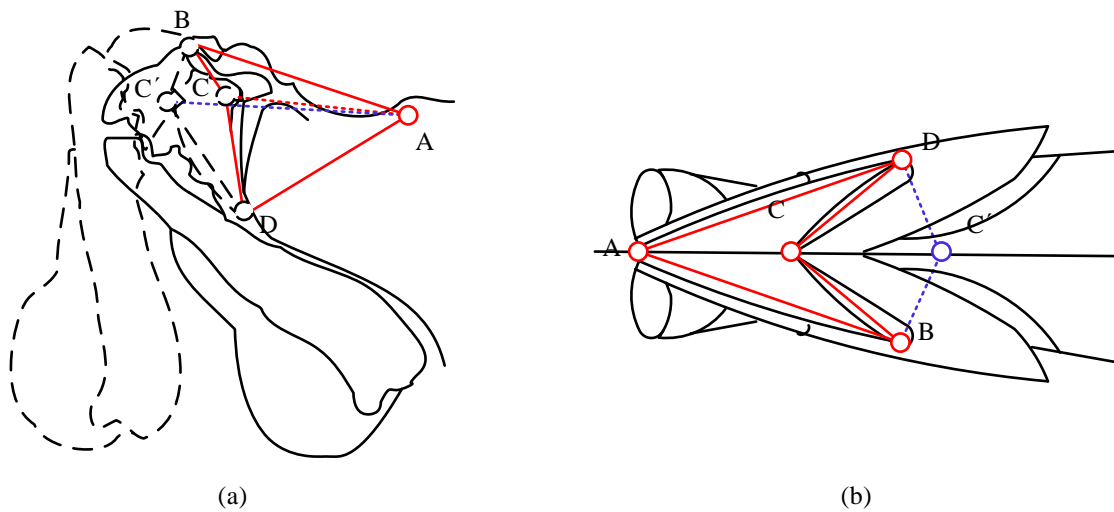


Figure 2.8. Concave four-bar linkages in biological systems: (a) mantis shrimp's strike; (b) teleost fishes' mouth.

2.4 Kinematic Analysis of Contact-Aided CFB Mechanism

In this section, the kinematics of a CFB mechanism is investigated. The centrodes of this mechanism are also explored and a contact-aided CFB mechanism proposed to mimic the complex movements of finger joints. This over-constrained structure also increases its stiffness.

2.4.1 Fixed and Moving Centrodes of CFB Mechanism

The centrode, an important characteristic in planar kinematics, is a path traced by the instantaneous centre of rotation of a rigid link moving in a plane [117]. The motion of the coupler link with respect to the ground link is pure rotation around the instantaneous

centre. The fixed centrode can be found by drawing the trajectory of the intersection of the crank link and follower link.

For crossing linkages, the length of one diagonal increases if, and only if, the other decreases [118]. Figure 2.9 shows the CFB linkage and its fixed and moving centrodes. Four links of the CFB mechanism AD , CD , BC , AB are indicated by a , b , c and d respectively. C_m and C_f respect moving and fixed centrodes respectively. θ_2 , θ_3 and θ_4 are four orientation angles of link vectors. The links are now drawn as position vectors that form a vector loop with the vector loop equation is being:

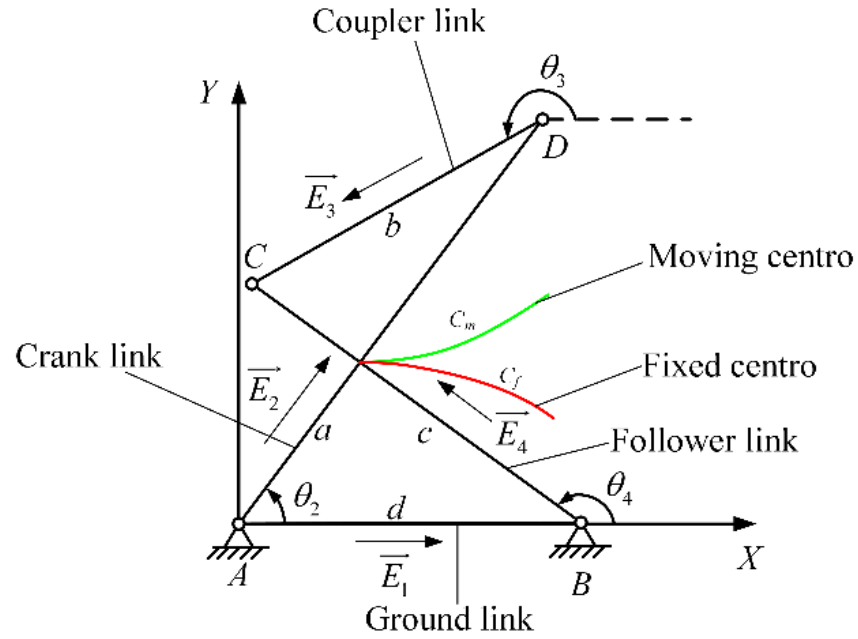


Figure 2.9. Position vector loop of CFB linkage and centrodes.

$$\vec{E}_2 + \vec{E}_3 - \vec{E}_4 - \vec{E}_1 = 0 \quad (2.1)$$

The solution of this equation can be derived [119] as following:

$$\theta_{4,2} = 2 \arctan \left(\frac{-N \pm \sqrt{N^2 - 4MP}}{2M} \right) \quad (2.2)$$

$$\theta_{3,2} = 2 \arctan \left(\frac{-N \pm \sqrt{N^2 - 4QR}}{2Q} \right) \quad (2.3)$$

where

$$M = \cos \theta_2 - K_1 - K_2 \cos \theta_2 + K_3 \quad (2.4)$$

$$N = -2 \sin \theta_2 \quad (2.5)$$

$$P = K_1 - (K_2 + 1) \cos \theta_2 + K_3 \quad (2.6)$$

$$Q = \cos \theta_2 - K_1 + K_4 \cos \theta_2 + K_5 \quad (2.7)$$

$$R = K_1 + (K_4 - 1) \cos \theta_2 + K_5 \quad (2.8)$$

$$K_1 = \frac{d}{a} \quad (2.9)$$

$$K_2 = \frac{d}{c} \quad (2.10)$$

$$K_3 = \frac{a^2 - b^2 + c^2 + d^2}{2ac} \quad (2.11)$$

$$K_4 = \frac{d}{b} \quad (2.12)$$

$$K_5 = \frac{c^2 - d^2 - a^2 - b^2}{2ab} \quad (2.13)$$

Equations (2.2) and (2.3) have two solutions. According to Grashof condition, if the sum of the shortest and longest link of a planar quadrilateral linkage is less than or equal to the sum of the remaining two links, then the shortest link can rotate fully with respect to a neighbour link. That is to say, only those CFB mechanisms satisfied with the condition $s + l \leq p + q$ are considered where s is the shortest link, l is the longest, and p and q are the other links. That means, the discrimination under the radical is positive and the solution is not complex conjugate. There are two values of θ_3 and θ_4 corresponding to any one value θ_2 . These are referred to the crossed and open linkage configurations or the linkage two circuits (Figure 2.10) [120]. A Grashof linkage is defined as crossed if the two links adjacent to the shortest link cross one another and open if they don't cross one another in this position [119]. In addition, the two shortest links ($AB=CD$) are also contained in the Grashof linkage. In other words, the CFB mechanisms can be obtained by using the Grashof condition and the shortest rule.

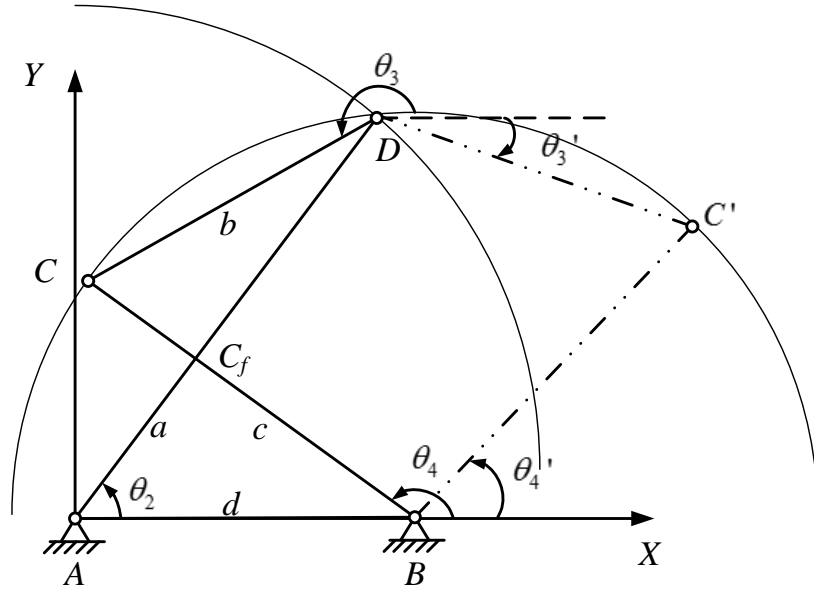


Figure 2.10. Two solutions to the crossed and open configurations of the four-bar linkage.

According to Kennedy-Aronhold Theorem [121], the centrode is found at the intersection of the extensions of the crank and the follower. In the case of CFB mechanism, the centrode is always between the coupler link and the ground link. As shown in Figure 2.10, AB is fixed as a frame and AD rotates clockwise with respect to A . The locus of centres of instantaneous rotation for D is a line along AD and for C is the line along CB . Therefore, the instantaneous centre of rotation for coupler link CD is C_f , the crossing point of AD and CB . Assuming A is the original position of the fixed coordinate system, the fixed centrode is the crossing point of two vector \overrightarrow{AD} and \overrightarrow{BC} . Therefore, the locus of fixed centrodes can be expressed as

$$\overrightarrow{C_f} = \frac{a \tan \theta_4}{\tan \theta_4 - \tan \theta_2} + j \frac{a \tan \theta_4 \tan \theta_2}{\tan \theta_4 - \tan \theta_2} \quad (2.14)$$

where θ_2 is an independent variable, θ_4 can be obtained from Equation (2.2).

The moving centrodes can be obtained by attaching the coordinate system to coupler link CD with C as the original point and having the same rotation with angle DCB decreasing, as shown in Figure 2.11.

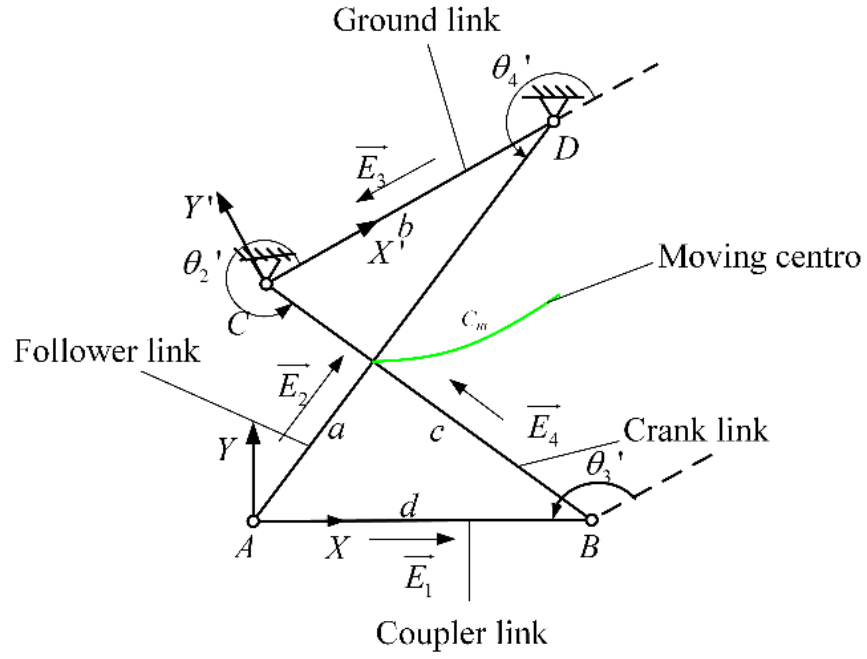


Figure 2.11. Moving centrodes at coordinate system $X'CY'$.

By using the same expression method, the vector of the moving centrode with respect to the coordinate system $X'CY'$ can be expressed as

$$\overrightarrow{C_m'} = \frac{b \tan \theta_4'}{\tan \theta_4' + \tan \theta_2'} + j \frac{b \tan \theta_4' \tan \theta_2'}{\tan \theta_4' - \tan \theta_2'} \quad (2.15)$$

where

$$\theta_4' = -3\theta_2 - \theta_3 \quad (2.16)$$

$$\theta_2' = \theta_4 - 2\theta_2 - \theta_3 \quad (2.17)$$

The transformation matrix of coordinate system $X'CY'$ with respect to XAY is expressed as

$${}^c_A T = \begin{bmatrix} -\cos(2\theta_2 + \theta_3) & \sin(2\theta_2 + \theta_3) & a \cos \theta_2 + b \cos \theta_3 \\ -\sin(2\theta_2 + \theta_3) & -\cos(2\theta_2 + \theta_3) & a \sin \theta_2 + b \sin \theta_3 \\ 0 & 0 & 1 \end{bmatrix} \quad (2.18)$$

The vector of moving centrode with respect to the coordinate system XAY can be expressed as

$$\overrightarrow{C_m} = {}^c_A T \overrightarrow{C_m'} \quad (2.19)$$

Partial trajectories of centrodes with a rotational angle of the crank link of 35° are shown in Figure 2.12. The motion of the coupler link with respect to the ground link is

uplicated by making these two centrodes roll against one another without slipping. Due to the pure rolling of the two curves, they have the same length.

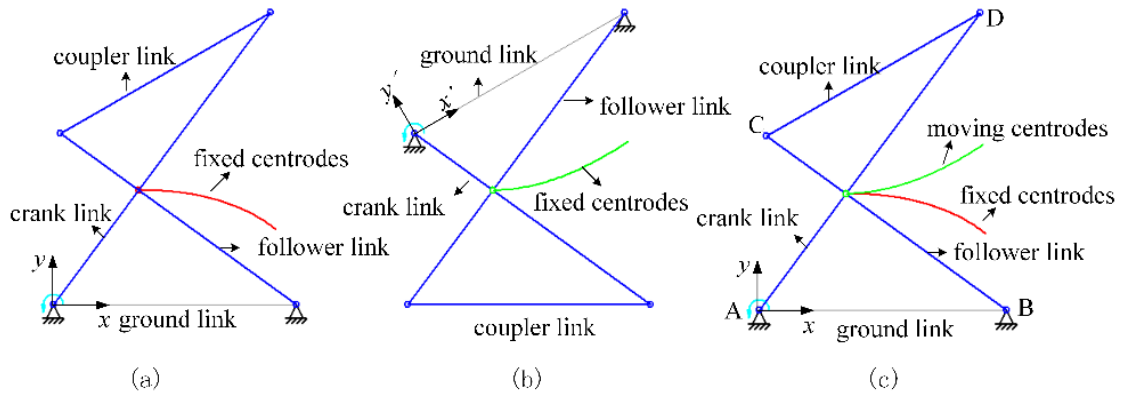


Figure 2.12. CFB mechanism and trajectories of its centrodes: (a) produced by trajectory of fixed centrodes; (b) produced by trajectory of moving centrodes; (c) trajectories integrated into one figure.

2.4.2 Design of Contact-Aided CFB Mechanism

The contact-aided mechanism was first introduced in [122]. Cannon and Howell proposed a novel design of a compliant rolling-contact element capable of performing the functions of a bearing and a spring [123]. The application of contact surfaces enhances the functionality of a compliant mechanism to be capable of performing certain kinematic tasks similar to a rigid body. Due to the characteristics of the centrodes, a contact-aided CFB mechanism with a much higher stiffness is created by adding a high kinematic pair between the coupler and the ground link. Figure 2.13 shows a contact-aided CFB mechanism with a limited rotating range of 90° .

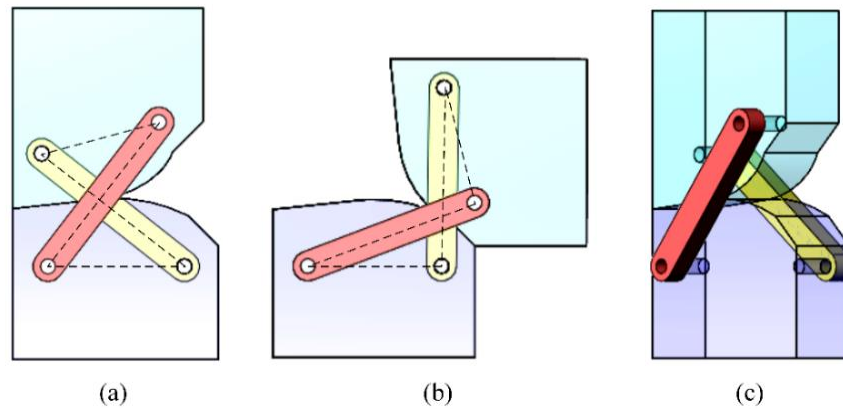


Figure 2.13. Contact-aided CFB mechanism: (a) Initial position; (b) Final position; (c) Side view of the assembly.

Based on the above design process for centrodes and a contact-aided CFB linkage, a prosthetic leg can be developed with the bending angle of 90° , as shown in Figure 2.14.

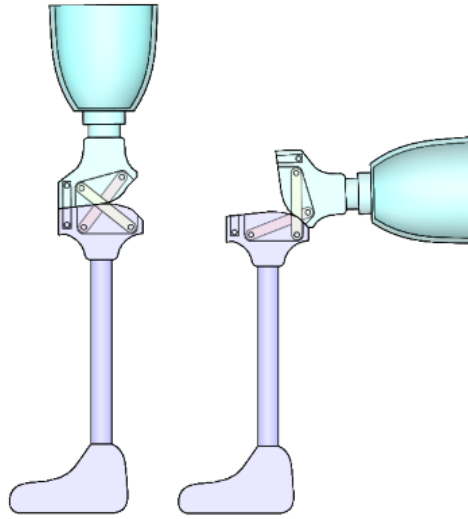


Figure 2.14. Prosthetic leg using a contact aided CFB linkage.

2.5 Contact-Aided CFB-Based Anthropomorphic Finger

This section first investigates gripping configurations of the human hand for different objects. The development process of a CFB-based anthropomorphic finger is then presented. Finally, a two-fingered gripper with the joint is prototyped and tested.

2.5.1 Gripping Analysis and Design of Finger Joints

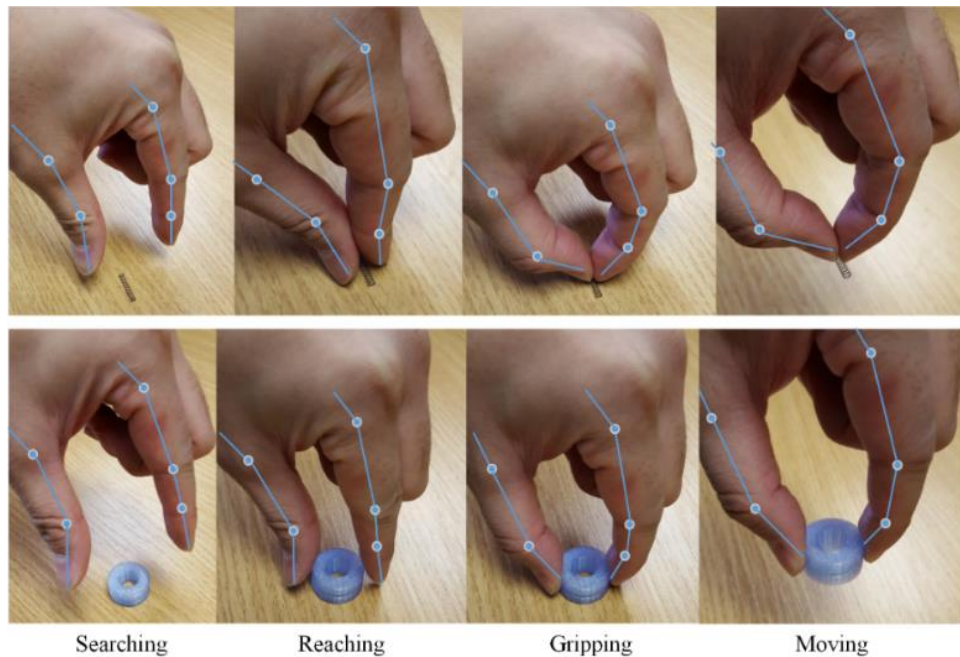


Figure 2.15. Gripping process for objects in different sizes and shapes.

Configurations of the human hand are different in gripping various sizes and shapes of objects. Nevertheless, the gripping processes are similar, typically including searching, reaching, gripping and moving [124]. Two gripping examples are considered and various configurations of fingers are observed. The two objects are a compression spring with a diameter of 2.5mm and a length of 15mm and a cylindrical block with a diameter of 22mm and a height of 11mm, as shown in Figure 2.15.

By analysing the gripping processes of the two objects, the fingernails and fingertips play significant roles. For a small diameter object, such as the spring, the fingernails and the fingertips cooperate to enclose and hold with a very small gripping force. For a larger part such as the plastic wheel, soft fingertips that deform during contacting apply a large range of frictional forces and moments [125]. Therefore, the design of the finger should combine the functions of a fingernail and a soft fingertip.

2.5.2 Design Process of a Two-Joint Finger

Taking the thumb finger as an example, the MCP and IP joints need to be considered during the design. The action ranges of extension/flexion as to MCP and IP joints are 10H/55 and 15H/80 respectively (see Table 2.2 in section 2.2), as shown in Figure 2.16. The thumb finger is the only one which has hyper extension at the MCP joint which means it has the largest bending range of the five fingers. In order to mimic the ranges of motion of the two joints, two CFB linkages are adopted, one for mimicking the IP joint and the other for the MCP joint.

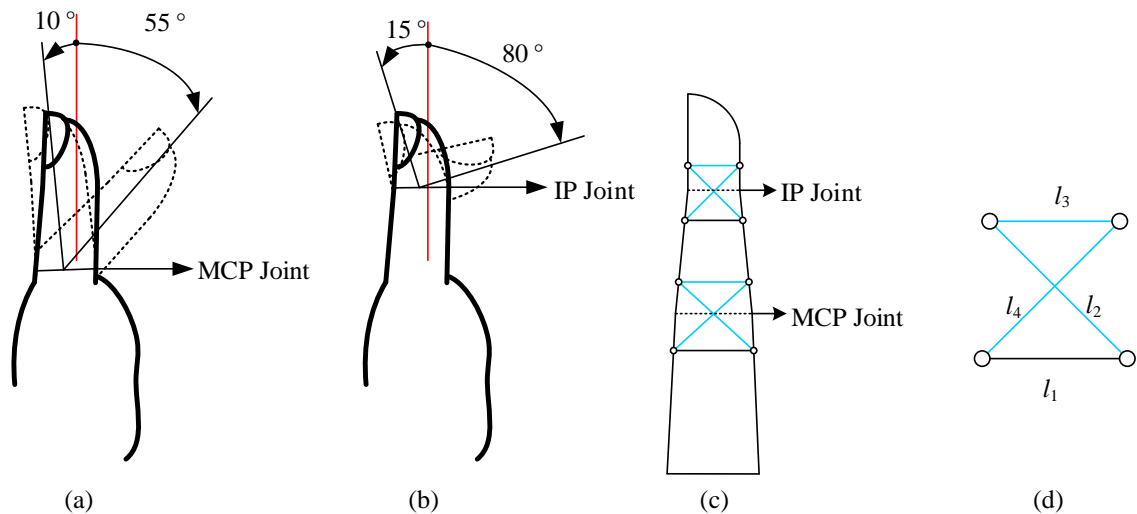


Figure 2.16. Extension/flexion ranges of two joints of thumb finger and equivalent CFB mechanisms of the joints: (a) extension/flexion range of MCP joint; (b) extension/flexion range of IP joint; (c) replacing of each joint with CFB linkage; (d) indication of each link of CFB linkage.

According to the approach proposed in Sections 2.4.1 and 2.4.2, the extension/flexion ranges of these two CFB mechanisms determine their ranges of motion, the fixed and moving centrodes of the mechanisms can thus be obtained. The synthesized two-joint finger which has the same motion range as human thumb is shown in Figure 2.17.

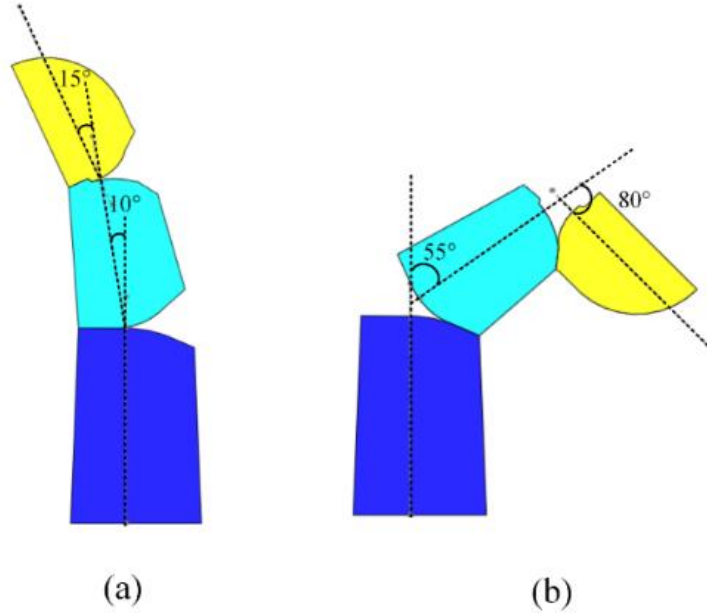


Figure 2.17. Side view of two-joint finger connecting with fixed and moving centrodes: (a) hyper extension of the finger; (b) flexion range of the finger.

Table 2.4 shows the geometric parameters of the two finger joints where l_1 indicates ground link, l_2 the drive link, l_3 the follower link and l_4 the coupler link, as shown in Figure 2.16(d).

Table 2.4. Geometric parameters of the two-joint finger

Property	IP joint	MCP joint
l_1 (mm)	18	25
l_2 (mm)	24	32
l_3 (mm)	16	22
l_4 (mm)	24	32
Angular ranges (°)	15H/80	10H/55

2.5.3 Prototype and Testing

The gripping analysis of the human hand (see Section 2.5.1) indicates that fingernails and soft fingertip play critical roles in specific gripping tasks. A 3D model considering these details is designed in order to mimic the human finger. Two joints of the finger are

decoupled with a tendon for driving two phalanges. The finger is symmetrically divided into front and back halves which make manufacturing and assembly simple and efficient. The detailed design of the two-joint finger is shown in Figure 2.18.

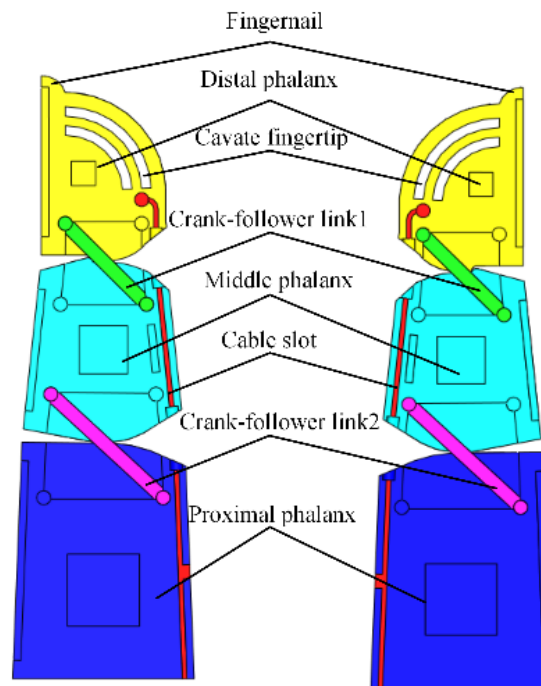


Figure 2.18. 3D model of a two-joint finger.

A 3D printed prototype is shown in Figure 2.19. The material used for the outside layer of the phalanges is silicone elastomer while the material for crank link and follower links of CFB mechanism is polylactide (PLA). Nylon rope passes through cable slots between which a compression spring is placed for returning it back to the original position.

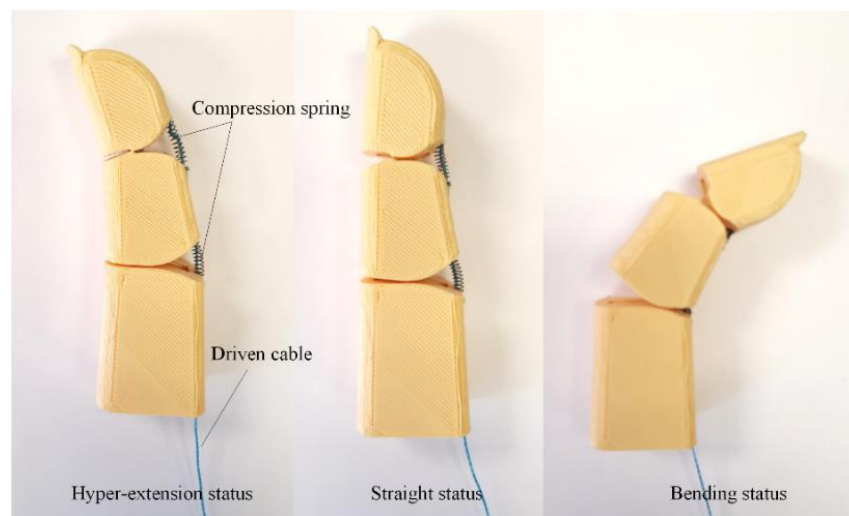


Figure 2.19. Contact-aided joints and motion of a robotic finger.

A two-fingered hand developed for manual gripping test is shown in Figure 2.20. The palm holder contains a differential pulley which drives the two fingers in underactuated motion. A wide range of objects with various sizes and weights used for grasping include a plastic cup, tiny spring and pinecone, etc. as shown in Figure 2.21. The fingernail is used for gripping the tiny spring. The combination of fingernail and fingertip ensures successful gripping of a ballpoint pen. The soft fingertips provide a large friction force and moment for the cuboid-shaped battery. The differential drive contributes to the irregular non-centred pinecone gripping. The 3D printed gripper is utilized to grip a wide range of objects. Gripping configurations for different sizes and weights are various. The testing successfully verifies the feasibility of the design approach.

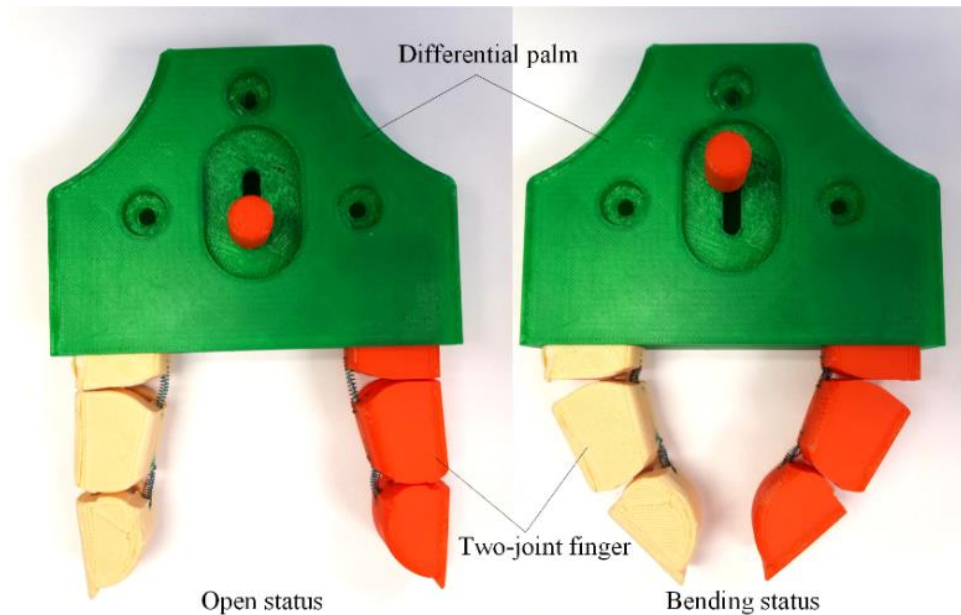
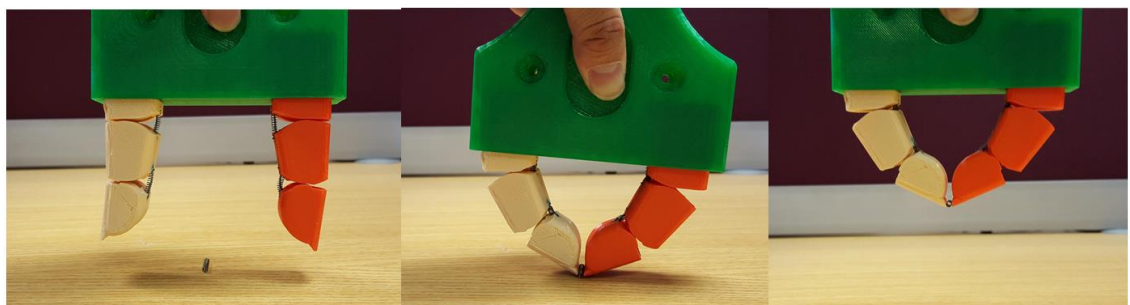
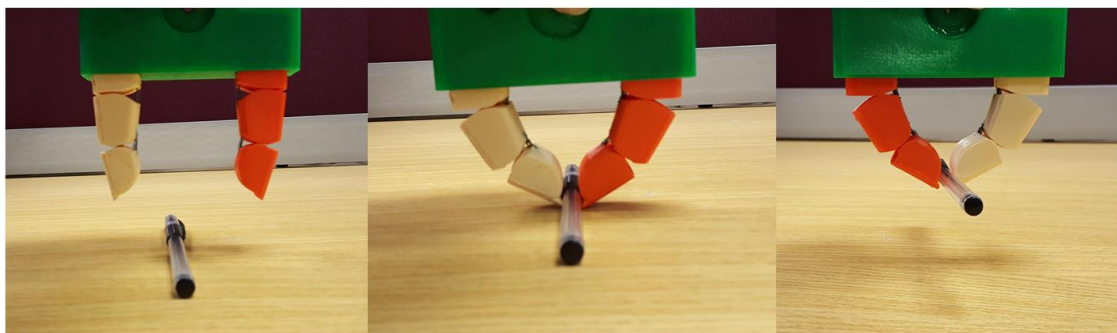


Figure 2.20. Two-fingered hand at open and bending statuses.

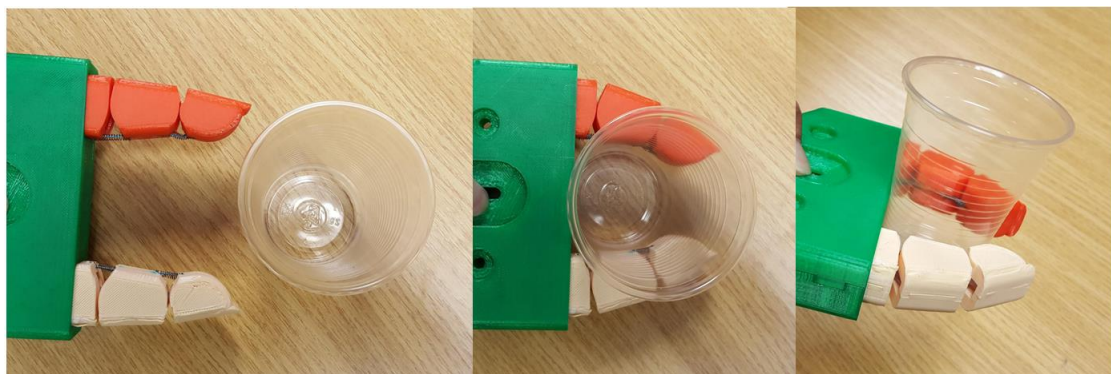


(a) tiny cylindrical spring, 0.2g, $\Phi 2.8\text{mm} \times 15\text{mm}$

Figure 2.21. Gripping testing on a variety of objects (to be continued)



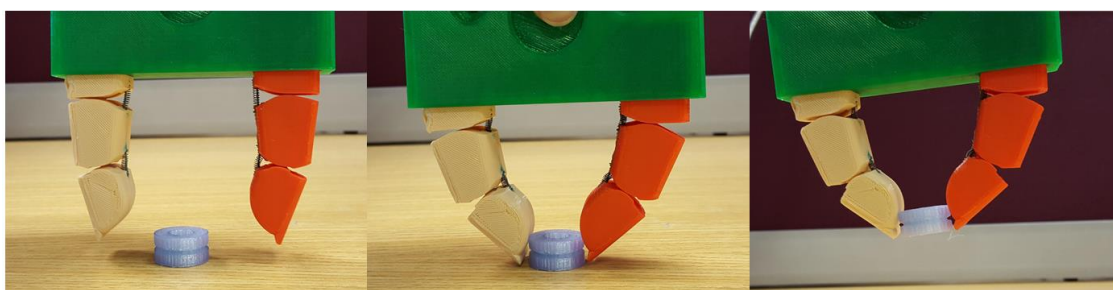
(b) lying cylindrical ball pen, 15g, $\Phi 8\text{mm} \times 130\text{mm}$



(c) frustum plastic cup, 5.6g, $\Phi 45\text{mm} \times \Phi 74\text{mm} \times 88\text{mm}$

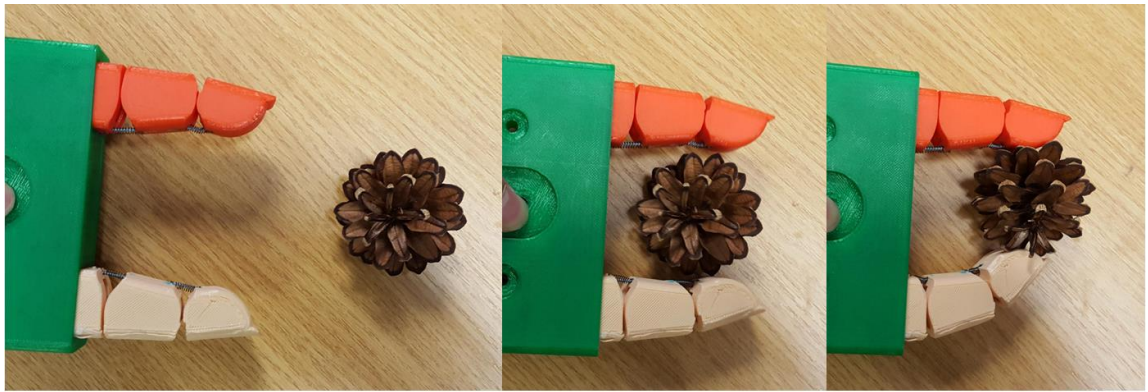


(d) 9V battery, 45g, $48.5\text{mm} \times 26.5\text{mm} \times 17.5\text{mm}$



(e) Cylindrical plastic part, 8g, $\Phi 20\text{mm} \times 4\text{mm}$

Figure 2.21. Gripping testing on a variety of objects (to be continued)



(f) irregular shape, pinecone, 10g

Figure 2.21. Gripping testing on a variety of objects (continued).

2.6 Summary

This chapter has provided a detailed analysis of human grasping behaviours and a novel design of anthropomorphic finger. The human articular system was presented and human grasping behaviours analysed. The biological mimicking methods provided an inspiration for a finger joint design. The kinematics of a contact-aided CFB mechanism was presented and a design approach for mimicking human finger joints proposed. The gripping process of the human hand indicates the significant role of the fingernail and soft fingertip which were proposed for prototyping. A two-joint thumb finger was developed to verify the proposed non-revolute design. The prototype was manufactured by 3D printing with rigid and soft materials and successfully tested with a variety of objects which verified the feasibility of the biomimetic design.

CHAPTER 3 – CFB-Based Multi-Mode Fingertip

In chapter 2, a natural gripping system was investigated and articular system of human hand was presented. A novel type of anthropomorphic finger based on CFB linkage was proposed. By analysing the gripping processes of the synthesized anthropomorphic finger hand, fingernails and the fingertips play significant roles. This chapter will focus on a systematic analysis of RRRR linkage which has four rotating joints and included CFB linkage and its application as a fingertip with multiple gripping modes.

3.1 Flexible Gripping in Manufacturing

The flexibility of the gripper means that it can grip a large number of objects. The objects that can be gripped primarily depend on the fingertip (or jaw) of the gripper. The gripping force is also variable according to the form and condition of the active surfaces between the objects and the fingertip (such as coefficient of adhesive friction). So it is essential to ensure good contact between the objects and fingertip for safe gripping. In addition, an appropriate design of workpieces for robotic gripping is also important in industrial applications. The flexibility of the human hand would be more superior than any existing gripper system, as it can naturally cope with numerous objects from a thin needle to a basketball (if the hand is large enough). There are special fingertips for gripping only limited objects, such as a gripper for automotive assembly, see Figure 3.1(a). Industrial fingertips are always specialized to ensure compliance in manipulating several workpieces, see Figure 3.1(b). Some fingertips consider flexible contact or are self-adjustable to grip complex objects with different shapes, see Figure 3.1(c). Obviously, the more flexible the fingertip, the more objects it can grip.

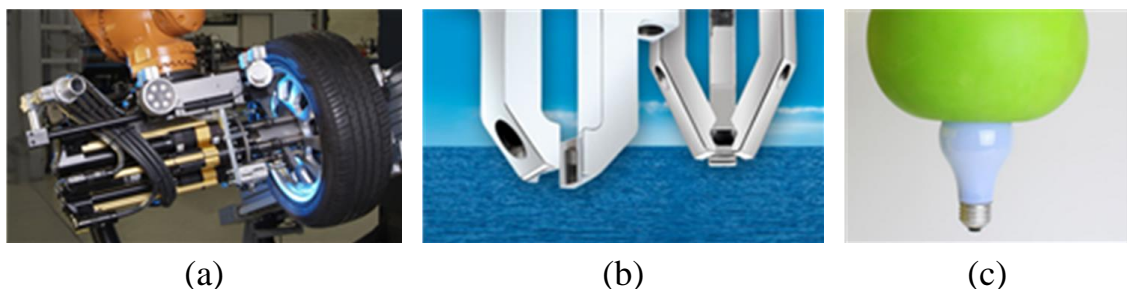


Figure 3.1. Special, specialized and flexible fingertips: (a) specific clammer for automobile assembly; (b) industrial robot gripper; (c) soft ball gripper.

One way to boost the flexibility of the gripper is by changing fingertips. Figure 3.2 presents a set of fingertips [2]. The fingertips can be replaced manually or automatically to be able to meet specific handling tasks. For quick, correct conditions, an automatic quick-change operation is required. It also depends on the economic and technical

requirements. A specific unit between the finger and fingertips makes the change process smooth. However, the change cycle is inefficient during a manufacturing process.

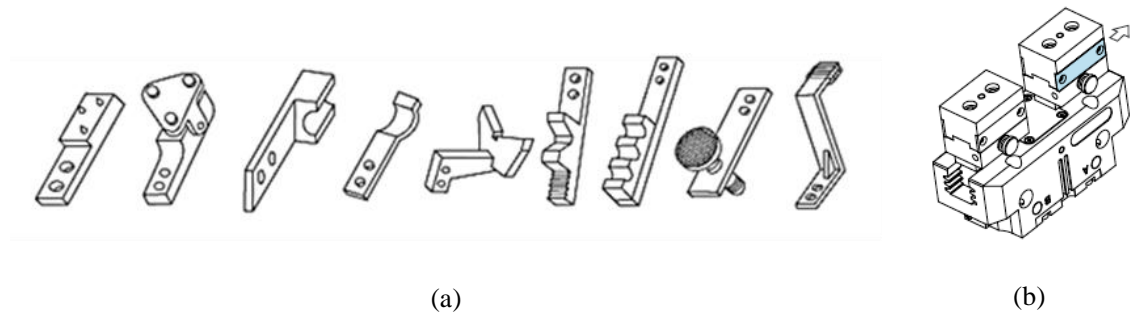


Figure 3.2. A set of fingertips and the changing unit [2]: (a) various finger tips; (b) driving platform.

Another method of increasing flexibility is the use of rotary units to construct a multi-gripper group which can grip different objects without changing fingertips due to the multiple fingertips, see Figure 3.3. The grippers can be used simultaneously or successively for gripping. These grippers are able to work independently and are always used for handling one or multiple types of objects. According to Figure 1.1 in Introduction, operating time and handling time comprise the whole time consuming of the handling process. Multigrippers will multiply the operating time which is an efficient approach. To prevent this happening, a multi-mode concept works for various functions is presented.

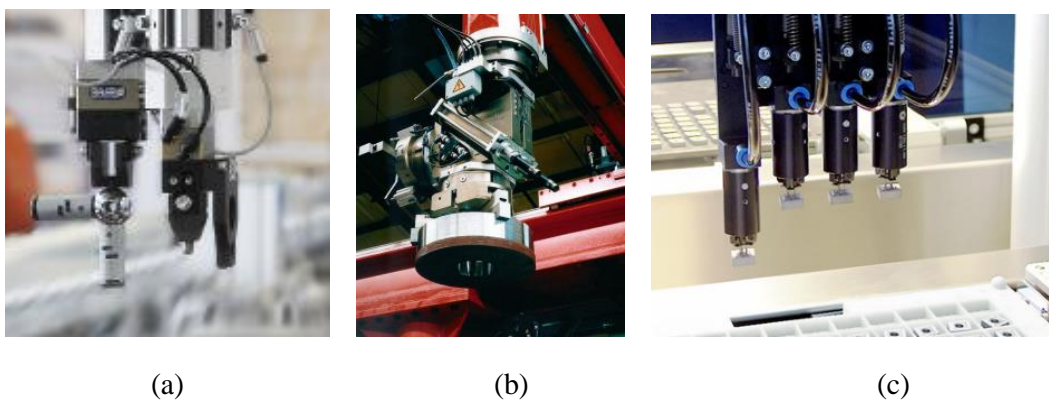


Figure 3.3. Multi-grippers: (a) multiple gripper for successively assembly; (b) multiple gripper in industrial picking; (c) multiple gripper for endurance test of keyboard.

Small and medium-scale size or meso-scale size (see Section 1.3.1) manufacturing lines demand more flexible gripping technology. This is because the aim of this technology is always to grip a broad range of objects. This chapter provides a multiple-mode (multi-mode) fingertip which is totally different from existing artificial fingertips. Due to the close relationship between the specific fingertip and four-bar linkage, the classification of planar four-bar linkage is first followed by the atlas of the simplest ones. Specifically, CFB mechanisms are investigated based on the same method. Kinematic equilibrium of CFB mechanism provides a new design vision for multi-mode development for practical application. The CFB mechanism as a multi-mode fingertip on a gripper increases its flexibility for meso-scale size objects gripping them with its angular mode and gripping macro-scale size objects with passive-adjusting mode. To standardize the novel designed fingertip, kinetostatic analysis of the CFB-based fingertip is conducted. Two tables referring to the transfer coefficient of a CFB-based fingertip for a two-fingered and three-fingered gripper hand are provided.

3.2 Types of Planar Four-Bar Linkages

The functions of linkages are classified into function, path and motion generation according to the primary goal of a design. A four-bar linkage is the simplest movable closed chain linkage and contains four links and a loop of four joints. According to the relationship of the four axes of the linkages, there are planar, spherical and Bennett four-bar linkages with the axes parallel, intersecting at a single point or angular position, respectively. The planar four-bar linkage plays an important role in machines [126, 127] because of its wide variety of movements guided by the planar four-bar linkage. Applications include pantographs, train suspensions, stroke engine and biological system mimicking [114]. In this section, basic types of planar four-bar linkage are investigated. Coupler curves and cognate mechanisms of basic types of planar four-bar mechanism are presented by using Roberts-Chebyshev theorem (see **Appendix D**). The relationship of straight-line mechanisms of the most common type (approximate and exact) is summarized along with some new discoveries (see **Appendix E**).

A planar four-bar linkage comprises four links that can be seen as two levels connecting with one rod. The force rotates one level and the power transfers to another level through a center rod. In a four-bar mechanism, the torque is engaged to a drive link while the force and motion are transferred to a follower link through a coupler link. Therefore, the four links are named the drive link, coupler link, follower link and ground link where the drive and follower links are mounted to coupler and drive link, see Figure 3.4 (a). This type of planar four-bar mechanism is also named a planar RRRR

(4R) mechanism because of the four revolute (R) joints. These definitions are consistently used throughout this thesis.

The other two types of planar four-bar mechanisms (slider-crank and double slider mechanisms) are two special configurations with a follower link or drive and follower links infinite in length. The slider-crank linkage is connected by three R joints and one prismatic (P) joint, on RRRP linkage. The order of P and R can be changed to represent different versions of slider-crank mechanisms. For example, if the slider acts as a coupler link, the mechanism is called RRPR or RPRR mechanism. The RRRP mechanism is often used to transform rotary motion into translation motion, see Figure 3.4(b). The double slider mechanism refers to two sliders which is connected by one coupler link. This mechanism is a PRRP mechanism which contains two R joints and two P joints and is always used to transform two translation motions into rotary motion, see Figure 3.4(c).

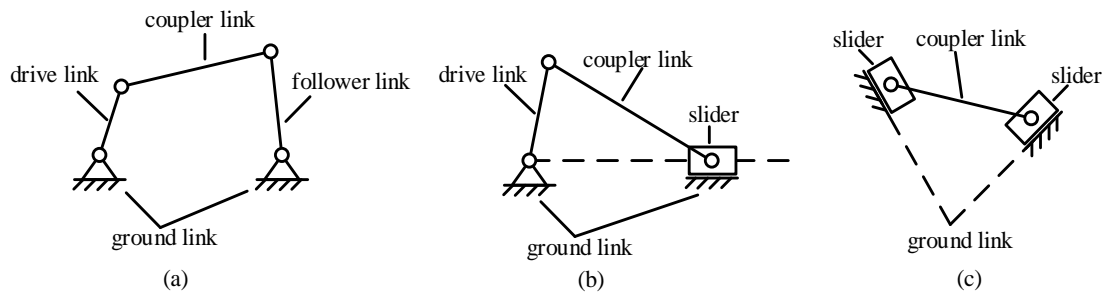


Figure 3.4. Three basic types of planar four-bar mechanisms: (a) RRRR mechanism, (b) RRRP mechanism, (c) PRRP mechanism.

3.2.1 RRRR Mechanisms

There are two classification approaches for a planar quadrilateral mechanism or RRRR mechanisms. The first approach depends on the dimension of each link (Grashof condition [128] and McCarthy expansion [129]). The other depends on configurations of the linkage.

The Grashof condition states:

If the sum of the shortest and the longest link of an RRRR linkage is less than or equal to the sum of the remaining two links, the shortest link can rotate fully with respect to neighbouring links.

It can be written as $s+l \leq p+q$, where s is the shortest link, l is the longest link and p and q are the neighboring links. Types of RRRR linkages are shown in Figure 3.5.

If a link can rotate a full 360 degrees, it is called as a crank. For a limited range of angles which do not include 0 degrees or 180 degrees, it is called rocker.

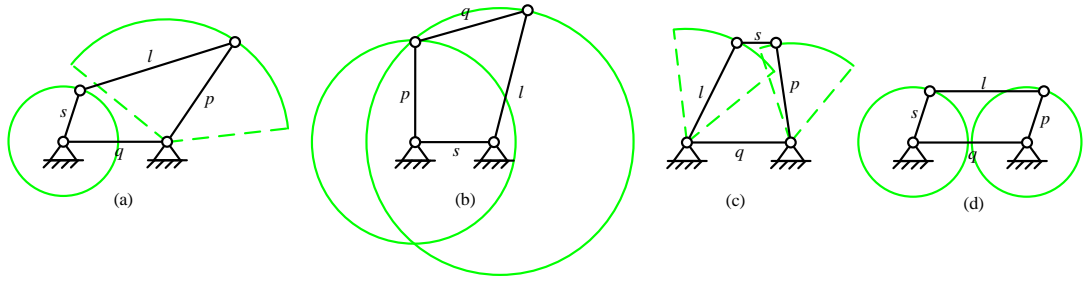


Figure 3.5. Types of mechanisms resulting from the Grashof condition: (a) cank-rocker, $s+l < p+q$; (b) double crank, $s+l < p+q$; (c) double rocker, $s+l > p+q$; (d) parallelogram, $s+l = p+q$.

The configurations of an RRRR linkage are classified into three types: convex, concave and cross [130] (Figure 3.6). This classification considers the rotation angle of the vertices changing while the length of each link is preserved and the lengths of the diagonals. By analyzing the characteristics of the three types of configurations, it can be seen that:

- (1) Convex and concave cases do not have crossed links. Only the cross cases have two crossed links.
- (2) All four internal angles of the convex and cross cases are less than 180 degrees. The concave case has one reflex angle which is more than 180 degrees.
- (3) The angle-changing trend of convex and cross cases is the same. The concave case has a different angle change from the other two. In detail, the $\angle DAB$ of the convex and cross cases increases, while the opposite $\angle BAD$ increases and the other two opposite $\angle ABC$ and $\angle ADC$ decrease. The concave case shows that the $\angle DAB$ increases while the opposite $\angle DCB$ decreases and the other two opposite angles increase.
- (4) For convex and cross cases one diagonal increases if and only if the other decreases; for concave case one diagonal increases if only if the other increases.

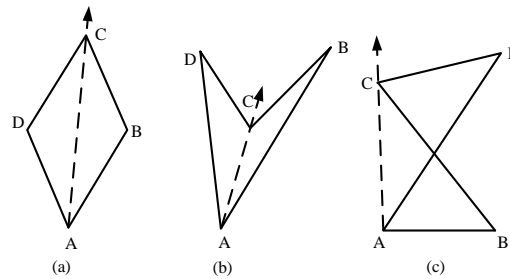


Figure 3.6. Three configurations of a planar four-bar linkage: (a) convex, (b) concave, (c) cross.

3.2.2 Configuration Zones of RRRR Mechanisms

A kinematic chain can be used to determine the configurations of a four-bar mechanism. Six postures can be calculated covering all solutions. A novel and comprehensive classification of RRRR linkage based on its configuration is proposed.

RRRR linkages can be looked as two sets of dyad which is the simplest kinematic chain of two binary links, one connecting joint and two free joints. The angles of the dyad can be zero, acute, right, obtuse, reflex and straight. Therefore, the dyad has six configurations in total, as shown in Figure 3.7. Zero and straight angles are special cases with folded and stretched in-line configurations. The right configuration transforms the position of the acute and obtuse angles. In this section, general configurations with acute, obtuse and reflex angles are mainly considered. Since a reflex angle is necessary for a concave four-bar linkage, acute and obtuse angles exist in all three configurations of a four-bar linkage.

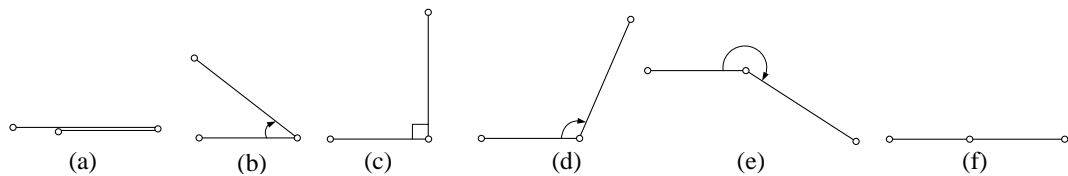


Figure 3.7. Six configurations of dyad with (a) zero, (b) acute, (c) right, (d) obtuse, (e) reflex and (f) straight angles.

To analyze the classification of RRRR linkage, take the acute-angle dyad as an example (Figure 3.8). This separates the planar area into seven areas and boundaries (dotted line). By connecting any single point located in each area and the two free joints of the dyad, it is possible to obtain three categories of RRRR linkage with different configurations i.e. convex, concave and cross.

If the one binary link (such as AB) is fixed as a ground link. These three categories of RRRR linkage can be further divided into seven subcategories, which contain two types of cross four-bar (CFB) mechanisms, four types of concave mechanisms and one type of convex mechanism. Convex mechanism has been extended, such as the Grashof conditions. Until now, the research on concave and CFB mechanisms has not been well explored, even though six out of seven categories are non-convex types.

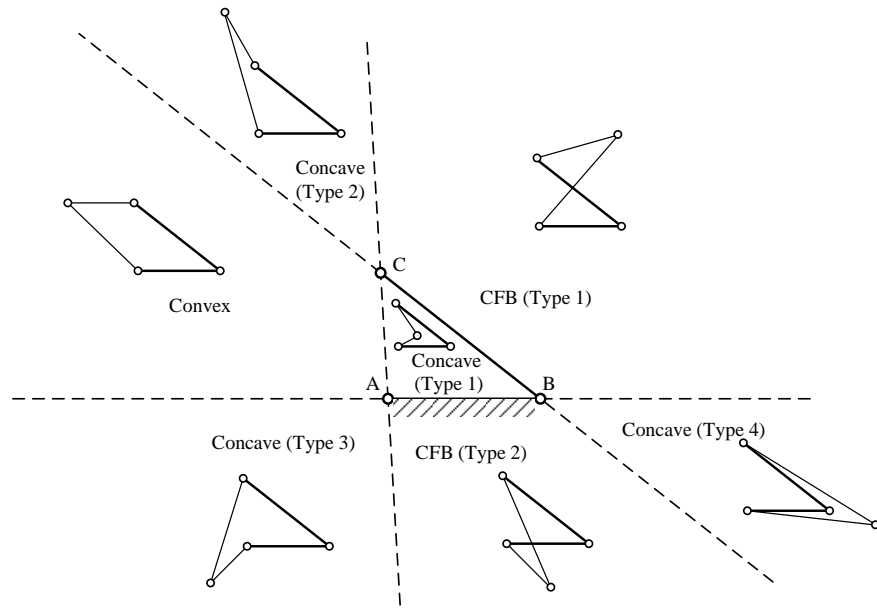


Figure 3.8. Classification of RRRR mechanisms based on acute-angle dyad.

In the same way, the other two configurations of the dyad with obtuse and reflex angles are used to classify RRRR mechanisms, as shown in Figures 3.9 and 3.10. The seven types of mechanisms comprise the same the three types of classification. The acute- and obtuse- angle have the same allocation of the seven types which means that the position of each type is identical. However, the classification based on reflex-angle have an inverse allocation direction.

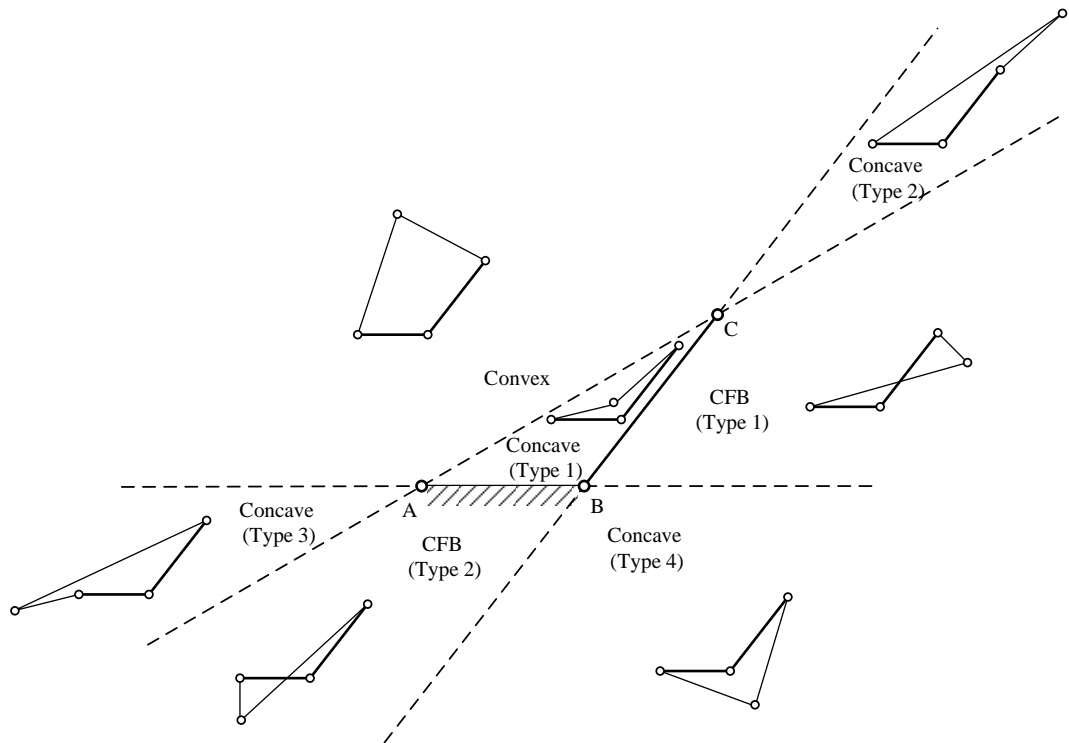


Figure 3.9. Classification of RRRR mechanisms based on obtuse-angle dyad.

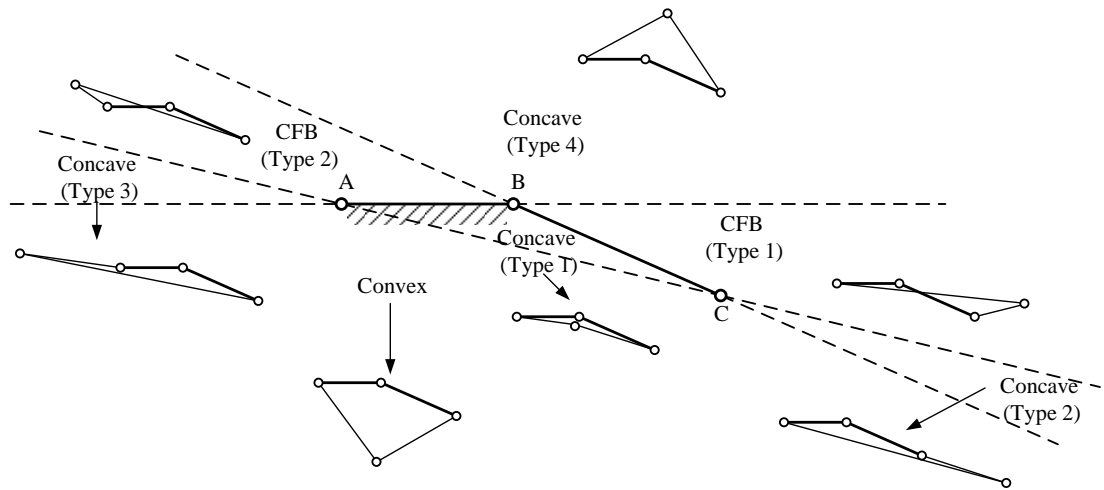


Figure 3.10. Classification of RRRR mechanisms based on reflex-angle dyad.

Further, if the two free joints A and C are connected with points located at the boundary (dotted lines), there exists some special configurations to transform between neighboring areas, see Figure 3.11. In these configures, two links align or coincide with each other, a torque applied on the other side cannot induce rotation to the coincident link, which is said to be at its dead or toggle point. There is also an undetermined position at joint B if two added links coincide with the dyad; these are known as singularity configurations.

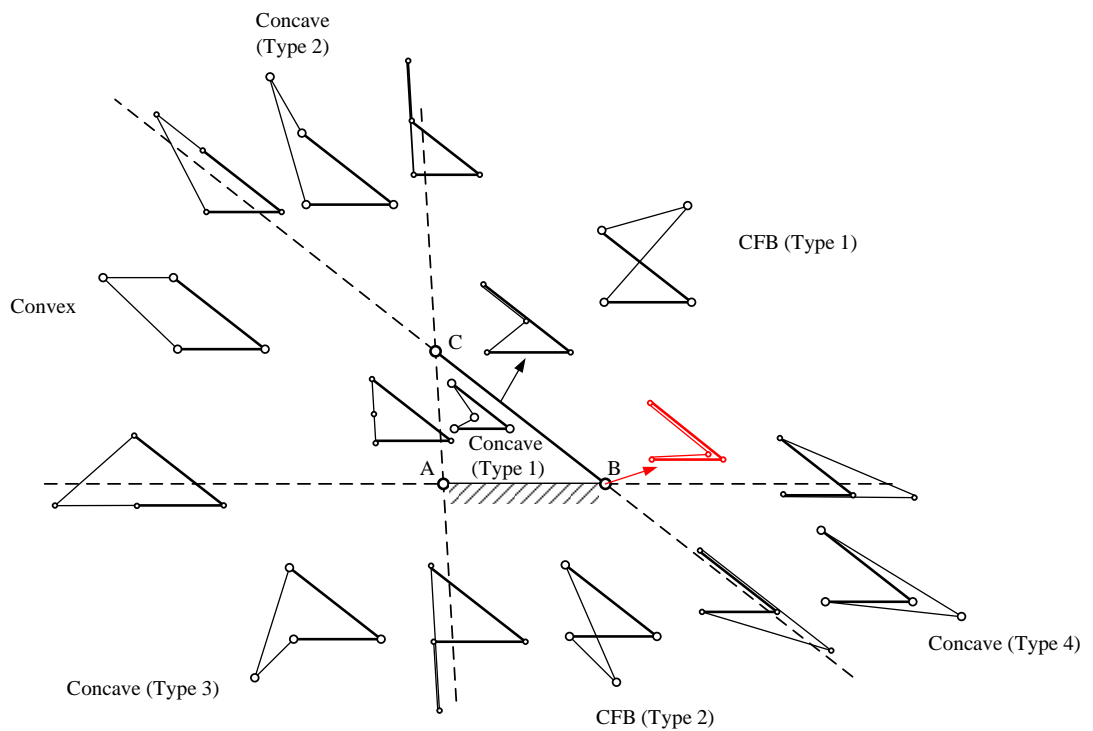


Figure 3.11. Configurations of the whole series of the RRRR mechanisms

The most specific configuration of an RRRR mechanism is based on the folded and stretched in-line configurations of dyads. It is a branched or transition configuration, as shown in Figure 3.12.

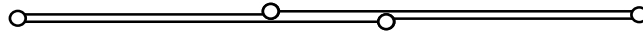


Figure 3.12. Transition configuration of RRRR mechanism.

3.2.3 Basic Planar Four-Bar Mechanisms

According to the classifications, configurations and related applications, the basic types of planar four-bar mechanisms are summarized in Figure 3.13. The five basic mechanisms can be transformed into various cases by using inversion, expansion, cognate and equivalent.

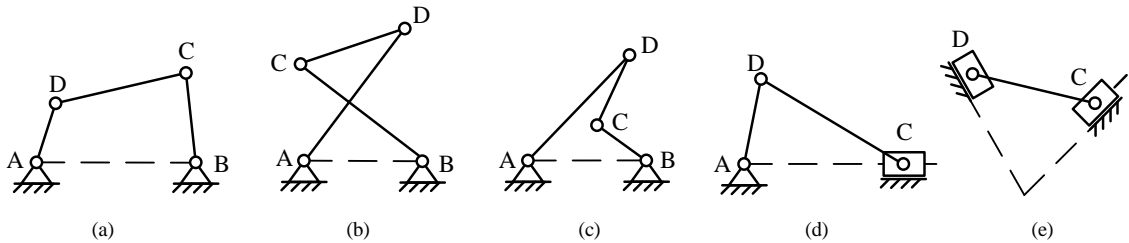


Figure 3.13. Basic four-bar mechanisms: (a) convex RRRR; (b) cross RRRR; (c) concave RRRR; (d) RRRP; (e) RPPR.

3.3 Configurations Zones of CFB Mechanisms

Biomimetics is a research area that imitates biological design to solve scientific problems. An American inventor Otto Schmitt first coined this word in the 1950s while trying to emulate the function of nerve cells in an artificial device. The word contains the Greek words bios (life) and mimetic (copy). The growth of biomimetic research has been rapid since 2001 and it has shown no sign of saturating until now. The endeavour of mimicking creatures is to understand the natural world and evolution through building models of natural processes. Therefore, the identification of configurations for planar four-bar mechanisms is better suited to the study of biological system than the Grashof-classification which is used for engineering. The identification of configuration zones in this section is more about the change of the structural elements through evolution. Four-bar linkages have been widely used in knee joint mimicking [131]. The CFB mechanism as a knee joint indicates **less energy consumption** than a revolute knee joint. The physical characteristics in terms of motors, weight, inertia and length

would be less for a knee mechanism based on a CFB linkage [132]. The classification of CFB mechanism results in a better understanding and application in the future design.

According to Section 3.2.2, there are two types of CFB mechanism classified based on configurations, see Figure 3.14 and is very easy to understand. The first shows a mechanism with a drive link and a follower link crossed, the other one with a crossing ground link and a coupler link.

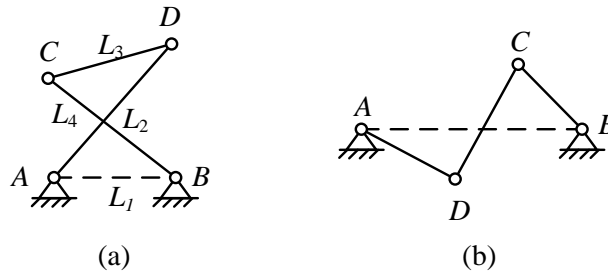


Figure 3.14. Two types of CFB mechanism: (a) Type 1 CFB mechanism with crossing drive and follower links; (b) Type 2 CFB mechanism with crossing ground and coupler links.

The planar four-bar mechanism is efficient at transferring motion and power. Four-bar linkages play significant role in machine design. Figure 3.15 shows one application of the CFB mechanism as a scale conversion, which is also called a function generator. The mechanism converts a linear scale into a logarithmic scale. Its error is less than 0.0037° for a 60° range of rotation of both crank and follower.

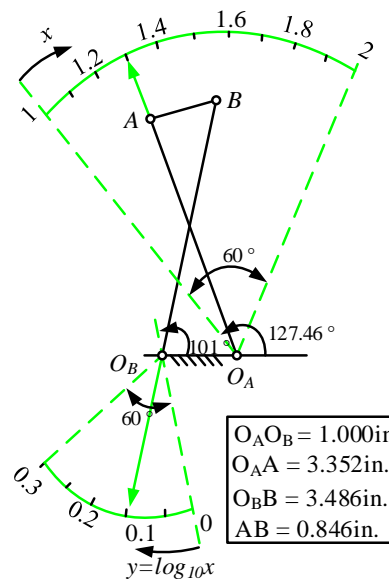


Figure 3.15. Cross four-bar mechanism and applications: a generator of the logarithmic function $y=\log x$ and the arcs of oscillation;

Two specific examples of these CFB mechanisms are antiparallelogram mechanism and Watt straight-line mechanisms (Figure 3.16). The curves of fixed and moving centrodes of the coupler link of antiparallelogram mechanism are two ellipses as shown in Figure 3.16(a). Figure 3.16(b) presents a coupler curve of the Watt straight-line mechanism which contains an approximate straight line segment.

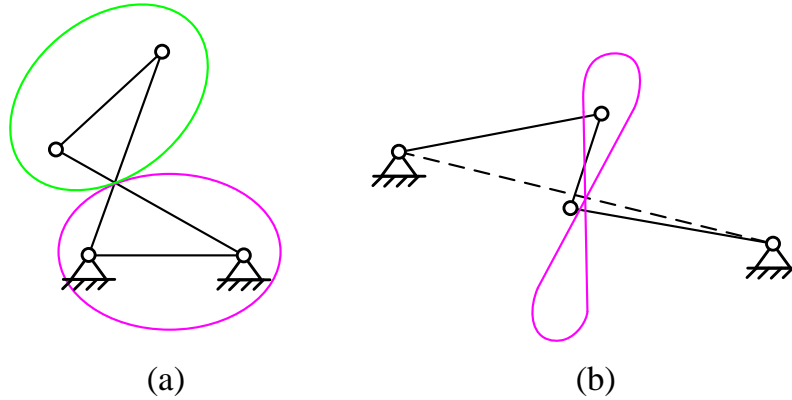


Figure 3.16. Specifications of an antiparallelogram mechanism and a Watt straight-line mechanism.

Possible variations in link lengths and working ranges play important roles in biomimicking, animal mechanics and mechanical functioning; they also provide a method to simplify the study of complex biological systems. A CFB mechanism with crossing drive and follower links was used to mimic a knee joint and has a potential application in mimicking finger joints. Therefore, a systematic classification of the variety of lengths of a CFB mechanisms is beneficial for further applications. For a biological replacement the full rotation of the drive link is not necessary; only a segment of the coupler curve or centrodes' trajectory is needed. The length of each link in the mechanism is a key factor in determining its type. According to this basic analysis, the relationship of the four links are shown in Table 3.1 where $L_1 = AB$, $L_2 = BC$, $L_3 = CD$, $L_4 = AD$ (Figure 3.14(a)). The dimensional relation is separated into two columns, the first one lists a general relationship of two links (L_1 and L_2) and the other column lists the subdivided relations of all potential dimensional relationship of the CFB mechanism. The existence column lists whether there exists a configuration or not. The feature column lists the area graph of the connecting joint of the added dyad. The dimensions of a given dyad are represented by L_1 and L_2 . The different equivalence of the links can be separated into two types, $L_1 = L_2$ and $L_1 \neq L_2$. The types of CFB

mechanisms and the position zones with different dimensional relationships are shown in Figures 3.17 and 3.18.

Table 3.1. Dimensional relation of each link and their position zones.

Dimensional Relation (= or \neq)			Existence (Yes/No)	Position Zone	
$L_1 = L_2$	$L_1 = L_2, L_3 = L_4$	$L_1 = L_2 = L_3 = L_4$	No	None	
		$(L_1 = L_2) \neq (L_3 = L_4)$	No	None	
	$L_1 = L_2, L_3 \neq L_4$	$L_1 = L_2 = L_3 \neq L_4$	Yes	2-segment curve	Two areas
		$L_1 = L_2 = L_4 \neq L_3$	Yes	2-segment curve	
		$(L_1 = L_2) \neq (L_3 \neq L_4)$	Yes	Areas exception of the above lines	
$L_1 \neq L_2$	$L_1 = L_3, L_2 = L_4$	$(L_1 = L_3) \neq (L_2 = L_4)$	Yes	1 point (antiparallelogram)	
	$L_1 = L_3, L_2 \neq L_4$	$L_1 = L_3 = L_4 \neq L_2$	Yes	1 point	2-segment curve
		$(L_1 = L_3) \neq (L_2 \neq L_4)$	Yes	3-segment curve	
	$L_1 = L_4, L_2 = L_3$	$(L_1 = L_4) \neq (L_2 = L_3)$	No	None	
	$L_1 = L_4, L_2 \neq L_3$	$L_1 = L_4 = L_3 \neq L_2$	Yes	1 point	2-segment curve
		$(L_1 = L_4) \neq (L_3 \neq L_2)$	Yes	3-segment curve	
	$L_2 = L_3, L_1 \neq L_4$	$L_2 = L_3 = L_4 \neq L_1$	Yes	1 point	1-segment curve
		$(L_2 = L_3) \neq (L_1 \neq L_4)$	Yes	3-segment curve	
	$L_2 = L_4, L_1 \neq L_3$	$(L_2 = L_4) \neq (L_1 \neq L_3)$	Yes	3-segment curve	
	$L_3 = L_4, L_1 \neq L_2$	$(L_3 = L_4) \neq (L_1 \neq L_2)$	Yes	3-segment line	
$L_1 \neq L_2 \neq L_3 \neq L_4$			Yes	Areas that exception of the above segments and points	

Figures 3.17 and 3.18 show two types of CFB mechanisms with different lengths of each link. According to the zones, there is only one anti-parallelogram CFB mechanism with given dyad and their opposite links unequal, however a parallelogram mechanism with four identical links can be obtained. It is impossible for a CFB mechanism to have four identical links. The position zones of $L_1 = L_2$ are equal to $(L_1 = L_2, L_3 \neq L_4)$, because there is no CFB mechanism with $L_1 = L_2, L_3 = L_4$. The geometrical synthesis processes of the position zones of a CFB mechanism is the same as the above mentioned synthesis process for RRRR mechanisms.

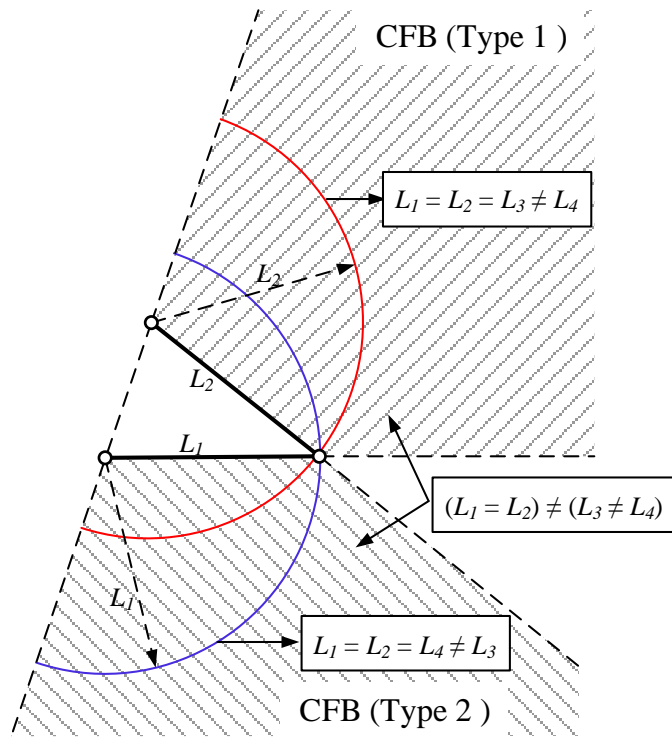


Figure 3.17. Position zones of CFB mechanism with $L_1 = L_2$.

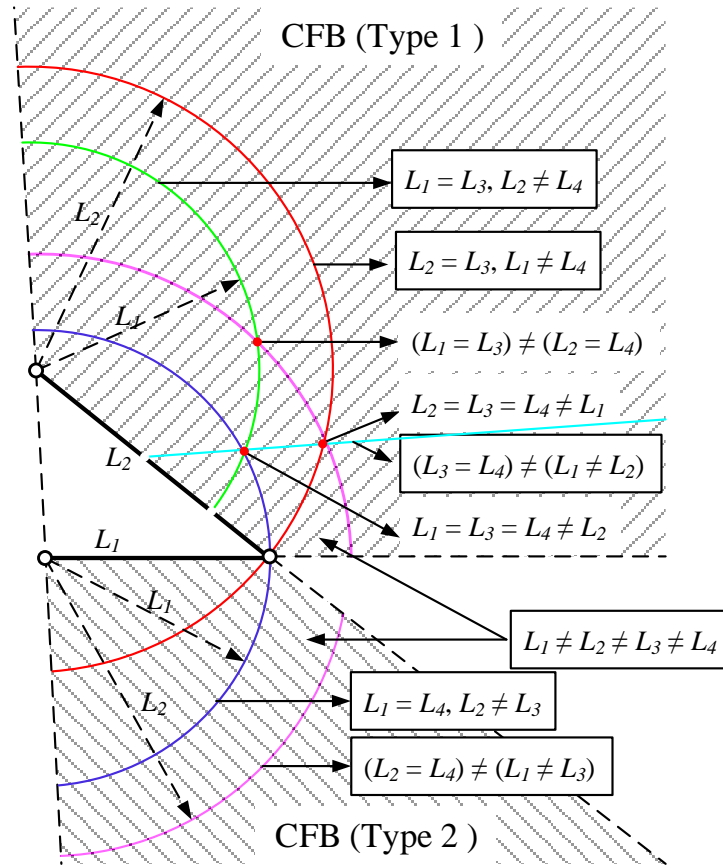


Figure 3.18. Position zones of CFB mechanism with $L_1 \neq L_2$.

3.4 Kinetic Equilibrium of a CFB Mechanism

In Chapter 2, the concept of the centrode has been presented as a path traced by an instantaneous centre. The fixed centrode is a path traced by the instantaneous centre of the coupler link. Therefore, a given position of a CFB mechanism will always have a force equilibrium configuration if a force is applied to the coupler link. If the acting line of the force direction passes through the instantaneous centre, the mechanism is in equilibrium. However if a distance e exists between the instantaneous centre and the line of force direction, the CFB mechanism will move until the centre and force are coincident. The two conditions are shown in Figure 3.19.

Two theorems of equilibrium of a CFB mechanism can be stated:

Theorem 1:

A requirement of static equilibrium is that the line of force direction is coincident with the instantaneous centre.

Theorem 2:

If the angle between the line of force direction and coupler link is fixed, the mechanism will move until the line of force direction coincident with the instantaneous centre.

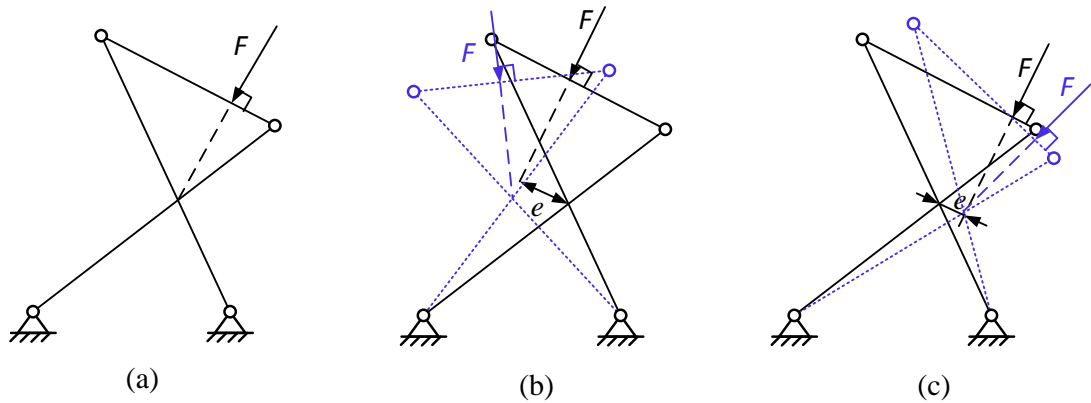


Figure 3.19. Two conditions of equilibrium of a CFB mechanism (F is perpendicular to the contacted link): (a) static equilibrium; (b) and (c) dynamic equilibrium at two sides.

3.5 CFB Mechanism for Multi-Mode Gripping

Gripping with the human hand is activated because the neural and visual systems work as sensors with the brain operating as a control and processing system. Progress in research and development for grippers has been made in underactuated grasping; for example, Birglen and Gosselin have used a five-bar linkage and a four-bar linkage connected in series for three-phalanx underactuated fingers [133]. Ceccarelli has

designed three-phalanx underactuated fingers with cross four-bar (CFB) linkages in series [134]. To create stable, encompassing grasps with subsets of fingers, soft fingertips that deform during contact and apply a larger spread of frictional forces and moments than their rigid counterparts have been studied [135]. The CFB linkage is found to be an excellent candidate to achieve passive-adjusting motion and has similar characteristics to a soft fingertip. A passive-adjusting mechanism system has characteristics such as adaptivity, under-actuativity, efficiency and multifunction whereby it can adjust itself automatically depending on the locations and shapes of objects.

A CFB linkage is shown in Figure 3.20(a). Crank link AD rotates from initial angle γ with respect to vertical line to angle γ' and the coupler link CD reaches position $C'D'$. In turn, the mechanism can adjust passively when one point of link CD contacts an object. If the positions of two points of the coupler link CD are determined, the configuration of the whole mechanism will be fixed. Reorientation of the CFB mechanism shows that the triangle BAD decreases while the other opposite triangles ABC and ADC increase. The diagonal AC increases while the other diagonals BD , decreases.

A soft-fingertip model comprising a CFB-damper-spring component is shown in Fig. 3.20(b). Friction is represented as f at the fingers' contact surfaces. The normal force applied on each fingertip is F_n . The masses of object and the CFB linkage are G_m and G_l respectively. K_s and R_d represent the stiffness of the spring and the damper ratio respectively. Analysis of contact positions should be conducted when applying it as a fingertip for gripping. Furthermore if the motion of one endpoint of link CD contacts with its symmetrical opposite then these two CFB mechanisms will be angular fingertips.

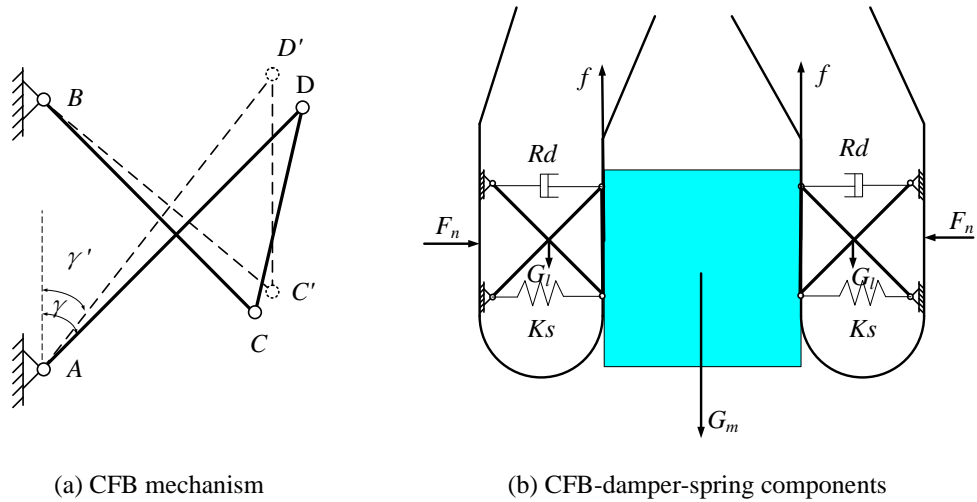


Figure 3.20. CFB mechanism as passive-adjusting fingertip

3.6 Equilibrium Analysis of a CFB Mechanism for Gripping

Section 3.4 has presented the dynamic equilibrium feature of the CFB mechanism and Section 3.5 discusses the potential application of a CFB to replace a human fingertip for passive-adjusting gripping. A detailed discussion of the CFB mechanism gripping application is presented in this section.

3.6.1 Simplified CFB Mechanism with Point Contact

According to the dynamic equilibrium analysis in Section 3.4, there are two potential directions of rotation for each CFB mechanism. One direction is for gripping and the other for position limitation. Other characteristics for gripping are that at least one point of the object contacts with the coupler link and the contact force is always perpendicular to the contact surface.

This gripping scenario is shown in Figure 3.21, where Figure 3.21(a) includes an initial position and half of the gripper. Suppose AB is a ground link of the CFB linkage with an angle α respective to the symmetrical line. The detailed length of each link and angle between nearby links are as shown. The spring and damper as integrated components of the system are ignored since space is limited. A simple method using magnet material will be proposed in development of meso-gripper in Chapter 5. In order to limit movement to one direction, a contact surface is imposed to the limited distance between B and D is shortest as shown, while the other side distance between A and C is free to change. In other words, there is only anticlockwise motion of the link CD starting from the initial position. A planar coordinate system xy has been created at point A with ground link AB placed on axis x . Rotate the xy system to make the axis x level. The four link lengths a, b, c, d and angles α, β, δ are now as shown in Figure 3.21(b). I is an intersection point of AD and BC ; this is known as the instantaneous centre of coupler link CD . Auxiliary line HI is always perpendicular to the coupler link CD . For the directions of the position vectors in Figure 3.21(b), $\theta_2, \theta_3, \theta_4$ are the angles of links AD, DC and BC respectively in relation to the x -axis, the objective being to determine the position of point H (or e). Suppose the coordinate of point H is (x, y) .

The coordinates of point I can be determined $I(x, y) = (\frac{a \tan \theta_4}{\tan \theta_4 - \tan \theta_2}, \frac{a \tan \theta_4 \tan \theta_2}{\tan \theta_4 - \tan \theta_2})$

The angle θ_3 can be represented according to geometrical analysis as

$$\theta_3 = \pi - \delta + \alpha \quad (3.1)$$

The vector loop equation of the CFB mechanism is as follows:

$$\overrightarrow{AD} + \overrightarrow{DH} - \overrightarrow{AB} - \overrightarrow{BC} - \overrightarrow{CH} = \vec{0} \quad (3.2)$$

Equation (3.2) can be separated into its real and imaginary components and set to zero.

$$a \cos \theta_2 - e \cos \theta_3 - d - c \cos \theta_4 - (b - e) \cos \theta_3 = 0 \quad (3.3)$$

$$a \sin \theta_2 + e \sin \theta_3 - c \sin \theta_4 - (b - e) \sin \theta_3 = 0 \quad (3.4)$$

The equation representing HI perpendicular to DH is as follows (“•” indicates dot product of two vectors):

$$\overrightarrow{HI} \bullet \overrightarrow{DH} = 0 \quad (3.5)$$

Substituting Equation (3.5) into Equation (3.6).

$$\left(\frac{a \tan \theta_4}{\tan \theta_4 - \tan \theta_2} - x \right) (x - a \cos \theta_2) + \left(\frac{a \tan \theta_4 \tan \theta_2}{\tan \theta_4 - \tan \theta_2} - y \right) (y - a \sin \theta_2) = 0 \quad (3.6)$$

The length of DH is:

$$|\overrightarrow{DH}| = e \quad (3.7)$$

Therefore,

$$(x - a \cos \theta_2)^2 + (y - a \sin \theta_2)^2 = e^2 \quad (3.8)$$

Substituting Equations (3.1), (3.3), (3.4), (3.6) and (3.8). There are six unknowns in five equations. Therefore e can be determined.

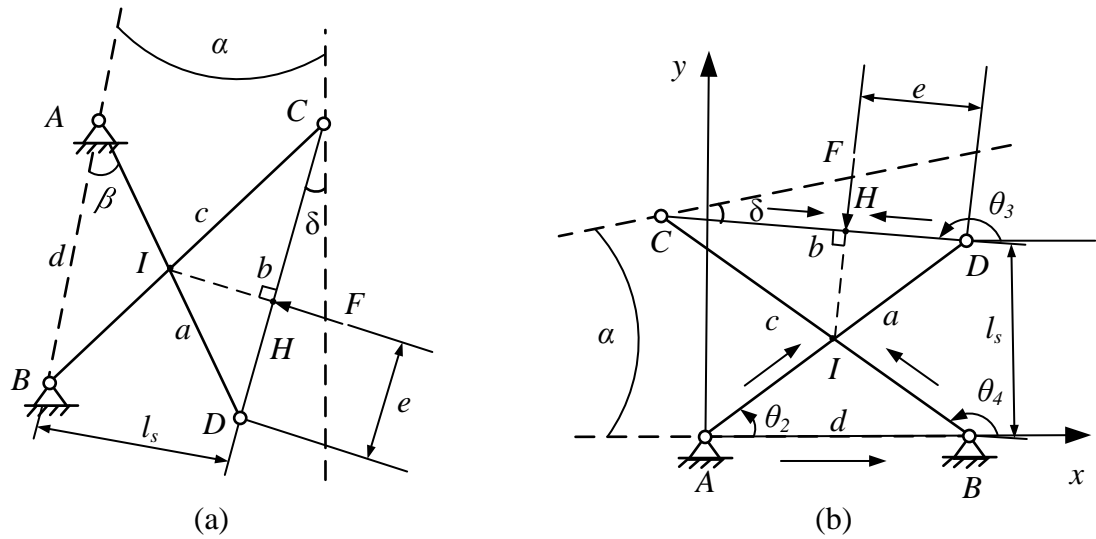


Figure 3.21. Initial position of CFB mechanism within coordinate system

By applying the same approach, another position with coupler link CD vertical is shown in Figure 3.22(a). The position of H_1 (or e_1) can be determined by the following equations.

$$\theta_3 = \pi + \alpha \quad (3.9)$$

$$\overrightarrow{AD} + \overrightarrow{DH} - \overrightarrow{AB} - \overrightarrow{BC} - \overrightarrow{CH} = \vec{0} \quad (3.10)$$

(3.11)

(3.12)



(b)

3.6.2 General CFB Mechanism with Point Contact

In real design cases, we need to leave some margin for link CD as contact surface. Therefore, as shown in Figure 3.23, a quadratic link $BCQP$ can be constructed by extending link BC to CP with length c_l and AD to DQ with length a_l and connecting the two end points P and Q as a contact surface.

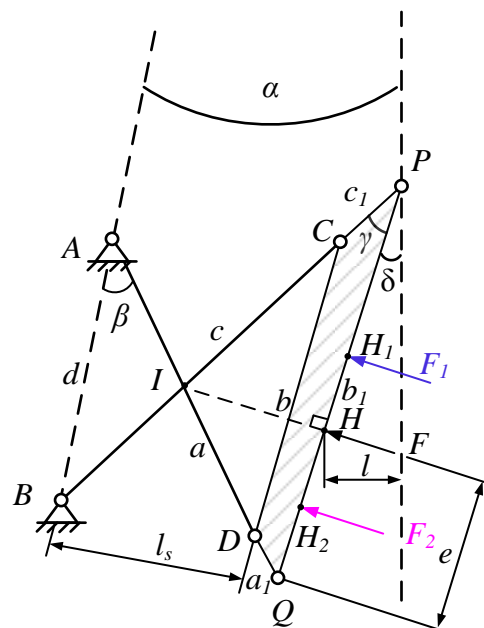


Figure 3.23. Force positions applied for CFB mechanism.

Force F is applied at point H and directs towards the instantaneous centre I when the CFB mechanism is in static equilibrium. If F_1 shown above F is applied at position H_1 , the mechanism will make an anticlockwise rotation, while F_2 makes the mechanism static because of the limitation between points B and D .

As shown in Figure 3.23, distance between B and D is l_s , which can only be extended. The length of l_s can be calculated using:

$$l_s = \sqrt{a^2 + b^2 - 4ad \cos \beta} \quad (3.13)$$

According the geometrical parameters, $\angle ABC$ can be derived as

$$\angle ABC = \gamma + \delta - \alpha \quad (3.14)$$

The length of AI is calculated:

$$AI = \frac{d \sin(\gamma + \delta - \alpha)}{\sin(\beta + \gamma + \delta - \alpha)} \quad (3.15)$$

Meanwhile,

$$IQ = AQ - AI = a + a_1 - AI \quad (3.16)$$

$$\angle IQP = \beta + \delta - \alpha \quad (3.17)$$

$$e = IQ \cos \angle IQP \quad (3.18)$$

Therefore, the distance e can be derived by solving Equations (3.15) to (3.18):

$$e = \left(a + a_1 - \frac{d \sin(\gamma + \delta - \alpha)}{\sin(\beta + \gamma + \delta - \alpha)} \right) \cos(\beta + \delta - \alpha) \quad (3.19)$$

The distance between the contact point H of force F and the vertical line passing through P is:

$$l = (b_1 - e) \cos \delta \quad (3.20)$$

According to Equations (3.19), distance e is influenced by distances a , a_1 and d ; the method for augmenting the angular mode is to increase the lengths a , a_1 or to decrease the ground link length d . The way to enlarge ranges of the two gripping modes is to increase b_1 or decrease e .

3.6.3 General CFB Mechanism with Surface Contact

For the gripping application shown in Figure 3.24, any one condition is regained when the contact surface PQ is in vertical direction which is typical of grasping for vertical surface objects, such as a cube. There is always one gripping point on PQ , above point H such as H_1 which achieves vertical gripping at static equilibrium. If the contact point above H_1 is contacting point for cube gripping, then gripping becomes even more stable than the static equilibrium condition, because there is a contact segment on PQ (or at least at two contacting points).

Assuming that AB moves towards being level and force F_I is applied to point H_I , the CFB mechanism is in static equilibrium exactly when PQ is vertical, that is to say H_I is the exact point at which it is at its final configuration. The static equilibrium position of the mechanism is shown in Figure 3.24.

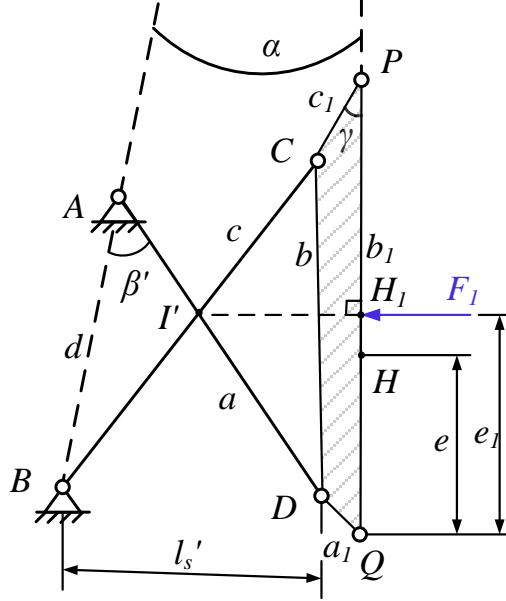


Figure 3.24. Gripping configuration with PQ in vertical position.

In this configuration, β' and l_s' are used to denote the altered position respectively. The instantaneous centre is I' . ADQ and BCP are not on a straight line in this configuration.

3.6.4 Summary of Multi-Mode Gripping with CFB Fingertip

According to the above analysis, for single contact point gripping with a CFB-based fingertip, there are two gripping modes separated into three segments, as shown in Figure 3.25, passive-adjusting (passive-stable and passive-equilibrium) mode and angular mode. The whole contacting surface can be separated into three segments. A gripping position lower than point H is angular mode while the upper positions are in passive-adjusting mode that the gripper passively adjusts its configuration depending on contact position of an object.

The configuration of the CFB mechanism is static at angular-gripping mode. Friction between PQ and contacted objects is applied to lift the latter. The coupler link PQ of the CFB mechanism rotates passively to the static equilibrium position if the gripping position is between H and H_I . The coupler link PQ of the CFB mechanism passively rotates to contact the surface of the object with at least two points if the contact point is above point H_I . Even though the configuration of the CFB is at a nonequilibrium position, lifting is more stable due to two points gripping on the coupler link maintains

the configuration of the CFB mechanism fixed. The outline of these two modes and three position zones are shown in Figure 3.25.

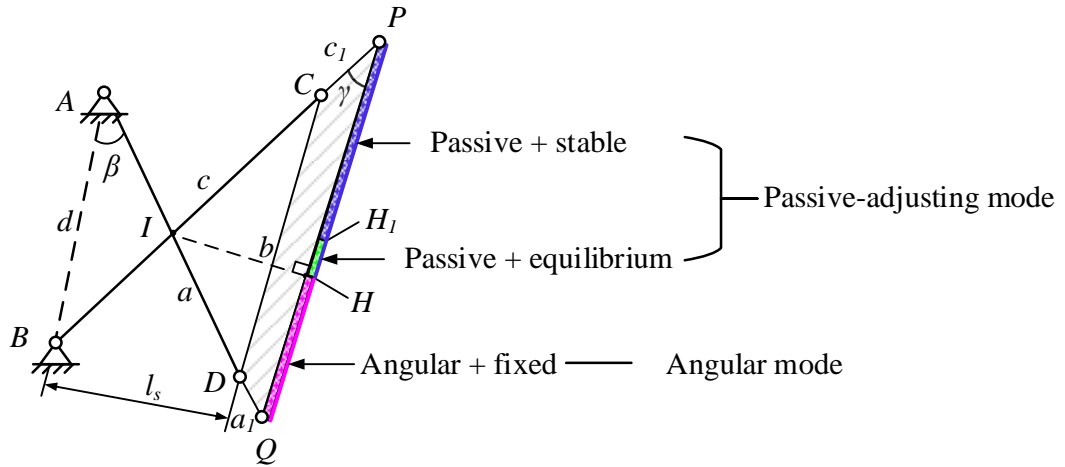


Figure 3.25. Two gripping modes and three position zones.

3.7 Gripping Capabilities of a CFB Mechanism

3.7.1 CFB Mechanism for Passive-Adjusting Gripping

Figures 3.26 to 3.28 illustrate the gripping process of different objects in passive-adjusting modes with a CFB-based gripper. Each claw of the gripper is integrated using a CFB linkage which works as a fingertip for passively adjusting the pad to the contact point of the object. There are two types of gripping configurations (passive-stable and passive-equilibrium) depending on the contact positions at the fingertip.

Figure 3.26 shows passive-stable gripping for vertical surface with more than two points on the contact surface where the gripping point is above H_l . The configuration of the coupler link is fixed safely on the vertical surface of the object.

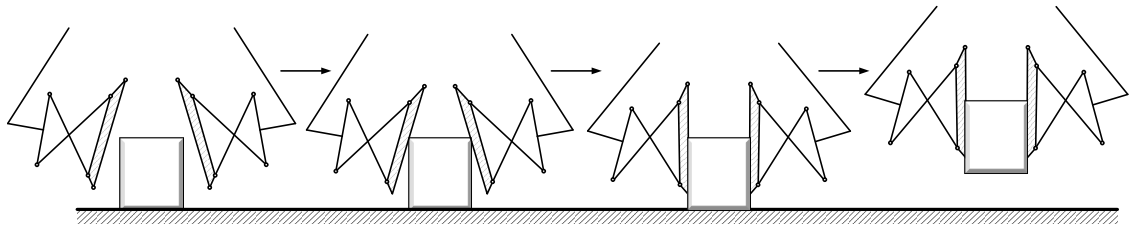


Figure 3.26. Passive-stable gripping for vertical friction of CFB-based fingertip.

Another passive-stable type is when the reaction force is at the contact point opposite to gravity. The configuration of CFB mechanism as a lifting posture in vertical gripping scheme is half mechanical locking and more stable than gripping only with friction. One example of this type is shown in Figure 3.27.

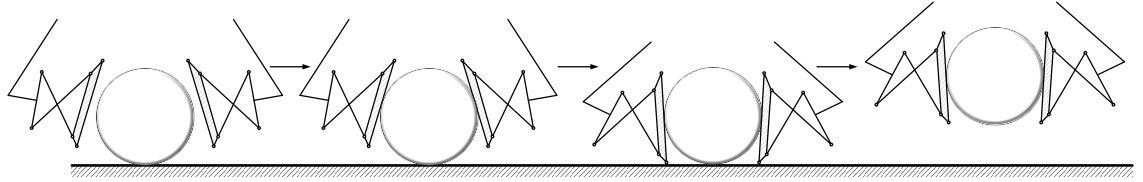


Figure 3.27. Passive-stable gripping for lifting posture of CFB-based fingertip.

Passive-equilibrium gripping is shown in Figure 3.28. The gripping points are located between H and H_l , which is a quite small range. Therefore it is quite difficult to distinguish this figure with Figure 3.26 in first two steps. However, when the contact position locates at this range, the CFB mechanism will move slightly and automatically to search the equilibrium position fixing the configuration in an angular configuration. The lifting force depends only on the friction between the coupler link and the contact point of the object.

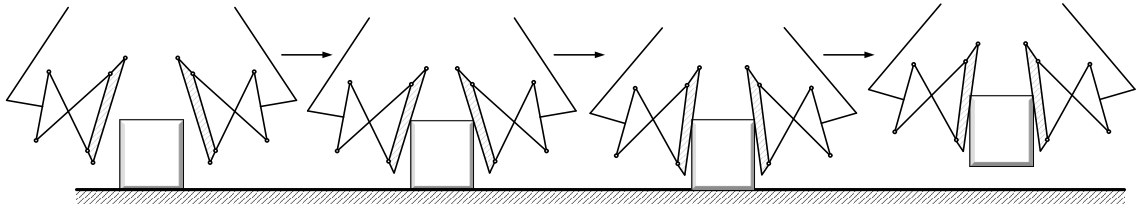


Figure 3.28. Passive-equilibrium gripping of CFB-based fingertip.

3.7.2 CFB Mechanism for Angular Gripping

Compared with passive-adjusting mode, two types of angular gripping mode depend more on the size of the objects. The mechanical intelligence makes the gripper adapt its configuration to the various objects. The following figures illustrate the gripping process for different objects.

Figure 3.29 shows a small object with dimension less than the maximum size in the angular configuration of the gripper. The coupler link of each side moves when it contacts the object. The object is lifted when the friction is big enough to support its weight.

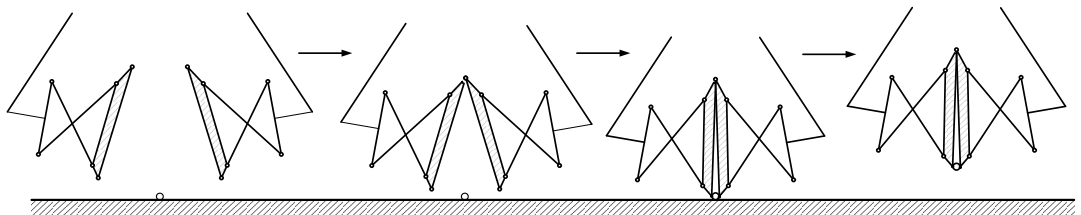


Figure 3.29. Contact-angular gripping of CFB-based fingertip (for small objects).

Another type of angular mode is as a gripping point below H , that is to say, the size is larger than the open size of the gripper in a contact-angular configuration, as shown in Figure 3.30. This gripping process is similar to small object types. The main difference is that two coupler links do not contact with each other, the angle between two contacting surface will not change.

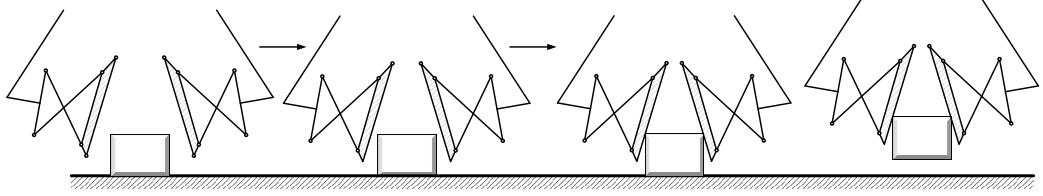


Figure 3.30. Contactless-angular gripping of CFB-based fingertip (for large objects).

3.8 Gripping Zone of CFB-Based Gripper

According to the configurations of the gripper analysed in Section 3.6, there are three zones on the contacting surface with different gripping configurations. The basic geometrical parameters and signs of the schematic are shown in Figure 3.31. There are two basic modes (passive-adjusting and angular) which can be further classified into four sub-modes (passive-stable, passive-equilibrium, contact-angular and contactless-angular). Gripping modes and the range of dimensions of gripped objects are summarized in Table 3.2.

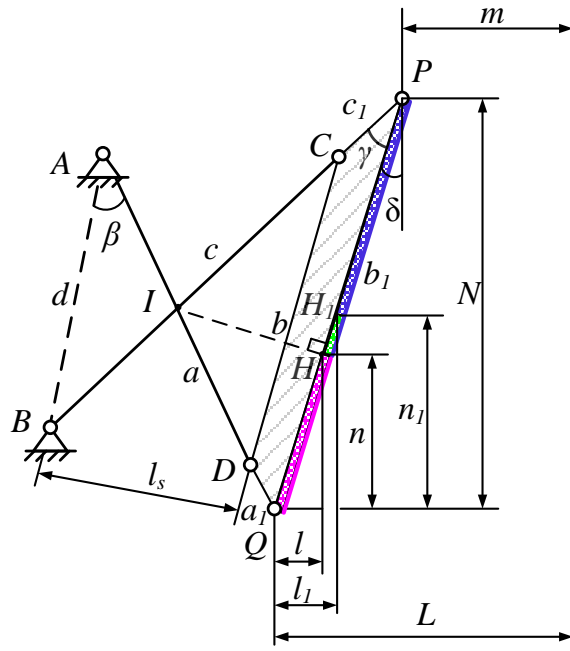


Figure 3.31. Schematic of gripper with multiple gripping positions.

By analysing the gripping ranges of various modes in Table 3.2, both the design criteria and functionality of the designed gripper are obtained. The height of the object is also an important parameter to consider. The higher the object, the easier and safer it is to be gripped with passive-stable mode. For short object, angular mode is used. The gripping only considers the fingertip is stiff without deformation. The advantages of the novel multi-mode gripper can be attributed to passive-adjusting, a type of mechanical intelligence. Before gripping, the size, weight and shape of the objects do not need to be considered. The gripper can passively adapt to them automatically. Auxiliary systems, such as a vision system, can be used to identify the gripping mode after equilibrium gripping and for determining the gripping force applied to objects.

Table 3.2. Gripping ranges of the four gripping modes

Category		Contacting position	Width	Height
Passive-adjusting mode	Passive-stable	H_1P	$>2(L-m-l_1)$	$n_1 - N$
			>0	$\geq N$
	Passive-equilibrium	HH_1	$2(L-m-l) - 2(L-m-l_1)$	$n - n_1$
			$>2(L-m-l_1)$	$>n_1$
Angular mode	Contactless-angular	HQ	$> 2(L-m-l)$	$0 - n$
			$2(L-m-l_1) - 2(L-m-l)$	$n - n_1$
	Contact-angular	HQ	$0-2(L-m-l)$	$>n$
			$0-2(L-m-l)$	$0 - n$

3.9 Kinetostatic Analysis of CFB-Based Fingertip

Kinetostatic analysis of the CFB fingertip involves the instantaneous kinematics and static condition of the CFB-based fingertip to react to the force produced by a finger (finger force in short). It refers to the relationship between the finger force and corresponding the reaction forces. The schematics at the static equilibrium condition of the fingertip are first determined. The objective of the analysis is to discover the relationship between the finger force and reaction force.

Based on the gripping processes and gripping ranges of various modes of the CFB-based fingertip, three configurations of CFB-based gripping are addressed to analyse the relationship between finger force and the reaction force at the contact surface, as shown in Figure 3.32. The vertical line passing through point P as a boundary separates all the

links on the left side, the second one with PQ coincident with the boundary, the last with PQ on the right hand. This classification concludes all four modes presented in Section 3.6. The Type I configuration shown in Figure 3.32(a) includes two angular modes and passive-equilibrium mode. The Type II configuration refers to passive-stable mode with vertical friction, see Figure 3.32(b). Type III, shown in Figure 3.32(c), is passive-stable mode with the half mechanical-locking characteristic. All configurations match with different force reaction situations.

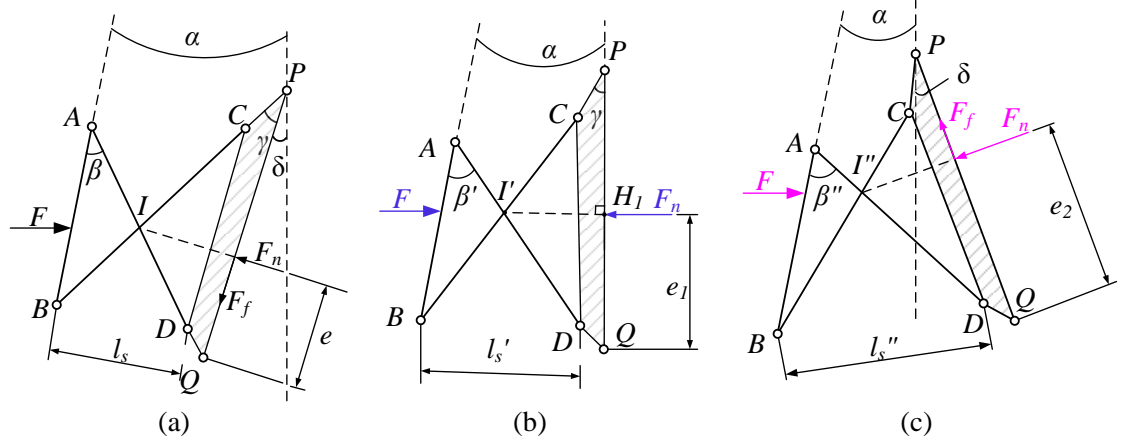


Figure 3.32. Type I, II and III configurations of CFB-based fingertip.

In total, there are three location areas of reaction forces on the contact surface between Q and H_I (shown in Figure 2.30) in the first configuration of the CFB-based fingertip. Positions between Q and H (including H) are in the same situation since the configuration is rigid with distance of BQ fixed. Positions at the passive-equilibrium range are different because of the free motion. However, the reaction forces involved in all the gripping processes are the same. There are the normal force F_n and friction force F_f , both of which are related to the angle δ of PQ with respect to vertical line.

The second configuration is a type of gripping with PQ against the vertical surface. Its force equilibrium equation is very simple, the magnitudes of normal force F_n and finger force F are equal.

The third configuration is the half mechanical-locking posture, normal force (F_n) and friction (F_f) force influencing each other according to a force analysis. Force diagrams of these three configurations are shown in Figure 3.33.

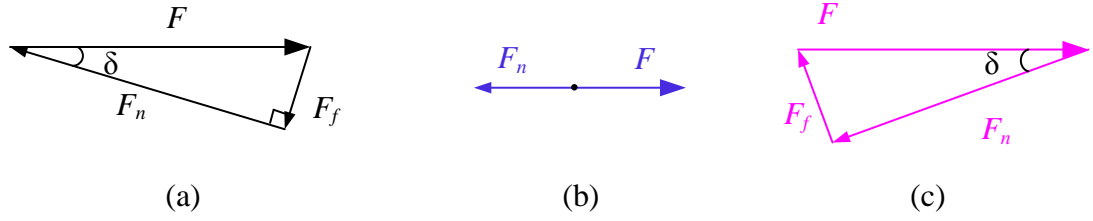


Figure 3.33. Force diagrams of three types of gripping configurations.

3.10 Gripping Force Analysis of CFB-Based Fingertip

A gripper should produce necessary forces to overcome the weights of objects and keep them against the fingertip during the gripping process. Safe gripping is a basic requirement. In other words, a gripper should not produce an excessive force which may damage the object especially if fragile. The gripping force is related to the shape of the fingertip and the posture of a gripper. The gripping environment is complicated, which also makes the force applied to grab an object complicated as this may depend on the solo finger forces, finger and friction forces on the fingertip or only the friction forces.

Due to its multi-mode characteristic, the corresponding force situations of the CFB-based fingertip are more complicated. Considering a two-fingered gripper with CFB-based fingertips, three types gripping are defined, as shown in Figure 3.34.

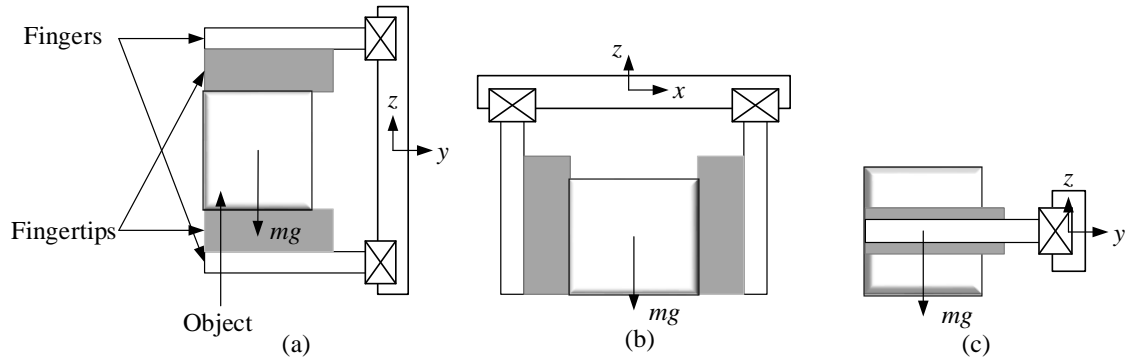


Figure 3.34. Three postures of gripping: (a) a horizontal gripper with horizontal object; (b) vertical gripper with horizontal object; (c) horizontal gripper with vertical object.

In order to calculate the gripping force required during a transportation process. The finger force and weight of the object are considered and their correlation analysed [136]. The necessary finger force can be calculated by the formula:

$$F = K_a K_e K_s mg \quad (3.21)$$

where

$$K_a = 1 + a/g ;$$

K_s = safety factor, varying from 1.2 to 2.0, which should be enhanced if a robot has a strong acceleration/deceleration or the possibility of impact during movement;

K_e = transfer coefficient, which is shown in Table 3.3 (Page 74);

F refers to the finger force per finger to hold an object with weight m at an acceleration a .

$g = 9.8m/s^2$, acceleration due to gravity. Required if acting against a .

Safety factor K_s depends on the application itself, the transporting route, workspace, arrangement of objects and human safety considerations. Factor K_a depends on the maximum acceleration of the gripped object. K_e is the transfer coefficient and relates to the fingertip configurations and the gripping postures; it is the ratio between the finger force F and object gravity force mg .

According to Section 3.7, the CFB-based fingertip has two main modes with three corresponding configurations, which depends on the size, shape and contact point of the object, shown in Figure 3.35. Meanwhile, there are three postures of a gripper in terms of horizontal gripper with a horizontal object, vertical gripper with a horizontal object and horizontal gripper with a vertical object.

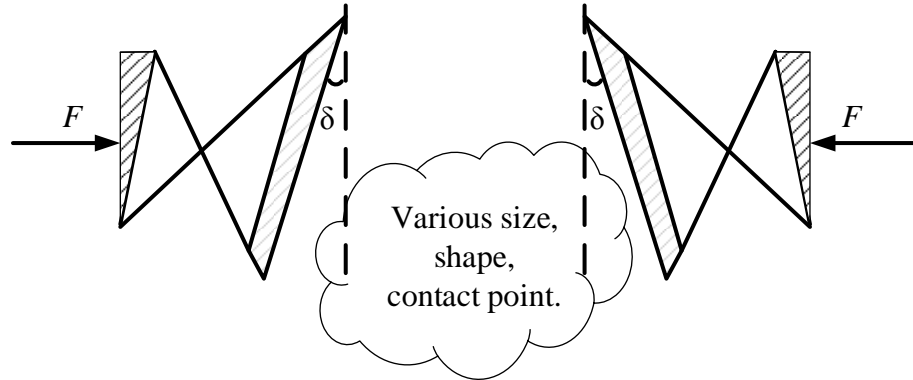


Figure 3.35. Gripping with CFB fingertip.

The following examples will present how factor K_e is derived with various configurations and gripping postures. In order to simplify analysis process, gripped objects are simplified with regular round surface or parallel surface for angular and parallel configurations of fingertip respectively.

Case 1:

Figure 3.36 shows a vertical gripper with a Type I configuration fingertip applying finger force F per finger to hold a horizontal object of weight m to move at an upward acceleration a . δ refers to the angle of the configuration in Types I and III. Friction force F_f is produced by F_n and equal to μF_n , the coefficient of friction between fingertip and object is denoted by μ .

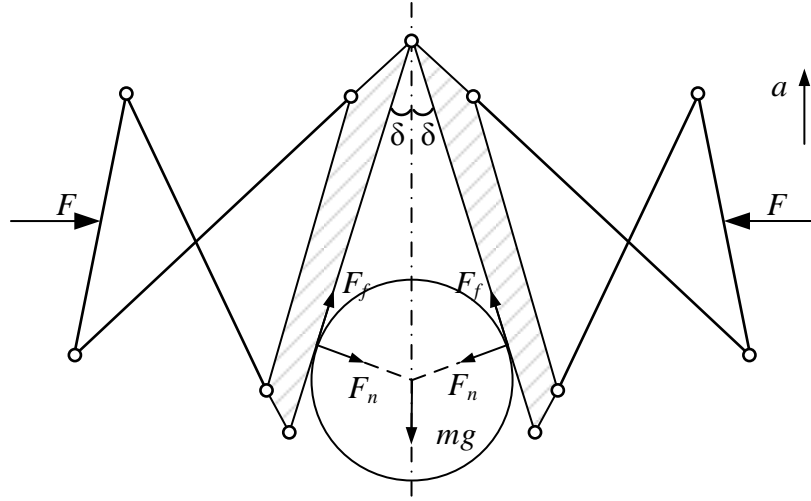


Figure 3.36. Vertical gripper with Type I configuration fingertip holding a horizontal object and decomposing forces on the object.

The force equilibrium equations in the vertical directions are as follows:

Vertical direction:

$$2\mu F_n \cos \delta - 2F_n \sin \delta - mg = ma \quad (3.22)$$

According to Figure 3.33(a),

$$F \cos \delta = F_n \quad (3.23)$$

Substituting Equation (3.23) into (3.22), we have

$$2\mu F \cos^2 \delta - 2F \sin \delta \cos \delta - mg = ma \quad (3.24)$$

$$F = \frac{1}{2(\mu \cos^2 \delta - \sin \delta \cos \delta)} \left(1 + \frac{a}{g}\right) mg \quad (3.25)$$

By considering Equations (3.21) and (3.25):

$$K_e = \frac{1}{2(\mu \cos^2 \delta - \sin \delta \cos \delta)} \quad (3.26)$$

Case 2:

A vertical gripper with Type II configuration fingertip applying finger force F per finger to hold a horizontal object of weight m to move at an upper acceleration a , as shown in Figure 3.37. Decomposing forces on object is also provided.

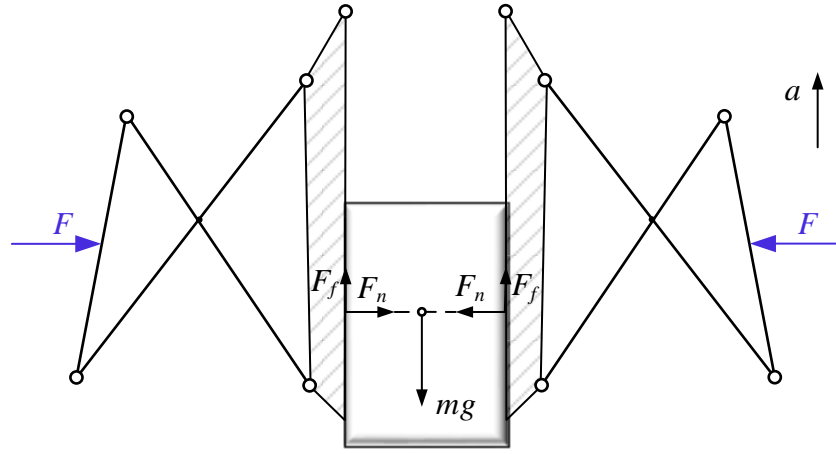


Figure 3.37. Vertical gripper with Type II configuration of fingertip holding a horizontal object and decomposing forces on the object.

K_e for this configuration can be derived as:

$$K_e = \frac{1}{2\mu} \quad (3.27)$$

Case 3:

A vertical gripper with Type III configuration of fingertip applying finger force F per finger to hold a horizontal object of weight m to move at an upper acceleration a . A minimum force needed to hold the object is to make the object to have a trend of moving downward. Therefore friction of the objects is pointing to upward. The decomposing forces of object is shown in Figure 3.38.

$$2F \sin \delta \cos \delta + 2\mu F \cos^2 \delta - mg = ma \quad (3.28)$$

$$K_e = \frac{1}{2(\sin \delta \cos \delta + \mu \cos^2 \delta)} \quad (3.29)$$

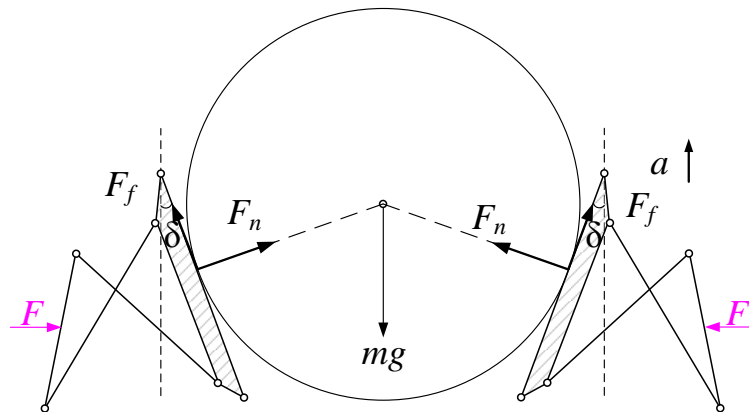


Figure 3.38. Vertical gripper with Type III configuration fingertip holding a horizontal object and decomposing forces on the object.

Case 4:

For a horizontal gripper with horizontal object, the situation is quite different. The magnitudes of finger force exerted by the upper finger and the lower finger are not equal because the difference between them is always the static weight of the object, as shown in Figure 3.39. An extreme static case is when $F_1=0$ and $F_2=mg$. Therefore, for an acceleration a , the force equilibrium equation is:

$$F_n - mg = ma \quad (3.30)$$

According to Figure 3.33(b),

$$F = F_n \quad (3.31)$$

From Equations (3.30) and (3.31), the value of K_e is

$$K_e = 1 \quad (3.32)$$

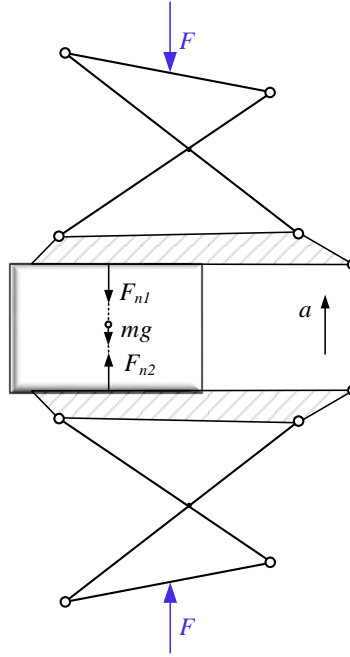


Figure 3.39. Horizontal gripper with Type I configuration fingertip holding a horizontal object and force analysis.

Case 5:

A diagram of a horizontal gripper with a vertical object is shown in Figure 3.40. A CFB-based fingertip is attached to each finger.

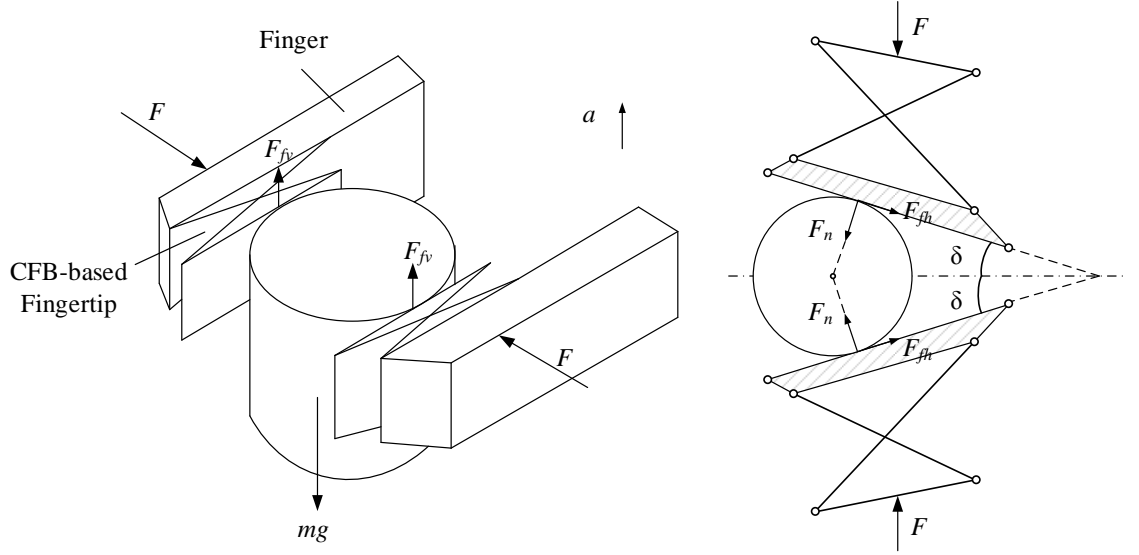


Figure 3.40. Diagram of a horizontal gripper with vertical object and a plan view.

Forces exerted to the object are analysed in the horizontal and vertical planes, as shown in Figure 3.40. Friction forces in the horizontal and vertical planes are denoted by F_{fh} and F_{fv} , respectively. From the horizontal plane, two equations are derived:

$$F_n \sin \delta = F_{fh} \cos \delta \quad (3.33)$$

$$F = F_n \cos \delta + F_{fh} \sin \delta \quad (3.34)$$

From the vertical plane, two equations are obtained:

$$2F_{fv} - mg = ma \quad (3.35)$$

$$F_{fv} = \mu F_n \quad (3.36)$$

By substituting Equations (3.35) and (3.36), one has

$$F = \frac{1}{\mu \cos \delta} \left(1 + \frac{a}{g}\right) mg \quad (3.37)$$

Therefore, transfer efficiency factor in this situation is

$$K_e = \frac{1}{\mu \cos \delta} \quad (3.38)$$

Other cases:

By using the same analysis process, the other two configurations for a vertical gripper can also be calculated. A total of nine situations considering the three configurations of the CFB-based fingertips and their transfer coefficients are summarized in Table 3.3. The same analysis process produces the results of a gripper with three fingers as shown

in Table 3.4. These equations summarized in table only consider regular cylinder, spherical or cubic blocks. It is impossible to consider all regular shapes even irregular shapes. Because the objects are various and this work is also not the focus of the thesis. Examples considered in this chapter are also what commercial gripper vendor always provided. The purpose of providing the detailed calculating process is to compare with present fingertips of commercial gripper tips. CFB fingertip is also a potential commercial product that can be chosen by end user. Relative patent on CFB fingertip has been applied.

Table 3.3. Transfer coefficient of CFB-based fingertip (two fingers).

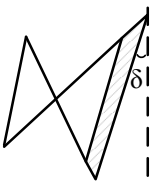
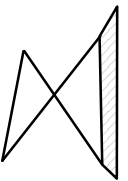
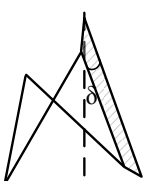
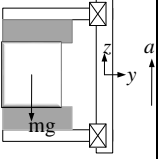
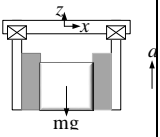
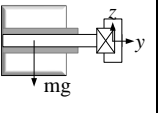

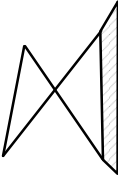
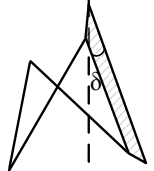
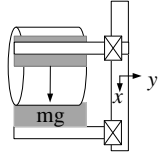
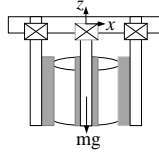
K_e		Type I configuration	Type II configuration	Type III configuration
				
Horizontal gripper with horizontal object		1	1	1
Vertical gripper with horizontal object		$\frac{1}{2(\mu \cos^2 \delta - \sin \delta \cos \delta)}$	$\frac{1}{2\mu}$	$\frac{1}{2(\sin \delta \cos \delta + \mu \cos^2 \delta)}$
Horizontal gripper with vertical object		$\frac{1}{2\mu \cos \delta}$	$\frac{1}{2\mu}$	$\frac{1}{2\mu \cos \delta}$

Table 3.4. Transfer coefficient of CFB-based fingertip (three fingers).

K_e		Type I configuration	Type II configuration	Type III configuration
				
Horizontal gripper with horizontal/vertical object		1	1	1
Vertical gripper with horizontal object		$\frac{1}{3(\mu \cos^2 \delta - \sin \delta \cos \delta)}$	$\frac{1}{3\mu}$	$\frac{1}{3(\sin \delta \cos \delta + \mu \cos^2 \delta)}$

3.11 Summary

A geometrical approach in 2D space was used to investigate the classification of the planar four-bar mechanisms and included CFB mechanisms. The atlas of planar four-bar and CFB mechanisms were provided. A multi-mode fingertip based on a CFB linkage was presented. Firstly, the kinetic equilibrium as a specific characteristics and its potential application for gripping was investigated. A new type of fingertip based on CFB linkage was then developed for multi-mode gripping and the gripping range and force of each configuration analysed. Finally, a methodology of calculating the CFB-based gripping force was provided and tables on transfer coefficient summarized for typical shapes and configurations.

CHAPTER 4 – RCM-Based Multi-Motion Finger

In Chapter 3, a multi-mode CFB-based fingertip was presented. The contact position between the novel tip and the object determines the configuration of the tip and gripping effect. As a novel type of fingertip, the calculation of the gripping force is also required. Therefore, the force calculation equation and transfer coefficient were also provided. In addition to the fingertip, the finger itself is an entry point for the novel development of a robotic gripper hand, since finger grippers are the most commonly used grippers.

Generally, a gripper has two opposing fingers or three fingers can be postured as in a lathe chuck. Sometimes the fingers are driven simultaneously in order to centre a gripped part, while differential gripper benefits gripping of irregular shaped parts [28]. Centred gripping provides some flexibility in the location of components at the pick-up point. Traditional two-fingered grippers can be split into parallel motion and angular motion. The underactuated finger is one type of mechanically adaptive design that is widely used in the development of gripper or robotic hands [137]. Some of these underactuated designs are based on linkages while others are tendon-driven systems [138, 139]. It is recognized that tendon systems are limited to small grasping forces and not suitable for manipulations.

Grasping tasks for flexible or fragile objects are however handled using either vacuum or magnetic grippers. The gripper tip is placed in contact with the object either in a magnetic or a vacuum field. Any pick-up point errors in placement of the object will result in a similar error at the destination; therefore, these types are not appropriate for high accuracy applications. In this chapter, a remote-centre-of-motion (RCM)-based finger solution is provided and analysed. Angular, parallel and underactuated motion of the RCM-based gripper is presented. The static force of the finger for various applications is investigated. The development of RCM-based finger provides a novel design which has unique reconfigurable characteristics with parallelogram linkages.

4.1 Kinematic Analysis of Double-Parallelogram RCM Mechanism

The RCM mechanism is a form of minor-mobility mechanism with constructing linkages rotating around a fixed point distal from it. It is a kind of parallelogram-based mechanism which can be applied in several different backgrounds. Due to its mechanical safety for surgery, RCM mechanisms are widely used as a wrist of minimally invasive surgery (MIS) robots [140] to provide a fixed point moving around the surgical incision.

A telerobotic system manipulator with a remote centre of motion was first developed by Taylor [140], with a variety of RCM robots subsequently developed in the area of surgery equipment (Figure 4.1). The concept and mechanism were also used in MIS for precision operations as a steady hand [141, 142]. Bai extended the mechanism to multiple RCMs for complicated applications by investigating the relationship between the RCM mechanism and a deployable mechanism. A multiple RCM mechanism [143] was proposed and some applications demonstrated, such as foldable stages and a surgical helmet for ophthalmology [144].

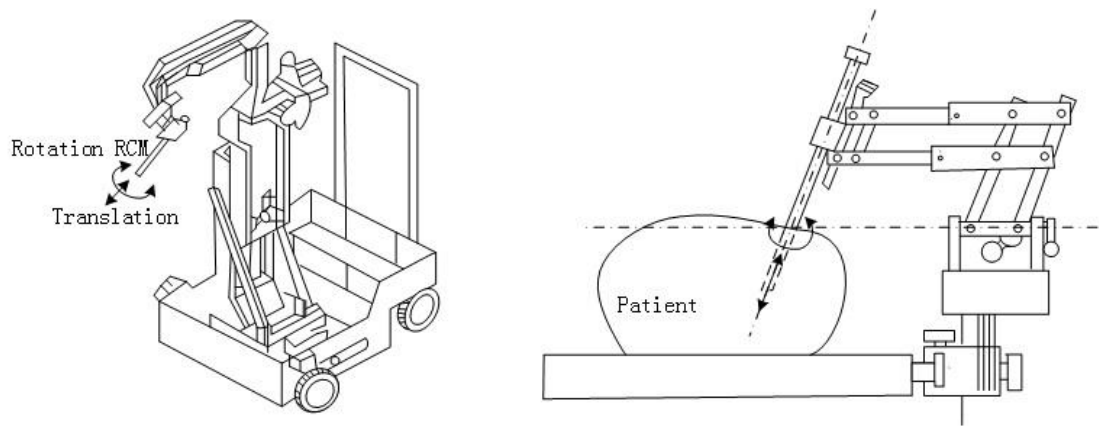


Figure 4.1. RCM Robot for laparoscopic surgery developed by Taylor [140].

For the purpose of analysing the kinematics and structural characteristics of a multi-RCM mechanism, it is necessary to analyse a special configuration of six-bar linkage as shown in Figure 4.2.

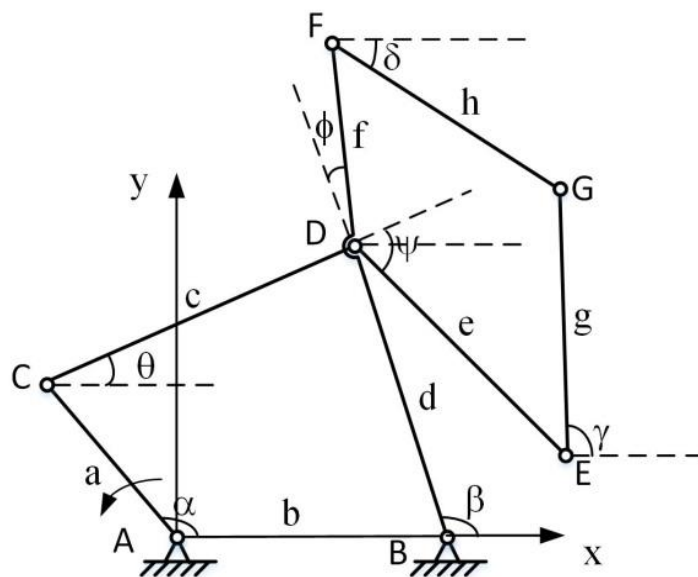


Figure 4.2. Schematic of a six-bar linkage

In Figure 4.2, the coordinate system xAy is fixed to the six-bar linkage. The x -axis is fixed at side link AB . A is at the origin and y -axis is perpendicular to x . The dimensions of six links and rotation angles are represented as shown in Figure 4.2 where AC is the input link, and EG is the output link.

Two crossed links (CDE and BDF) are angulated links with bend angles ψ and ϕ . The other four angles β , θ , δ and γ are the rotation angles of each link, while angle α is the input angle.

This six bar linkage has two four-bar loops (loop $ABDC$ and loop $DEGF$). The displacement equations of the linkage are as follows:

Loop $ABDC$:

$$\overrightarrow{AC} + \overrightarrow{CD} = \overrightarrow{AB} + \overrightarrow{BD} \quad (4.1)$$

$$ae^{j\alpha} + ce^{j\theta} = b + de^{j\beta} \quad (4.2)$$

$$\begin{cases} a \cos \alpha + c \cos \theta = b + d \cos \beta \\ a \sin \alpha + c \sin \theta = d \sin \beta \end{cases} \quad (4.3)$$

Loop $DEGF$:

$$\overrightarrow{DF} + \overrightarrow{FG} = \overrightarrow{DE} + \overrightarrow{EG} \quad (4.4)$$

$$fe^{j(\beta-\phi)} + he^{j(-\delta)} = ee^{j(\theta-\psi)} + ge^{j\gamma} \quad (4.5)$$

$$\begin{cases} f \cos(\beta - \phi) + h \cos(-\delta) = e \cos(\theta - \psi) + g \cos \gamma \\ f \sin(\beta - \phi) + h \sin(-\delta) = e \sin(\theta - \psi) + g \sin \gamma \end{cases} \quad (4.6)$$

Equations (4.3) and (4.6) represent a system of 4 equations with 5 unknowns and can also be viewed as 4 equations with 4 unknowns if input angle α is a given variable.

The trajectories of E and G can be calculated by the following equations,

Trajectory of point E :

$$\overrightarrow{AE} = \overrightarrow{AC} + \overrightarrow{CD} + \overrightarrow{DE} = ae^{j\alpha} + ce^{j\theta} + ee^{j(\psi-\theta)} \quad (4.7)$$

$$\begin{cases} x_E = a \cos \alpha + c \cos \theta + e \cos(\psi - \theta) \\ y_E = a \sin \alpha + c \sin \theta + e \sin(\psi - \theta) \end{cases} \quad (4.8)$$

Trajectory of point G :

$$\overrightarrow{AG} = \overrightarrow{AB} + \overrightarrow{BF} + \overrightarrow{FG} = b + de^{j\beta} + fe^{j(\beta-\phi)} + he^{j(-\delta)} \quad (4.9)$$

$$\begin{cases} x_G = b + d \cos \beta + f \cos(\beta - \phi) + h \cos(-\delta) \\ y_G = d \sin \beta + f \sin(\beta - \phi) + h \sin(-\delta) \end{cases} \quad (4.10)$$

Let the numerical dimensions of the mechanism be: $a=30$, $b=40$, $c=50$, $d=45$, $e=45$, $f=30$, $g=40$, $h=40$, $\varphi=20^\circ$, $\psi=70^\circ$. A crank-and-rocker mechanism (loop $ABDC$), is obtained with input angle α changing from 0° to 360° . The trajectories of joints E and G are simulated as shown in Figure 4.3.

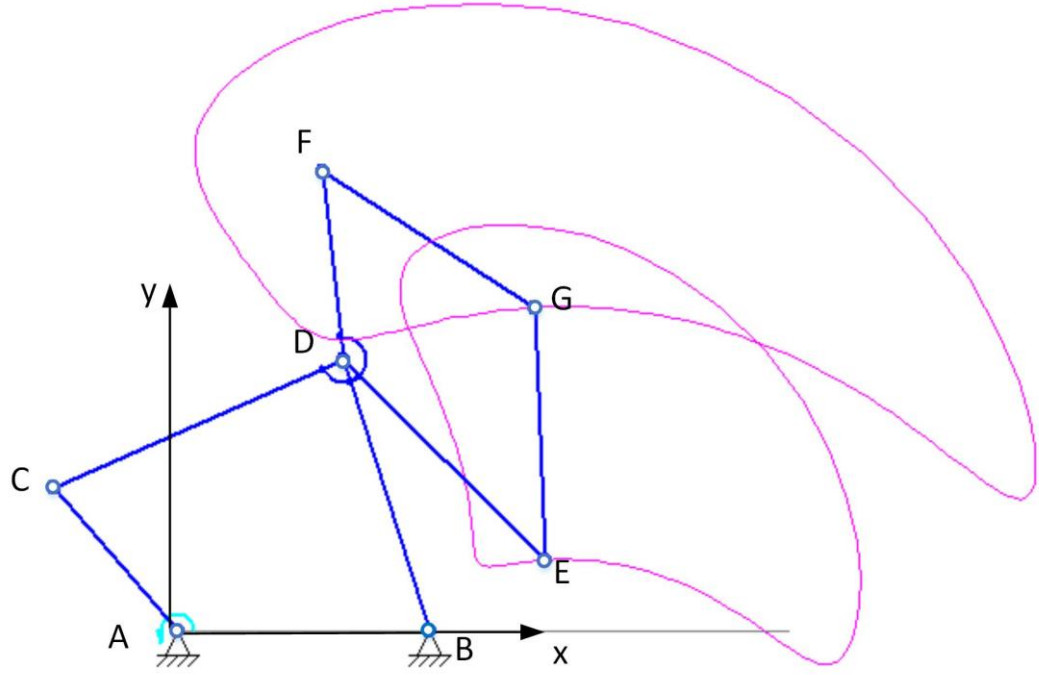


Figure 4.3. Trajectories of joints E and G

If loops $ABDC$ and $DEGF$ are parallelograms, then the geometric relations of this mechanism should maintain constrains where $a=d$, $b=c$, $\alpha=\beta$, $\theta=0$, $f=g$, $e=h$, $\delta=\psi$, $\gamma=\alpha-\varphi$. Equations (4.7) and (4.9) then become:

$$\overrightarrow{AE} = c + ae^{j\alpha} + he^{j\psi} \quad (4.11)$$

$$\overrightarrow{AG} = c + ae^{j\alpha} + he^{j\psi} + fe^{j(\alpha-\phi)} \quad (4.12)$$

From Equations (4.11) and (4.12), we obtain

$$\overrightarrow{EG} = fe^{j(\alpha-\phi)} = \overrightarrow{DF} \quad (4.13)$$

Equation (4.13) reveals that \overrightarrow{EG} is always equal to \overrightarrow{DF} because link BDF rotates around a fixed point B , so link EG will also rotate around a fixed point O_1 with the same geometric characteristics (Figure 4.4). The geometric condition ensures DBO_1E is

a parallelogram, subsequently forming a six-bar mechanism with two parallelograms and a virtual remote centre.

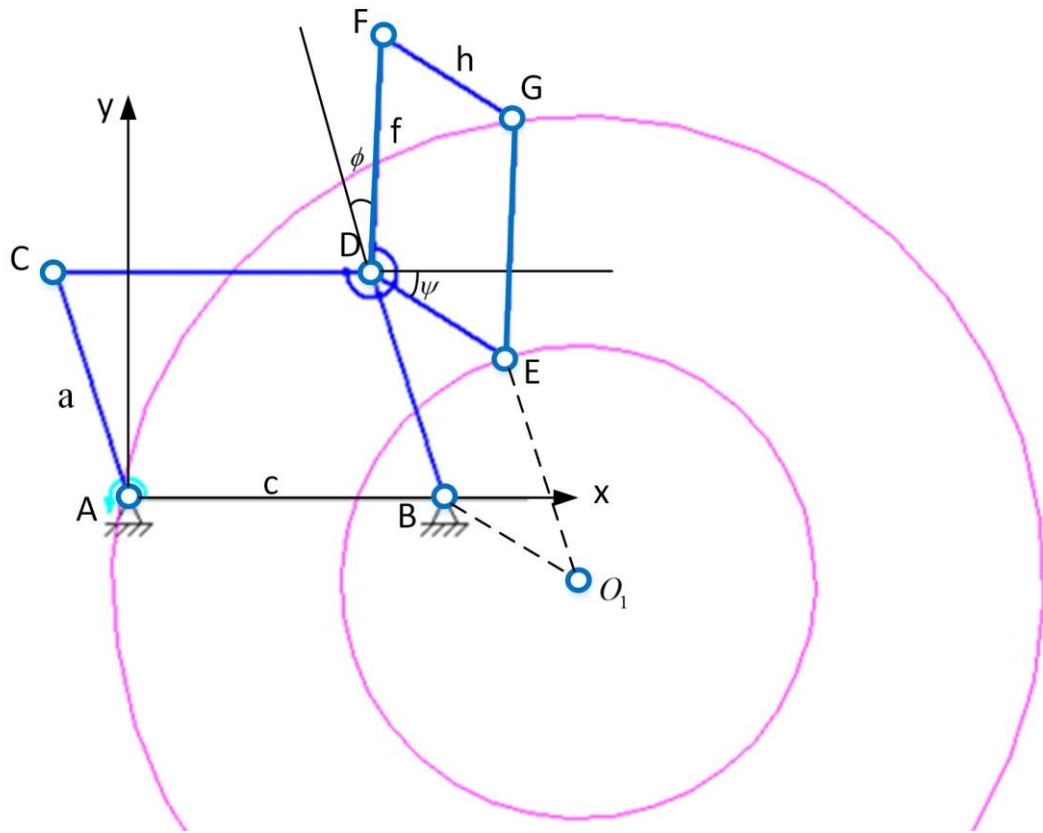


Figure 4.4. A type of six-bar mechanism with one remote centre

4.2 Motion Transmission of RCM-Based Fingers

Gripper fingers are set in motion to build up gripping forces on objects. Angular, parallel and underactuated motion of the finger is commonly generated for object gripping. Angular motion refers to the end part of fingers pivoting on one point virtually or actually. Parallel motion of finger is always driven in a linear slot to move towards each other. Underactuated motion means the number of actuators is less than the full degrees of freedom to be driven [145].

The most investigated underactuation is actually position limitation with springs. Underactuation is an intermediate solution between full-actuation (each joint has one independent motor and complex control for versatile motion) and simple-actuation (few actuators and simple control for specific motion). An underactuated gripper or hand is also an intermediate type which may not be so versatile or stable across the full range. It is less expensive, providing average control and requiring few actuators to do more complicated work [146]. The number of actuators of an underactuated hand is less than

the DOF of the hand. The gripper mechanism requires an intelligence which allows it to envelope the shape of objects automatically using its fingers. The intelligence is usually governed and implemented by the springs and mechanical limits for position control. The control strategy is simple and direct without any specification. An example of a two-DOF finger is shown in Figure 4.5. The diagram of the finger shows a five-bar linkage which has two coincident joints with one link length 0. Closing is enabled by a force acting at the arrow position. Before the first phalange contacts the object, the second joint of the five-bar linkage is mechanically limited and the adjacent two links connected by spring. The mechanism is actually a one DOF four-bar linkage. After contact of the first phalange, the mechanical limit is released and one link fixed. In another configuration a one-DOF four-bar mechanism is generated until the second phalange contacts with the object.

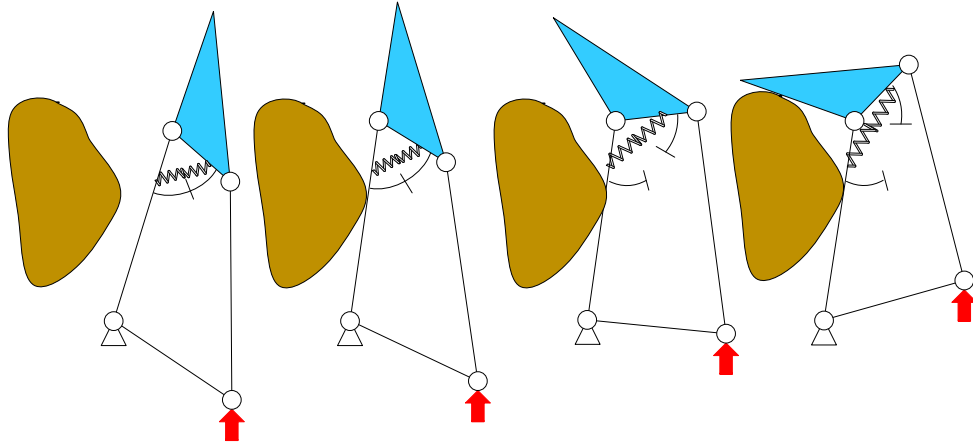


Figure 4.5. Gripping sequence of the underactuated gripper [141].

In this section, the motion transmissions of RCM-based finger with angular, parallel and underactuated are investigated. This is the first mechanism which includes three types of the gripping motion and can be further used to develop fingers with multi-mode gripping capabilities.

4.2.1 Angular Motion of RCM-Based Finger

The kinematic diagram of the RCM mechanism is shown in Figure 4.6. Point O is a remote centre of the RCM mechanism. The initial position (solid lines) of the RCM mechanism is determined by the ground link AB which is at angle θ between AB and the horizontal line. Links BDF and CDE are angulated with angles α and β respectively. The main lengths of the mechanism are a , b , c and d .

According to the kinematic analysis of the RCM mechanism in Section 4.1, links BDF and GEO are identical in dimension and have the same rotating motion. Angles CAC'

and EOE' are identical and equal to δ . Link EG acting as a fingertip for grasping has angular motion. The rotating velocity of link EG is the same as driving link AC .

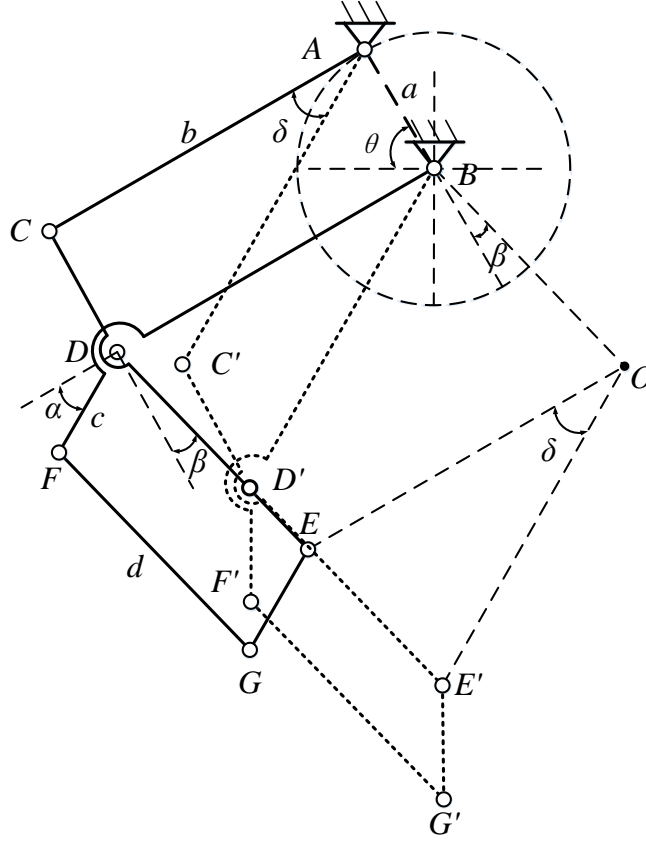
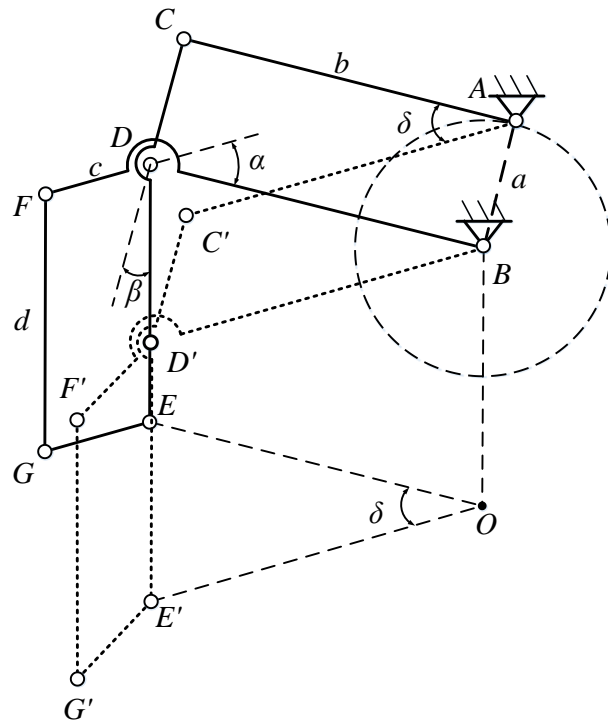


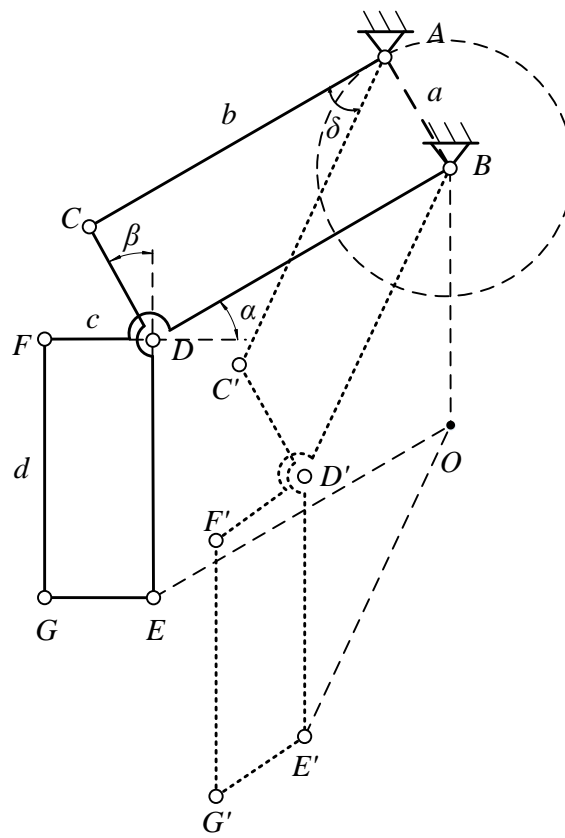
Figure 4.6. Kinematic diagram of two positions of the RCM mechanism.

4.2.2 Parallel Motion of RCM-Based Finger

Parallel motion applies to another link, DE , in the RCM mechanism. A viewing position of single finger is to make the DE or BO vertical. Comparing with Figure 4.6, two approaches can be used, one by rotating the whole mechanism until BO vertical, see Figure 4.7 (a); the other by changing the angles or directions of angulated links BDF and CDE . The former one is much easier for constructing an angular-parallel reconfigurable gripper. According to Figures 4.6 and 4.7 (a), the rotational angle of the whole mechanism with respect to frame point B is $\pi/2 - \theta + \beta$, which is solely related to the initial position of the angle of angulated link CDE .



(a)



(b)

Figure 4.7. Two approaches to obtain parallel gripping.

4.2.3 Underactuated Motion of RCM-Based Finger

Underactuated motion of the mechanism is obtained by changing the position of A to be movable. As shown in Figure 4.8, point A is a frame point, AC is a drive link and BO is vertical. DE of the RCM mechanism provides a translation motion and the RCM-based gripper imparts parallel gripping. If link BDF is stopped due to an obstacle, and point A is free with a circular motion, link CDE will continue to move. The rotating angle of link CDE is the same as link AB and equals to γ . The remote centre O also rotates an angle γ along a circle with radius d .

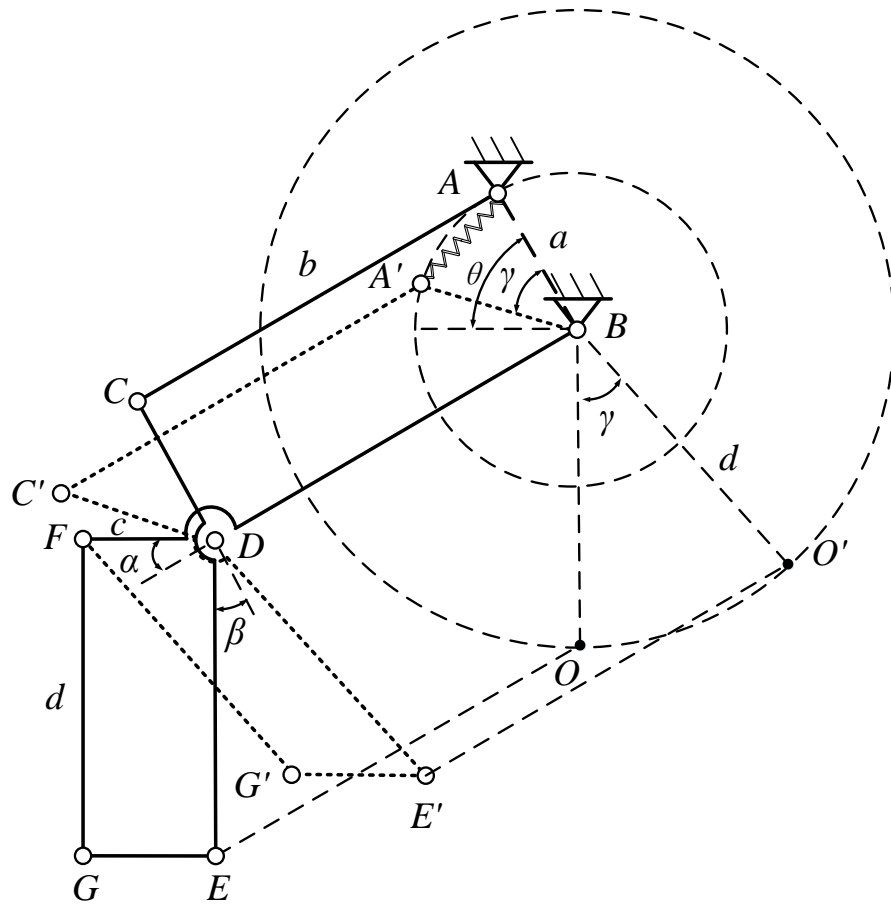


Figure 4.8. RCM-based mechanism for underactuated grasping.

From Sections 4.2.1 to 4.2.3, the following conclusions can be drawn: the angular motion of the RCM-based finger can be obtained from the furthest link EG ; the extended coupler link CDE of the first four-bar loop can be used for parallel gripping if the initial position of BO is vertical. Releasing of one frame point A generates underactuated motion. Therefore, the RCM-based finger has three motion-modes: angular, parallel, and underactuated. The angular and parallel modes are specific

Substituting Equation (4.14) into Equation (4.15),

$$\tau = Fl \quad (4.16)$$

where ω is the angular velocity of drive link, v_x is the velocity of acting point and parallel to GE , l is the perpendicular line between rotating centre and force direction.

In Figure 4.9, OH can be derived as,

$$OH = \sqrt{b^2 + e^2 + 2be \cos \alpha} \quad (4.17)$$

According to geometrical parameters, l is obtained:

$$l = b \cos \alpha + e \quad (4.18)$$

The relationship between the output of the actuator and the gripping force is

$$\tau = F(b \cos \alpha + e) \quad (4.19)$$

If the friction between the contact surface and the grasped object is considered, as in Figure 4.10, the following equation is obtained by applying virtual work,

$$\tau\omega = Fv_x + fv_y \quad (4.20)$$

Using a similar calculating process, the relationship between the actuator output and the gripping force and friction is as follows,

$$\tau = F(b \cos \alpha + e) + fb \sin \alpha \quad (4.21)$$

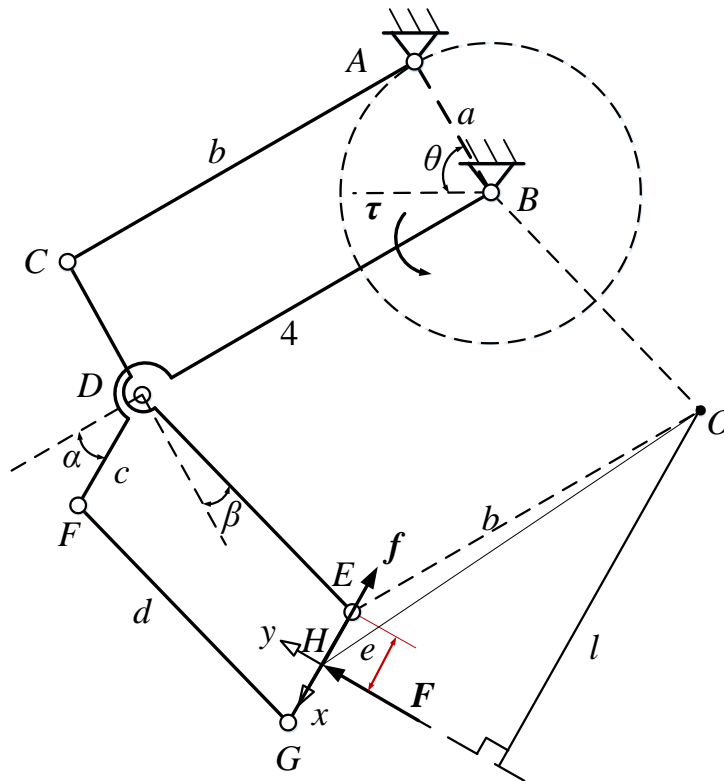


Figure 4.10. Static analysis of RCM-based finger with angular motion (considering friction).

4.3.2 Static Analysis of RCM-Based Finger with Parallel Motion

A kinematic representation of the RCM-based parallel gripping finger is shown in Figure 4.11 (friction free model). F is the action force of the mechanism at the specific position. The velocity polygon of link CDE is constructed at the right hand side. Applying the principle of virtual work,

$$\tau\omega = Fv_y \quad (4.22)$$

The vertical component of v is

$$v_y = b\omega \sin \varphi \quad (4.23)$$

Substituting Equation (4.23) into Equation (4.22), we obtain

$$\tau = Fb \sin \varphi \quad (4.24)$$

where ω is the angular velocity of drive link BD and b , its length.

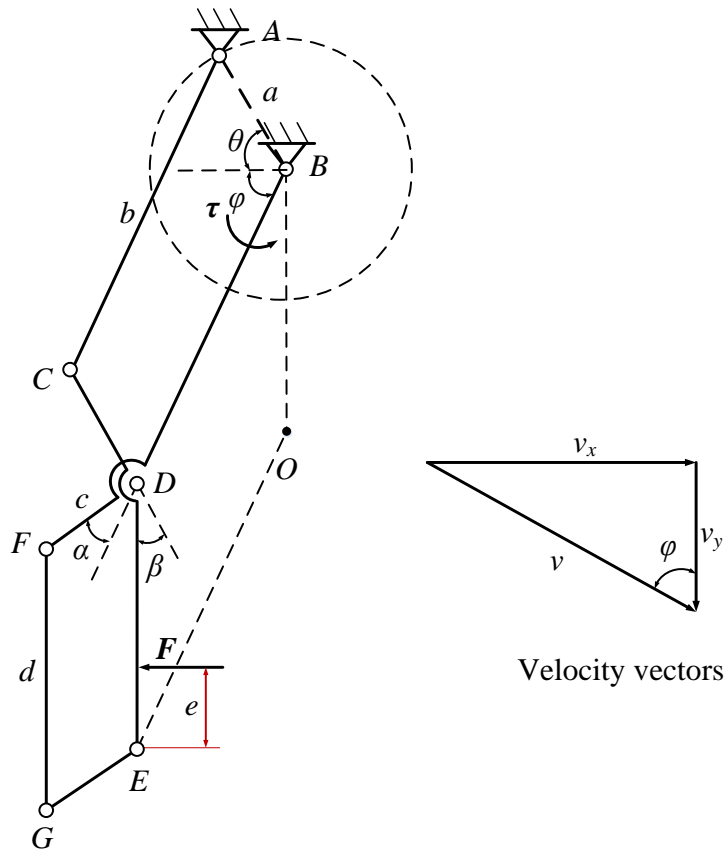


Figure 4.11. Static analysis of RCM finger with parallel motion (friction free).

By considering the friction at the contacting point between the fingertip and the grasped object (Figure 4.12), the input and output virtual powers of the finger is obtained

$$\tau\omega = Fv_x + fv_y \quad (4.25)$$

In the same way, the relationship between the actuator output and the gripping force and friction is obtained

$$\tau = Fb \sin \varphi + fb \cos \varphi \quad (4.26)$$

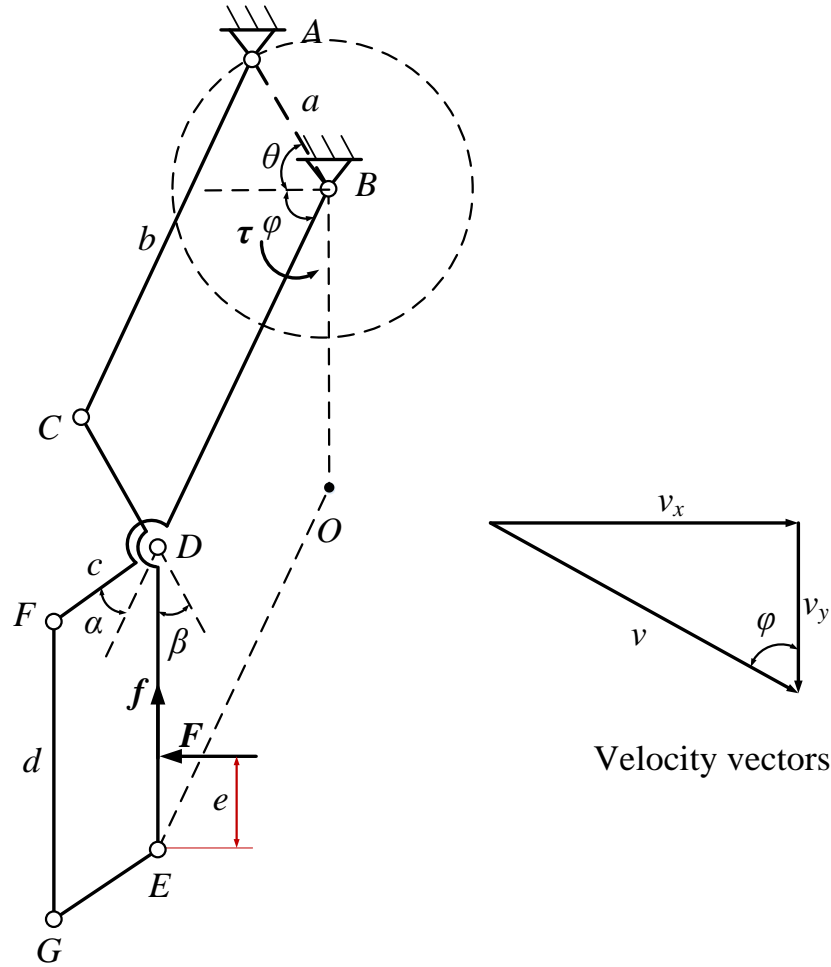


Figure 4.12. Static analysis of RCM finger with parallel motion (considering friction).

4.3.3 Static Analysis of RCM-Based Finger with Underactuated Motion

The analysis method for the underactuated finger what it generates an external wrench onto a fixed object was presented in [145]. The stable and unstable grasps of two-phalanx underactuated fingers of general architecture were analysed. Figure 4.13 shows a two-phalanx finger with two contacts and its stable and unstable configurations. The analysis disclosed that the process of closing will force the finger to lose contact with one of the phalanges, usually the proximal one. Because the wrench of distal link caused by contact force has the same direction with drive torque. The parallel

configuration of the two-phalanx finger is also shown to be unstable in paradoxical equilibrium [146], a peculiar unstable behaviour that no equilibrium possible, see Figure 4.14; this refers to distal contact only.

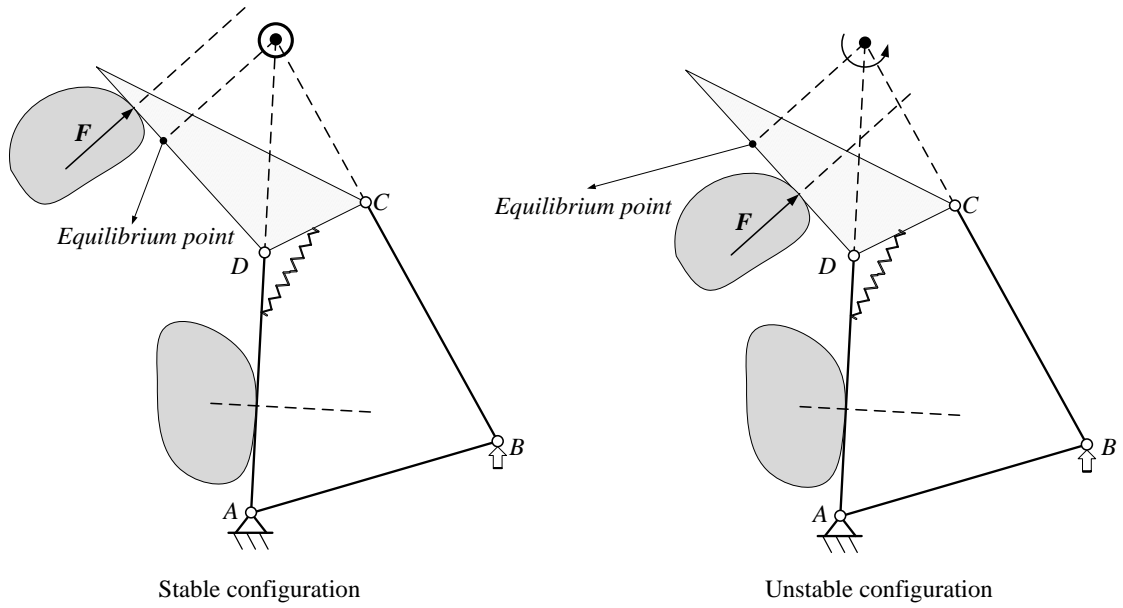


Figure 4.13. Stable and unstable configurations with two contact points.

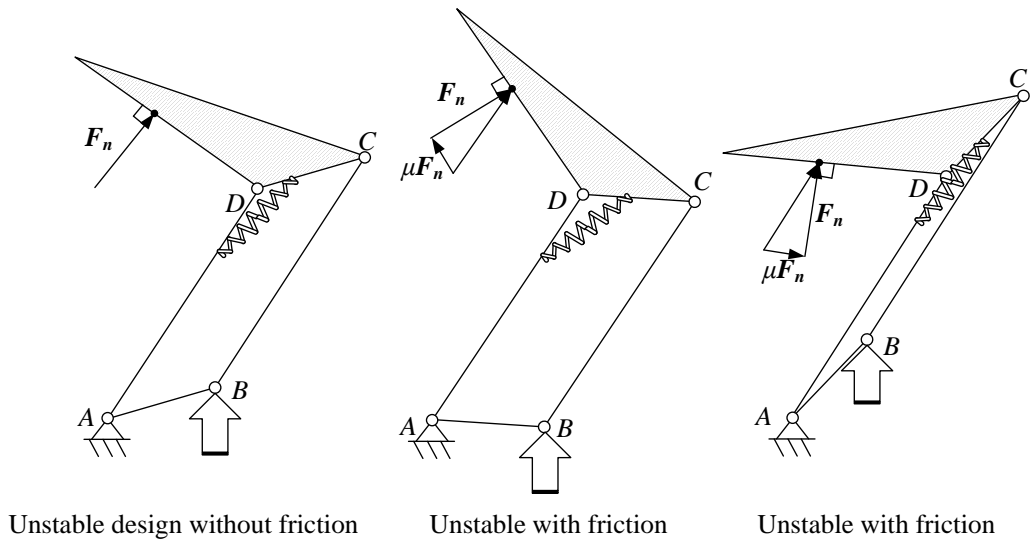


Figure 4.14. Unstable design of underactuated finger in paradoxical equilibrium without and with friction.

For linear contact with distal phalanx, it is shown that the two phalanx self-adaptive finger is stable if and only if the location of the equilibrium position is between both contact points of the line [147] as shown in Figure 4.15.

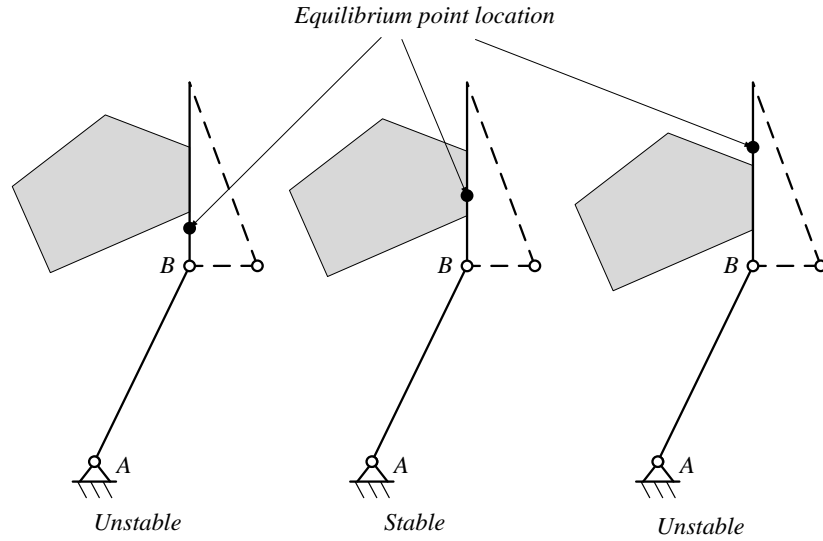


Figure 4.15. Stability of planar pinch grasp depending on the equilibrium location.

The above stability analysis refers to fingertip upward. In practical gripping for assembly, there is always vertical grasping as shown in Figure 4.16 where the configurations in paradoxical equilibrium, unstable and stable status without friction are shown. Three different-shaped objects are grasped by the same two-phalanx finger in three different configurations. The instant centre of the parallel-configuration gripper is a point at infinity position. Therefore if the direction of the action force is parallel-to-parallel links, it is a paradox equilibrium position as presented before. Figure 4.16 (b) shows an unstable position with angle α between drive link and the action force far from the finger. Figure 4.16 (c) is a stable configuration with an angle β as shown. A larger angle ψ and deeper gripping position make the stable configuration much easier to obtain.

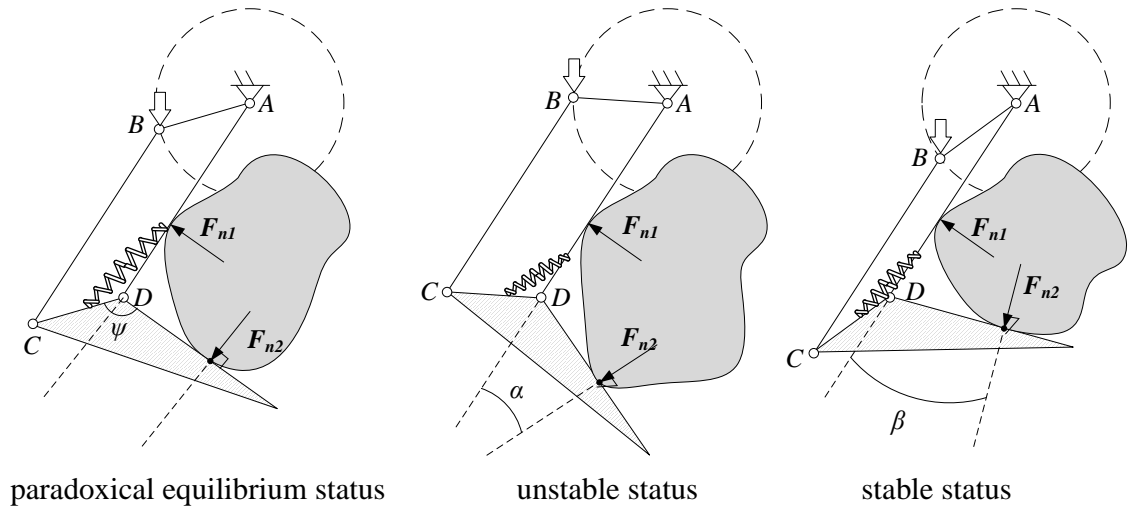


Figure 4.16. Vertical grasping in paradoxical equilibrium, unstable and stable statuses without friction.

The underactuated parallel finger with friction is analysed as shown in Figure 4.17. The equilibrium position of the finger with parallel condition between the parallel links and action force is shown in Figure 4.17(a). In the same configuration of gripping, however, if the friction between the gripping surface and the gripped object is higher, then the gripping action is changed to a stable state. That is to say, the larger the coefficient of friction of the fingertip, the more stable the underactuated gripping.

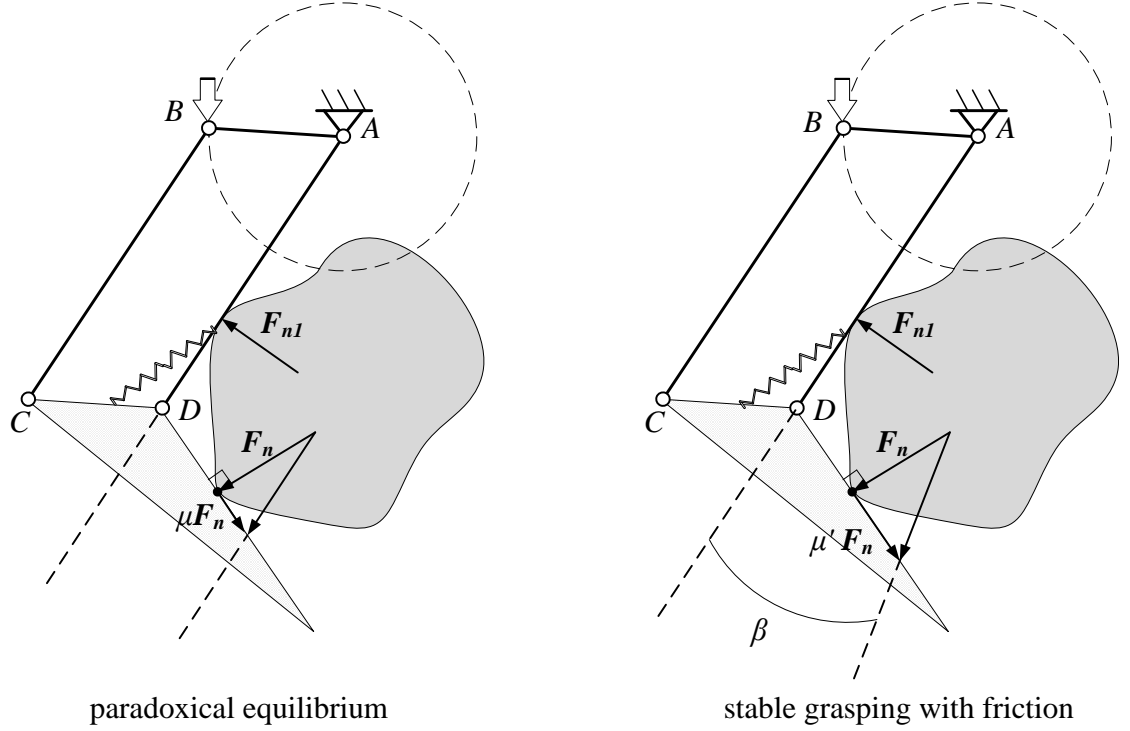


Figure 4.17. Vertical grasping in paradoxical equilibrium and stable grasping with friction.

Figure 4.18 shows two configurations of the RCM-based underactuated finger. The input torque of drive link AB is τ . One end of spring with stiffness K is fixed at point A . The rotating angle of link AB is γ . The contact points of the two-phalanx finger have grasping forces of F_1 and F_2 respectively and their location with offset lengths e_1 and e_2 are as shown in the figure.

The increased length of spring can be simplified. As shown in Figure 4.19, the initial length of spring is x and the final length after extension is $A'P$. The increased length Δ is $A'P - x$, which can be replaced by length AA' . Therefore:

$$\Delta = AA' = 2a \tan(\gamma / 2) \quad (4.27)$$

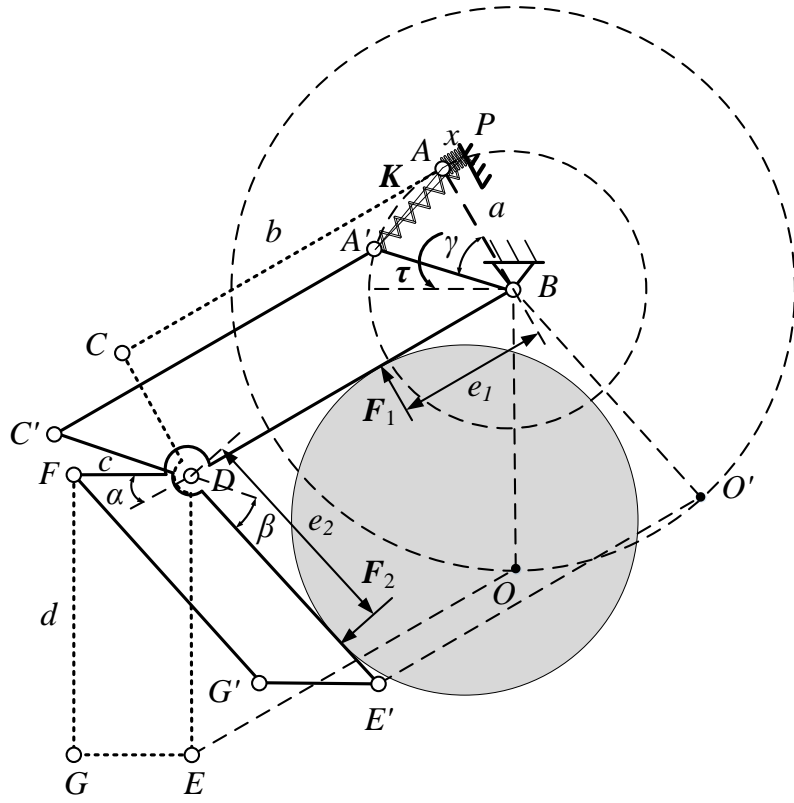


Figure 4.18. Kinematic representation of RCM-based underactuated gripping.

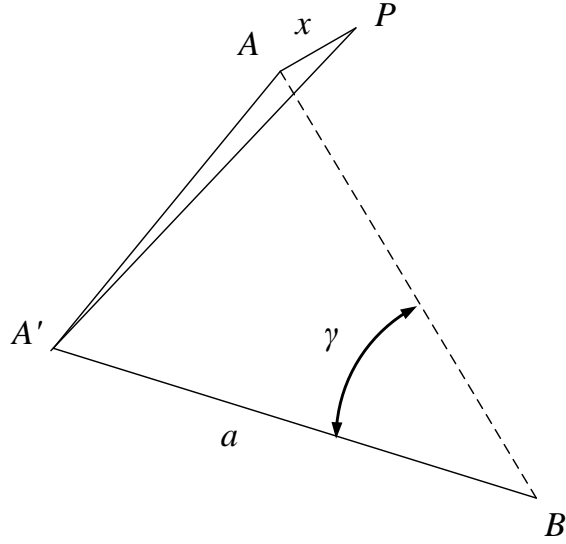


Figure 4.19. Spring changing in the two-phalanx finger.

Here force F_1 make the proximal phalanx contact the object without any motion, therefore the virtual power is 0. If there is a constant angle θ passing simultaneously by links AC and BD , then equating the input and output virtual power of the system,

$$\tau \dot{\gamma} = K \Delta \cos(\gamma / 2) a \dot{\gamma} + F_1 e_1 \dot{\gamma} + F_2 e_2 \dot{\gamma} \quad (4.28)$$

The parallel type of a two-phalanx underactuated finger is reported to be unstable for grasping [145] because of the instant centre between the ground link and coupler link is located at an infinite position with only distal contact. The instant stability analysis of two-phalanx configurations with point contact is shown in Figure 4.20. The “lock” symbol has been used to indicate which joint holds the triggered element and the “unlock” symbol for a released joint [148]. In these two diagrams, the stable and unstable regions of the gripper are marked. Both of them are five-bar mechanisms, where axis of the ground link is coincident in Figure 4.20(a).

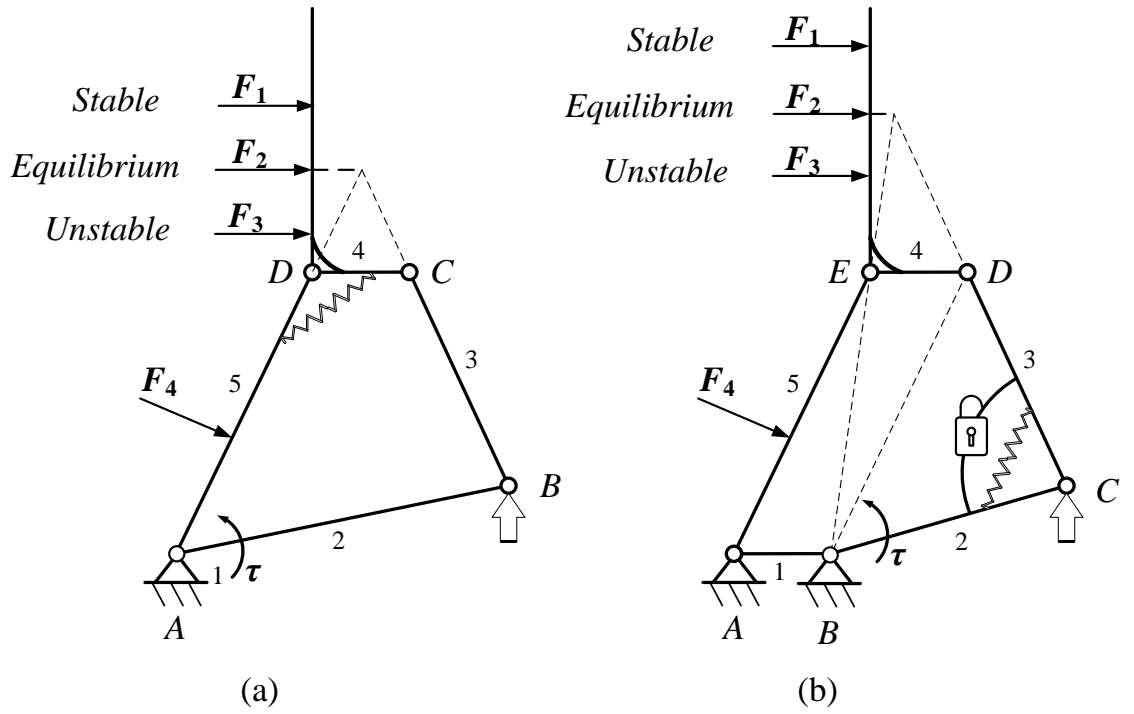


Figure 4.20. Stable grasping region of the two configurations.

By applying the approach shown in Figure 4.20(b), a modified grasping underactuated RCM-based finger is proposed, see Figure 4.21. In this mechanism, joint G is locked before the proximal phalanx contact objects. The joint is actuated if the proximal phalanx encounters an obstacle. There are two pivot points for this structure when compared to the structure shown in Figure 4.18.



This chapter has provided a novel finger design which is based on an RCM mechanism. The kinematics of the RCM was firstly investigated. Due to its geometrical characteristics, its multiple modes of motion were investigated in terms of angular, parallel and underactuated. The RCM mechanism was first developed for robotic finger design as a class of reconfigurable finger. Static analysis of the three configurations was also conducted. For the underactuated type, grasping stability was then investigated. It has been shown that the grasping position and coefficient of friction of the fingertip are influential factors for stable grasping.

CHAPTER 5 – Development and Testing of Robotic Gripper Hands

The gripper acts as a bridge between the robotic arm and the world around it. The design of a mechanical gripper requires an in-depth knowledge of mechanism design including kinematic analysis and dimensional synthesis. Chapters 2, 3 and 4 discussed significant components of mechanical grippers in terms of finger joints, fingertips and fingers. The finger joints are unique for anthropomorphic finger design. Fingertip and adaptive fingers are two novel applications for gripper design, thanks to their multi-mode and multi-motion characteristics. This chapter mainly focuses on the development of adaptive and reconfigurable gripper hands based on the aforementioned multi-mode fingertip and multi-motion finger and aims to develop a type of meso-scale gripper for miniaturized product assembly.

5.1 Gripper Hands with Meso-Scale Gripping

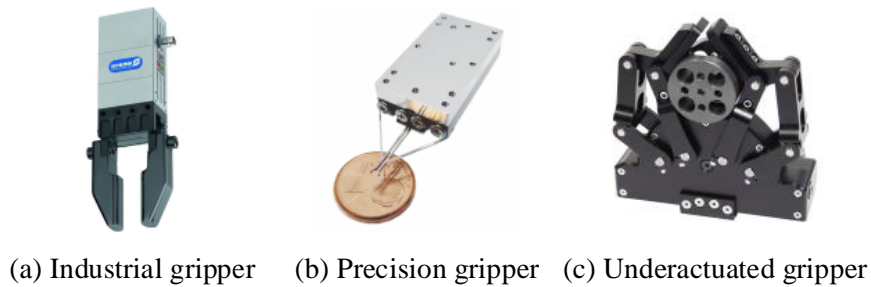


Figure 5.1. Three general types of gripper hands

Grippers and robotic hands are essential end-effectors of robotic manipulators. The development of grippers or robotic hands able to pick up various objects has attracted much attention within the research community over the last four decades. Grippers vary from simple configurations, such as parallel/angular two-jaw designs, to complex, dextrous hand with advanced sensors, control units and servomotors. The initial gripper application used in industry was for picking up raw and finished parts [10]. The majority of grippers are variations of three fundamental designs, namely: parallel, angular and three-fingered grippers. A two-fingered gripper has the minimum number of fingers and the minimum complexity of a hand. According to typical types of industrial gripper applications, the minimum gripping force of a parallel gripper is difficult to control especially for small objects with quite low weights. Angular grippers can be adjusted to various angles according to workpieces and space limitations. Robotic grippers that mimicking human hands have also been investigated and applied in industry. Within such systems, fingers are the most important components of a precision grasping “hand” [149]. These can mainly be classified into three types: low-

cost grippers for industrial production, precision grasping and underactuated grasping [27], as shown in Figure 5.1. Recent research on universal high flexibility, multi-functional robotic grippers has been carried out and some systems have been developed [150]. However, it is still difficult to accurately grip very small, fragile and light objects with such grippers. With the development of micro-scale technologies in electronics, optics and biology, micro-grippers are required for micro-robot and micro-assembly applications. Micro-grippers also require to grip and handle micro-objects securely and accurately with the range below $100\mu\text{m}$, preferably with no gripper changes. Some specifically designed micro-grippers are able to handle objects ranging from nanometers up to $500\mu\text{m}$. In a variety of circumstances a robot has to switch hands for gripping objects with various sizes, shapes and ranges of gripping force. A general purpose “hand” that can accomplish all of these tasks will make gripping much more efficient and reduce changeover time. This type of gripper hand will benefit a lot for the upcoming booming of collaborative robot for industrial application.

The main contribution of the thesis is to overcome the technical issues in design and develop grippers with mesoscopic gripping range to bridge the micro- and macro grippers. In recent years, applications in industrial assemblies within a size range from 0.5mm to 100mm are increasing due to the large demands for new products, especially those associated with digital multimedia. Research on grippers or robotic hands within the meso-scale of this range has not been explored in any great detail. This chapter outlines the development process of a gripper to bridge the gap between micro-grippers and macro-grippers by extending the gripping range to the meso-scale, particularly without the need to switch grippers during industrial assembly. To address this gap, a meso-scale gripper (meso-gripper) which has metamorphic characteristics and two gripping modes is proposed, developed and tested. A definition of meso-scale artificial gripping has been presented in the Introduction, Section 1.42. The meso-gripper researched in this work has two modes of operation: passive-adjusting and angular gripping, adapting to the various shapes of objects automatically using appropriate configurations. This form of gripping and the associated mechanism are both novel in their implementation and operation.

This chapter is organized as follows. Firstly, human gripping behaviours are investigated by considering variant shapes and sizes. Gripping processes for tiny and general sized objects are analysed. Then a detailed design and analysis of a type of meso-gripper are addressed by integrating an RCM mechanism with a CFB linkage. The passive-adjusting and angular gripping modes are then analysed and a dual functional

mechanism design proposed. In Section 5.2, a geometric constraint method is then demonstrated which facilitates task-based dimensional synthesis after which the kinematics of synthesized mechanism is investigated. The modified gripper is then developed by considering stiffness and layout. In Section 5.3, actuation and transmission mechanisms of gripper are selected for specific design requirements. Three types of differential mechanisms are used to increase the gripper's flexibility according to underactuated requirements. Finally, physical prototypes are fabricated using 3D printing. Three types of gripper hands are developed. The first one is a meso-gripper with manual actuation. The second is precision-power integrated gripper which has been patented. The third is a reconfigurable gripper which is implemented by considering multiple modes of the RCM mechanism. The meso-gripper and reconfigurable gripper are successfully tested for universal object gripping.

5.2 Development of a Meso-Gripper

5.2.1 Analysis of Human Grasping Behaviours

Two manual gripping examples were considered and various configurations of fingers observed to help define the functionality of the proposed meso-gripper. These examples comprise two parts, a very thin hex socket screw with a diameter of 1.5mm and a plastic cuboid with dimensions 28mm × 24mm × 17 mm. Both were observed to be processed in four steps, namely: searching, reaching, gripping and moving [124] (Figure 5.2). First step searching refers to a combination work with visual system, same function as human eye during human gripping process. The objective for each step in assembling these two parts is the same but the configurations are different due to size and shapes of the parts.

The gripping process of a hex socket is as follows:

- a. Distal segments of thumb and index fingers contact each other, then move to the hex socket;
- b. The contacted fingers reach above the hex socket;
- c. The hex socket is gripped by fingertips;
- d. The hex socket is moved;

The gripping process for plastic cuboid is

- a. The thumb and index fingers move to the plastic cuboid;
- b. Distal segments of thumb and index fingers reach and contact two edges of the cuboid;
- c. Pads of thumb and index fingertips grip the sides of the part for clamping;
- d. The cuboid is moved.

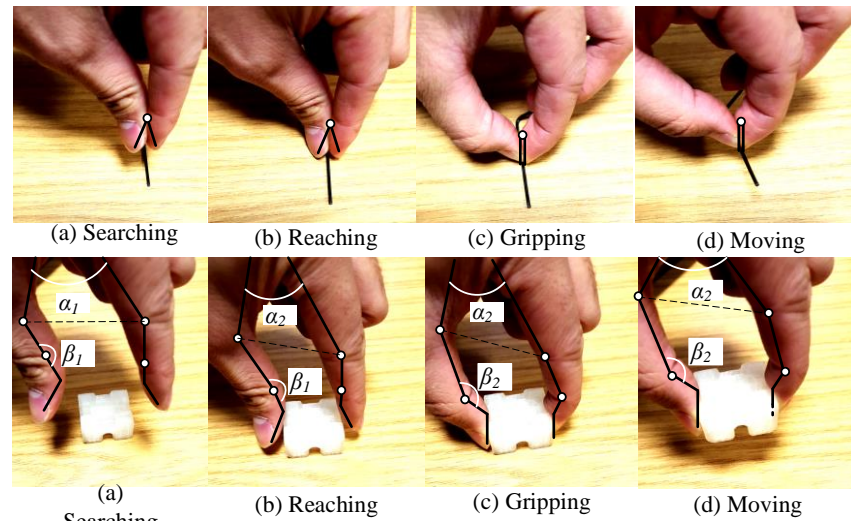


Figure 5.2. Gripping processes for a hex socket and plastic cuboid

Comparing these two processes, gripping the hex socket screw requires only one DOF while gripping the cuboid requires two DOFs (see Figure 5.2). This analysis greatly simplifies the finger design for gripping these objects. Two DOFs, one for positioning and another for clamping, are the minimum number of DOF required in these gripping processes.

By considering the analysis of gripping processes and the proposed CFB fingertip and RCM finger, an overall gripper model was obtained. The gripping process mimics the human hand as shown in Figure 5.3. The process shows that the integrated mechanism passively adapts to parallel sides of a cuboid.

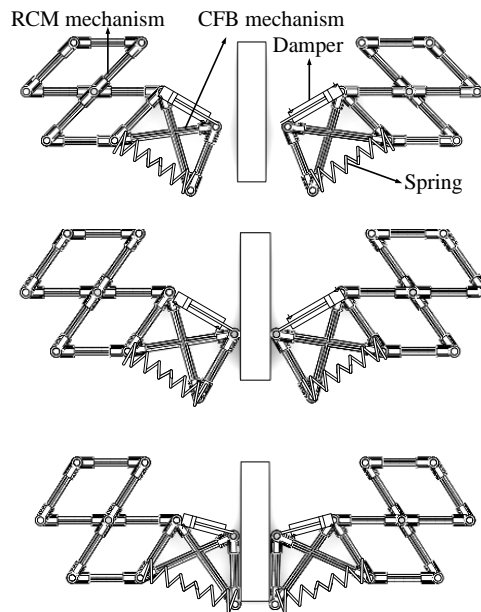


Figure 5.3. Sequential gripping process of the integrated mechanism

5.2.2 Metamorphic Gripping of the Multi-Mode Gripper

Considerable development in theoretical research on metamorphic mechanisms [151] has been made in the past 15 years such as the metamorphic hand [152] and walking machines. Schematic of a meso-gripper during passive-adjusting mode as shown in Figure 5.4(a), has two DOFs when considering one side of the gripper. The DOFs of the mechanism will reduce to one if one point of CFB mechanism touches the object. If two points of the coupler link in the CFB linkage touch an object, the DOF degrades to -1, i.e. it is over-constrained. Therefore, the meso-gripper is an example of metamorphic mechanism. A detailed analysis of this characteristic is now outlined.

The process of cuboid gripping (shown Figure 5.3) is similar to the four steps shown in Figure 5.2. The object M is supposed to be fixed to the frame while point I of the CFB mechanism slides on the surface of the object until point H contacts it as shown in Figure 5.4(a). The solid line diagram shows the point at which the mechanism reaches the cuboid and the dashed diagram the final configuration. The equivalent mechanism during the gripping process is shown in Figure 5.4(b). The DOF (F) analysis of this mechanism during this process is calculated using the Gruebler's equation where n = number of moving links, p_l = number of lower pairs, p_h = number of higher pairs:

$$\text{Searching step: } F = 3n - 2p_l - 2p_h = 3 \times 8 - 2 \times 11 = 24 - 22 = 2$$

$$\text{Reaching step: } F = 3n - 2p_l - 2p_h = 3 \times 9 - 2 \times 13 = 27 - 26 = 1$$

$$\text{Gripping step: } F = 3n - 2p_l - 2p_h = 3 \times 7 - 2 \times 11 = 21 - 22 = -1$$

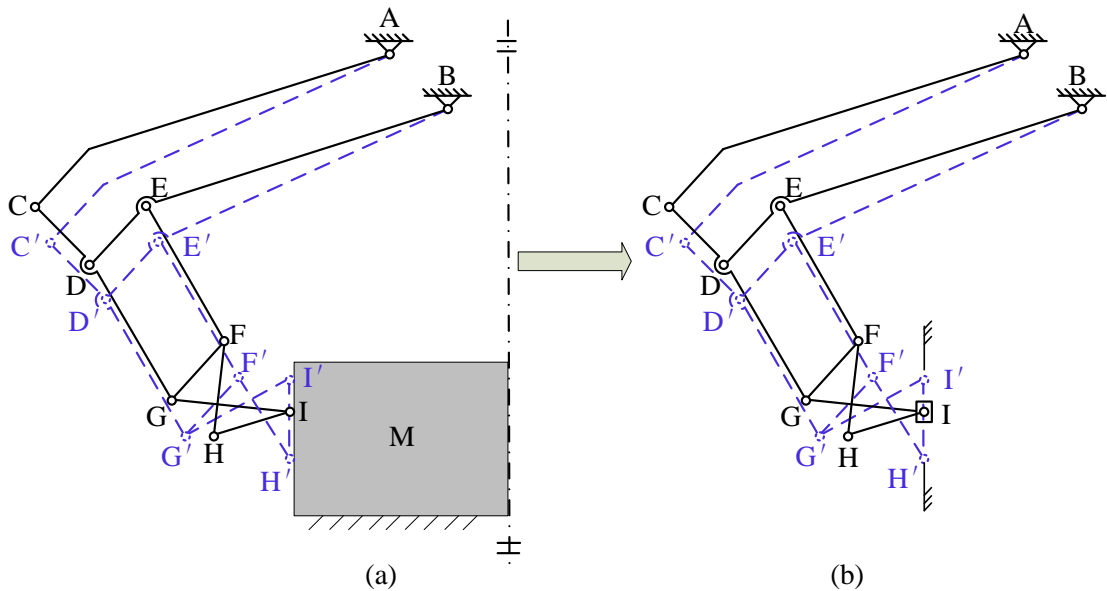


Figure 5.4. Metamorphic gripping and equivalent mechanism

The number of movable links of the mechanism changes during the gripping process, causing a subsequent change in its topology.

The angular gripping mode of the gripper has a similar motion to the passive-adjusting mode. The DOFs and topology of the mechanism vary at different gripping steps.

5.3 Dimensional Synthesis of the Meso-Gripper

Geometric constraint programming was proposed to solve the general kinematic synthesis problem, such as planar four-bar linkages for motion generation, path generation and function generation [153]. Detailed dimensional synthesis and kinematic analysis of the multi-RCM mechanism can be found in [143]. The design process of a meso-gripper relating this approach will be presented in this section.

5.3.1 Task-Based Dimensional Synthesis

The objective of dimensional synthesis is to determine the value of each geometric parameter of a mechanism by taking account of its desired performance. Geometric parameters vary with the design criteria. Gripping range is one of the most important criteria which differentiate the meso-gripper from other designs. The dimensions of the mechanism are dependent on the task requirements.

A geometrical constraint approach is proposed to help design mechanisms over a specific gripping range. The approach is closely related to the synthesis of multi-RCM mechanisms [143]. It is a specific dimension synthesis approach relating to RCM-based mechanisms. The differences mainly lie on the considerations of the prototype design and the manufacturing requirements. According to motivation scenario in section 1.3.1, a gripper for product assembly needs to grip objects ranging from a minimum of 1mm to a maximum of 55mm. To design a precision gripper with the aforementioned RCM and CFB mechanisms with multiple gripping modes, **task requirement** for a multiple ranges of objects are defined as follows:

- (1) The gripping range of the meso-gripper should be 0-55mm.
- (2) The range of angular gripping mode is 0-6mm.
- (3) The range of passive-adjusting mode is 6-55mm.
- (4) The mechanism of the gripper should be compact.

5.3.2 Dimensional Synthesis Process

A flow diagram of synthesis approach for meso-gripper is shown in Figure 5.5.

The seven-step synthesis process incorporating the geometrical constraint approach is outlined as follows:

Step 1. **Determination of initial positions according to the task requirements:** Figure 5.6 provides an enlarged range of 0-60mm, with 5mm margin for the optimization. The RCM point and the first frame point are determined by considering

the compactness of the whole gripper. Because of symmetrical structure of the gripper, 3mm and 30mm in the figure show half side of it and are introduced in section 5.3.1.

Step 2. Design of the CFB linkage: The dimensions of the CFB linkage are shown in Figure 5.7. The length of follower link should be longer than the crank link to build an appropriate angular configuration for angular gripping. The other dimensions aims to make the mechanism compact enough and easy to manufacture. The connecting link will connect with the RCM mechanism.

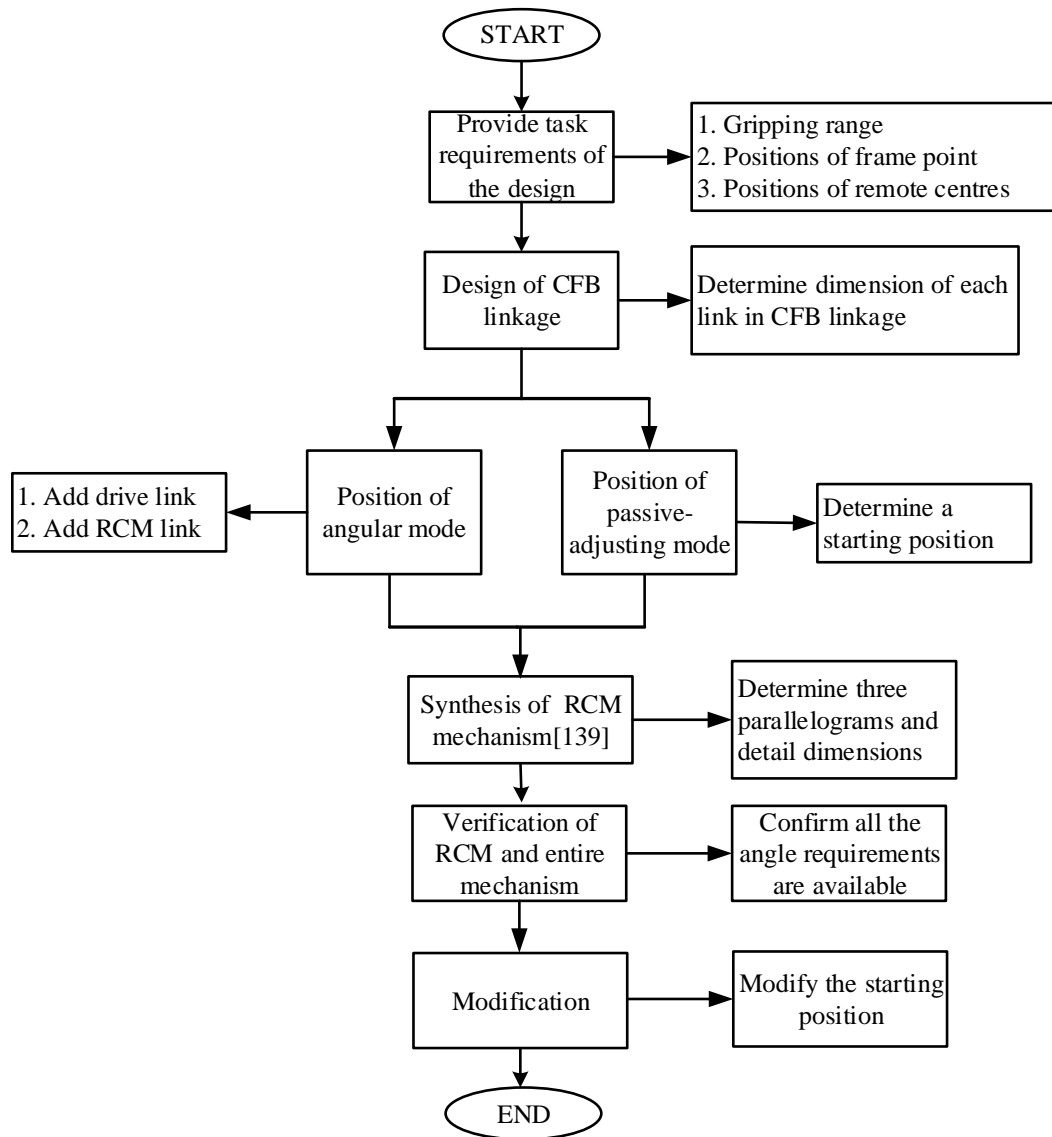


Figure 5.5. Flow diagram of synthesis approach for meso-gripper.

Step 3. Determination of position at angular gripping mode: The CFB linkage is incorporated into the graph obtained from Step 1. The length of drive link is set at 40mm i.e. larger than 30mm which is at the borderline limit. A circle of 40mm radius is

drawn with the RCM point its centre. The two endpoints of the coupler link are positioned on the symmetrical line and 3mm borderline respectively. One endpoint of connecting link is placed on the circle and a line drawn from the RCM point to the end of the circle, making the angle between it and connecting link of the CFB linkage 150° . The position of the CFB linkage at angular gripping mode is then determined, as shown in Figure 5.8. An initial position according to the task requirement is determined in this step.

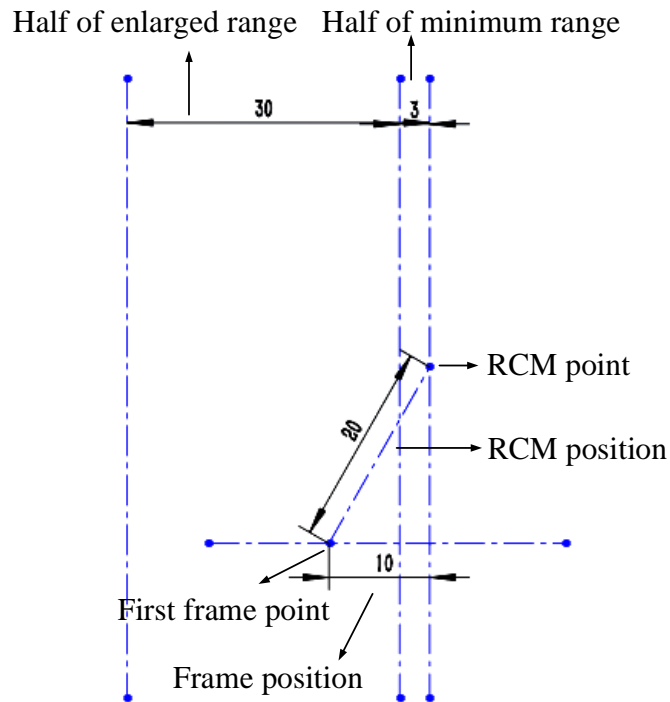


Figure 5.6. Objective gripping range and key points

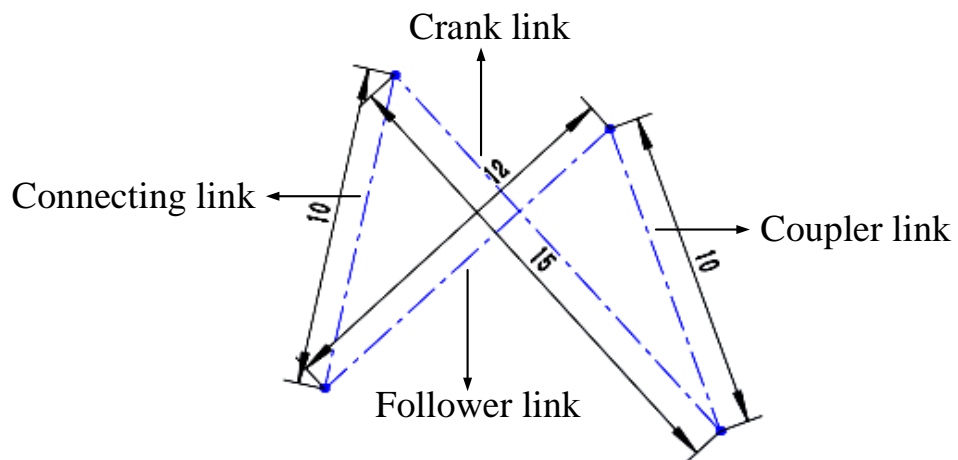


Figure 5.7. CFB linkage with integer dimensions

Step 4. **Determination of position at initial passive-adjusting mode:** As is shown in Figure 5.9, one end of the coupler link is positioned at the 30mm borderline, connecting one endpoint of the connecting link at the circle. This makes the angle between the connecting link and the RCM line 150° .

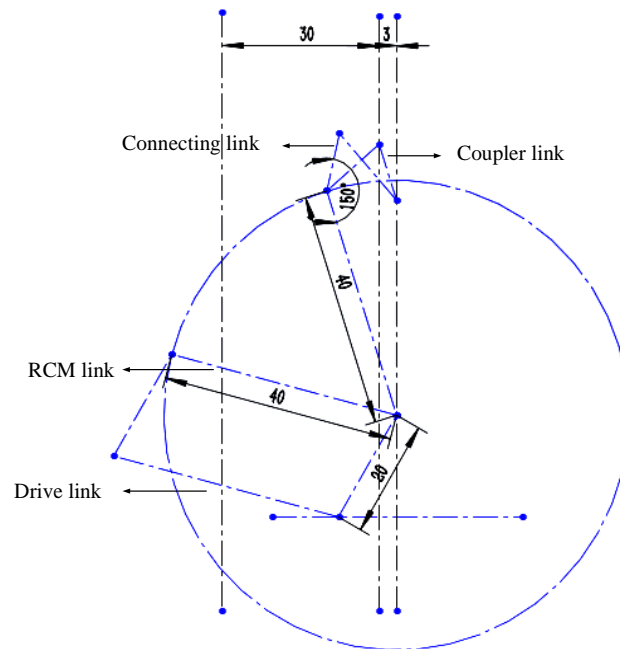


Figure 5.8. Position determination of CFB linkage (initial position according to task requirement)

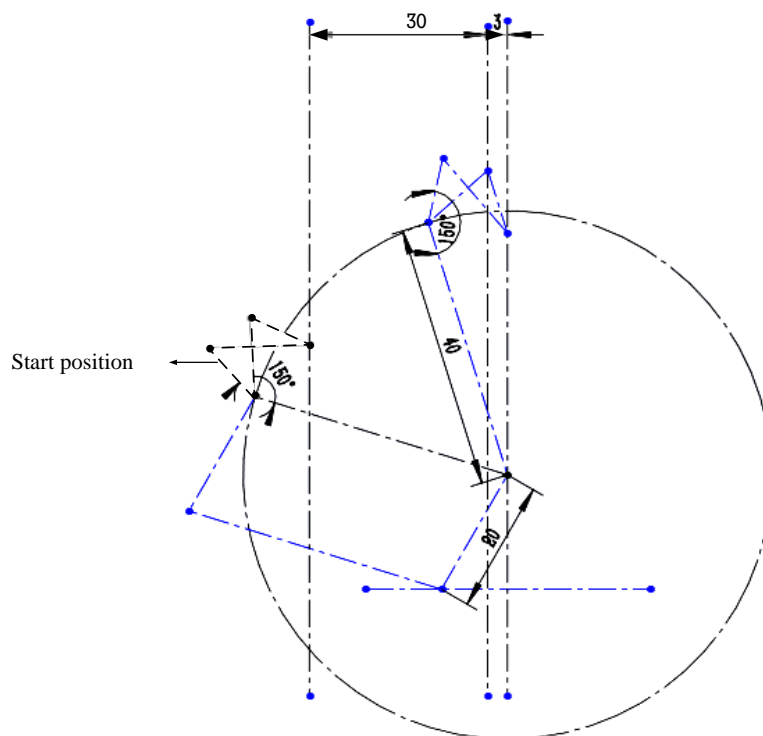


Figure 5.9. Initial position of CFB linkage

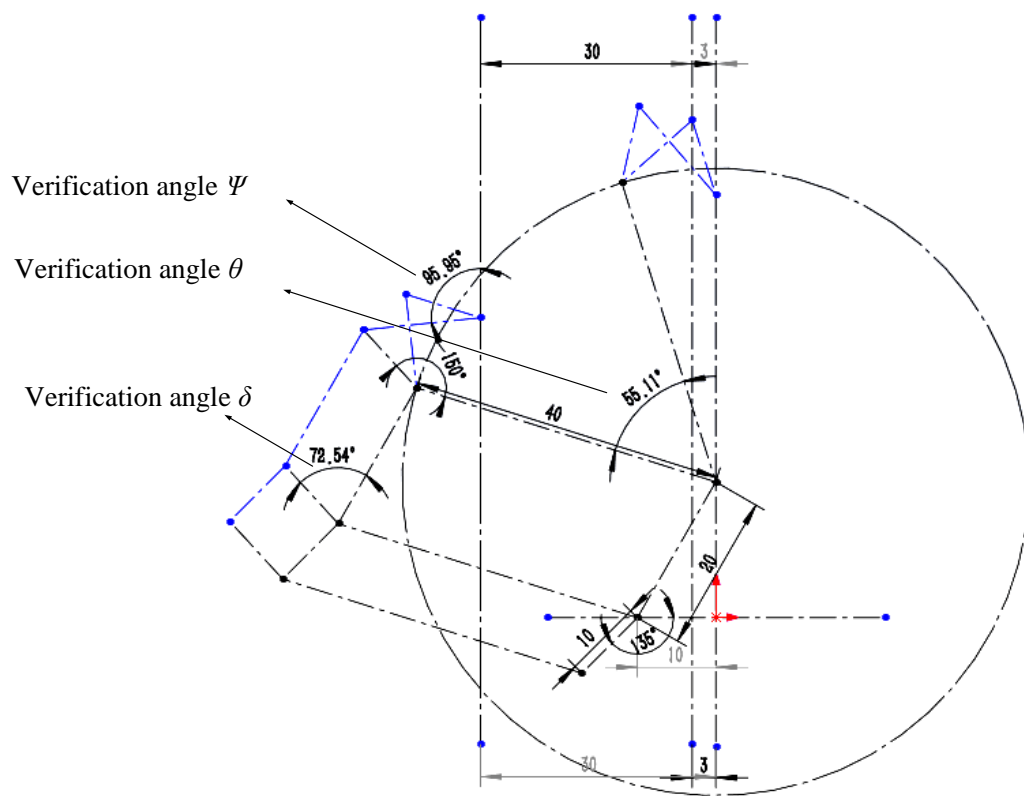


Figure 5.11. Verification of designed mechanism.

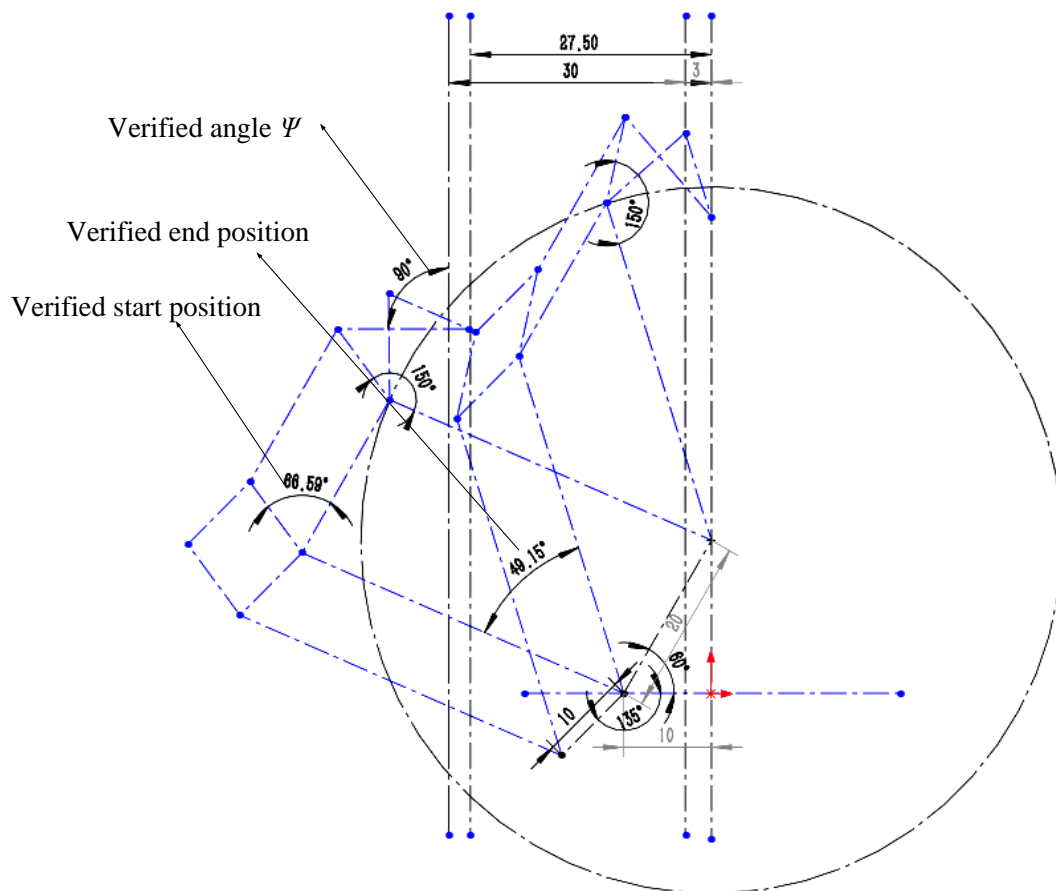


Figure 5.12. Final design after verification.

5.3.3 Kinematic Analysis of the Synthesized Meso-Gripper

In order to verify the parameters of the synthesized mechanism, a kinematic analysis of the mechanism is carried out. The most important geometric parameters are the drive angle and the motion between the contact surface and the object. Two different modes of gripping: passive-adjusting and angular gripping are now analysed. The rotating angle of driving link and the distance moved by point *I* on the contacting surface are the basic parameters required for further design of the drive method and the subsequent gripping force analysis.

As shown in Figure 5.13, the solid line diagram shows the final position for gripping a 55mm object and the dashed line diagram shows the initial position of the mechanism. Point *I* slides on the object surface using a slide link as shown. From this the rotating angle (*RA*) of the drive link is 6.42° and slide distance of point *I* about *y* axis (*U_y*) is 4.3mm.

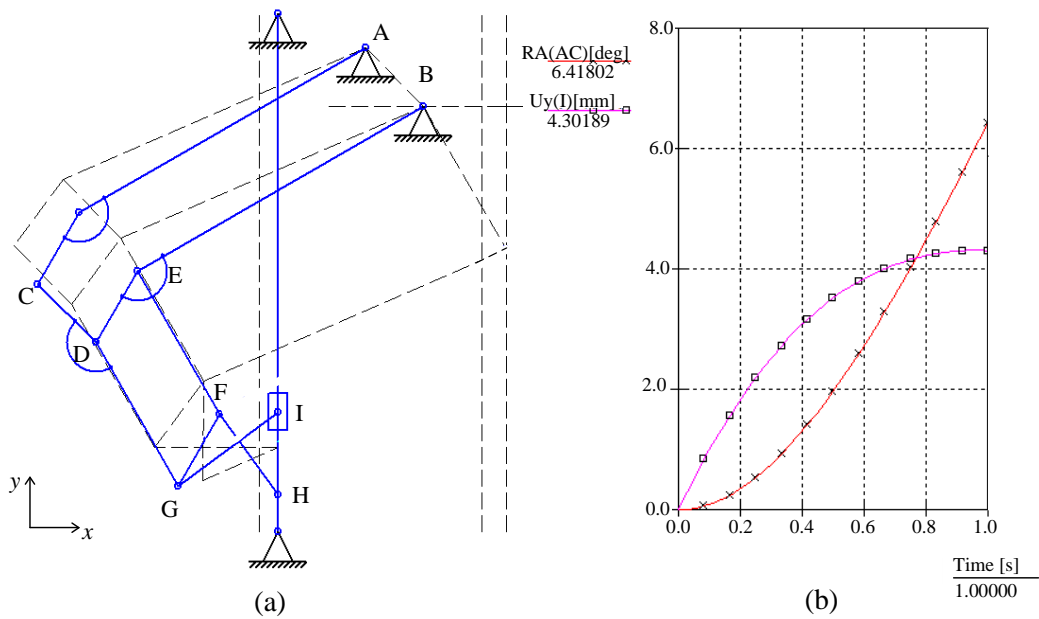


Figure 5.13. Gripping a 55mm object during passive-adjusting mode (a) Equivalent schematic; (b) Range of rotating angle of drive link AC and sliding distance of point I.

As shown in Figure 5.14, the gripping process for an object of 6mm requires a maximum rotating angle (*RA*) of drive link AC of around 2.9° and contacting point *I* sliding around 1.28mm.

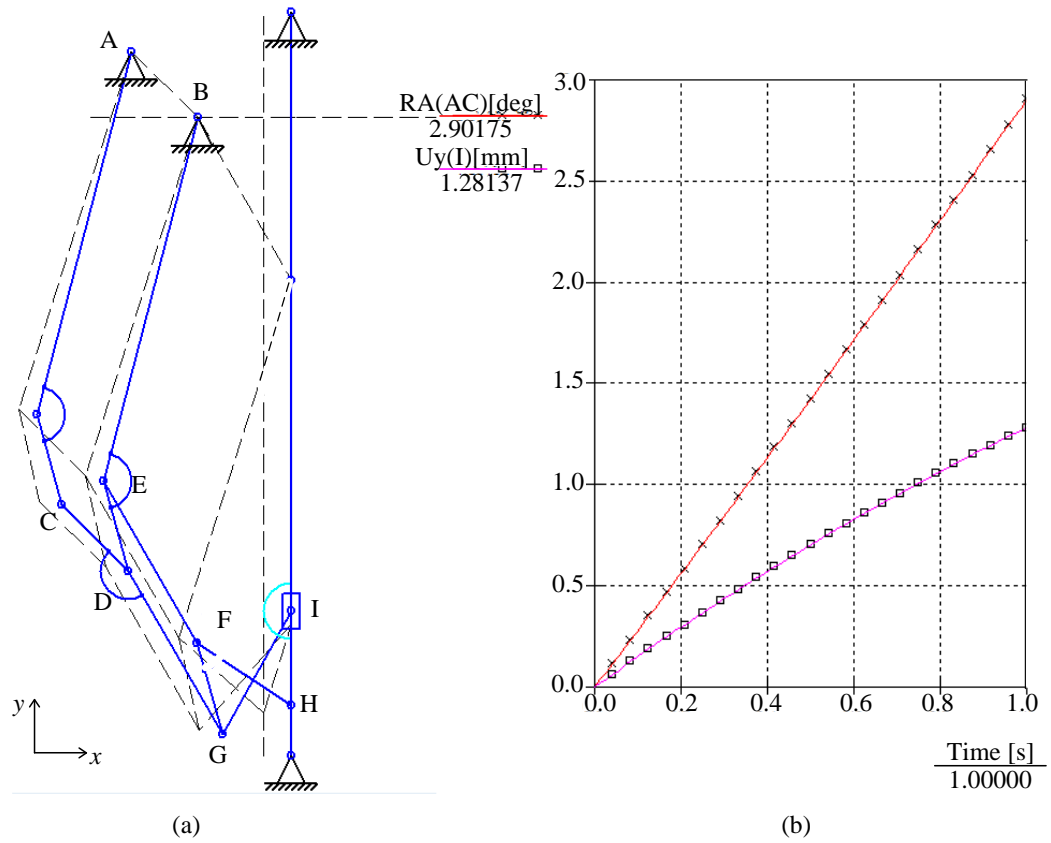


Figure 5.14. Gripping an object of less than 6mm at angular mode. (a) Equivalent schematic; (b) Range of rotating angle of drive link AC and sliding distance of point I.

5.4 Modified Multi-Mode Gripper

In Section 5.3, a geometrical constraint method was presented to design a gripper for a required gripping range. Kinematic analysis of the mechanism provides an understanding of the gripping process and determines the drive position. In this section, a modified design is presented by considering the mechanism and layout of the assembly for prototyping and manufacturing.

5.4.1 Modified Schematic of the Gripper

As shown in Figure 5.15(b), the integrated mechanism has four layers at the position of cross four-bar mechanism illustrated due to its multiple joints. This layout leads to the tip of the gripper being less stiff for accelerated gripping. So it is more advantageous to reduce the layers of the mechanism to provide a smaller gripping torque at the tip linkages.

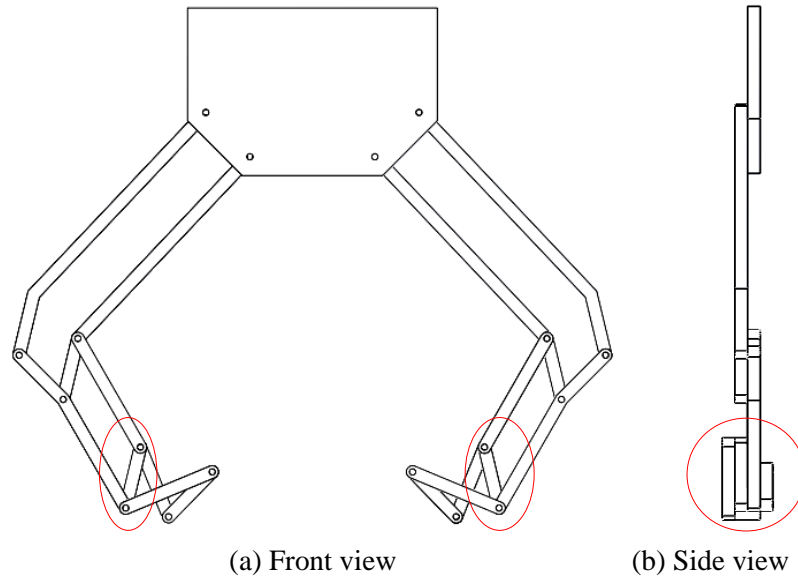


Figure 5.15. Layout of the meso-gripper assembly.

The CFB mechanism should be modified by changing the multiple joint of the connecting link into a single joint with the coupler link of the mechanism reduced in size to provide adequate space for the tip contact surface, as shown in Figure 5.16.

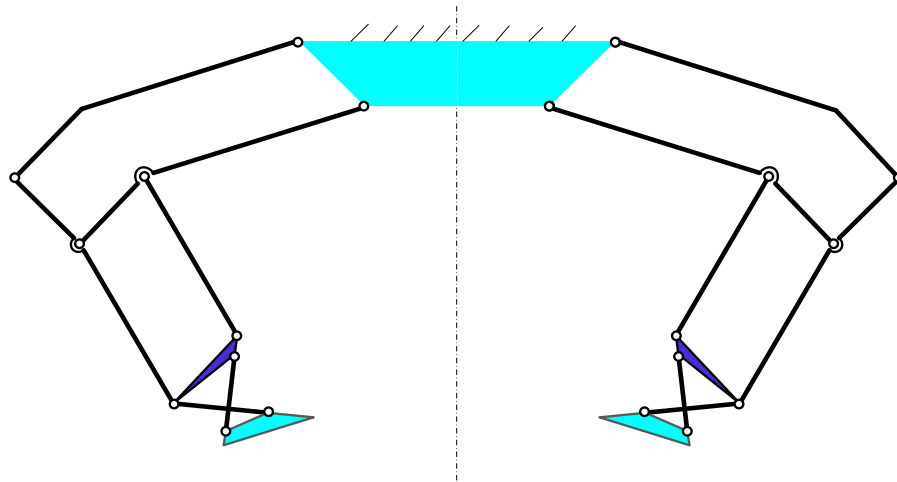


Figure 5.16. Modified schematic considering layers and contact surfaces.

Figures 5.17 and 5.18 show the kinematics of the meso-gripper at passive-adjusting and angular gripping modes. The rotating angles of the drive link at these two modes are around 8.65° and 2.91° and the sliding distances of contacting point I are 2.94mm and 1.24mm respectively.

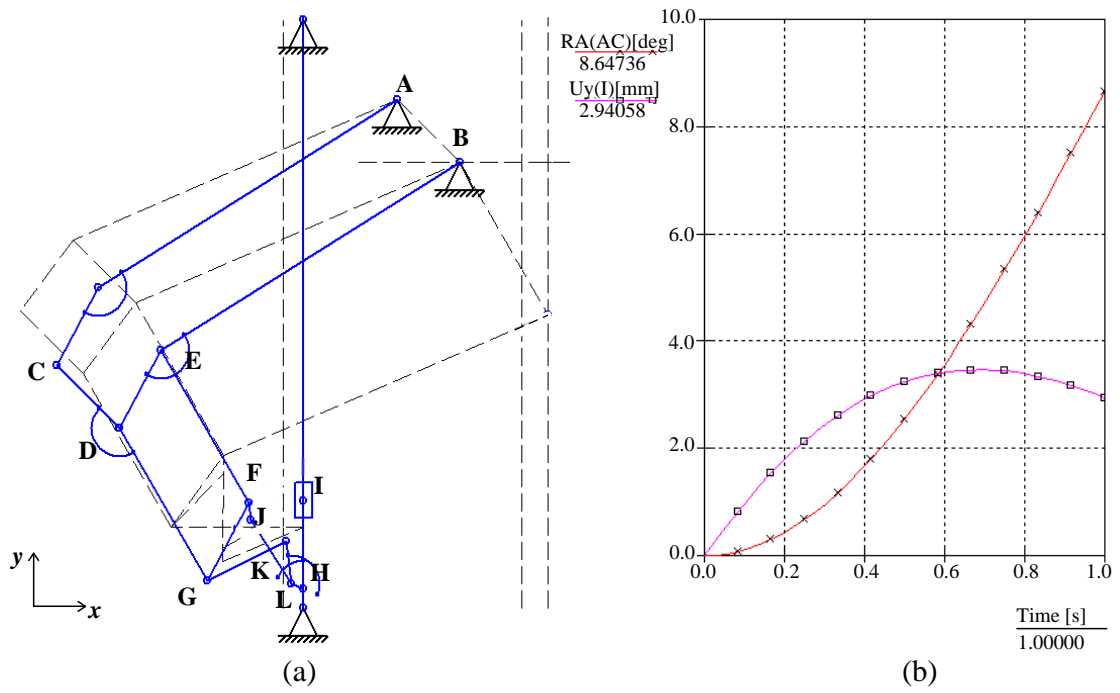


Figure 5.17. Kinematic analysis of the meso-gripper at passive-adjusting mode.

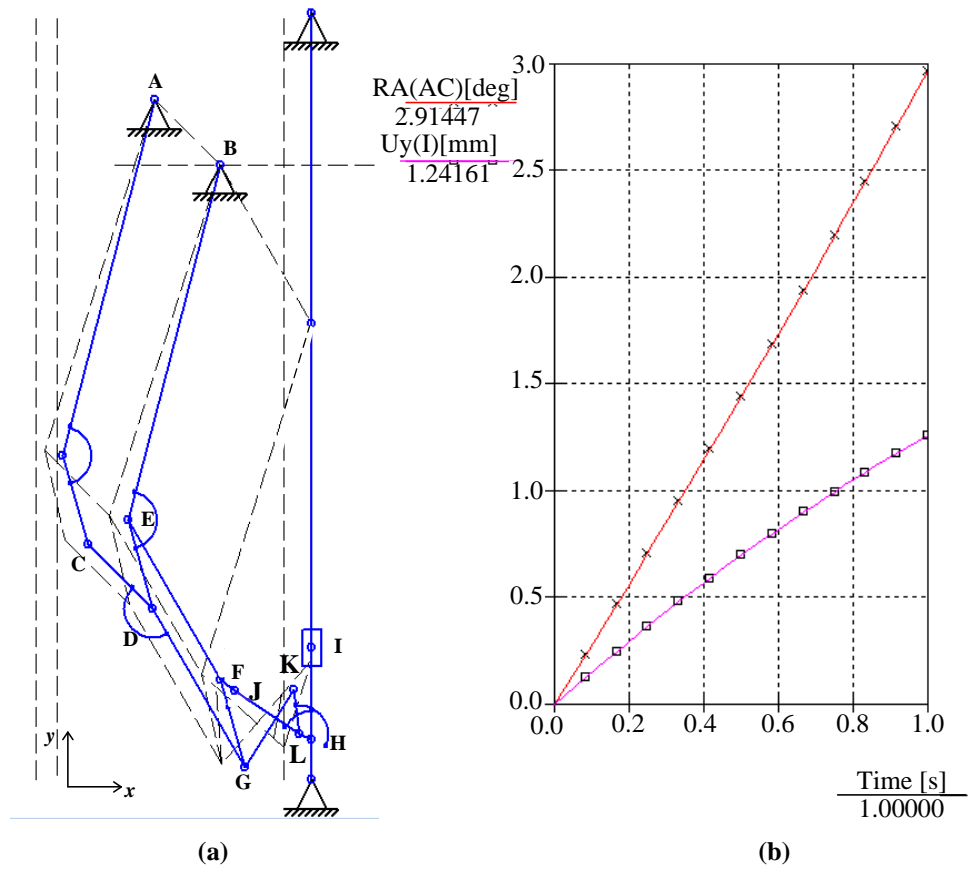


Figure 5.18. Kinematic analysis of the meso-gripper at angular mode.

5.4.2 Modified RCM-Based Finger

A typical RCM mechanism is a 6-bar over-constrained mechanism containing 3-parallelogram loops as shown in Figure 5.19(a). The mechanism transfers to one DOF by removing one connecting link of the parallelogram loop as shown in Figure 5.19(b). However, this simplification reduces the stiffness of the mechanism because one supporting link is removed. At passive-adjusting mode, the weight of the object and associated acceleration may result in a very large torque on some links; meanwhile the meso-gripper must be designed to be compact with each component being very small. This requires that the stiffness of the whole mechanism must be considered. Jensen [154] provided a design with pulley coaxial with the pivot by fixing connecting links on the pulley wheel as shown in Figure 5.20(a). Tendon- or belt-actuated mechanisms are limited to small gripping forces and lead to increased friction and elasticity. In this section an alternative approach to increase the stiffness of RCM mechanism is proposed by using redundant links as detailed in Figure 5.20(b).

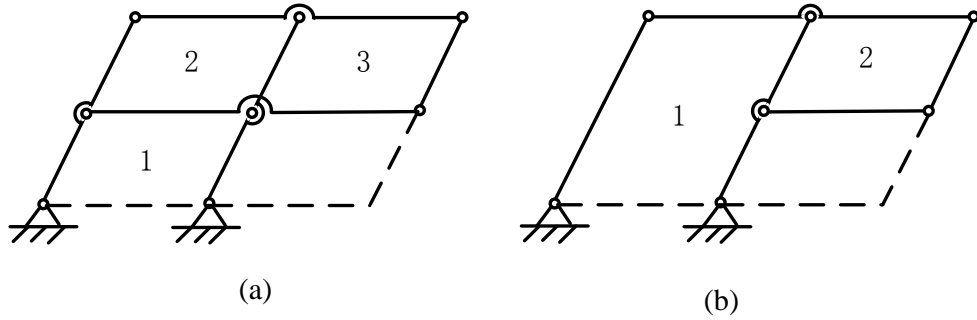


Figure 5.19. Simplification of RCM mechanism

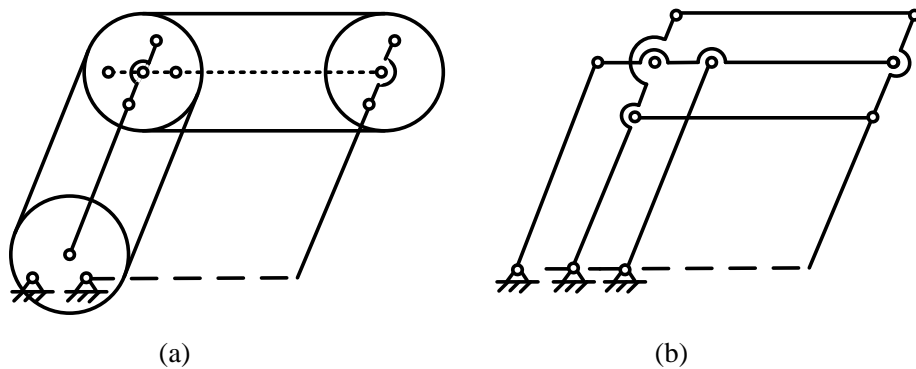


Figure 5.20. Pulley-driven mechanism and the equivalent mechanism

The modified RCM mechanism is developed as shown in Figure 5.21(a). Due to its geometric characteristics, the dimensions of the mechanism are determined by simplifying the angulated link, as shown in Figure 5.21(b).

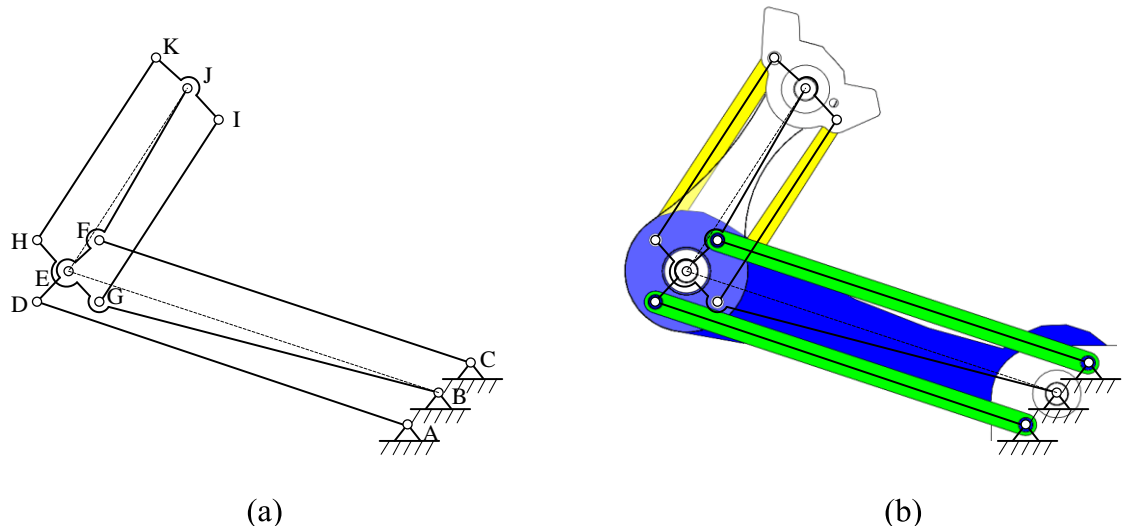


Figure 5.21. Modified schematic and 3D drawing of RCM

5.4.3 Modified CFB-Based Fingertip

A CFB linkage in Chapter 3 was used for passive adjustment due to the complicated contacting surfaces. References [155, 42] propose a method to exactly duplicate the kinematic characteristics of a rigid-link four-bar mechanism by using the centroids of the four-bar linkage. An overconstrained mechanism may be the best choice for machine design when larger and variable loads must be sustained by means of mass and compliance, especially when the maintenance of mechanical accuracy is important [156]. The continuous trajectories of fixed and moving centroids are the contact-aided surfaces for exactly duplicating the kinematic characteristics of rigid four-bar linkage.

According to the kinematic analysis shown in Figure 5.22, the drive angles of the crank links are calculated as 18.06° and 5.65° for adjusting and angular modes respectively. The larger angle of 18.06° should be selected to generate trajectories of fixed and moving centroids of the modified CFB mechanism.

The initial and final positions of the modified CFB mechanism are obtained while trajectories of the fixed and moving centroids of the mechanism are generated. By copying the corresponding files of the trajectories to the 3D modelling software (Solidworks), the over-constrained mechanism, considering the dimensions of crank and connecting links, is generated as shown in Figure 5.23(c).

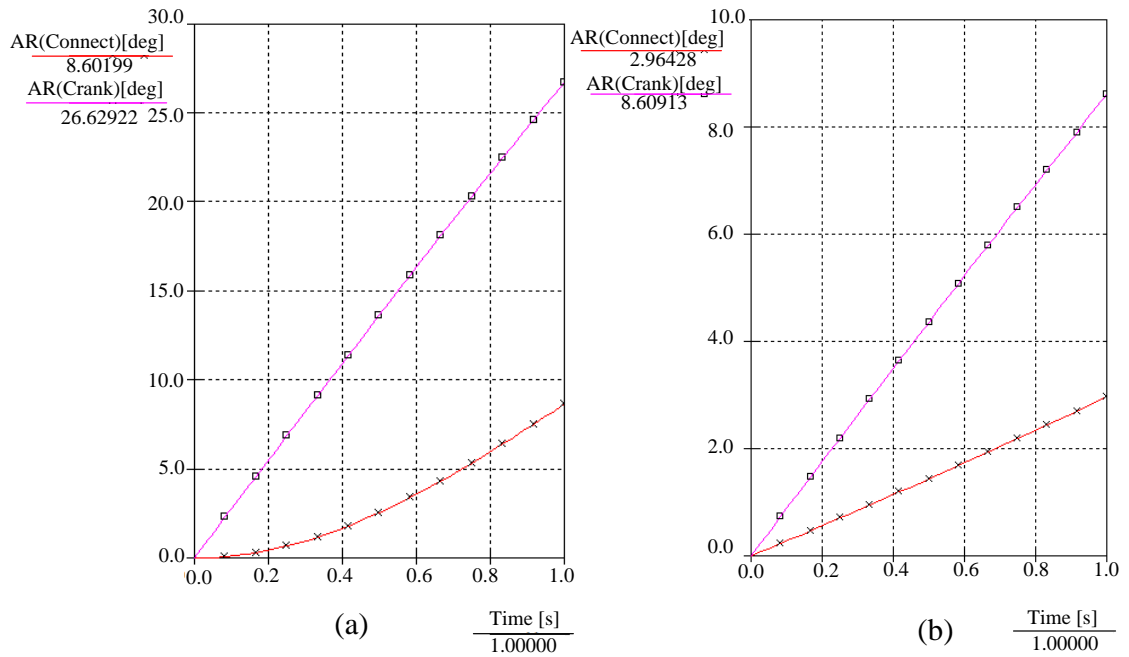


Figure 5.22. Relative angles of connecting and crank links for passive-adjusting and angular gripping modes

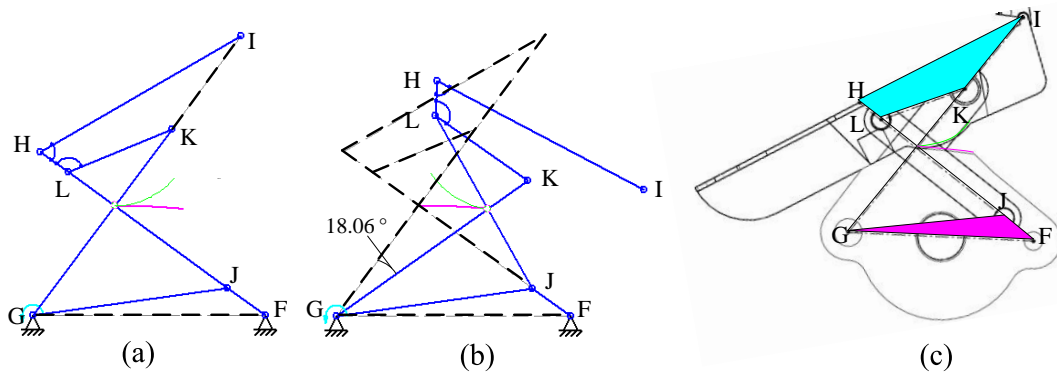


Figure 5.23. Initial and final positions of modified CFB Mechanism

5.5 Actuation and Transmission

5.5.1 Actuation

Robotic actuation provides a gripping action performed by an energy source. Considering the characteristics, the energy can be pneumatic, hydraulic and electrical. Generally speaking, motors are used to convert electricity into translation or rotation motion to produce mechanical energy. The gripping action can be conducted by different elements such as vacuum cups or fingers. The relationship between the drive and motion is shown in Figure 5.24.

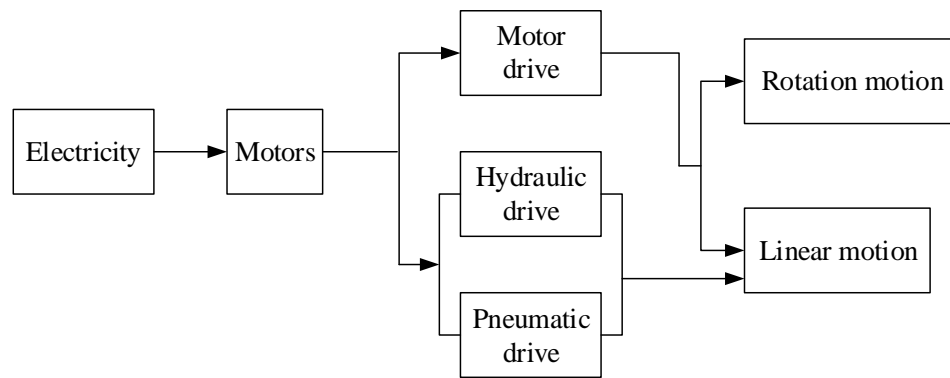


Figure 5.24. Relationship between drive and motion

The process of automation process is quite different from one to another. Choosing a gripper/hand there is a need to consider both economical and practical factors in automation projects, such as the task speed, gripping speed, parts, precision requirements and environmental needs.

A hydraulic drive needs hydraulic power generation components, complicated control equipment and perfect sealing technologies. Pneumatic drive are imprecise, difficult for positioning, speed and force/torque control. The maintenance requirements for both present significant costs. For instance, in some clean-area applications in electronic components manufacturing, the leaking oil or air contaminants are not acceptable. Electric drives with motors have more advantages when compared with the aforementioned two types. It is much easier to control position, speed and force/torque control, robust construction and high reliability, low cost, easy to integrate sensors and building distribution network. There are no air lines or oil pipes. The motor drive is much cleaner and available for a clean environment.

The speed and cost of a pneumatic drive are advantages. The disadvantages of it are that it has a slightly lower power to weight ratio than hydraulics and it is not as programmable or flexible as electricity.

5.5.2 Differential Force Transmission

The concept of underactuation [27] in robotic gripping with fewer actuators than DOFs allows the two fingers to adjust to irregular shapes without the need for complex control strategies and sensors. Differential mechanisms are used in robotic hands to provide underactuation, such as a movable pulley, seesaw mechanism, fluidic T-pipe and planetary and bevel gear differentials [157]. This differential system always locates at the transforming box of the gripper/hand. The most often used differential system would be a movable pulley. As shown in Figure 5.25, the two ends of the tendon are fixed

symmetrically in the two fingers' pulley wheels. The actuated power is distributed to the two fingers to facilitate gripping of non-centred or irregularly shaped objects.

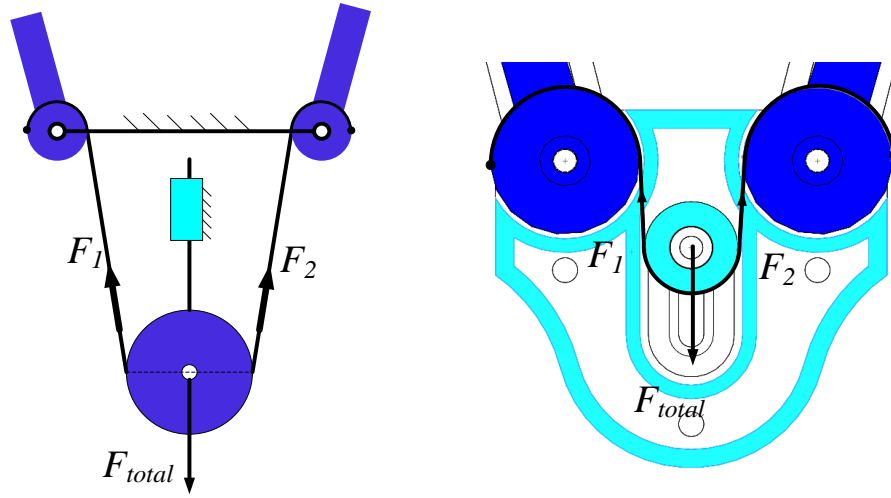


Figure 5.25. Movable pulley for differential force transmission.

In order to obtain more outputs, multiple differential devices can be added in parallel as shown in Figure 5.26, a differential system with four outputs which leads to an underactuated transmission for more phalanges. These two types of movable pulley differential systems have been used in the meso-gripper and precision-power gripper developed in this thesis. Some other differential systems using planetary gears can be found in [158].

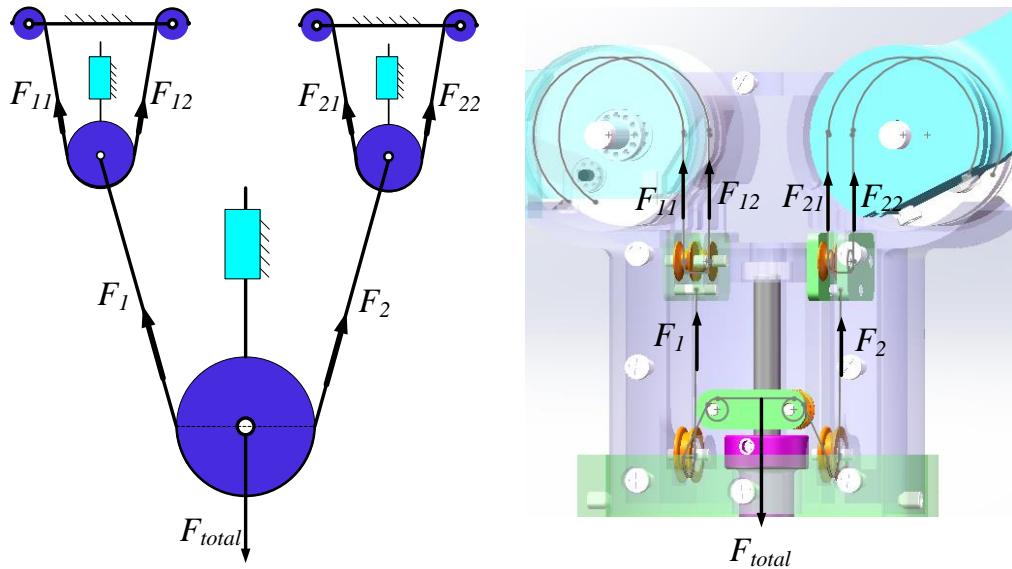


Figure 5.26. Differential mechanisms with four outputs.

Another differential or adaptive method for underactuation was presented in [159]. A breakaway clutch was provided by utilizing helical gears, as shown in Figure 5.27. As a consequence of the thrust load produced by a drive helical gear during motion, the driven gears can slide along the vertical axis. This motion may be triggered if one phalange is contacting an object while another is contactless or still on the way. The motion cannot reverse when the driven gear is not meshed due to the worm gear mesh in the next stage attached to each finger. This mechanism was used in reconfigurable hand development.

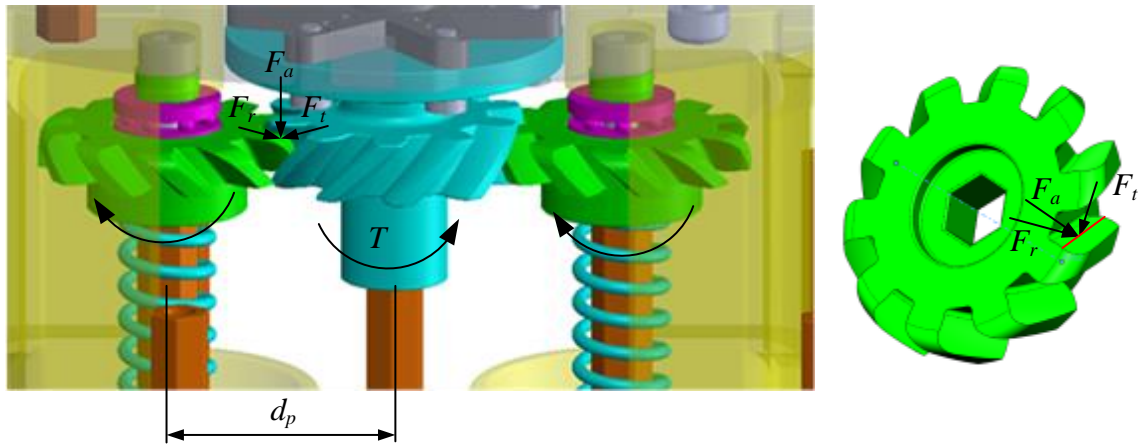


Figure 5.27. Breakaway clutch mechanism for differential transmission.

5.6 Prototyping and Testing

Based on the aforementioned design approaches and corresponding development process, three types of robotic grippers with different configurations and functions were developed. The first one is named meso-gripper following its main functions. This gripper has three different gripping modes for larger range gripping, specifically for meso-scale objects. The detailed idea generation, dimensional synthesis approach and optimization process have been provided in Sections 5.1, 5.2 and 5.3. The second gripper is a power-precision gripper, which has a power grasping capability compared to the meso-gripper due to the more complicated differential system. The third type is a reconfigurable gripper hand which has more functions with changeable fingertips for various objects. The modular finger makes the gripper easily transformable from two-fingered to three-fingered. The three types of hand/grippers are shown in Figure 5.28.

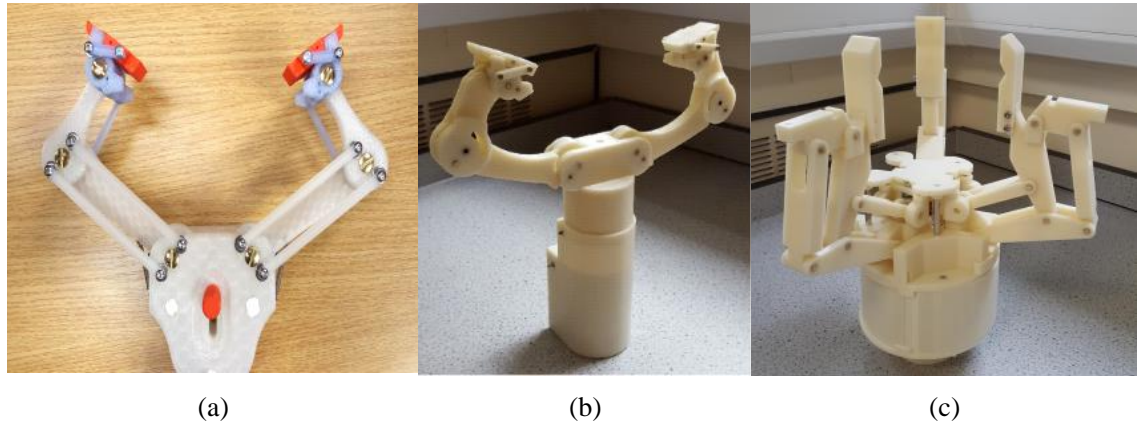


Figure 5.28. (a) passive-adjusting meso-gripper; (b) power-precision gripper; (c) reconfigurable gripper hand.

5.6.1 Meso-Gripper

The 3D model of the meso-gripper integrating passive-adjusting and angular gripping modes is shown in Figure 5.29. The whole design was scaled up to 200% for better 3D printing. The gripping range for passive-adjusting mode is 12-110mm and for angular gripping mode 0-12mm. The gripper hand is designed to mimic human grasping functions for handling solutions of meso-scale objects including small, fragile and light objects. It aims to provide a single hand or gripper that can handle components within the aforementioned meso-scale ranges to reduce assembly time and per unit cost of manufacture.

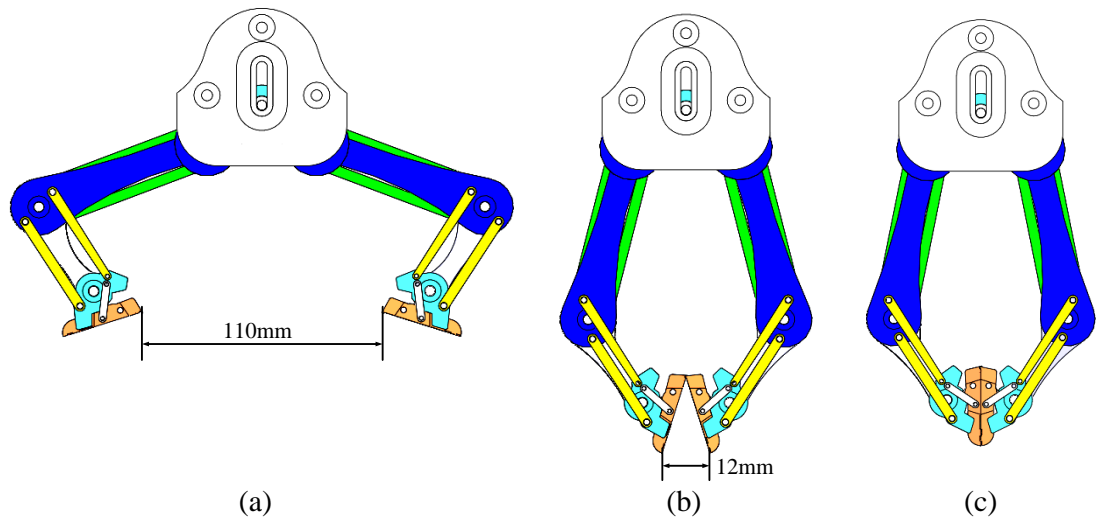


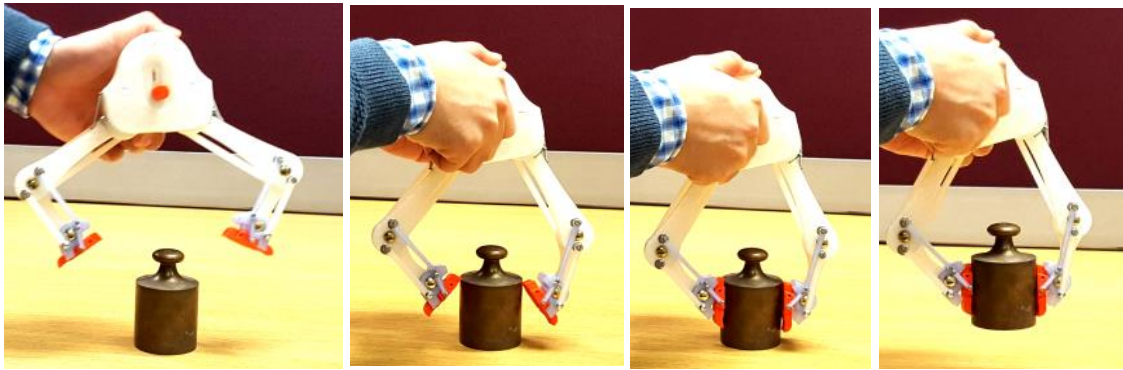
Figure 5.29. Meso-gripper with two modes

Most of the components of the gripper were manufactured via 3D printing. The material used for the gripper body is polylactide thermoplastic (PLA). For the coupler

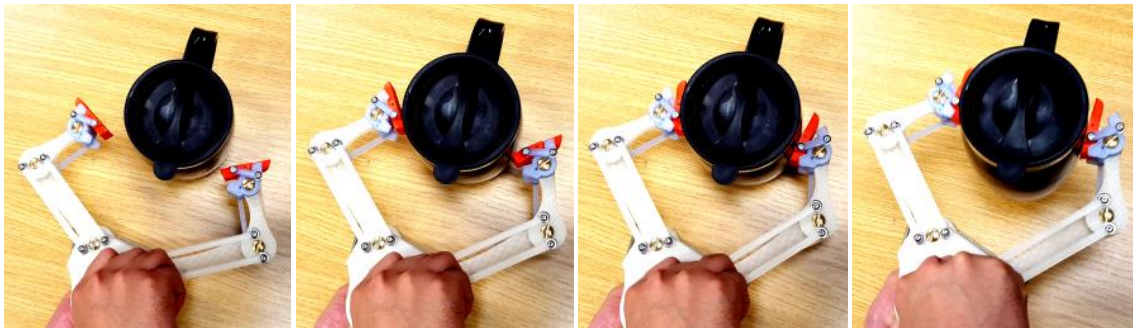
link of the CFB linkage a silicone elastomer was used. The prototype of the gripper can grip various objects manually using both modes.

As shown in Figure 5.30, objects used for testing the gripper's capabilities include regular shapes (cylinder, cone, hexagon) and irregular shapes (flat, sharp and pinecone). The sizes of these objects varied from 0.5 to 105mm with gripping loads varying from 0.5g to 1000g. For different types of objects the gripping approach was different, e.g. vertical gripping, horizontal gripping, passive-adjusting mode gripping or angular gripping. In all cases the meso-gripper performed successfully.

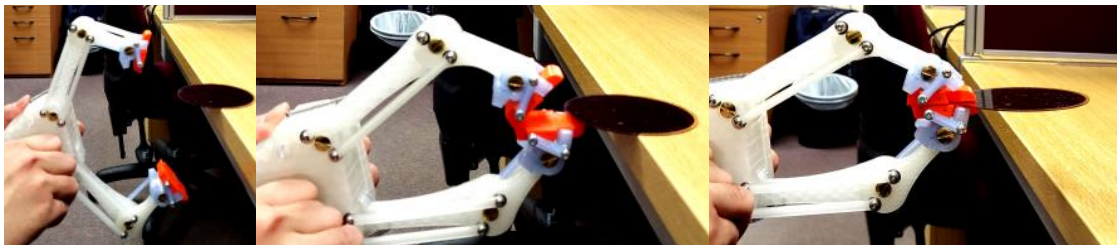
(<https://www.youtube.com/watch?v=TceAuoeYDb0>)



(a) Weight, 1Kg, dimensions: $\Phi 50\text{mm} \times 55\text{mm}$

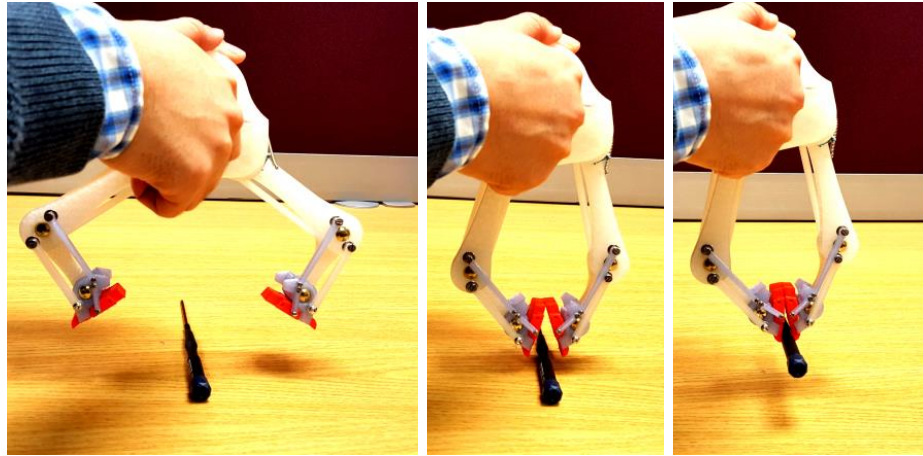


(b) Café cup, 450g, dimensions: $\Phi 105\text{mm} \times 120\text{mm}$

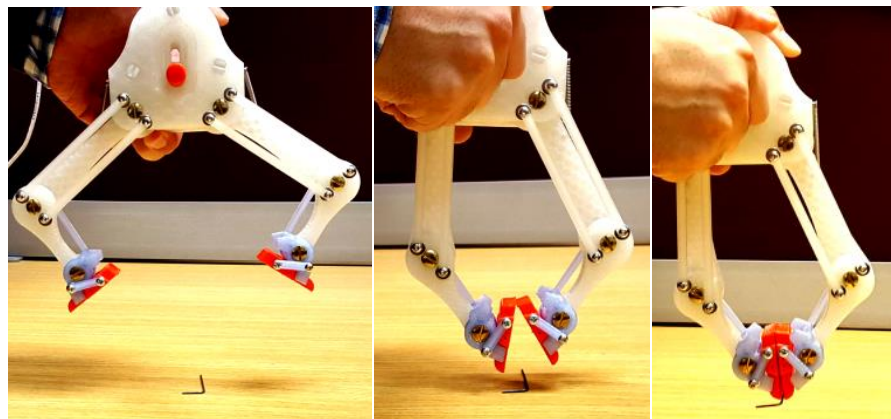


(c) Wafer, 9.5g, dimensions: $\Phi 76\text{mm} \times 0.8\text{mm}$

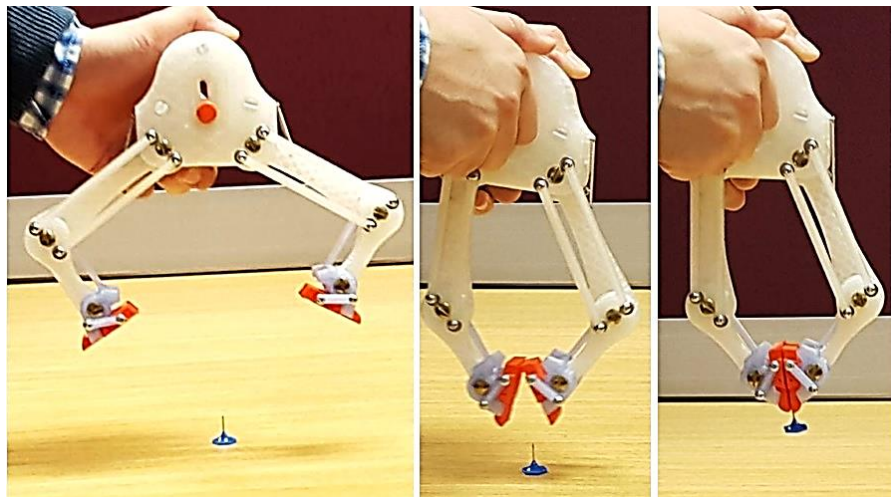
Figure 5.30. Gripping tests for different objects (to be continued).



(d) Screw driver, 12g, dimensions: $\Phi 7\text{mm}$ - $\Phi 10\text{mm}$

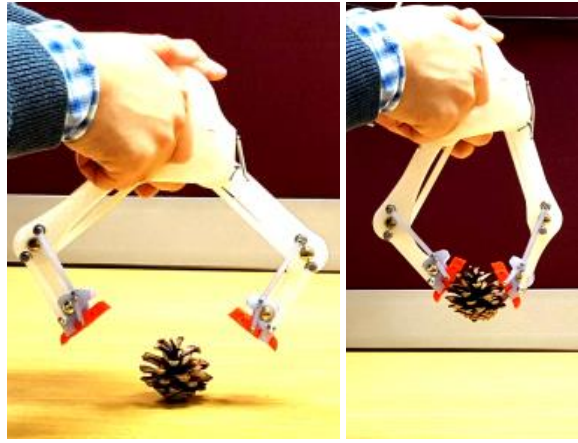


(e) Hex wrench, 0.5g, dimension: $\Phi 1.5\text{mm}$



(f) Stick pin, 0.5g, dimensions: $\Phi 0.5\text{mm}$ - $\Phi 1\text{mm}$

Figure 5.30. Gripping tests for different objects (to be continued)



(g) Pinecone, 10g, irregular shape

Figure 5.30. Gripping tests for different objects (continued).

5.6.2 Power-Precision Gripper

A precision-power integrated gripper with four differential outputs is shown in Figure 5.31. In addition to precision and passive-adjusting gripping modes, it can also be used for power grasping.

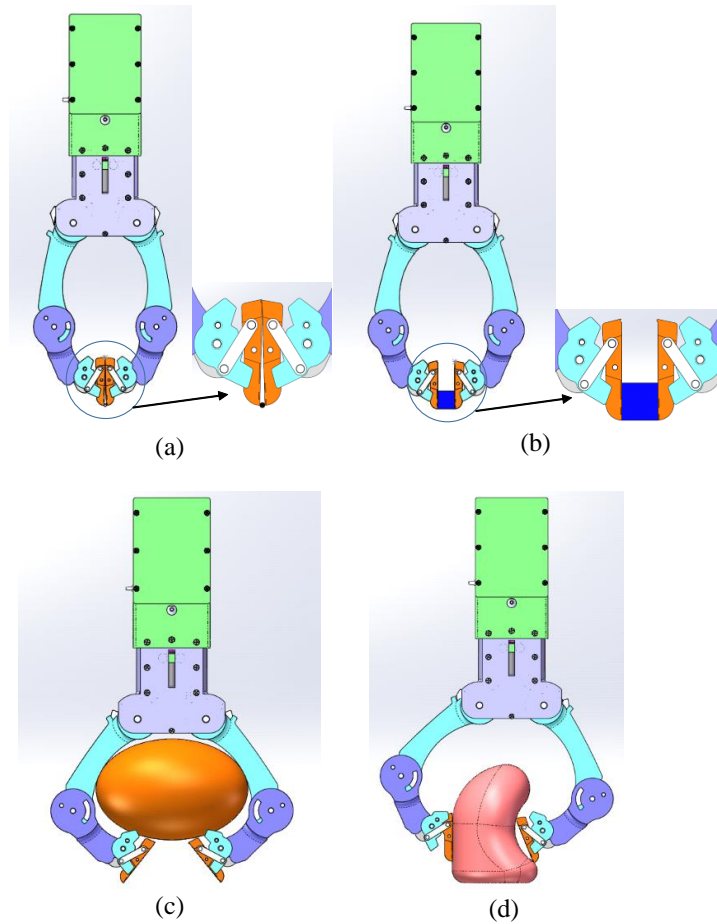


Figure 5.31. Four modes of power-precision gripper. (a) precision gripping; (b) passive-adjusting modes; (c) differential modes; (d) power modes.

The diagram of four-output differential mechanism with two differential ends being connected to the left and right link drive members as shown in Figure 5.32. The diagram can also be found in Figure 5.26, Section 5.5.2. The internal proximal link has a first end rotatably attached to the link drive member and a second end attached to the first end of a distal finger member. Therefore, the differential force can be transformed from drive to the distal finger. This is the most different characteristic and related solutions for power gripping. More details can be found in the patent [44].

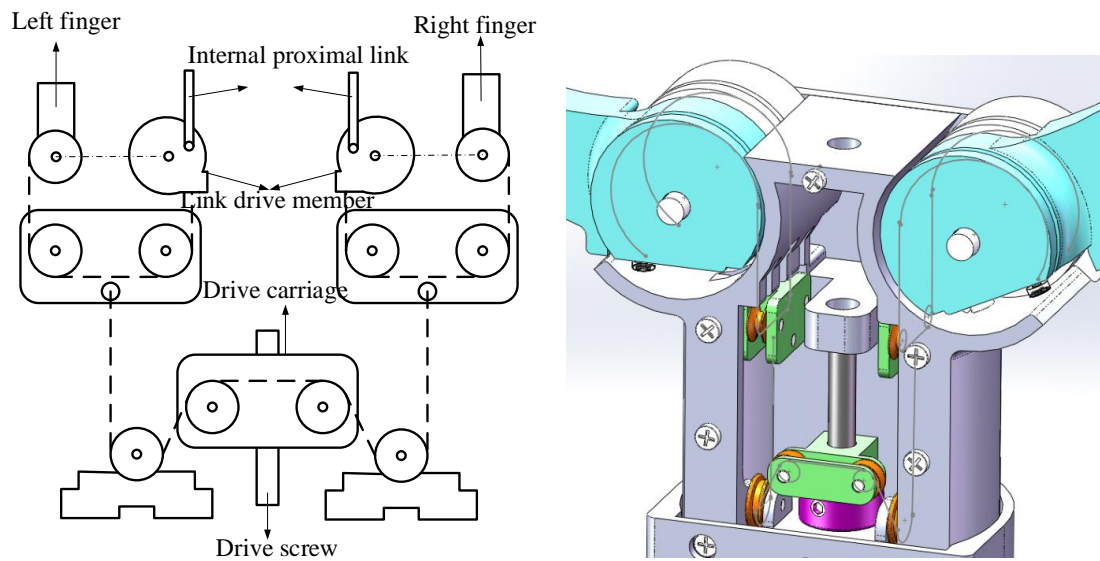


Figure 5.32. Transmission diagram and 3D drawing of four-output differential mechanism

5.6.3 Reconfigurable Hand

Static analysis of the RCM finger in Section 4.3.3 indicates that RCM mechanism has parallel and angular motion with respect to two inner links. This characteristic means that RCM mechanism can provide two types of motion as a gripper finger. The changeable tips provide the gripper reconfigurable functions that are able to grip a wider variety of objects.

Pre-configuration gripping always means the gripper can transfer their configurations before gripping. Take the Barrett hand as an example, objects are classified and the gripping simulations are used to optimize gripping activities. In practical objects grasping activities, a transformation from 2-fingered to 3-fingered is necessary. A platform with changeable fingertips and transformable fingers is developed, as shown in Figure 5.33.

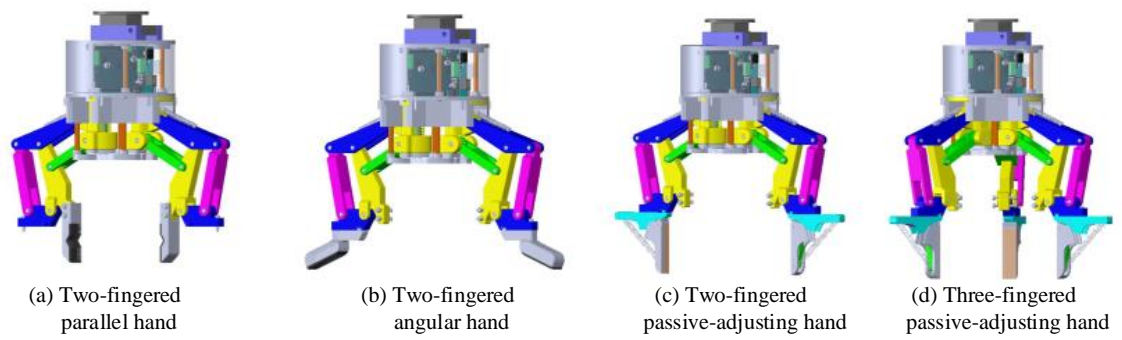


Figure 5.33. Reconfigurable hand

The subassemblies of the main body of the reconfigurable hand are shown in Figure 5.34. A platform with one end connecting with the actuator and the other coupled with helical gear can support two or three fingers. The finger assembly contains helical and worm gear sets for power transforming and fast-changing heads for fingertips. Fingertips are components or assemblies for different applications. Here three components are provided for three types of motion in terms of parallel, angular and passive-adjusting.

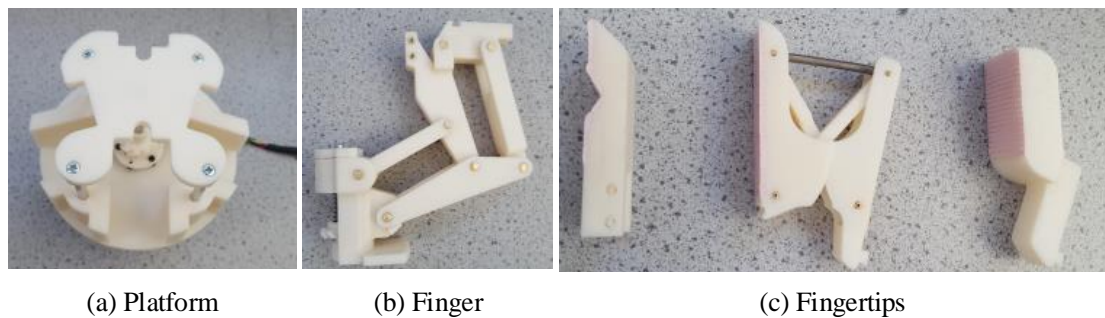


Figure 5.34. Independent assemblies of the main body

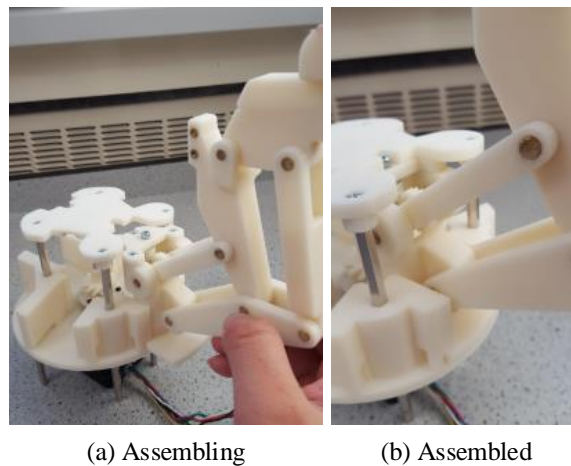


Figure 5.35. Finger assembly process

These components or assemblies can be assembled freely by considering practical grasping activities. Equally, manufacturers only need to purchase one gripper hand which can transform from two to three fingers and can also grasp by changing fingertips. The fast-changeable design make the transformation process easy and efficient. This is also a low-cost and affordable approach for a reconfigurable gripper hand. The finger assembly process is shown in Figure 5.35.

The power transforming mechanism of the gripper is based on a breakaway clutch mechanism, see Figure 5.36. Three fingers are driven by a single actuator through the breakaway clutch mechanism comprising helical gears. This type of underactuated principle is able to provide full action of each finger for object contact. The process is such that if one finger is blocked by the contact object, some other fingers will continue the closing sequence until all the fingers make contact.

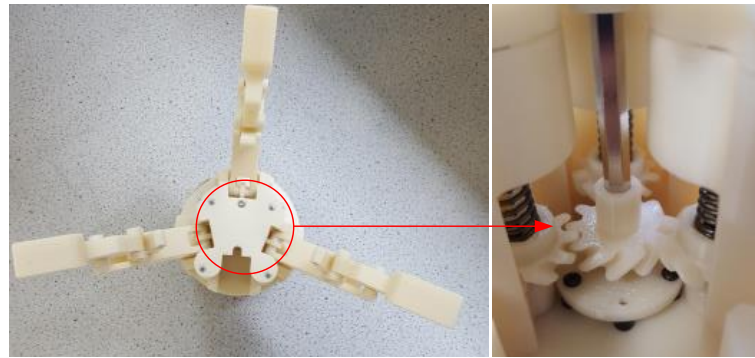


Figure 5.36. Breakaway clutch mechanism for three-fingered hand

A prototype of the gripper hand and the hand's grasping configurations are shown in Figure 5.37.

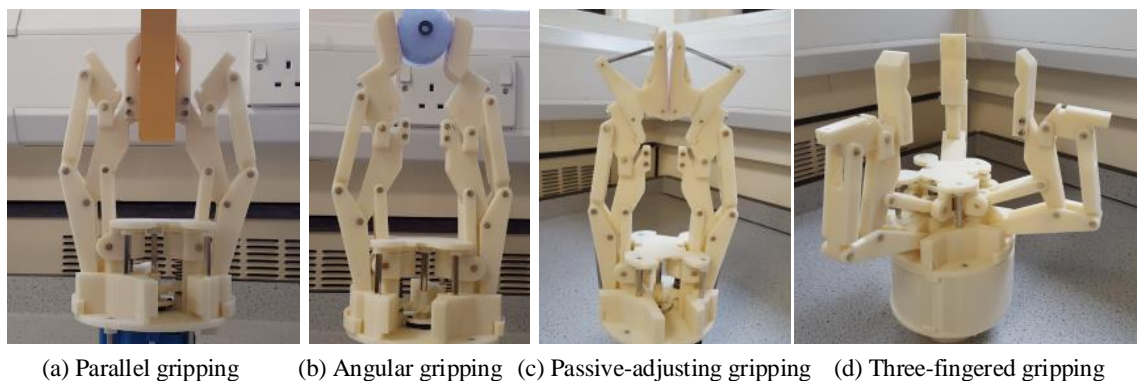


Figure 5.37. Prototype of reconfigurable hand

A comparison of these three types of gripper hands developed in the work is shown in Table 5.1.

Table 5.1. Comparison of developed gripper hands

	Functional Mode	Drive	Control
Meso-gripper	Angular mode, Passive-adjusting mode.	Manual	N/A
Power-precision gripper	Angular mode, Passive-adjusting mode, Power gripping mode.	DC motor	Position
Reconfigurable hand	Angular mode, Passive-adjusting mode, Parallel mode, 3-Fingered mode.	Stepper & driver	Position, speed, (torque)

5.7 Summary

This chapter has introduced the concept of the meso-scale for robotic gripper design as well as providing a formalization of a methodology for such gripping systems. It has also demonstrated and validated this methodology through the design, analysis and testing of a meso-gripper combining two integrated operational modes, passive-adjusting and angular gripping.

In order to mimic the gripping process of the human hand, a meso-gripper integrating a RCM mechanism and CFB linkage was developed by using a geometrical constraint approach for dimensional synthesis of the mechanism. The kinematics of the synthesized mechanism were analysed. The modified design considered the stiffness and layout of the mechanism providing a self-checking approach before manufacturing. A 3D-printed operation prototype was tested for gripping different types of objects. The results show the gripper with passive-adjusting and angular gripping modes can achieve universal gripping within the meso-scale at scales as small as 0.5mm with a gripping load of as little as 0.5g. The general purpose meso-gripper successfully addresses the gap identified in the introduction. In addition, another two gripper hands based on the proposed design approach were also successfully developed and tested.

CHAPTER 6 – Conclusions

6.1 General Conclusions

This thesis has presented a design process for a class of novel robotic gripper hands or end-effectors. Reconfigurable topology and variable mobility of the design offer versatility, adaptability and low cost for the changing environment and demand. To meet requirements of fast-shifting and customised manufacturing in the 3C industry, affordable and adaptive end-effectors for miniaturized product assembly are necessary to research and develop.

The thesis first investigates the key challenges and unmet needs in this research area, analyses potential objects and defines a meso-scale gripping range. A general development process has also been considered. Based on the investigation and outlines of design process of a novel gripper, the following three chapters provide three important components and their novel development. Chapter 2 referred to a novel CFB-based finger joint design for mimicking a human hand joint. Chapter 3 analysed CFB linkages and its potential application as fingertip. Chapter 4 provided an RCM-based finger which contains three motion modes in terms of angular, parallel and underactuated grips. The previous chapter (Chapter 5) describes the detailed development process of the novel adaptive gripper hands. Three types of gripper hands have been developed as examples of the methodology and solutions.

6.2 Contributions

The development of adaptive or reconfigurable hands has been conducted by many groups worldwide, each one having distinctive characteristics. This thesis has defined a class of adaptive hands with their own novel and distinctive features. The miniaturized manufacturing process, especially an assembly process, by mimicking the human hand and then integrating meant that mechanisms synthesis and multi-mode, reconfigurable and metamorphic concepts, the functional gripper hands were finally invented.

Before the development of each significant component of the adaptive gripper hands, some simple and general four-bar or six-bar mechanisms were also reviewed. These mechanisms are fundamental for such novel applications and gripper design. Taking the CFB mechanism as an example, if the gripping capability is not brought into this simple mechanism, it is impossible to discover its multi-mode function for different type of object gripping and stability analysis. The RCM mechanism is in the same situation. This six-bar linkage had been specific to a steady-hand system for minimal invasive surgery (MIS). An extension for gripper finger design provides a more profound meaning. The RCM-based finger contains inherent angular, parallel and underactuated

modes and is a perfect choice for a gripper finger. No one had thought out or developed one gripper hand which integrates these three different motion modes until now. Another significant advancement is that all of these modes can be actuated with only one actuator.

The design of each type of gripper hand has many advantages: less complicated, cheaper, mechanical intelligence, less need for control. Even though the prospect cost for this type is not as low as some simple parallel or angular grippers. The general cost considers multiple modes for various objects, saving time for change over during the manufacturing process, etc. The design is also a valuable attempt to promote the development of adaptive gripper hands.

The critical issues facing manufacturers and the assembly industry are based around three challenges: versatility, adaptability and low cost. The adaptive gripper hands researched make versatile manipulators that can achieve combined tasks, decreased changing times and costs and accommodate uncertain grasping tasks and unstructured ambient conditions. The design of each type of gripper hand has achieved a phased objective.

6.3 Future Work

Much research work and technologies still need to be addressed in the future work.

All the gripper hands presented in the thesis were 3D printed. For precise force testing, these models are not sufficient.

The analysis must be extended to dynamic situations for reliable product development.

For complex handling tasks, adaptive control, tactile and vision sensings can significantly increase performance. Force and position control is not difficult for the last type of reconfigurable hand. In some situations, stiffness, compliance control and sensory feedback also need to be considered.

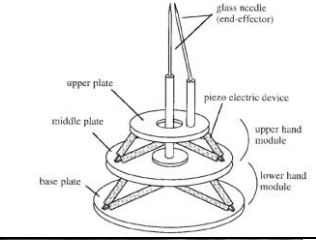
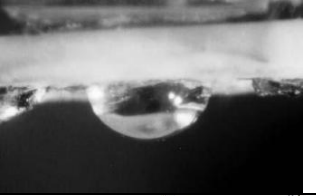
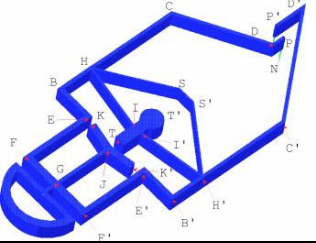
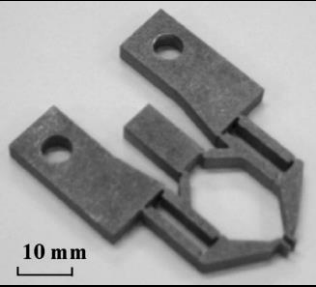
Grasping planning and manipulation are becoming more and more important because of the wide application of robots needing stable and fast motions when carrying out complex tasks as well as interaction with humans and the ambient environment. Current versions of gripper hands do not yet possess these functions.

Appendix A – Specifications of Commercial Robotic Grippers/Hands

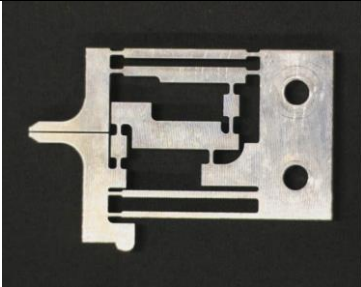
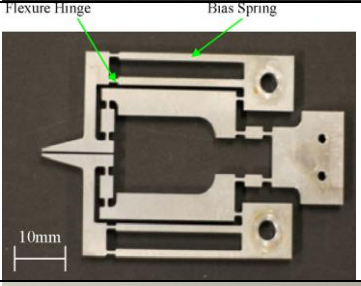
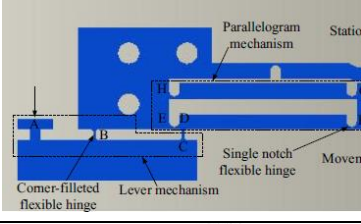
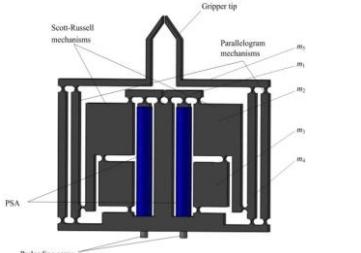
Company	Type		Actuator	Stroke(mm)		Gripper force(N)		Load(Kg)	Finger length(mm)	Weight(Kg)
				Maximum	Minimum	Maximum	Minimum			
Festo	2-Finger parallel	DHPS-6/35	Pneumatic	4/25		910	25			0.019-1.285
	2-Finger angular	DHWS-10/40	Pneumatic	Angle:40 °		25/200	0			0.04-0.775
	2-Finger radial	DHRS-10/40	Pneumatic	Angle:180 °		30/200				0.044-0.829
	3-Finger parallel	DHDS-16/50	Pneumatic	5/12		87/750				0.096-0.92
IAI	2-Finger slider	RCP	Electric	30	4	220	10			0.085-1.6
	2-Finger lever	RCP	Electric	Angle:180 °		90	6.4			0.2-1.4
	3-Finger slider	RCP	Electric	14	10	102	22			0.6-1.2
	3-Finger lever	RCP	Electric	Angle:19 °		50	18			0.6-1.1
PHD	2-Finger parallel	Preci-parallel	Pneumatic	26	6.5	3581	124		191(max)	0.08-1.96
		Micro-parallel	Pneumatic	13	4	123	11		100(max)	0.036-0.28
		Heavy	Electric	26	6.5	1703	179		190(max)	1.22-6.12
	2-Finger angular	Micro-angular	Pneumatic	Angle:40 °	Angle:40 °	133	13		80(max)	0.034-0.244
	3-Finger parallel		Pneumatic	40	6	6459	196		200(max)	0.12-7.05
Robohand	2-Finger parallel	DPE-400	Electric	20	10	1334	445		125(max)	2.52
		DPE-200	Electric	25	25	111	111		76.2(max)	0.53
		DPE-100	Electric	4	4	5	5		50(max)	0.23
		Preci-parallel	Pneu/Hydra	30	10	11475	176		500(max)	0.5-8.7
		Industry	Pneumatic	70	4	28000	36		406(max)	0.024-9
		Heavy	Pneumatic	350	19.05	3520	222		813(max)	0.3-15.8
	3-Finger parallel		Pneu/Hydra	70	4	11190	422		406(max)	0.24-43.9
	2-Finger angular		Pneumatic	Angle:180 °	Angle:0 °	7911	32		280(max)	0.09-6.7
Robotiq	2-Finger adaptive	85	Electric	85/85	1/43	220	5	5	100	0.85
	2-Finger adaptive	140	Electric	140/140	1/90	110	10	2.5	150	1

	3-Finger adaptive		Electric	155/155	1/20	60	15	2.5/10	150	2.3
Schunk	2-Finger parallel	EGP 40	Electric	12		140	40	0.7	50	0.35
		WSG 50	Electric	110		80	5	0.4	170	1.2
		PG-plus 70	Electric	60		200	30	1	140	1.2
SMC	2-Finger parallel	MHQJ2	Pneumatic	28	4	227	7.8			0.9-1.96
	2-Finger toggle	MHT2	Pneumatic	Angle:28 °	Angle:-3 °	Moment:106N.m	Moment:12.4N.m		32	0.79-2.9
	2-Finger angular	MHC	Pneumatic	Angle:30 °	Angle:-10 °	Moment:0.038N.m	Moment:0.017N.m		20	0.095-0.22
	3-Finger parallel	MHR	Pneumatic	18	6	59	12		50	0.1-0.76
	To be continued									
	Continued									
	4-Finger parallel	MHS	Pneumatic	64	4	537	23		40	0.08-1.13
Sommer	2-Finger parallel	MGP80x	Pneumatic	24	2	400	6			0.008-0.46
	2-Finger parallel	GP12	Pneumatic	26	6	450	4			0.003-1.4
	3-Finger parallel	MGD80x	Pneumatic	24	2	1130	30			0.025-2
	3-Finger parallel	GD	Pneumatic	180	120	Moment:9N.m	Moment:0.12N.m			0.038-2
Univer	2-Finger angular	YMA10	Pneumatic	Angle:30 °	Angle:10 °	Moment:3.05N.m	Moment:0.2N.m		30-85	
	2-Finger 180 ° angl	YMA20	Pneumatic	Angle:180 °	Angle:-3 °	78	6		60-90	
	2-Finger parallel	YMP10	Pneumatic	16	6	81	5		30-85	
	2-Finger parallel-G	YMP20	Pneumatic	30	4	318	16			
	3-Finger parallel	YMP50	Pneumatic	32	4	1310	16			
Yamaha	2-Finger parallel	Single cam type	Electric	23.5	3.2	40	5			0.09-0.58
	2-Finger parallel	Double cam type	Electric	19.3	5	250	50			0.2-0.8
	2-Finger parallel	Screw type	Electric	38	19	150	50			0.42-0.89
	3-Finger parallel		Electric	30	3.5	20	2.5			0.09-0.64

Appendix B – Micro - Nano Grippers

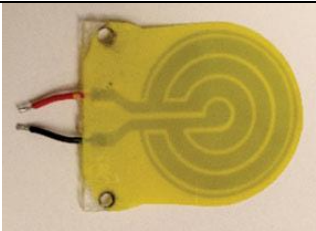
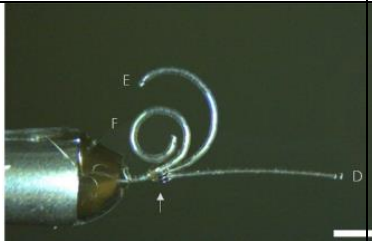
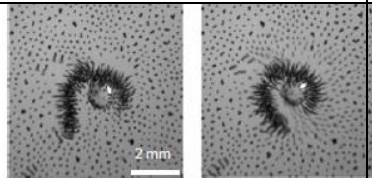
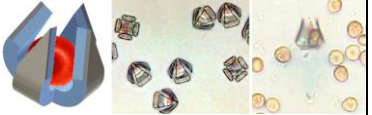
Date	Name	Schematic/prototype	specification	Power/actuator	manipulation	application
1999	Two-fingered micro-hand [48]		Parallel mechanisms; 3 DOFs translational motion; 3 dimension region; 0.1μm accuracy.	Piezoelectric device, 16μm for 150V Master-slave system,	Moving, catching, rotating, releasing	Assembling micro-machines, Manipulating biological cells, Performing micro-surgery.
2003	Electroadhesive microgripper [49]		400-900mm diameter half-spherical lens.	3KV/m power	Air, gas or vacuum environment catching and moving.	Delicate, polished and/or coated optical and electro-optical microcomponents.
2004	Contact-aided compliant mechanism[50]		Translation input to output curves; 130×36×136.35 mm; Homopolymer polypropylene sheet; 2 dimension region;	Stepper motor	Curve paths	Cell harvesting, Tissue culture sample cutting
2007	Monolithic compliant-flexure-based microgripper [51]		Spring steel; Grasping size range: 200–800m, Two dimension. Displacement amplification: 3.0; Maximum stroke: 170μm	Lead–zirconate–titanate (PZT) piezoelectric actuator;	Clamping and releasing	Assembly of miniaturized gear systems
To be continued						

Continued

2009	Compliant-based microgripper [52]		Translation to rotation; Amplification mechanism; wire electro-discharge machining Two dimension. amplification: 3.68 maximum stroke: 100 μm	PZT actuator	Clamping and releasing	Manipulation
2009	Hybrid flexure-based microgripper [53]		Parallel motion; wire electro-discharge machining Two dimension. amplification: 2.85 Maximum stroke: 100 μm	PZT actuator	Clamping and releasing	Assembly operations
2014	Monolithic compliant gripper[54]		Lever mechanism and parallelogram mechanism; Two dimension. control: PID algorithm, visual and force feedback; grasping range: 200 μm ; amplification: 6.0	Stack piezoelectric ceramic actuator (SPCA) actuator	Clamping and releasing	Micro-assembly
2014	SR-based compliant gripper[55]		Scott-Russell mechanism; Control: labview real time; Two dimension and three dimension. Grasping range: 1000 μm ; amplification: 22.2;	Stack PZT actuator	Clamping and releasing	Micromanipulation and microassembly

To be continued

Continued

2014	Electrostatic/gecko-like adhesive gripper[56]		Hybrid electrostatic/ dry adhesive; 2-4KV high voltage; Microwedges;	5kV DC-DC converter	Pneumatic air slide actuator	Manufacturing, mobile robots, and grappling objects in a space environment
2015	Microrobotic tentacles [57]		Shape-engineered elastomeric microtubes microtube inner diameter: 100-125 μ m; tube-wall: 8-32 μ m; long: 5-8mm; liquid-phase poly (dimethylsiloxane) (PDMS) grasping radius range: 185 μ m; grasping force range: 0.78mN;	Pneumatic actuator(PDMS /polyimide-based pneumatic balloon actuator)	Spiraling motion	Vivo biomedical manipulation
2011	Colloidal asters [58]		Colloidal structures; ferromagnetic colloidal suspension; viscous drag force: 10 ⁻⁶ N; viscous torque: 10 ⁻⁹ Nm;	Alternating magnetic field	Capture, transport, and position	Self-assembled microrobots.
2014	Self-folding Grippers [59]		Material: biocompatible and bioresorbable silicon monoxide and silicon dioxide; Folding angle:100 °; Folding radii: 765nm; Thickness: 3-27nm.	Release of residual stress	Folding and release	Single cell capture,

Appendix C – Grasp Taxonomy

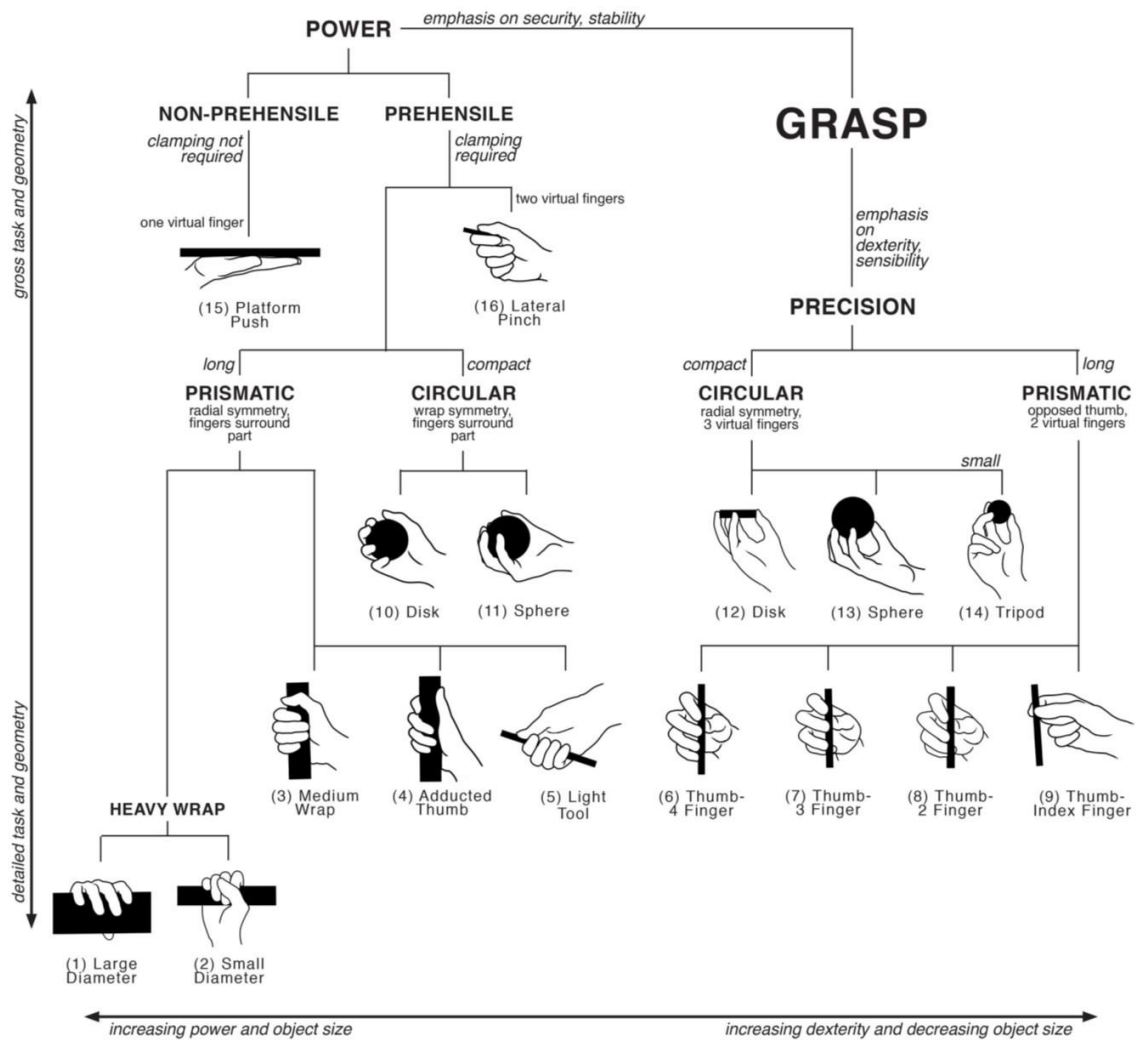


Figure C.1. Cutkosky grasp taxonomy [71]















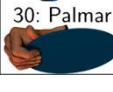
		Power					
Opp: VF:		Palm		Pad			
		3-5	2-5	2	2-3	2-4	2-5
Thumb Abducted			1: Large Diameter  2: Small Diameter  3: Medium Wrap  10: Power Disk  11: Power Sphere 	31: Ring 	28: Sphere 3 Finger 	18: Extension Type  26: Sphere 4-Finger 	19: Distal Type 
Thumb Adducted		17: Index Finger Extension 	4: Adducted Thumb  5: Light Tool  15: Fixed Hook  30: Palmar 				

Figure C.2. GRASP taxonomy that incorporates all previous grasp classifications [71]
(to be continued)







Opp: VF:	Intermediate		
	Side		
	2	3	3-4
Thumb Abducted	23: Adduction Grip 		21: Tripod Variation 
Thumb Adducted	16: Lateral  29: Stick  32: Ventral 	25: Lateral Tripod 	

Figure C.2. GRASP taxonomy that incorporates all previous grasp classifications [71]
(to be continued)













		Precision				
Opp: VF:		Pad				Side
		2	2-3	2-4	2-5	3
Thumb Abducted		9: Palmar Pinch 	8: Prismatic 2 Finger 	7: Prismatic 3 Finger 	6: Prismatic 4 Finger 	20: Writing Tripod 
		24: Tip Pinch 	14: Tripod 	27: Quadpod 	12: Precision Disk 	
		33: Inferior Pincer 			13: Precision Sphere 	
Thumb Adducted					22: Parallel Extension 	

Figure C.2. GRASP taxonomy that incorporates all previous grasp classifications [71]
(continued)

Appendix D – Cognate of Planar Four-bar Mechanisms and Their Extensions

D.1 Coupler-Point Curves and Cognate Mechanisms

The outputs of a four-bar mechanism can be derived from the follower link or the coupler link. The curve generated by the point located at the coupler link is named coupler-point curve. The curves with respect to the ground link are generally much more complex. In the early days when the computation at ability was not as fast as today, a large atlas of coupler curves for different points was published in a set of charts of over 7000 curves [160]. Designers needed these to predict the relative motion of machine components to select mechanisms that match up with the potential applications.

A more interesting fact of the coupler-point curves is that two other four-bar mechanisms have identically the same curves as the first one. These are known as the cognates or Roberts-Chebyshev cognates, which is revealed in a theorem by Roberts and Chebyshev. The cognate mechanisms are two additional alternatives which may be more favourable than the first four-bar mechanism with respect to transmission angle and space requirement.

These independent discoveries are attributed to the two scientists Roberts (1875 in UK) and Chebyshev (1878 in Russia) using geometric approaches. Figure D.1 shows a general four-bar mechanism and its cognate mechanisms. The proof of the Roberts-Chebyshev theorem is not so difficult. If the approach is true, the only requirement for proof is to show that the derived pivot O_3 is fixed and coincident with the other cognate mechanisms. A simplest approach using complex numbers was proposed by J. B. Schor (1941). This also shows that triangle $O_1O_2O_3$ is similar to the coupler link ABC . Cayley provided a new way to simplify the determination of the link lengths of the cognate mechanisms, see Figure D.2.

The construction process of the cognate mechanisms is given by the following steps (Figure D.1):

- (1) From O_1 and C construct a parallelogram O_1ACA_1 locating A_1 ;
- (2) From O_2 and C construct a parallelogram O_1B_1CB locating B_1 ;
- (3) Construct the triangle similar to triangle ABC and merge one edge with the A_1C . Make the direction of the triangle the same as triangle ABC .
- (4) Construct another triangle similar to triangle ABC and merge one edge with the $C B_1$. Make the direction of the triangle the same as triangle ABC .
- (5) From C_1 and C_2 construct a parallelogram $CC_2O_3C_1$ locating O_3 ;

(6) O_3 is the frame point, $O_1A_1C_1O_3$ and $O_2B_1C_2O_3$ are two cognate mechanisms.

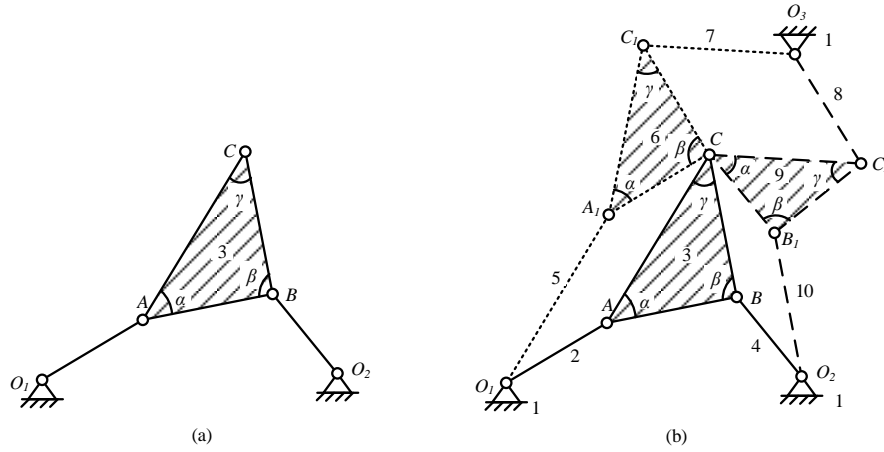


Figure D.1. (a) General four-bar linkage (O_1ABO_2); (b) two cognate mechanisms ($O_1A_1C_1O_3$ and $O_2B_1C_2O_3$).

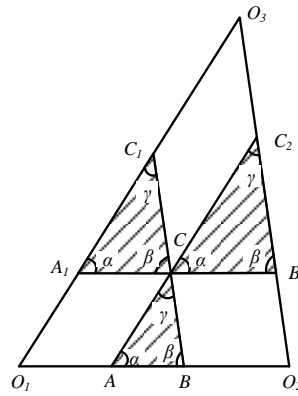


Figure D.2. Cayley's diagram plan.

D.2 Extension of Translation-Body Six-Bar Mechanisms

As shown in Figure D.3 (b), the whole system has ten links from 1 to 10. Assuming the angular velocities of links 2 to 10 are ω_2 to ω_{10} , respectively. Since the parallelograms O_1ACA_1 , O_2B_1CB and $CC_2O_3C_1$, the equivalent angular velocities of the links in the system are as followings: $\omega_2 = \omega_6 = \omega_8$; $\omega_4 = \omega_9 = \omega_7$; $\omega_5 = \omega_3 = \omega_{10}$.

Because C and C' in Figure D.3 (a) has the same curve during the motion process and link 2 and link 8 have the same angular velocity, an important usage of cognate mechanism is to build a rigid body rather than a single point to trace a coupler curve. With regard to the relationship between angular velocities $\omega_2 = \omega_8$, if the right cognate mechanism is to move to make link 2 and link 8 merge into one link 2-8 and configure itself without change (Figure D.3 (b)), points C and C' will trace the same

curve. By connecting C and C' , the system is a seven-bar mechanism where CC' is a translation body that traces the original coupler-point curve, see Figure. D.3 (c). The overconstrained link $O_2 B_1$ can be removed to obtain a simplified six-bar mechanism as shown in Figure. D.3 (d).

The construction process for the translation-body six-bar mechanism is as follows:

- (1) Construct a cognate four-bar mechanism and detach it with an original four-bar mechanism;
- (2) Keep the configuration of the cognate four-bar mechanism and move it to make links with the same angular velocity connect to each other;
- (3) Draw a link to connect the two coupler-point;
- (4) Remove one redundant link of the cognate four-bar mechanism.
- (5) Another transformation-body six-bar mechanism can be constructed in the other side.
- (6) The two transformation links can also be connected together to make a larger transformation body.

To determine the link lengths and structural features, a construction diagram plan is shown in Figure D.4.

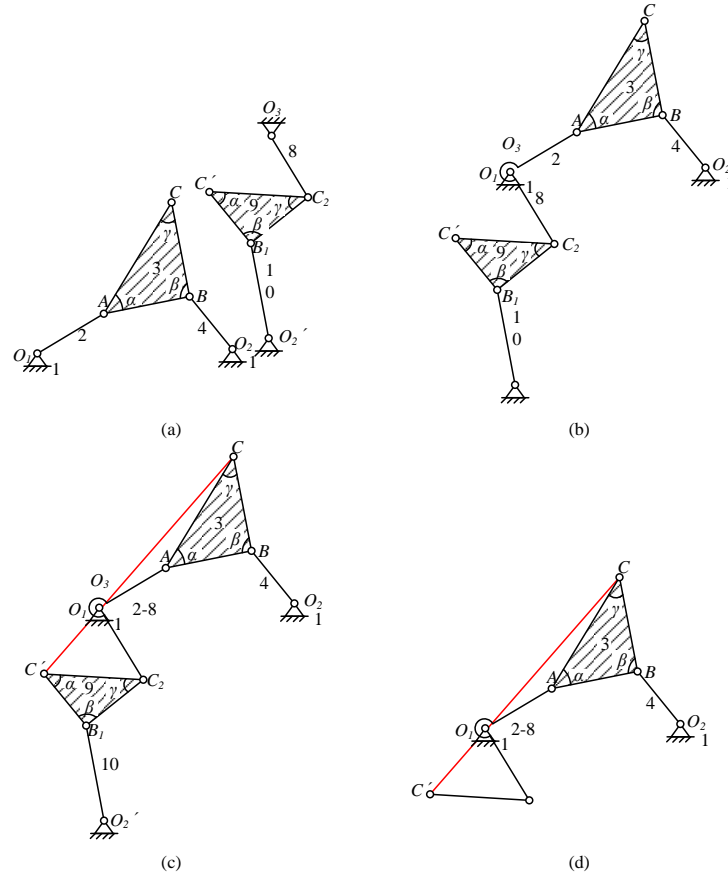


Figure D.3. Construction process of transformation-body six-bar mechanism.

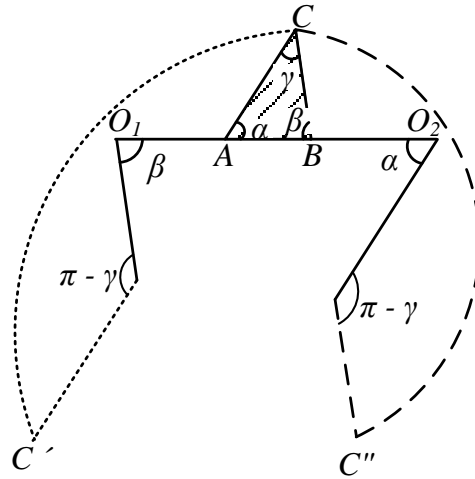


Figure D.4. Diagram plan for constructing transformation-body six-bar mechanism.

D.3 Extension of Cognate Six-Bar Mechanisms

Another interesting transforming approach to obtain a same coupler-point curve with the four-bar linkage is provided in [160]. A six-bar mechanism with the same coupler curve may avoid a bifurcation point existing in a four-bar mechanism. As shown in Figure D.5 (b), a cognate six-bar mechanism is constructed based on a four-bar mechanism O_1ABO_2 .

The construction process of the cognate six-bar mechanism is as follows:

- (1) From O_1 and C construct a parallelogram O_1ACA_1 locating A_1 ;
- (2) From O_2 and C construct a parallelogram O_2B_1CB locating B_1 ;
- (3) Construct a triangle similar to ABC and make it reverse and upside down. Merge the same length edge with O_1A_1 .
- (4) Draw a link by connecting B_1 and the noconnecting point of the triangle named B' .
- (5) Another cognate six-bar mechanism can be constructed in the other side.

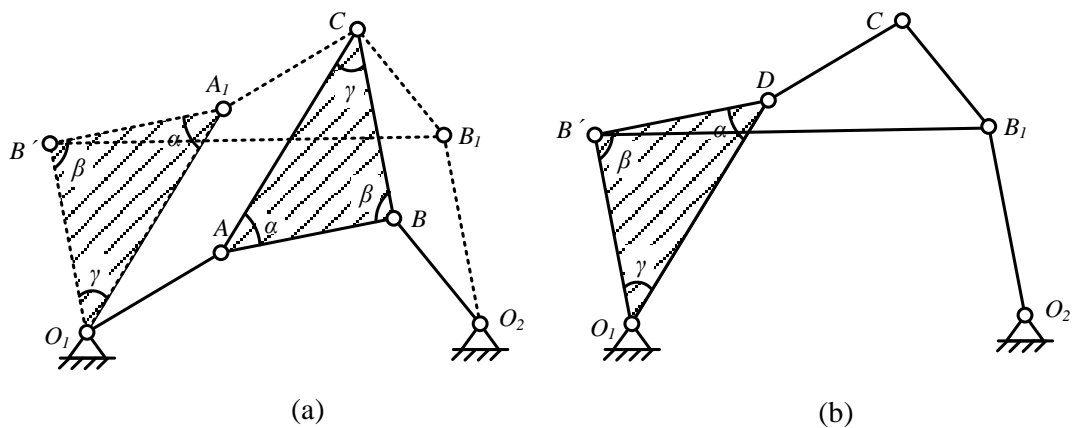


Figure D.5. (a) Construction process, (b) cognate six-bar linkage.

A construction diagram plan for determining the link lengths and structural features is shown in Figure D.6.

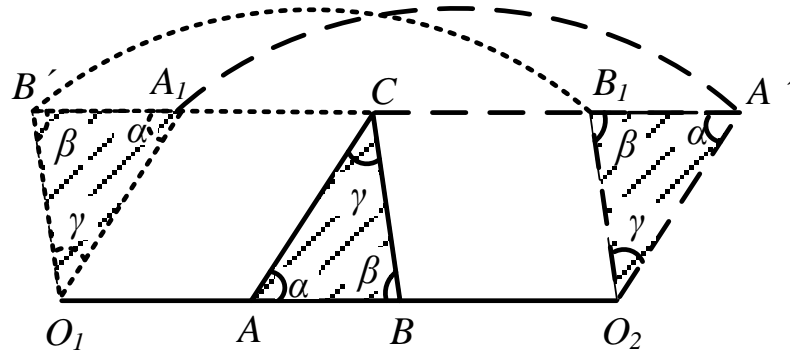


Figure D.6. Diagrammatic plan of cognate six-bar mechanism.

D.4 Cognate Four- and Six-Bar Mechanisms of Basic Four-Bar Mechanisms

In Section 3.1, the basic four-bar mechanisms are summarized. In order to investigate the coupler-point curve of these basic mechanisms, some useful specific types are constructed with a general triangle or a three-joint linear link as a coupler link. Diagrammatic plans for constructing cognate four- and six-bar mechanisms were also investigated according to the processes given in Sections D.1, D.2 and D.3.

Figure D.7 shows diagrams of a Type I four-bar mechanism which has a coupler link with the downward facing triangle head. The investigation shows that diagrams are rotated 180° with respect to the frame line.

Figure D.8 shows a four-bar mechanism with a three-joint linear coupler link. The internal triangles of the coupler link can be seen as $\alpha = 0$, $\beta = \pi$, $\gamma = 0$. Figure D.8 (b) shows three four-bar mechanisms with the same curve at point C. Figures (c) and (d) have transformation-body CC' , which has the same tracing curve with point C. Real-line sketches in Figures (e) and (f) show two cognate six-bar mechanisms.

Figure D.9 shows a general cross four-bar mechanism and its cognate mechanisms. The internal triangles of the coupler link can be seen as $\alpha = 0$, $\beta = 0$, $\gamma = \pi$. Details of these diagrams are as shown in the figure.

A concave four-bar mechanism and its cognate mechanisms is shown in Figure D.9. The two cognate four-bar mechanism implies that the structures are similar to cognates of the CFB mechanism. The concave four-bar mechanism is actually a specific moving range of the CFB mechanism. Therefore, the transformation-body six-bar mechanisms and cognate-six bar mechanisms can be derived from similar process as for the CFB mechanism.

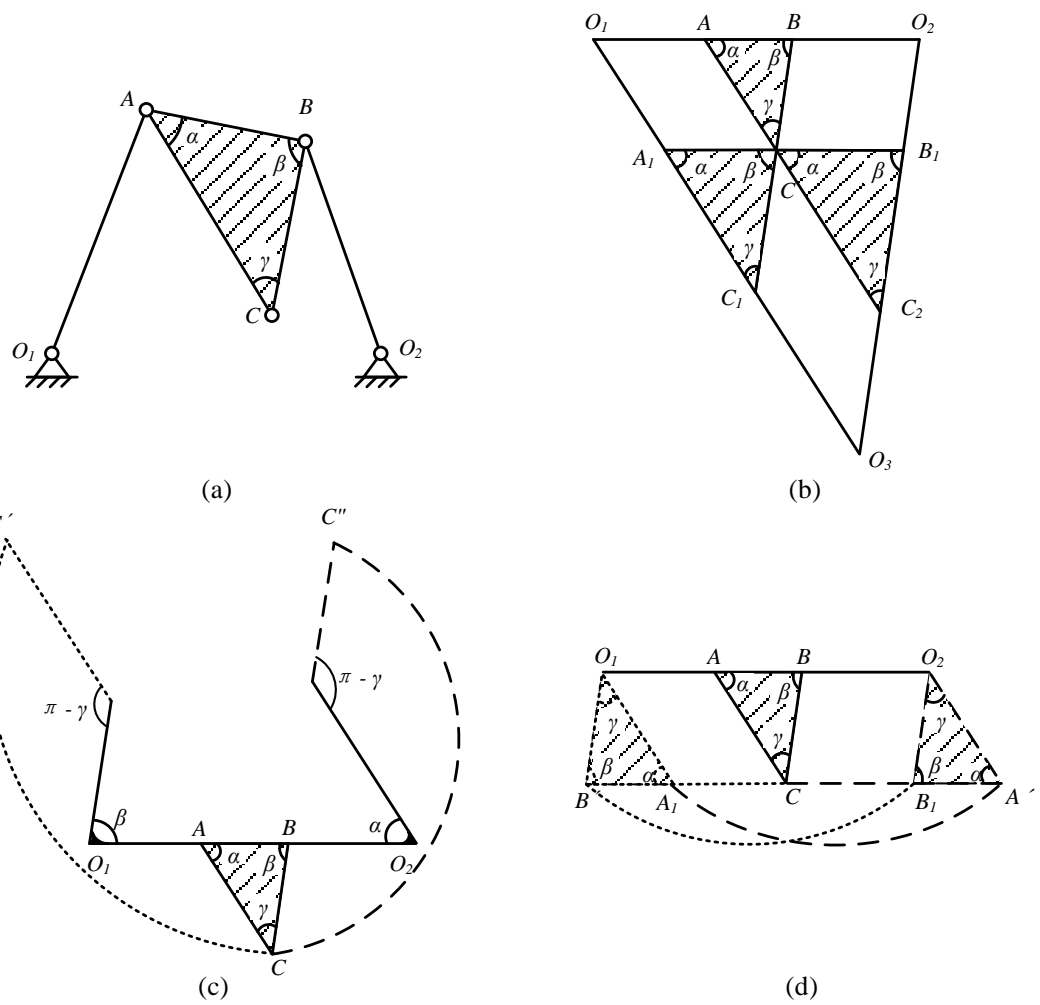


Figure D.7. Diagram plans of Type I four-bar mechanism: (a) sketch of the mechanism, (b) for cognate four-bar mechanism, (c) for transformation-body six-bar mechanism, (d) for cognate six-bar mechanism.

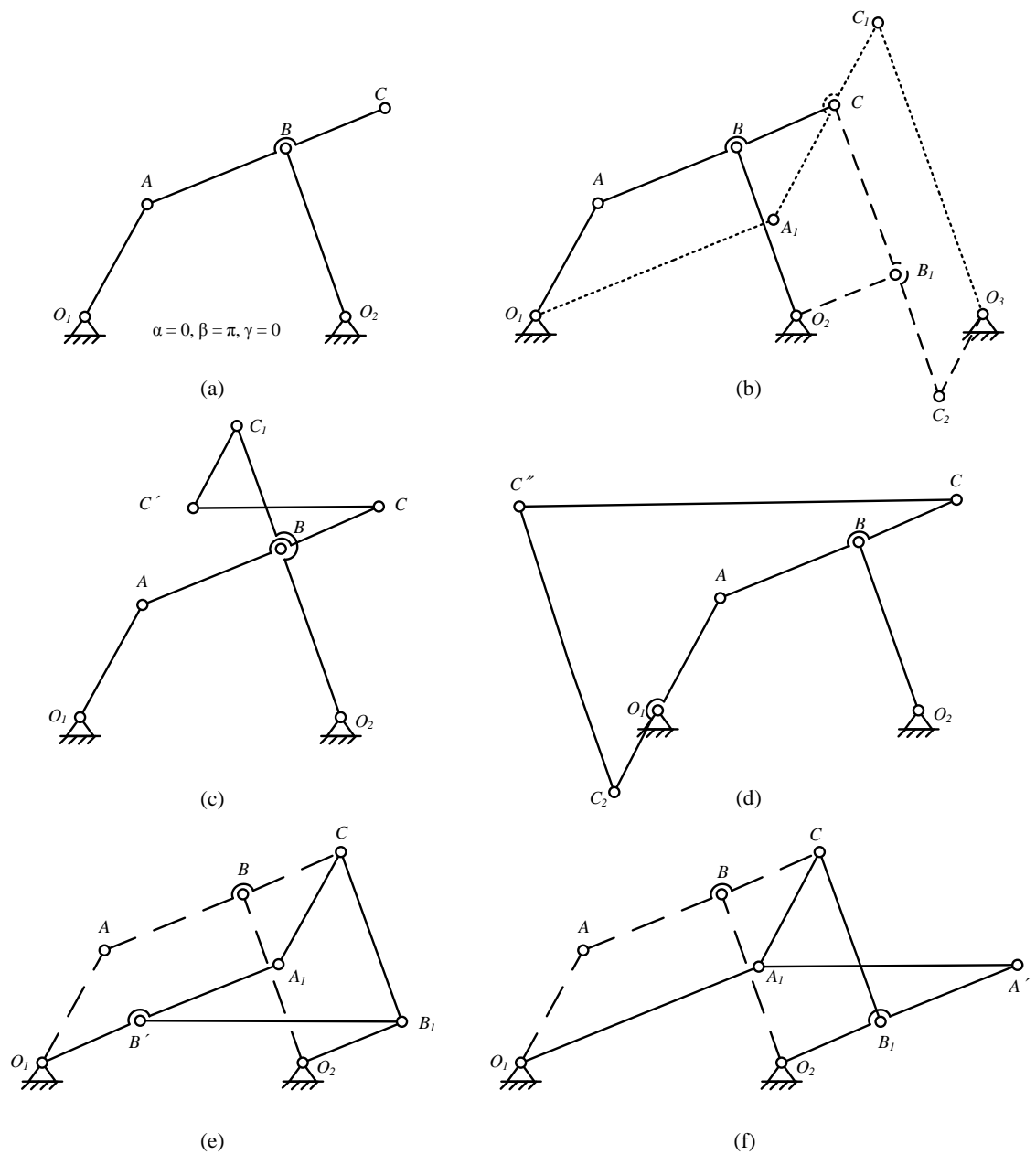


Figure D.8. Type II four-bar linkage and its cognate mechanisms: (a) four-bar linkage with three-joint linear coupler link, (b) cognate four-bar mechanisms, (c) and (d) transformation-body (CC) six-bar mechanisms, (e) and (f) cognate six-bar mechanisms.

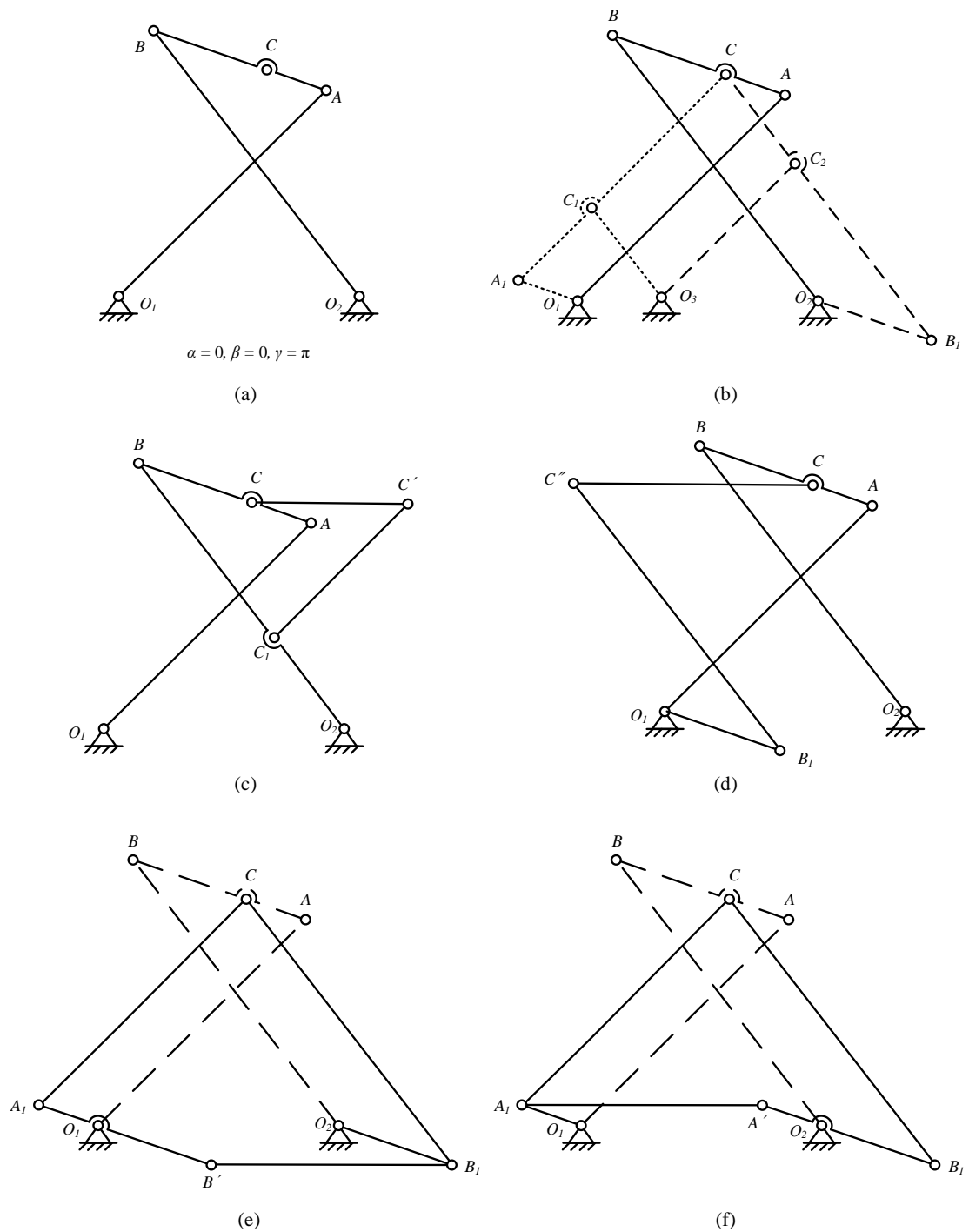


Figure D.9. Type III (CFB) mechanism and its cognate mechanisms: (a) four-bar linkage with crossing drive link and follower link, (b) cognate four-bar mechanisms, (c) and (d) transformation-body (CC) six-bar mechanisms, (e) and (f) cognate six-bar mechanisms.

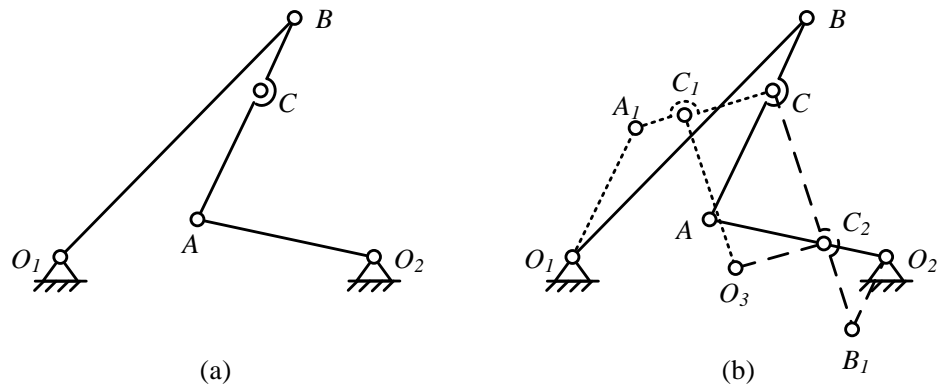


Figure D.10. Type IV (Concave) mechanism and its cognate four-bar mechanisms.

Figure D.11 shows a slider-crank mechanism with a coupler point C . Only one cognate four-bar mechanism is derived. It is also a slider-crank mechanism. The diagram plan for slider-crank mechanism is shown in Figure D.12.

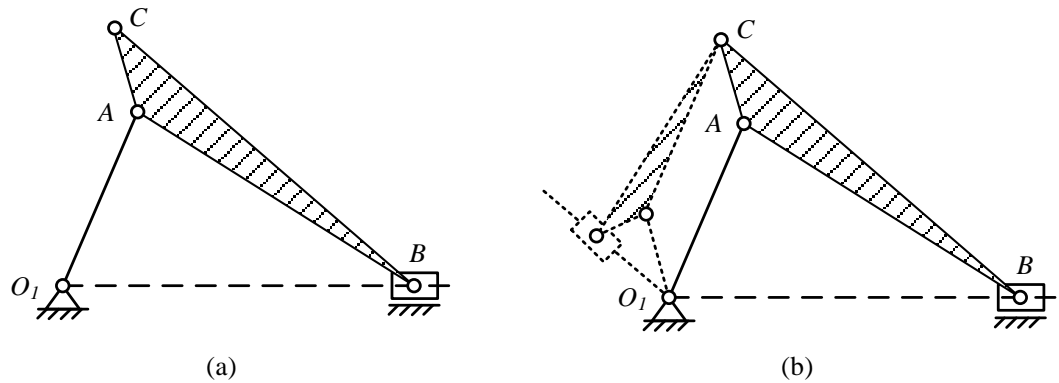


Figure D.11. (a) Type V (Slider-crank) mechanism and (b) its cognate four-bar mechanism.

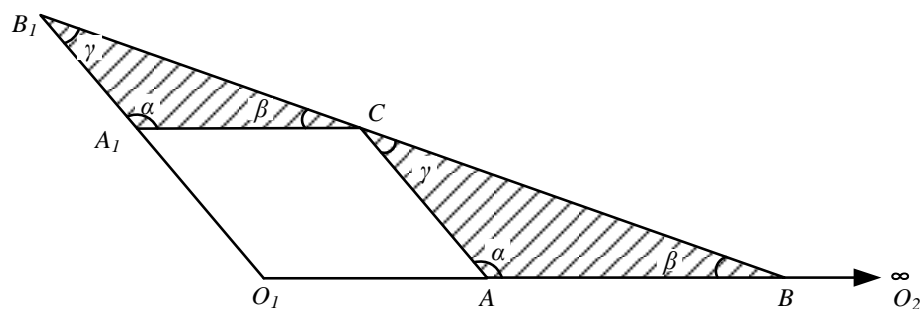


Figure D.12. Diagram plan of cognate slider-crank mechanism.

Appendix E – Cognate of Straight-Line Mechanisms and Their Extensions

A four-bar mechanism and cognates with the same coupler-point curves have been presented in Appendix D. The mechanism, in early applications, composing revolute-connected links was mainly used to transform the continuous rotation of a water wheel into reciprocating motion to suit piston pumps (Figure E.1). The mechanism works as a power transmission as well as a motion transformer.

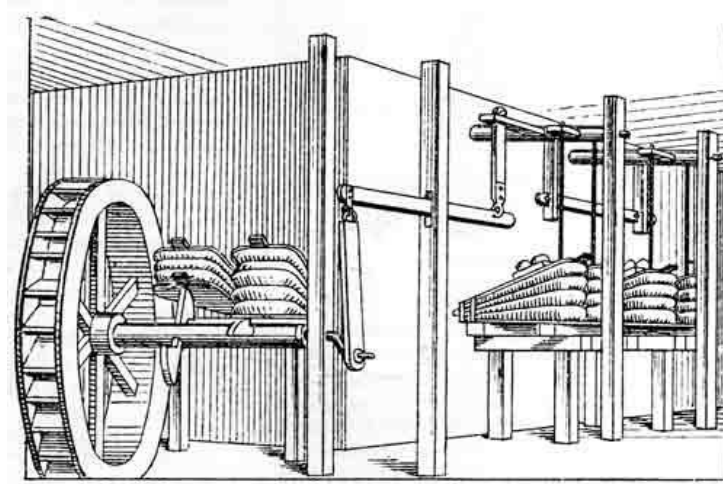


Figure E.1. Blowing engine by Vanuccio Biringuccio, about 1540. (From Theodor Beck, *Beiträge zur Geschichte des Maschinenbaues*, Berlin, 1899. p. 120)

The great interests in approximate straight-line mechanisms start from applications in steam engines. As noted, Watt had shown the way in 1784 when he invent a four-bar linkage whose couple point guided the upper end of the piston rod along an approximate straight line, see Figure E.2. The almost rectilinear portions of the curve or the approximate straight-line segments were emphasized for the application. After then the first analytical investigation of a coupler curve was undertaken by Prony [161]. The deviations of Watt's straight-line mechanism were examined. Watt's straight-line mechanism also inspired mechanical engineers and mathematicians to find a new way to use a planar four-bar linkage on the motion output of coupler not the follower link.

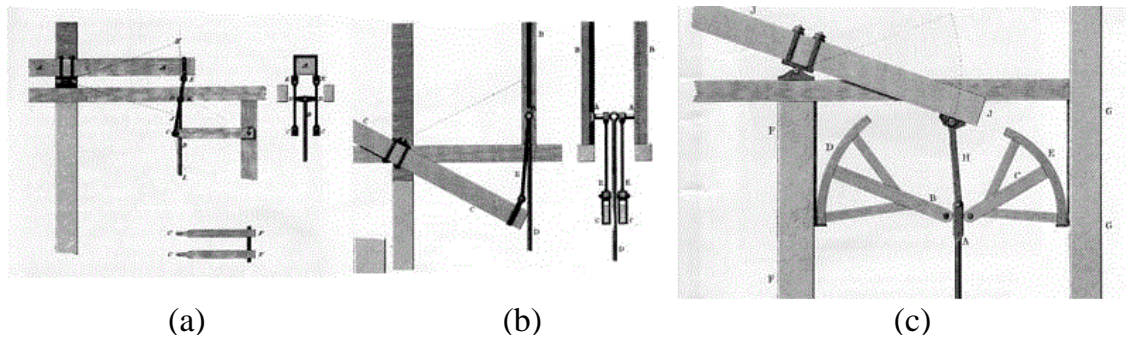


Figure E.2. Watt's mechanisms for double-acting engine: (a) straight-line mechanism; (b) crosshead and guide arrangement; (c) flexible cords mechanism. (From British Patent 1432, April 28, 1784)

E.1 Straight-Line Mechanisms

A large amount of usage of linkage-type use is closely allocated with “straight-line motion”. Almost all the textbooks on mechanisms or kinematics devote some space to introducing this “straight-line motion”. The first investigation of straight-line motion was led in sixteenth century by Cardano (1501-1571), as shown in Figure E.3 (a), a two circle system. The radius of the large circle is twice the small circle with the small one rotating inside the large one. The centre of the small circle is hinged with a link, the other end of which is hinged at the centre of large circle. All points of the circumference of the small circle trace straight-line segments. All points in the plane of the small circle describe ellipses. These facts were proved by De La Hire (1640-1718) at the end of the seventeenth century. Based on the hypocycloid, an English engineer James White developed a steam engine in 1801 (Figure E.3 (b)).

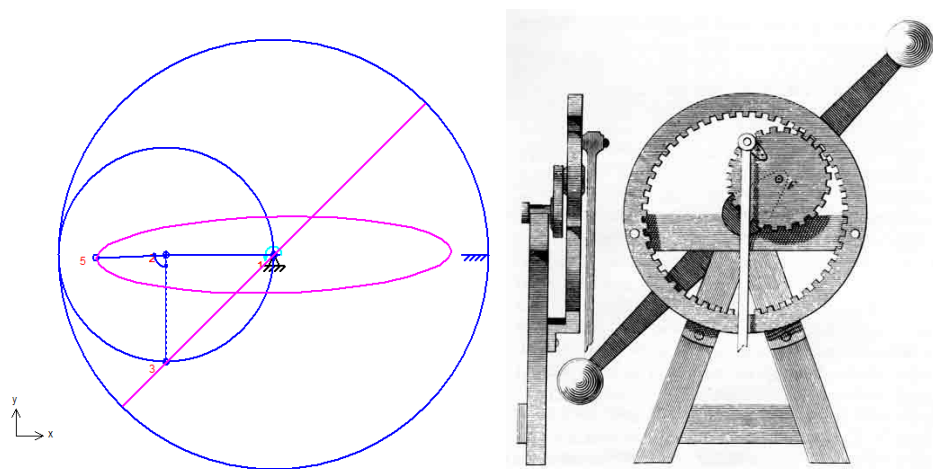


Figure E.3. (a) Cardanic circle system and (b) James White's hypocycloidal straight-line mechanism. (James White, *A New Century of Inventions*, Manchester, 1822, p 1.7)

Straight-line mechanisms can be classified into two groups: exact and approximate.

The only exact straight-line mechanism with four links was patented in 1803 by William Freemantle, an English watchmaker. The mechanism was latterly named the Scott Russell mechanism, after the name John Scott Russell (1808-1882), the prominent naval architect, see Figure E.4. In addition to this slide-crank exact straight-line mechanism, all the other exact types require six or more links, such as Peaucellier-Lipkin linkage (in 1864, eight-bar mechanism), Hart's inversor and A-rame mechanisms (in 1874, six-bar mechanism) and Quadruplannar Inversor or Sylvester-Kempe mechanism (in 1875, six-bar mechanism).

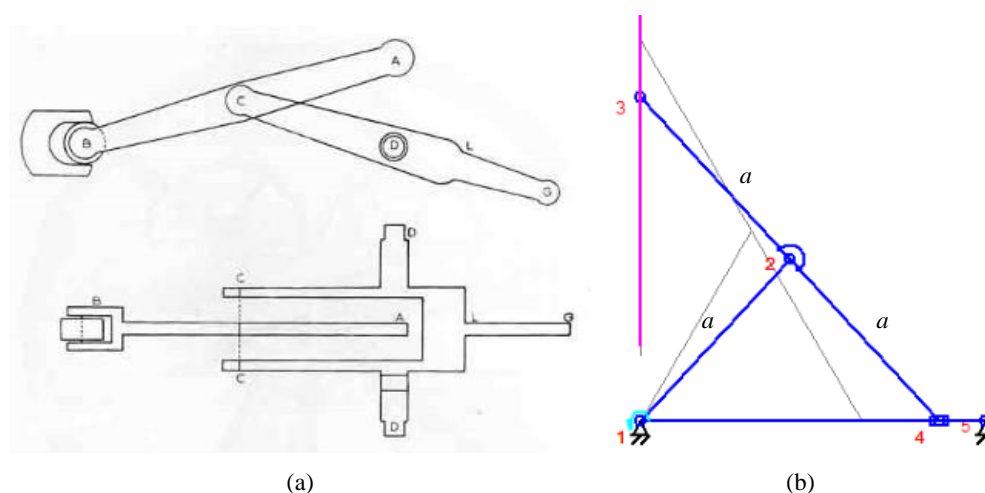


Figure E.4. (a) Freemantle straight-line mechanism. From British Patent 2741, Nov 17, 1803. (b) Scott Russell mechanism.

The symbol “ a ” in the figures represents dimension of the each segment of the link. In the following figures “ b ” or “ c ” have the same function to be distinguished “ a ” from different lengths.

The Scott Russell straight-line mechanism is actually based on the aforementioned Cardanic circle, see Figure E.5 (a). Three types of slider-based mechanisms can be derived as shown in Figure E.5. According to analysis of Cardanic circle, any two points on its circumference can be used to draw a straight line. In Figure E.5 (a), an angular link with three joints, two of which are on the circumference of the small circle and the third one on the centre, is used to construct a straight-line mechanism. Figure E.5 (b) and (c) is Reuleaux exact straight-line mechanism where a three-joint link with three joints locating at the circumference of the small circle and any two joints connecting with two sliders are employed to construct straight-line mechanisms.

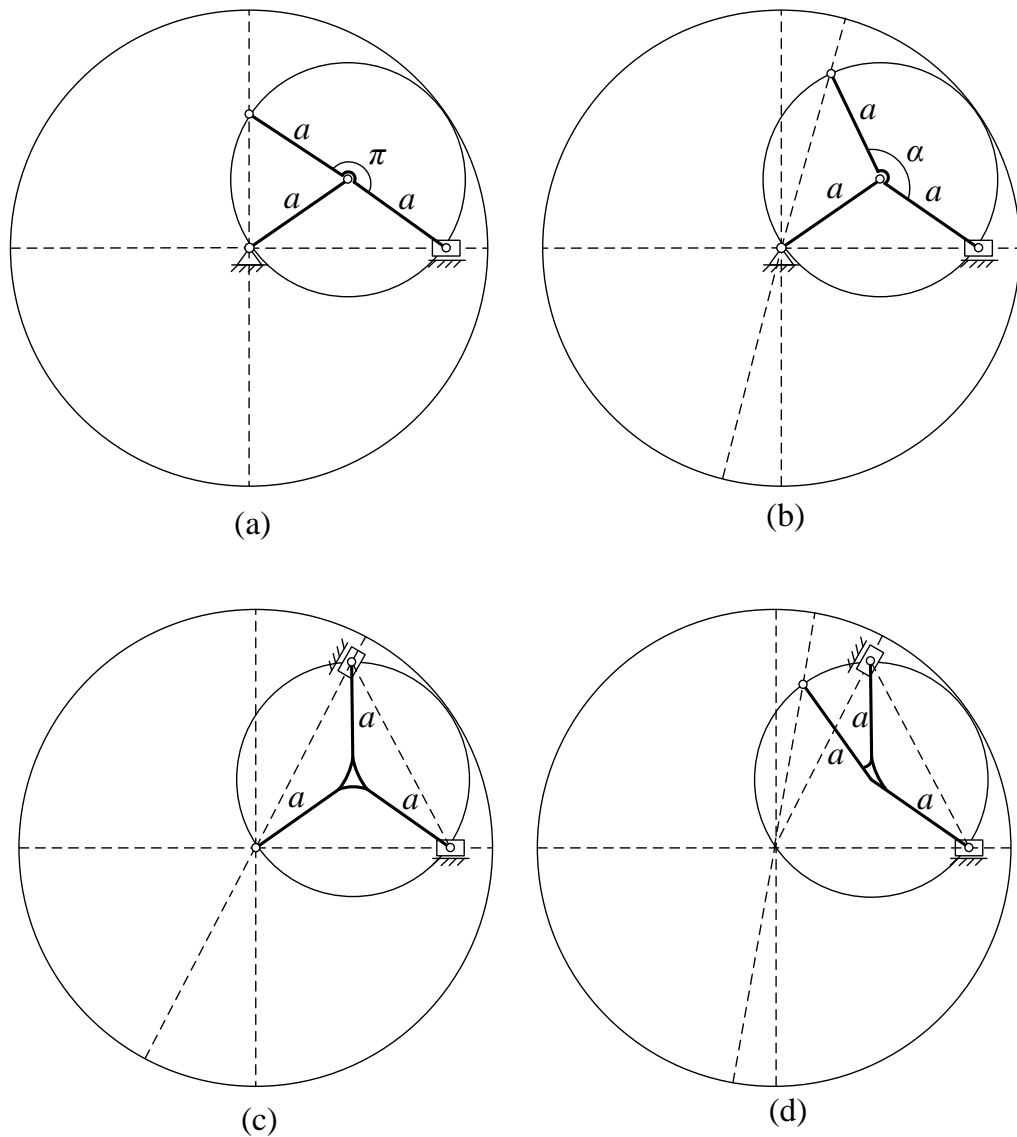


Figure E.5. Slider-based exact straight-line mechanisms: (a) Scott Russell straight-line mechanism; (b) angular Scott Russell straight-line mechanism; (c) double-slider Reuleaux straight-line mechanism; (d) angular double-slider Reuleaux straight-line mechanism.

The best known research on straight-line mechanisms was developed by James Watt (1736-1819) for guiding the piston of the early steam engines. In 1784, a patent of Watt's steam engine disclosed a four-bar linkage in which the central point of the coupler link is constrained to travel in an approximate straight line (Figure E.6).

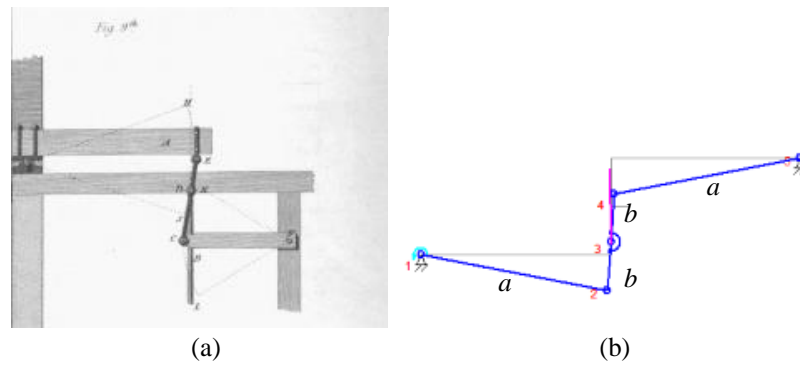


Figure E.6. Watt's approximate straight-line mechanism.

Some other approximate straight-line mechanisms were developed in the following years, see Figure E.7. Oliver Evans devised his straight-line mechanism (Evans linkage) in 1805 and used it on his Columbian engine. The practical advantage of lighter working beam than the Watt engines. Richard Roberts (1789-1864) invented a straight-line mechanism for the first metal planing machines in 1820. In 1867, Chebyshev developed a new straight-line mechanism based on the investigation of Watt and Evan's straight-line mechanism. Hoecken's straight-line mechanism was first published in 1926 by Karl Hoecken (1874-1962). The significant advantages are as follows: (1) Grashof crank-rocker; (2) nearly constant velocity along the center portion of the straight-line segment.

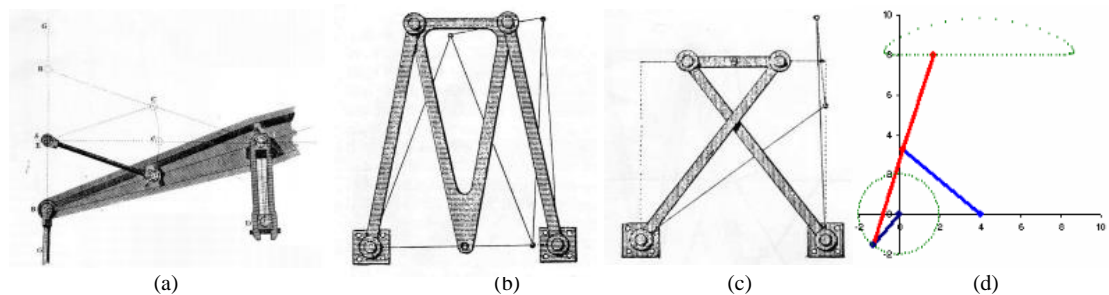


Figure E.7. Some other approximate straight-line mechanisms: (a) Evans linkage; (b) Roberts linkage; (c) Chebyshev linkage; (d) Hoecken linkage.

E.2 Cognate and Transformation-Body Mechanisms of the Straight-Line Mechanisms

The symmetrical slider-crank straight-line mechanism is shown in Figure E.8. The mechanism is entirely defined by specifying the length a . The red trajectory is the straight line trace of coupler point C. The cognate mechanism is drawn as a dashed line. The following figures have similar expressions with this design.

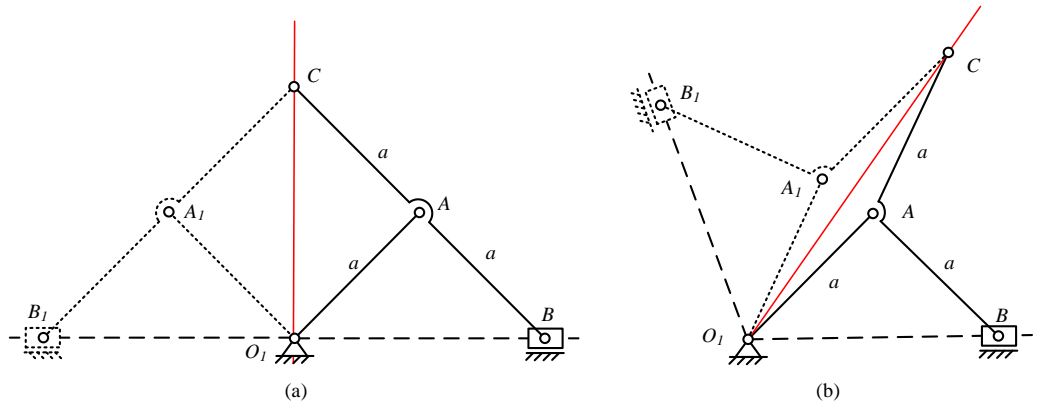


Figure E.8. Cognates of two types of symmetrical slider-crank straight-line mechanism

The combined form of original and cognate mechanisms is a pantograph mechanism [162], which is used to trace a path to an enlarged or a reduced scale, see Figure E.8 (a). The motion of Point B_1 is derived from point B , point O_1 being the supporting point. The combined form shown in Figure E.8 (b) is a Sylvester plagiograph or skew pantograph, which can turn the graph through any required angle.

If the configuration of the cognate four-bar mechanism is kept and then moved to make links with the same angular velocity connected and welded to each other, the two types of four bar mechanism with the same straight line motion in the original mechanism are shown in Figure E.9. Connecting line B_1C and BC 'of the scissor-like mechanism in Figure E.9 (a) are parallel with each other during the moving process. The angle α constructed by the connecting line B_1C and BC 'in Figure E.9 (b) is constant. The most familiar usage of these two type of linkages are deployable/foldable mechanisms [163, 164], as shown in Figure E.10.

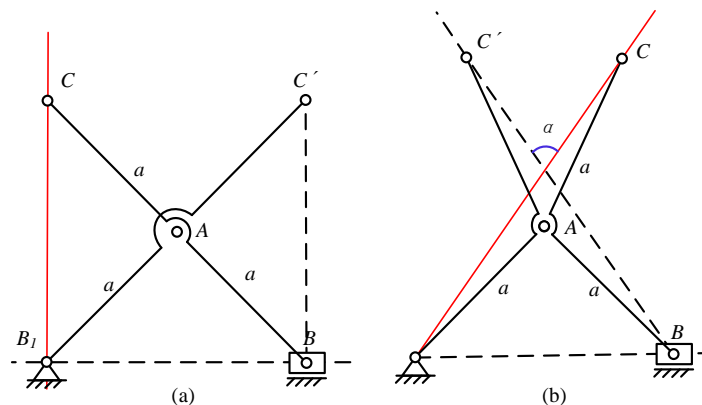


Figure E.9. Extending mechanisms of the two types of symmetrical slider-crank straight-line mechanism: (a) scissor-like mechanism; (b) angulated scissor-like mechanism.

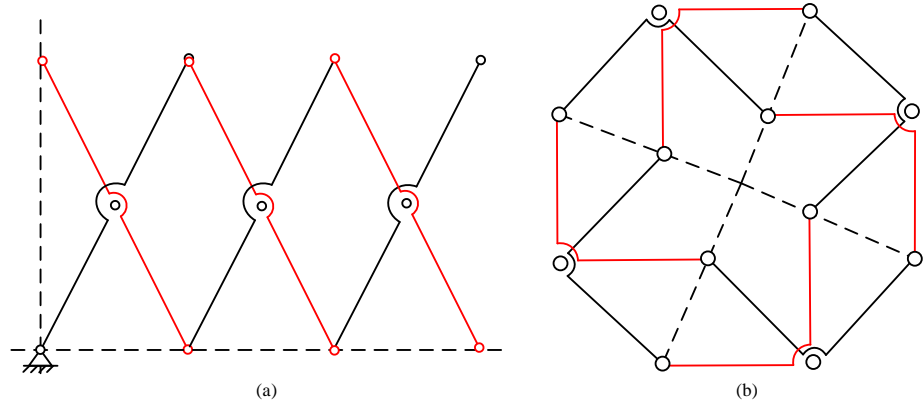


Figure E.10. Deployable mechanisms constructed by pantograph and plagiograph linkages.

Cognate mechanisms and their correlation of approximate straight-line mechanisms have been comprehensively investigated in [165]. The four- and six-bar cognate and transformation-body mechanisms of the typical approximate straight-line mechanisms are constructed according to the processes provided in Appendix D.

The cognate mechanism of the Watt's straight-line mechanism is a type of Evans mechanism as shown in Figure E.11. The length of O_1A_1 in Evan's straight-line mechanism can be freely chosen; however a larger value reduces the deviation of the coupler point from a . Watt straight-line mechanism shown in Figure E.11 is usually considered the most accurate because of the two arms O_1A and O_2B are equal in length.

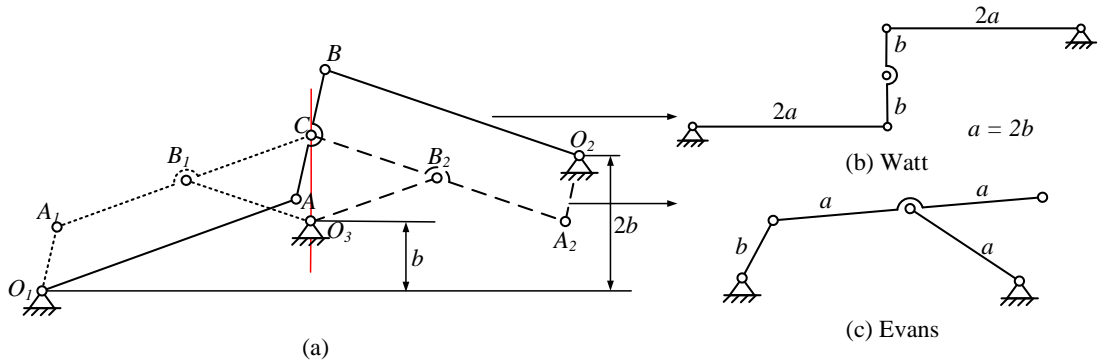


Figure E.11. Watt straight-line mechanism and its Evans cognate mechanism.

The six-bar cognate mechanism and transformation-body mechanism are shown in Figure E.12. Because of the symmetrical characteristic of this mechanism, there is only one mechanism for each category.

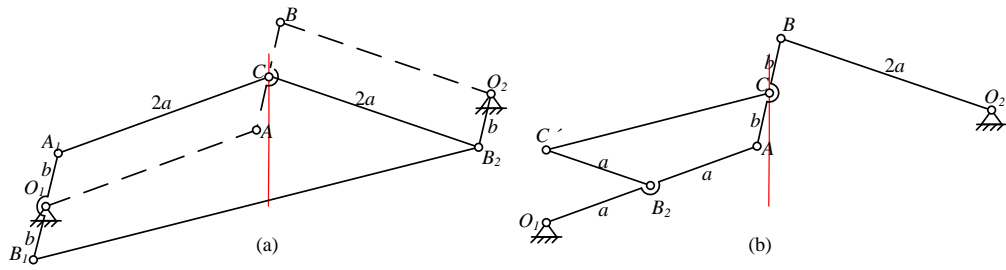


Figure E.12. Six-bar cognate and transformation-body of Watt straight-line mechanism.

A seven-bar transformation-body mechanism is synthesized by connecting the two sides of the transformation link is shown in Figure E.13.

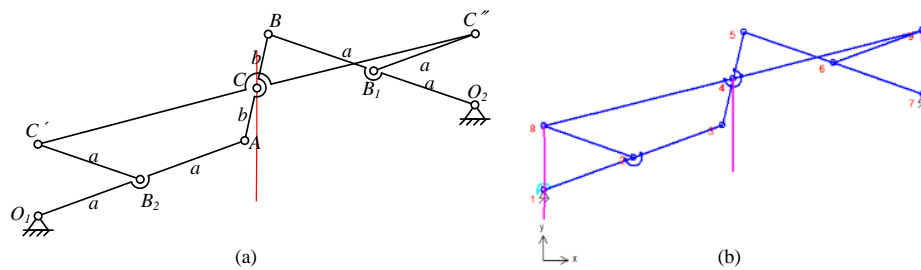


Figure E.13. Seven-bar transformation-body mechanism

Cognates of the symmetrical Roberts straight-line mechanism (Figure E.14) is a type of Watt mechanism. The two cognates are the same mechanism. The same situation is also shown in Figure E.15. The connected transformation-body mechanism has a similar triangle CC'' with respect to ACB . $O_1A-O_1B_2$ and $O_2B-O_2B_2$ are two hinged links, see Figure E.16. A simulation model verifies the result of geometrical design.

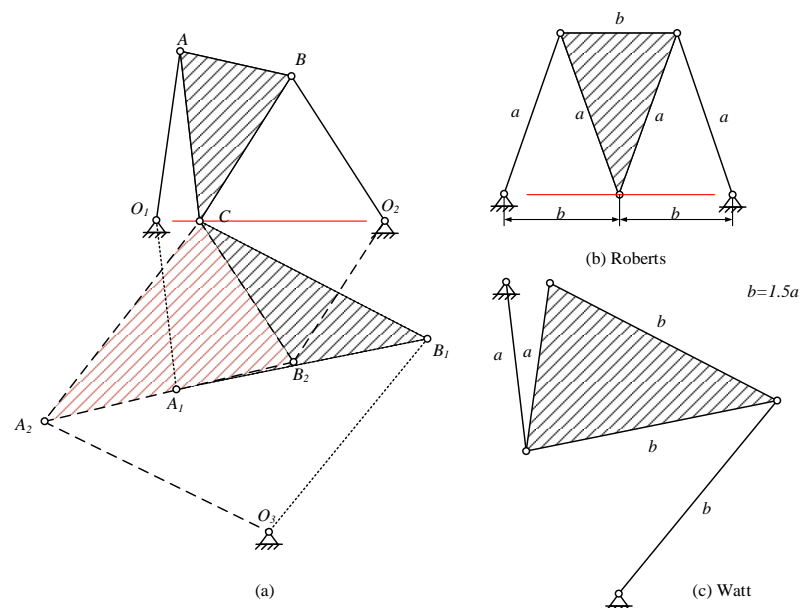


Figure E.14. Symmetrical Roberts straight-line mechanism and its cognates

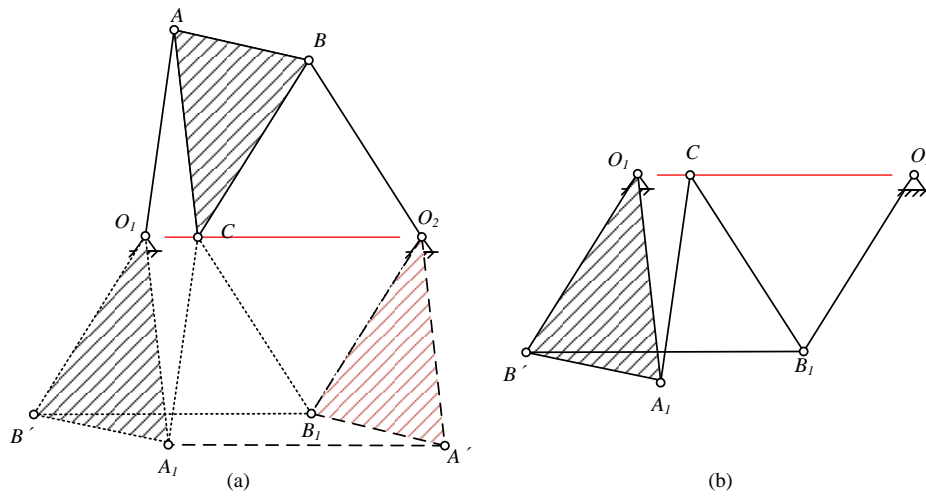


Figure E.15. Six-bar cognates of symmetrical Roberts mechanism.

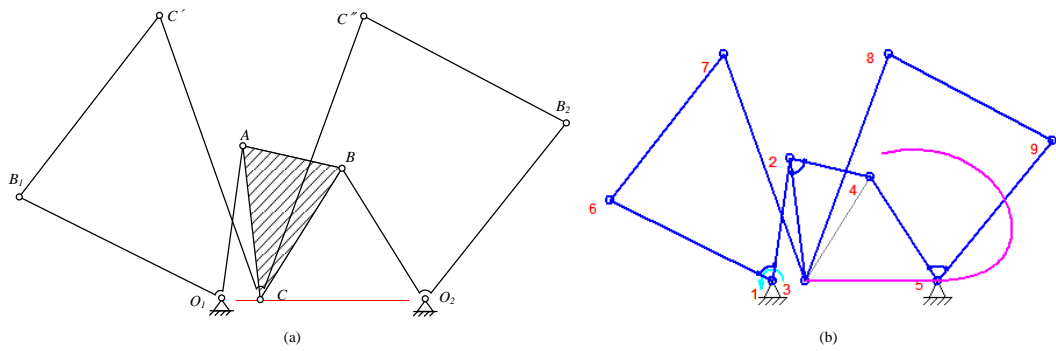


Figure E.16. Transformation-body of the symmetrical Roberts mechanism.

Cognates of symmetrical Chebyshev mechanism are shown in Figures E.17 and E.18. The transformation-body mechanism is shown in Figure E.19.

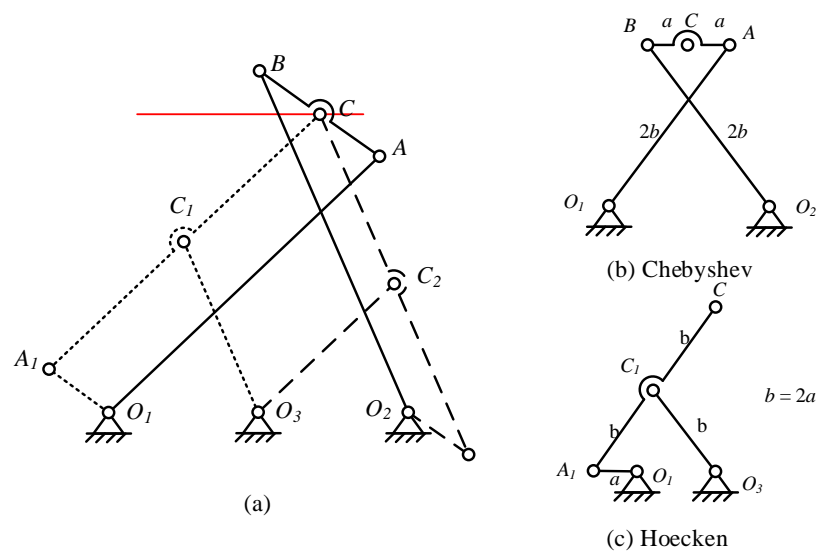


Figure E.17. Symmetrical Chebyshev straight-line mechanism and its cognates

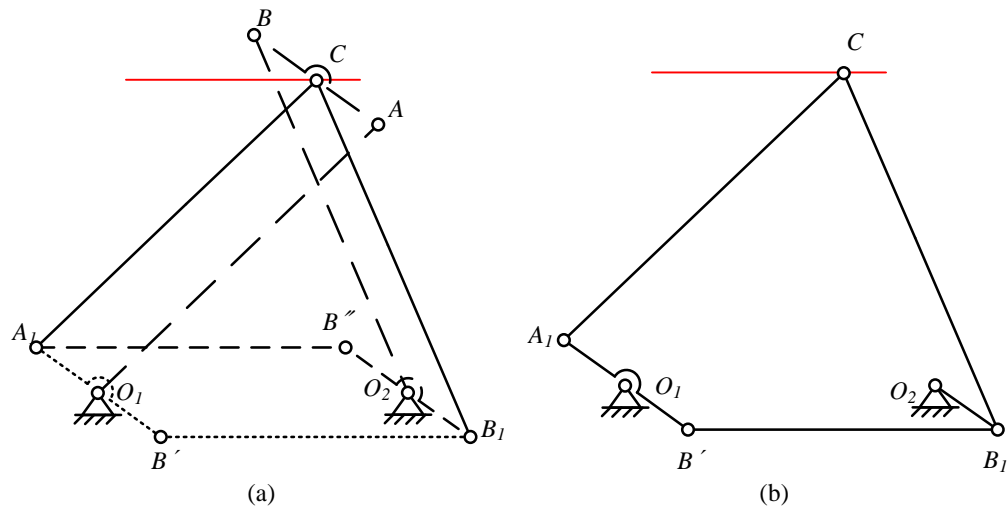


Figure E.18. Six-bar cognates of symmetrical Chebyshev mechanism.

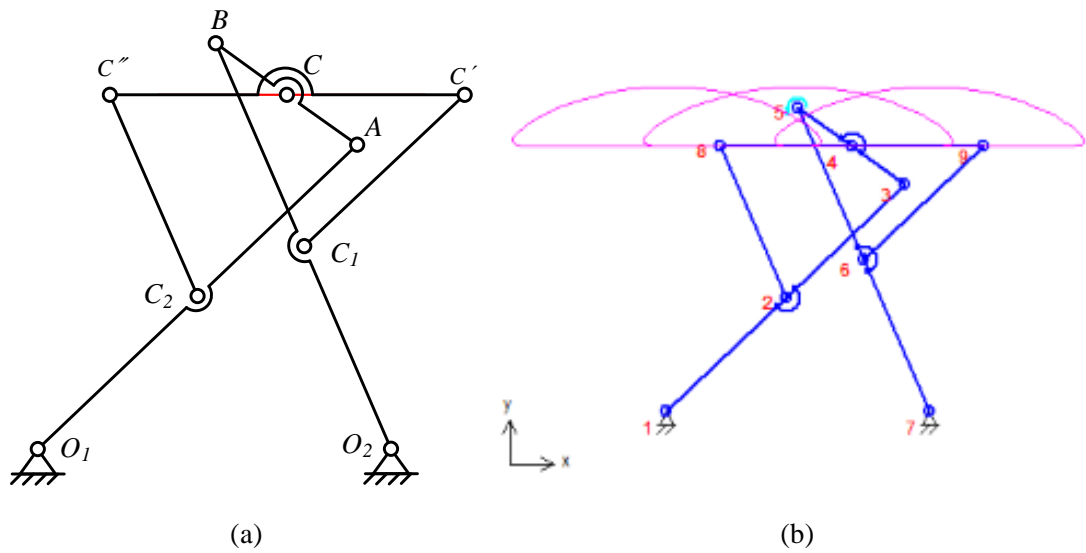


Figure E.19. Transformation-body of the symmetrical Chebyshev mechanism.

By considering the cognate relation of symmetrical Chebyshev and Hoecken straight-line mechanisms, four-bar cognates of Hoecken mechanism have two types: one is symmetrical Chebyshev and the other is identical to itself, as shown in Figure E.20. However, six-bar cognates and transformation-body mechanisms of the Chebyshev mechanisms are different, shown in Figures E.21 and E.22.

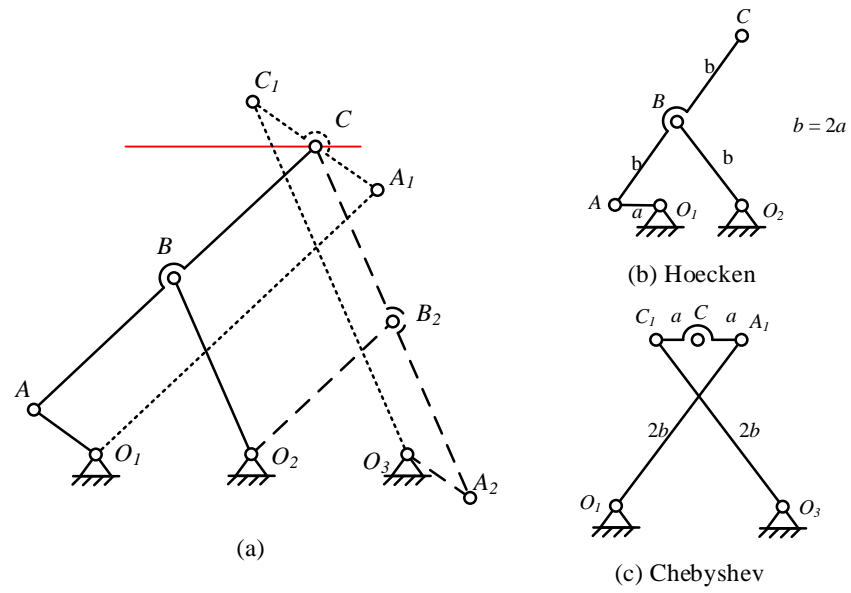


Figure E.20. Hoecken straight-line mechanism and its cognates.

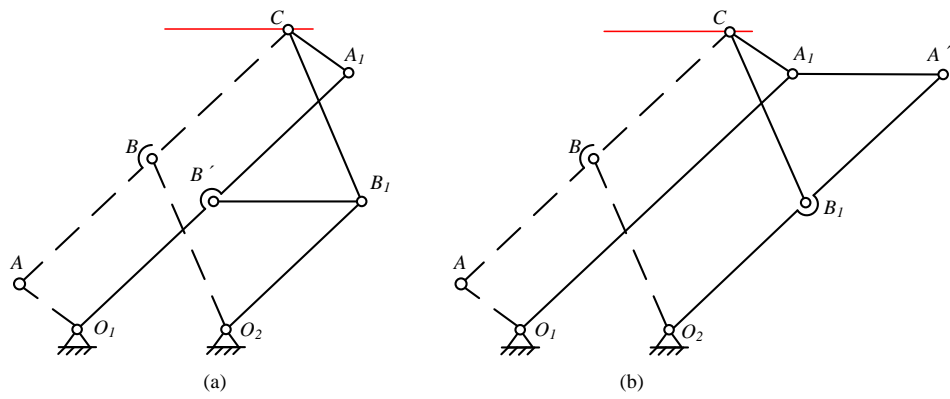


Figure E.21. Six-bar cognates of Hoecken mechanism.

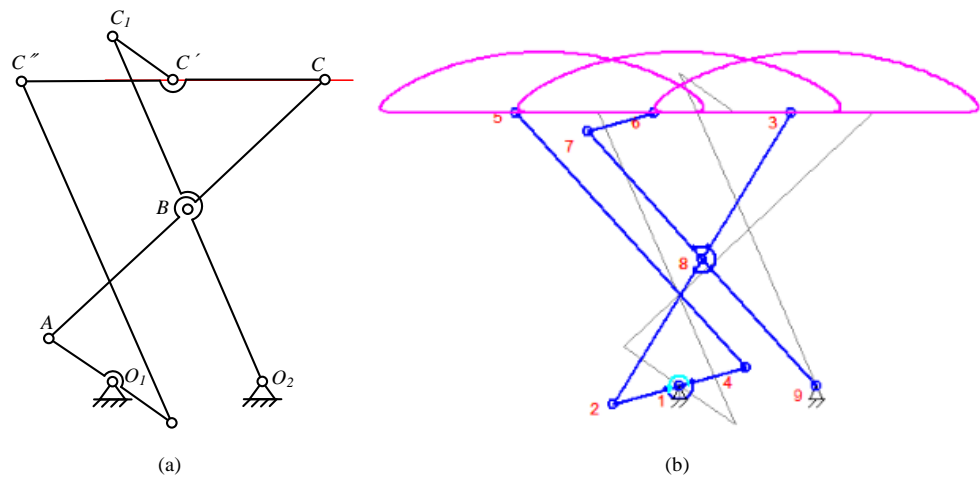


Figure E.22. Transformation-body of the Hoecken mechanism.

E.3 Correlation of Straight-Line Mechanisms and Their Cognates

Correlations of the exact and approximate straight-line four-bar mechanisms are summarized in Table E.1.

Table E.1. Correlation of the exact and approximate straight-line four-bar mechanisms.

Straight-line mechanisms	Four-bar cognate 1	Four-bar cognate 2	Number of six-bar cognates	Number of transformation-body
Scott Russell (Exact)	Scott Russell	None	None	None
Symmetrical Watt	Evans	Evans	1	1
Symmetrical Roberts	Watt	Watt	1	1
Symmetrical Chebyshev	Hoecken	Hoecken	1	1
Hoecken	Chebyshev	Hoecken	2	2

Appendix F – Synthesis of Multi-RCM Mechanism

F.1 Analysis of a Mechanism with Multiple Remote Centres

For the purpose of obtaining a mechanism with more remote centres, a parallelogram $GHJI$ is added to the former schematic. In other words, another set of crossed links $G-EFIH$ is added to construct a parallelogram, as shown in Figure F.1.

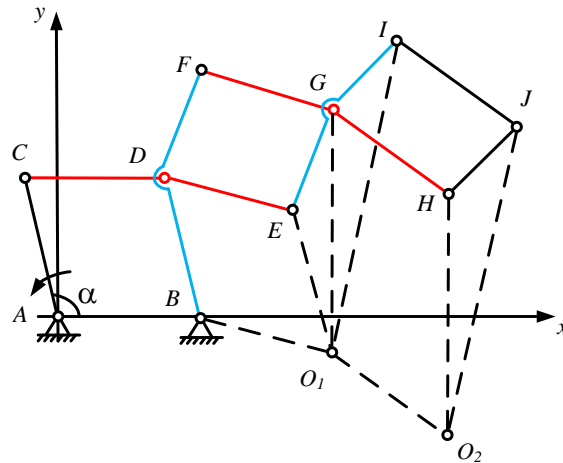


Figure F.1. A serially combined mechanism with planar scissor-like element

As shown in Figure F.1, a serially combined mechanism is constructed with two scissor-like elements (SLE) [143], $D\text{-}BCFE$ and $G\text{-}EFIH$. There are altogether three parallelogram loops in this mechanism. The degree of freedom of this mechanism is obtained by Gruebler's equation:

$$M=3L-2J-3G=3\times 8-2\times 10-3\times 1=1 \quad (\text{F.1})$$

where M = degree of freedom or mobility,

 $L = \text{number of links,}$

J = number of joins,

G = number of grounded links.

Link CDE is driven by link AC with translational motion because of a parallelogram loop $ABDC$. In the same way, link FGH does translational motion for another parallelogram loop $DEGF$. $\angle GEO_1$ is drawn to equivalent to $\angle FDB$. Since BO_1 is parallel to DE with a constant direction. Then point B is a fixed as a rotation centre. As O_1 within link GEO_1 corresponding to B within link FDB ; therefore, O_1 is also a fixed point. Link JHO_2 is equivalent to link IGO_1 and rotates around a fixed point O_2 as loop $GHJI$ is a parallelogram.

According to this analysis, a conclusion is finally obtained: Links CDE , FGH and IJ make translational motion and the points on them have the same linear velocity. Links

FDB , GEO_1 and JHO_2 , rotating around B , O_1 and O_2 respectively, have the same angular velocity. Point O_1 and point O_2 are virtual centres of the eight-bar mechanism.

The mechanism will also be movable, if links GEO_1 and JHO_2 are hinged to frame at O_1 and O_2 , while the mechanism turns out to be over-constraint, as shown in Figure F.1. If seven links (AC , CD , DF , FG , GI , IJ and JH) are removed from three loops ($ABDC$, $DEGF$ and $GHJI$), the simplified mechanism is a Watt-II mechanism (Figure F.2), a multi-loop kinematic chain with only one degree of freedom. It is concluded that RCM mechanisms and the mechanisms with multi-loop kinematic chain are interrelated.

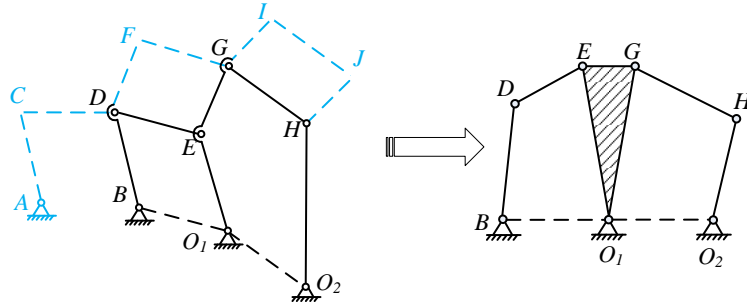


Figure F.2. The simplified mechanism and Watt- II mechanism.

According to the method provided, multi-RCM mechanisms can also be obtained by adding scissor-like elements and homologous mechanisms with multi-loop kinematic chain will also be obtained by removing links. A five-RCM mechanism is constructed by adding four scissor-like elements as shown in Figure F.3(a). A mechanism with a five loop kinematic chain is obtained by removing several links, as shown in Figure F.3(b). There exists five parallelogram loops in this mechanism (BP_2O_1C , EO_1O_2F , HO_2O_3I , KO_3O_4L and NO_4O_5P).

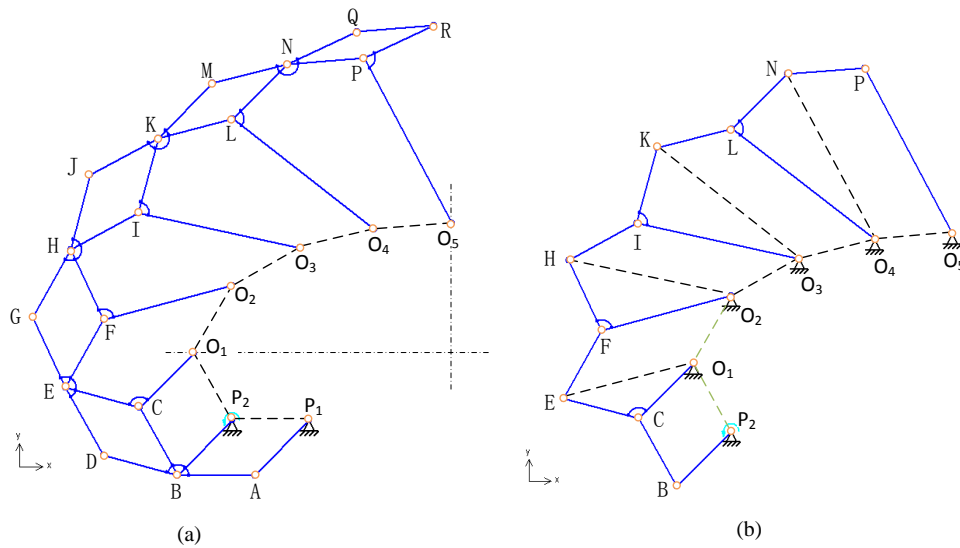


Figure F.3. A multi-RCM mechanism and its simplified mechanism.

F.2 Synthesis Procedure of a Multi-RCM Mechanism

This section provides a systematic procedure for the synthesis of a multi-RCM mechanism with two remote centres, if several constraints are known. The procedure is based on the analysis presented in section F.1. The process can be programmed for future development.

A synthesis approach is based on a multi-loop kinematic chain, because a multi-loop mechanism comprises few links and is compact. It can be seen as parallelogram-loop chains.

1. Firstly, a multi-loop kinematic chain is constructed by using the given fixed positions on the frame and remote centres.

2. Then an RCM mechanism is constructed by adding links to construct parallelograms.

3. The links connecting to the remote centres are removed and a multi-RCM mechanism obtained.

From this procedure, a conclusion is drawn that the limited space of the mechanism can be obtained by reducing the dimensions of the links that rotate around the remote centres. The synthesis procedure is shown in Figure F.4.

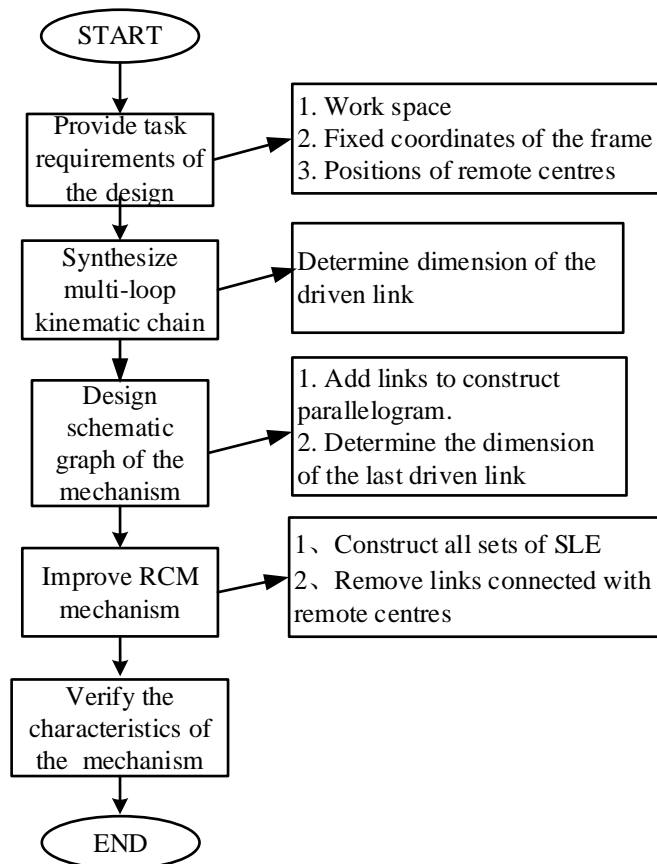


Figure F.4. Procedure of the synthesis approach.

F.3 Synthesis Example of Two-RCM Mechanism

It is assumed that a two-RCM positioning bracket is required with the connecting line P_1P_2 on the frame perpendicular to the connecting line O_1O_2 between two remote centres. The constraint condition is that all the links of the mechanism should be within the marked border lines in red, as shown in Figure F.5.

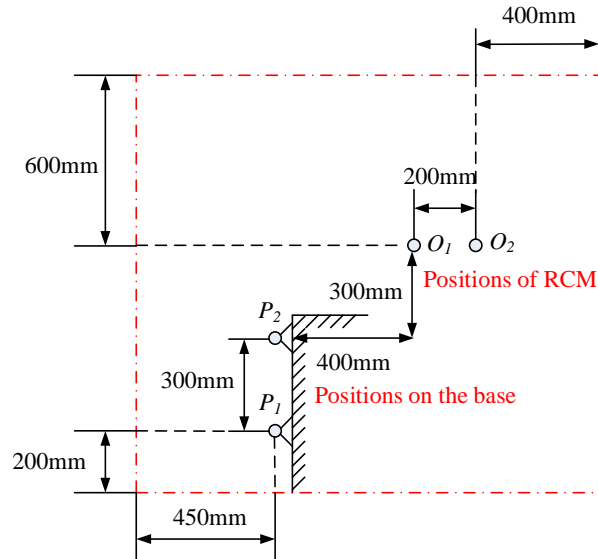


Figure F.5. Constraint condition and space for RCM mechanism.

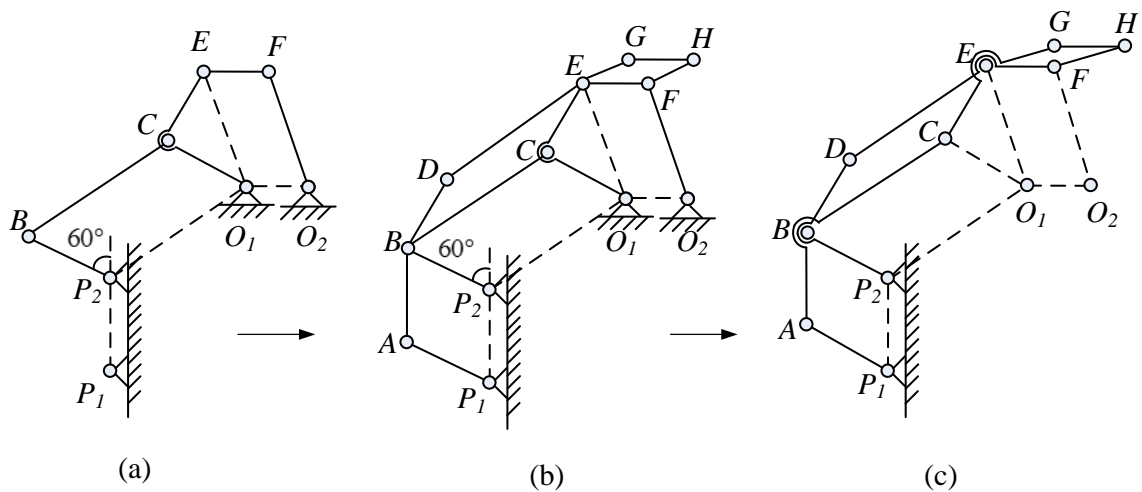


Figure F.6. Synthesis process of two-RCM mechanism: (a) multi-loop kinematic chain; (b) schematic with several parallelograms; (c) synthesized two-RCM mechanism.

According to the procedure in Figure F.4, two-RCM mechanism can be synthesised by four steps as follows:

Step1: Synthesize a multi-loop kinematic chain.

Suppose that an initial angle of driving link is 60° . A mechanism with two-loop kinematic chain is synthesized by connecting positions on the frame and two remote centres, as shown in Figure F.6(a). The dimension of the driven link ECO_1 is determined by the left and base border lines that form a limiting space. When the mechanism is in the limiting position, link ECO_1 will rotate an angle equal to $\angle CO_1P_2$. Let $\angle ECO_1=90^\circ$, $CE=300\text{mm}$ and $CO_1=300\text{mm}$ to make sure that $EO_1<450\text{mm}$.

Step 2: Construct parallelograms by adding links.

Figure F.6(b) shows the schematic graph of the constructed mechanism in which the dimension of HFO_2 is determined by the right and top border lines. If the mechanism is within a limiting position, link ECO_1 will rotate an angle equal to $\angle GEF$. Let $\angle GEF=30^\circ$ and $FH=200\text{mm}$ to make sure that $HO_2<600\text{mm}$.

Step 3: Optimized RCM mechanism.

Four links connecting with revolute pairs B and E are evolved to be two SLE, and then remove the fixed points O_1 and O_2 . Finally, a two-RCM mechanism is obtained in Figure F.6(c).

Step 4: Verification.

The mobility and motion range of the RCM mechanism are verified in Figure F.7. Figure F.7(a) shows an initial state of the two-RCM mechanism; Figure 17(b) shows the final state of two-RCM mechanism if the driving link rotates 60° .

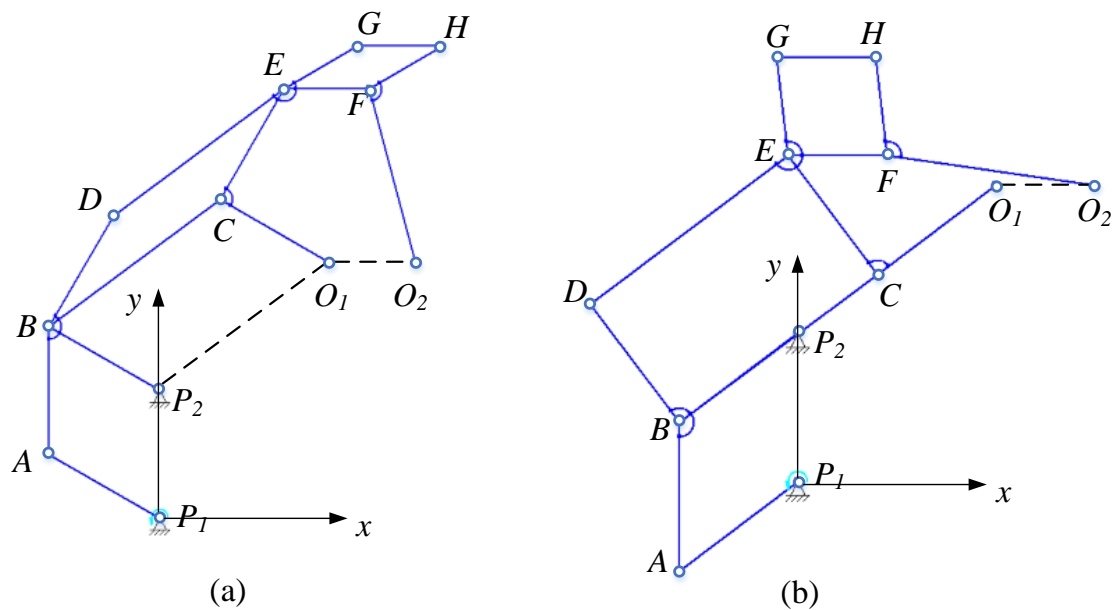


Figure F.7. Simulation of a two-RCM mechanism in software of SAM: (a) initial state of the mechanism; (b) final state of the mechanism with a rotation angle of 60° .

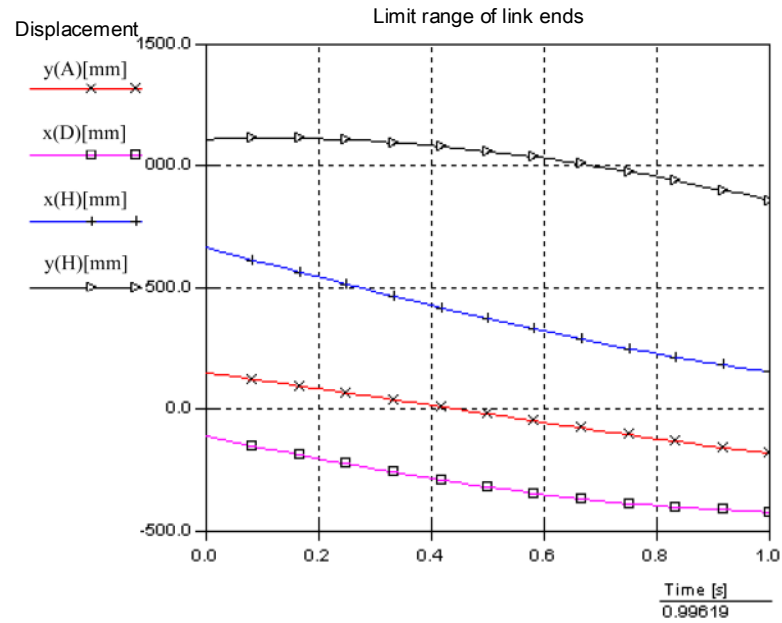


Figure F.8. Displacements of three link ends vs input angle

Joints A , D and H will reach to the furthest position distal from the origin point P_I during the rotation process of the mechanism. Figure F.8 illustrates displacements of three link ends, according to which all of them are within the space limits marked. The result shows that the synthesis method is correct and efficient enough to construct a two-RCM mechanism. This approach is also suitable for constructing a multi-RCM mechanism. A three dimensional model of the two-RCM mechanism is designed as shown in Figure F.9.

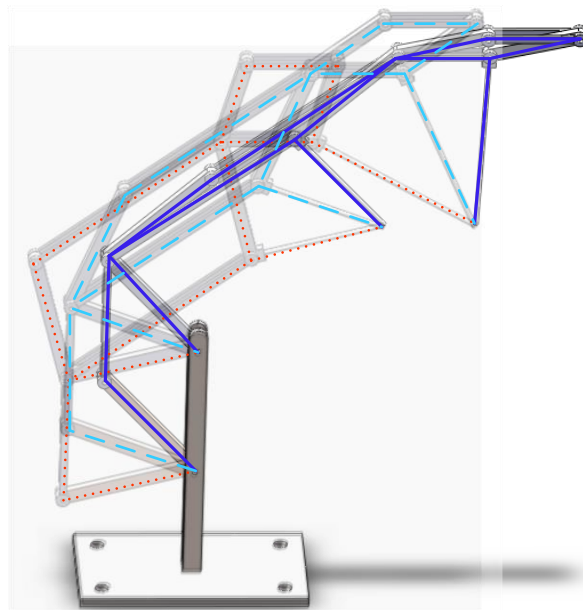


Figure F.9. 3D model of a two-RCM mechanism.

Appendix G – Implementation of Cognate Mechanisms by Software

The design processes of each type of cognate mechanism look very tedious. The final result is also very difficult to verify if geometric approaches were used manually. Some mathematical analysis software (such as Matlab, Mathematica) may work for development. However the coding process is also very tedious and slow. There are more than 1000 lines of Matlab code for the simple working model shown in Figure G.1. The programming for cognate mechanisms would be much more difficult to code using Matlab. In this section, a method using a combination of 3D modelling software (Solidworks) and planar mechanism analysis software (SAM) is presented to simplify the design and verification of such designs.

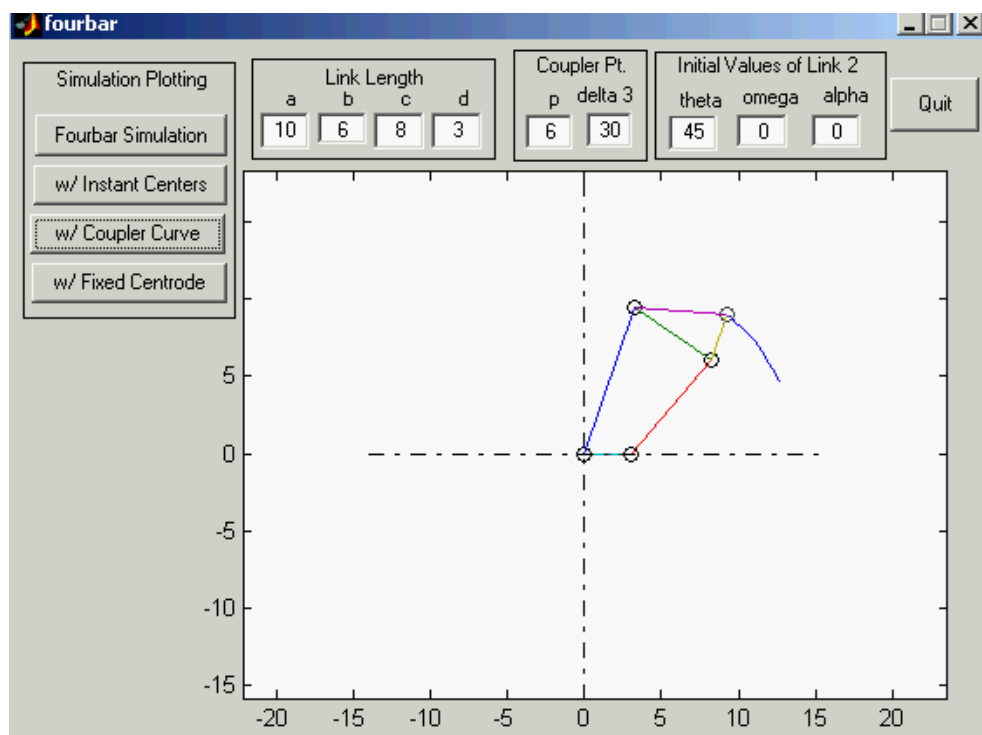


Figure G.1. Analysis programming for a four-bar mechanism using Matlab.

The design process would be simple if 3D modelling software and mechanism design software could be adopted to form parallelograms and similarly for determining the link lengths.

A mathematical calculation is the first step for a design. If the dimensions of each link have been given or calculated, the sketch can be drawn in the drawing environment of the software. Properties such as parameters relationships can be added to the sketch. Figure G.2 shows a sketch of a four-bar mechanism with detailed dimensions. In the sketch, O_1 is fixed to the original point and O_1O_2 is located on the horizontal line as a frame link, ABC is the coupler link and C thereof is the coupler point. All lengths of

each link of the mechanism are determined. According to the Grashof condition, this is a crank-rocker four bar mechanism. If the drive link is actuated, the mechanism will be movable; however, the curve trace of point C could not be captured in this modelling software unless a 3D model of each link is designed, using simulation for assembly. This is not a wise approach for complicated assemblies with an abundance of linkages. Another option is to import the sketch into a mechanism design software (such as Solidworks) for simulation. The outline sketch design for a mechanism is enough for simulation.

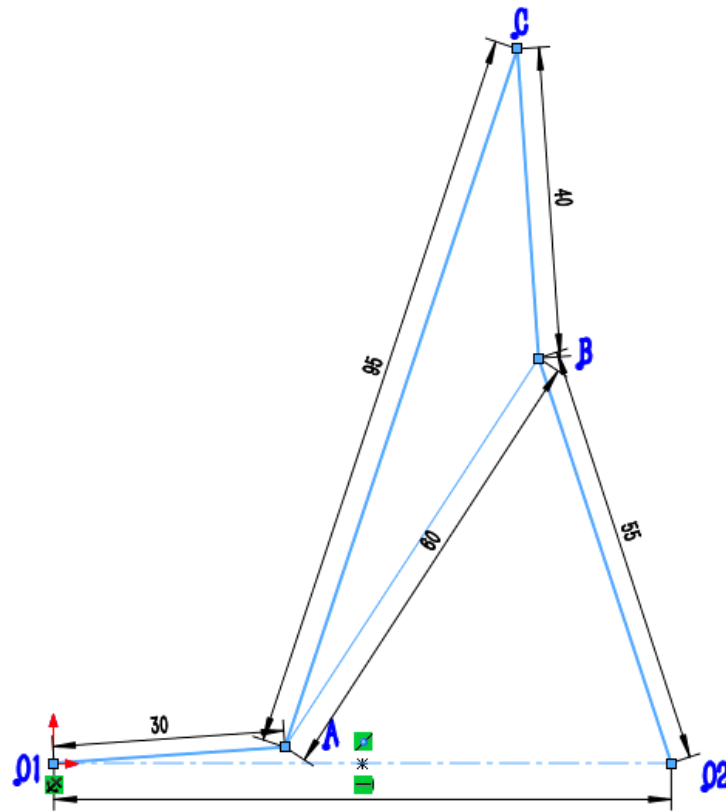


Figure G.2. Sketch drawing in 3D modeling software.

The file format may be changed for importing into a mechanism design software. The prepared sketch is used to construct beam elements in the software. Construction would be easier to follow in the 3D model design than drawing it in the mechanism design software environment (Figure G.3). In addition to path tracing, most of mechanism design software also has some other analysis functions, such as centrodes, displacements, velocities, acceleration, force and hodograph. Figure G.4 shows displacements of coupler point C in the x and y axes with respect to time.

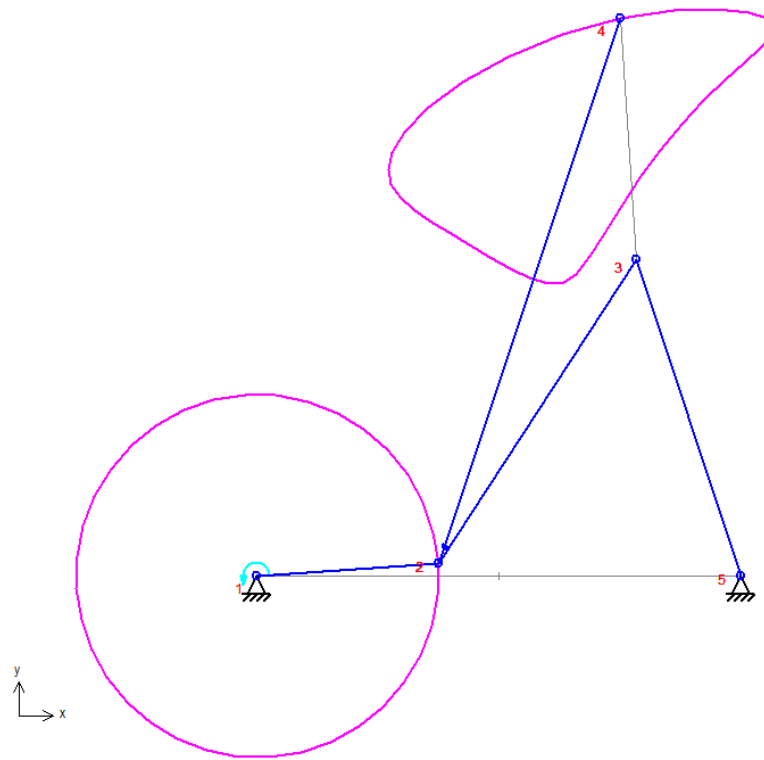


Figure G.3. Coupler-point curve of the four-bar mechanism.

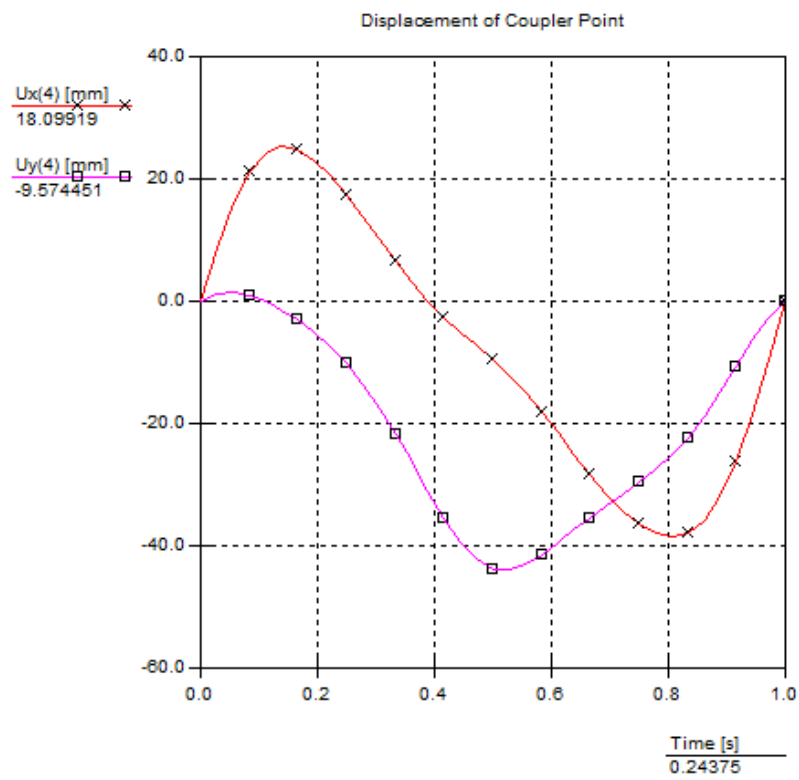


Figure G.4. Coupler-point curve of the four-bar mechanism.

The following steps for constructing cognate four- and six-bar mechanisms, transformation-body six-bar mechanisms in the 3D modelling software environment are actually possible and straightforward to conduct. Parallel lines and similar triangles are most important characteristics of the construction processes. In the software, geometrical relationships such as parallel, vertical, horizontal or fixed, scaling up/down of features, adding parameters such as angles and link lengths, can help deal with all the requirements of construction. An example of a constructing cognate six-bar mechanism shows how to use the software to assist mechanism design, see Figure G.5. According to construction process provided in Appendix E, a triangle is similar to a coupler triangle, and reversed and turned upside down. If the three angles of a triangle are determined, the entity can be scaled up or down or rotated to any orientation, as shown in Figure G.5.

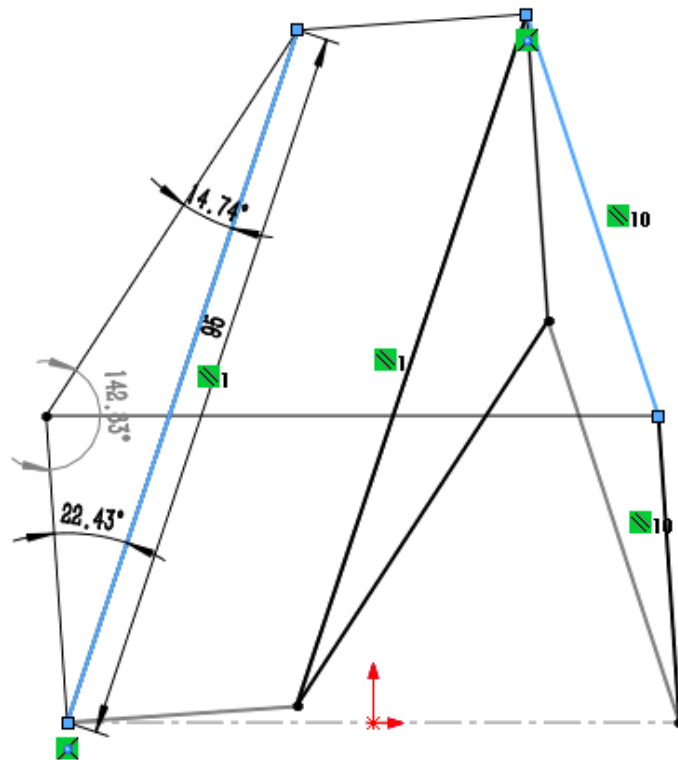


Figure G. 5. Construction of cognate six-bar mechanism.

In the same way, the cognate six-bar mechanism is imported into the mechanism design software and the final construction result is quickly verified, see Figure G.6. In the simulating mechanism, in order to draw the same coupler-point curve with the four-bar mechanism, the drive link should be link 2-6 which has the same angular velocity as the drive link of the four-bar mechanism.

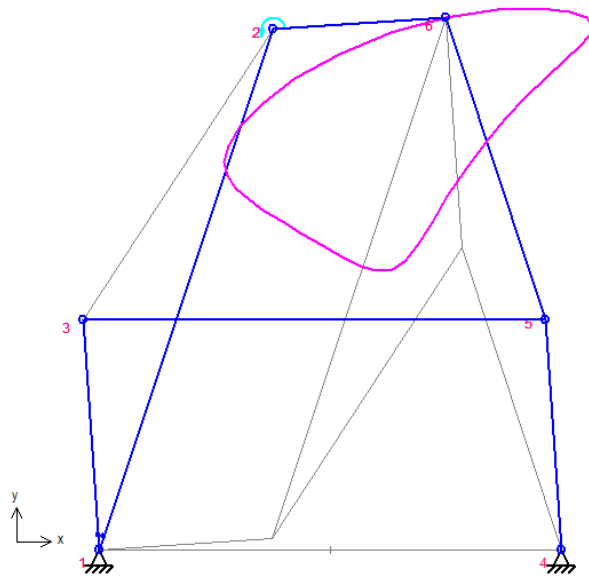


Figure G. 6. Cognate six-bar mechanism constructed in mechanism design software.

LIST OF PUBLICATIONS

- [1] Bai, G., Kong, X., inventor; Heriot-Watt University, assignee. (2017). Modular gripper. UK patent GB1719920.9.
- [2] Bai, G., Kong, X., inventor; Heriot-Watt University, assignee. (2017). An improved gripper. World patent WO PCT/GB2017/052396.
- [3] Bai, G., Kong, X., & Ritchie, J. M. (2017). Kinematic analysis and dimensional synthesis of a meso-gripper. *Journal of Mechanisms and Robotics*, 9(3), 031017.
- [4] Bai, G., Kong, X., & Ritchie, J. M. (2016, August). Kinematic analysis and dimensional synthesis of a meso-gripper. In *ASME 2016 International Design Engineering Technical Conferences and Computers and Information in Engineering Conference* (pp. V05AT07A064-V05AT07A064). American Society of Mechanical Engineers.
- [5] Bai, G., Wang, J., & Kong, X. (2016, July). A two-fingered anthropomorphic robotic hand with contact-aided cross four-bar mechanisms as finger joints. In *Conference on Biomimetic and Biohybrid Systems* (pp. 28-39). Springer International Publishing.
- [6] Bai, G., Qi, P., Althoefer, K., Li, D., Kong, X., & Dai, J. S. (2015, August). Kinematic analysis of a mechanism with dual remote centre of motion and its potential application. In *ASME 2015 International Design Engineering Technical Conferences and Computers and Information in Engineering Conference* (pp. V05BT08A011-V05BT08A011). American Society of Mechanical Engineers.

REFERENCES

- [1] National Research Council. (1998). Visionary manufacturing challenges for 2020. National Academies Press, 2.
- [2] Schunk, H., Steinmann, R., & Wolf, A. (2005). Grippers in Motion. Springer-Verlag Berlin Heidelberg.
- [3] Lee, J. (1988). Kinematic synthesis of industrial robot hand/gripper-a creative design approach. *Robotics and Autonomous Systems*, 4(3), 257-263.
- [4] Tischler, C. R., Samuel, A. E., & Hunt, K. H. (1995). Kinematic chains for robot hands-I. Orderly number-synthesis. *Mechanism and Machine Theory*, 30(8), 1193-1215.
- [5] Belfiore, N. P., & Pennestrì E. (1997). An atlas of linkage-type robotic grippers. *Mechanism and Machine Theory*, 32(7), 811-833.
- [6] Lanni, C., & Ceccarelli, M. (2009). An optimization problem algorithm for kinematic design of mechanisms for two-finger grippers. *Open Mechanical Engineering Journal*, 3, 49-62.
- [7] Li, G., Zhang, C., Zhang, W., Sun, Z., & Chen, Q. (2014). Coupled and self-adaptive under-actuated finger with a novel S-coupled and secondly self-adaptive mechanism. *Journal of Mechanisms and Robotics*, 6(4), 041010.
- [8] Konstantinov, M. S. (1975, September). Jaw-type gripper mechanisms. In *Proceedings of the 5 th International Symposium on Industrial Robots* (pp. 22-24).
- [9] Chen, F. Y. (1982). Gripping mechanisms for industrial robots: An overview. *Mechanism and Machine Theory*, 17(5), 299-311.
- [10] Lundström, G. (1974). Industrial robot grippers. *Industrial Robot: An International Journal*, 1(2), 72-82.
- [11] Monkman, G. J. (1992). Compliant robotic devices, and electroadhesion. *Robotica*, 10(02), 183-185.
- [12] Ragunathan, S., & Karunamoorthy, L. (2006). Modeling and dynamic analysis of reconfigurable robotic gripper system for handling fabric materials in garment industries. *Journal of Advanced Manufacturing Systems*, 5(02), 233-254.
- [13] Mantriota, G. (2007). Theoretical model of the grasp with vacuum gripper. *Mechanism and Machine Theory*, 42(1), 2-17.
- [14] Loucks, C., Johnson, V., Boissiere, P., Starr, G., & Steele, J. (1987, March). Modeling and control of the Stanford/JPL hand. In *Robotics and Automation. Proceedings. 1987 IEEE International Conference on* (Vol. 4, pp. 573-578). IEEE.
- [15] Jacobsen, S., Iversen, E., Knutti, D., Johnson, R., & Biggers, K. (1986, April). Design of the Utah/MIT dextrous hand. In *Robotics and Automation. Proceedings. 1986*

IEEE International Conference on (Vol. 3, pp. 1520-1532). IEEE.

[16] Kyberd, P. J., & Chappell, P. H. (1994). The Southampton hand: An intelligent myoelectric prosthesis. *Journal of Rehabilitation Research and Development*, 31(4), 326.

[17] Butterfaß, J., Grebenstein, M., Liu, H., & Hirzinger, G. (2001). DLR-hand II: Next generation of a dextrous robot hand. In *Robotics and Automation, 2001. Proceedings 2001 ICRA. IEEE International Conference on* (Vol. 1, pp. 109-114). IEEE.

[18] Lovchik, C. S., & Diftler, M. A. (1999). The robonaut hand: A dexterous robot hand for space. In *Robotics and Automation, 1999. Proceedings. 1999 IEEE International Conference on* (Vol. 2, pp. 907-912). IEEE.

[19] Tuffield, P., & Elias, H. (2003). The shadow robot mimics human actions. *Industrial Robot: An International Journal*, 30(1), 56-60.

[20] Lotti, F., Tiezzi, P., Vassura, G., Biagiotti, L., Palli, G., & Melchiorri, C. (2005, April). Development of UB hand 3: Early results. In *Robotics and Automation, 2005. ICRA 2005. Proceedings of the 2005 IEEE International Conference on* (pp. 4488-4493). IEEE.

[21] Carrozza, M. C., Cappiello, G., Micera, S., Edin, B. B., Beccai, L., & Cipriani, C. (2006). Design of a cybernetic hand for perception and action. *Biological Cybernetics*, 95(6), 629.

[22] Kawasaki, H., Komatsu, T., & Uchiyama, K. (2002). Dexterous anthropomorphic robot hand with distributed tactile sensor: Gifu hand II. *IEEE/ASME Transactions on Mechatronics*, 7(3), 296-303.

[23] Mouri, T., Kawasaki, H., Yoshikawa, K., Takai, J., & Ito, S. (2002, October). Anthropomorphic robot hand: Gifu hand III. In *Proc. Int. Conf. ICCAS* (pp. 1288-1293).

[24] Liu, J., & Zhang, Y. (2007, December). Mapping human hand motion to dexterous robotic hand. In *Robotics and Biomimetics, 2007. ROBIO 2007. IEEE International Conference on* (pp. 829-834). IEEE.

[25] Liu, H., Meusel, P., Seitz, N., Willberg, B., Hirzinger, G., Jin, M. H., & Xie, Z. W. (2007). The modular multisensory DLR-HIT-Hand. *Mechanism and Machine Theory*, 42(5), 612-625.

[26] Dai, J. S., & Wang, D. (2007). Geometric analysis and synthesis of the metamorphic robotic hand. *Journal of Mechanical Design*, 129(11), 1191-1197.

[27] Laliberté T., & Gosselin, C. M. (1998). Simulation and design of underactuated mechanical hands. *Mechanism and Machine Theory*, 33(1-2), 39-57.

[28] Gosselin, C., Pelletier, F., & Laliberte, T. (2008, May). An anthropomorphic underactuated robotic hand with 15 dofs and a single actuator. In *Robotics and*

- Automation, 2008. ICRA 2008. IEEE International Conference on (pp. 749-754). IEEE.
- [29] Martin, E., Desbiens, A. L., Laliberté T., & Gosselin, C. (2004). SARAH hand used for space operation on STVF robot. *Intelligent Manipulation and Grasping*, Genova, 279-284.
- [30] Dechev, N., Cleghorn, W. L., & Naumann, S. (2001). Multiple finger, passive adaptive grasp prosthetic hand. *Mechanism and Machine Theory*, 36(10), 1157-1173.
- [31] Pons, J. L., Rocon, E., Ceres, R., Reynaerts, D., Saro, B., Levin, S., & Van Moorleghe, W. (2004). The MANUS-HAND dextrous robotics upper limb prosthesis: Mechanical and manipulation aspects. *Autonomous Robots*, 16(2), 143-163.
- [32] Carbone, G., & Ceccarelli, M. (2008, May). Design of LARM hand: problems and solutions. In *Automation, Quality and Testing, Robotics, 2008. AQTR 2008. IEEE International Conference on* (Vol. 2, pp. 298-303). IEEE.
- [33] Zhang, W., Che, D., Chen, Q., & Du, D. (2009). A dexterous and self-adaptive humanoid robot hand: Gesture-changeable under-actuated hand. *Intelligent Robotics and Applications*, 515-525.
- [34] Li, G., Zhang, C., Zhang, W., Sun, Z., & Chen, Q. (2014). Coupled and self-adaptive under-actuated finger with a novel S-coupled and secondly self-adaptive mechanism. *Journal of Mechanisms and Robotics*, 6(4), 041010.
- [35] Dollar, A. M., & Howe, R. D. (2010). The highly adaptive SDM hand: design and performance evaluation. *The International Journal of Robotics Research*, 29(5), 585-597.
- [36] Odhner, L. U., Jentoft, L. P., Claffee, M. R., Corson, N., Tenzer, Y., Ma, R. R., Buehler, M., Kohout, R., Howe, R. D., & Dollar, A. M. (2014). A compliant, underactuated hand for robust manipulation. *The International Journal of Robotics Research*, 33(5), 736-752.
- [37] Meka, H2 compliant hand 2009. [Online]. Available: <http://mekabot.com/products/compliant-hand/>
- [38] 2G "Velo" Gripper. Retrieved from <http://www.willowgarage.com/velo2g>.
- [39] Kinovarobotics. Retrieved from <http://www.kinovarobotics.com/>
- [40] Robotnik. Retrieved from <http://www.robotnik.eu/robotic-hands/barrett/>
- [41] Robotiq. Retrieved from <http://robotiq.com/products/adaptive-robot-gripper/>
- [42] Bai, G., Wang, J., & Kong, X. (2016, July). A two-fingered anthropomorphic robotic hand with contact-aided cross four-bar mechanisms as finger joints. In *Conference on Biomimetic and Biohybrid Systems* (pp. 28-39). Springer International Publishing.
- [43] Bai, G., Kong, X., & Ritchie, J. M. (2017). Kinematic analysis and dimensional

synthesis of a meso-gripper. *Journal of Mechanisms and Robotics*, 9(3), 031017.

[44] Bai, G., Kong, X., inventor; Heriot-Watt University, assignee. (2018). An improved Gripper. World patent WO PCT/GB2017/052396.

[45] Bai, G., Kong, X., inventor; Heriot-Watt University, assignee. (2017). Modular gripper. UK patent GB1719920.9.

[46] Wang, L., & Xi, F. (Eds.). (2008). *Smart devices and machines for advanced manufacturing*. Springer Science & Business Media.

[47] Murray, R. M., Li, Z., Sastry, S. S., & Sastry, S. S. (1994). *A Mathematical Introduction to Robotic Manipulation*. CRC press.

[48] Tanikawa, T., & Arai, T. (1999). Development of a micro-manipulation system having a two-fingered micro-hand. *IEEE Transactions on Robotics and Automation*, 15(1), 152-162.

[49] Monkman, G. (2003). Electroadhesive microgrippers. *Industrial Robot: An International Journal*, 30(4), 326-330.

[50] Mankame, N. D., & Ananthasuresh, G. (2004). A novel compliant mechanism for converting reciprocating translation into enclosing curved paths. *Journal of Mechanical Design*, 126(4), 667-672.

[51] Nah, S. K., & Zhong, Z. W. (2007). A microgripper using piezoelectric actuation for micro-object manipulation. *Sensors and Actuators A: Physical*, 133(1), 218-224.

[52] Zubir, M. N. M., Shirinzadeh, B., & Tian, Y. (2009). A new design of piezoelectric driven compliant-based microgripper for micromanipulation. *Mechanism and Machine Theory*, 44(12), 2248-2264.

[53] Zubir, M. N. M., & Shirinzadeh, B. (2009). Development of a high precision flexure-based microgripper. *Precision Engineering*, 33(4), 362-370.

[54] Zhang, D., Zhang, Z., Gao, Q., Xu, D., & Liu, S. (2015). Development of a monolithic compliant SPCA-driven micro-gripper. *Mechatronics*, 25, 37-43.

[55] Ruffatto, D., Parness, A., & Spenko, M. (2014). Improving controllable adhesion on both rough and smooth surfaces with a hybrid electrostatic/gecko-like adhesive. *Journal of the Royal Society Interface*, 11(93), 20131089.

[56] Ai, W., & Xu, Q. (2014). New structural design of a compliant gripper based on the Scott-Russell mechanism. *International Journal of Advanced Robotic Systems*, 11(12), 192.

[57] Paek, J., Cho, I., & Kim, J. (2015). Microrobotic tentacles with spiral bending capability based on shape-engineered elastomeric microtubes. *Scientific Reports*, 5.

[58] Snezhko, A., & Aranson, I. S. (2011). Magnetic manipulation of self-assembled

colloidal asters. *Nature Materials*, 10(9), 698-703.

[59] Malachowski, K., Jamal, M., Jin, Q., Polat, B., Morris, C. J., & Gracias, D. H. (2014). Self-folding single cell grippers. *Nano Letters*, 14(7), 4164-4170.

[60] Ford, M. (2015). *Rise of the Robots: Technology and the Threat of a Jobless Future*. Basic Books.

[61] Blanes, C., Mellado, M., Ortiz, C., & Valera, A. (2011). Review. Technologies for robot grippers in pick and place operations for fresh fruits and vegetables. *Spanish Journal of Agricultural Research*, 9(4), 1130-1141.

[62] Gafford, J., Ding, Y., Harris, A., McKenna, T., Polygerinos, P., Holland, D., Walsh, C., & Moser, A. (2015). Shape deposition manufacturing of a soft, atraumatic, and deployable surgical grasper. *Journal of Mechanisms and Robotics*, 7(2), 021006.

[63] Rangunathan, S., & Karunamoorthy, L. (2006). Modeling and dynamic analysis of reconfigurable robotic gripper system for handling fabric materials in garment industries. *Journal of Advanced Manufacturing Systems*, 5(02), 233-254.

[64] Yeung, B. H., & Mills, J. K. (2004). Design of a six DOF reconfigurable gripper for flexible fixtureless assembly. *IEEE Transactions on Systems, Man, and Cybernetics, Part C (Applications and Reviews)*, 34(2), 226-235.

[65] Cohen, R. G., & Rosenbaum, D. A. (2004). Where grasps are made reveals how grasps are planned: Generation and recall of motor plans. *Experimental Brain Research*, 157(4), 486-495.

[66] Ansuini, C., Giosa, L., Turella, L., Altoè G., & Castiello, U. (2008). An object for an action, the same object for other actions: Effects on hand shaping. *Experimental Brain Research*, 185(1), 111-119.

[67] Wimmer, R., & Boring, S. (2009, February). HandSense: Discriminating different ways of grasping and holding a tangible user interface. In *Proceedings of the 3rd International Conference on Tangible and Embedded Interaction* (pp. 359-362). ACM.

[68] Hemmert, F., Hamann, S., Löwe, M., Wohlauf, A., & Joost, G. (2010, January). Shape-changing mobiles: Tapering in one-dimensional deformational displays in mobile phones. In *Proceedings of the Fourth International Conference on Tangible, Embedded, and Embodied Interaction* (pp. 249-252). ACM.

[69] Cipriani, C., Controzzi, M., & Carrozza, M. C. (2009, June). Progress towards the development of the smart hand transradial prosthesis. In *Rehabilitation Robotics, 2009. ICORR 2009. IEEE International Conference on* (pp. 682-687). IEEE.

[70] Kamakura, N., Matsuo, M., Ishii, H., Mitsuboshi, F., & Miura, Y. (1980). Patterns of static prehension in normal hands. *American Journal of Occupational Therapy*, 34(7),

437-445.

- [71] Cutkosky, M.R., & Wright, P.K. (1986). Modeling manufacturing grips and correlations with the design of robotic hands. *IEEE International Conference of Robotics and Automation*, 3, 1533-1539.
- [72] Rosheim, M. E. (1994). *Robot Evolution: the Development of Anthrobotics*. John Wiley & Sons.
- [73] Kapandji, A. I. (2006). *Articulate Physiology*. Paris: Maloine.
- [74] Feix, T., Pawlik, R., Schmiedmayer, H. B., Romero, J., & Kragic, D. (2009, June). A comprehensive grasp taxonomy. In *Robotics, Science and Systems: Workshop on Understanding the Human Hand for Advancing Robotic Manipulation* (Vol. 2, No. 2.3, pp. 2-3).
- [75] Feix, T., Romero, J., Schmiedmayer, H. B., Dollar, A. M., & Kragic, D. (2016). The grasp taxonomy of human grasp types. *IEEE Transactions on Human-Machine Systems*, 46(1), 66-77.
- [76] Ernst-Friedrich Schimke. (1978) *Planung und Einsatz von Industrierobotern: Arbeitsplatzanalysen, Auslegung und Anwendung von Handhabungssystemen*. VDI-Verlag.
- [77] Feix, T., Bullock, I. M., & Dollar, A. M. (2014). Analysis of human grasping behavior: Object characteristics and grasp type. *IEEE Transactions on Haptics*, 7(3), 311-323.
- [78] Steinhauser, M. O., & Hiermaier, S. (2009). A review of computational methods in materials science: Examples from shock-wave and polymer physics. *International Journal of Molecular Sciences*, 10(12), 5135-5216.
- [79] Hunt, K. H. (1978). *Kinematic Geometry of Mechanisms* (p.287). Oxford: Clarendon Press.
- [80] Boubekri, N., & Chakraborty, P. (2002). Robotic grasping: gripper designs, control methods and grasp configurations-a review of research. *Integrated Manufacturing Systems*, 13(7), 520-531.
- [81] Kong, X., & Jin, Y. (2016). Type Synthesis of 3-DOF multi-mode translational/spherical parallel mechanisms with lockable joints. *Mechanism and Machine Theory*, 96, 323-333.
- [82] Kuribayashi, K., Tsuchiya, K., You, Z., Tomus, D., Umemoto, M., Ito, T., & Sasaki, M. (2006). Self-deployable origami stent grafts as a biomedical application of Ni-rich TiNi shape memory alloy foil. *Materials Science and Engineering: A*, 419(1), 131-137.
- [83] Hao, G., & Kong, X. (2012). A novel large-range XY compliant parallel

manipulator with enhanced out-of-plane stiffness. *Journal of Mechanical Design*, 134(6), 061009.

[84] Birglen, L. (2010). From flapping wings to underactuated fingers and beyond: a broad look to self-adaptive mechanisms. *Mechanical Sciences*, 1(1), 5-12.

[85] Laliberté T., & Gosselin, C. M. (2001, June). Underactuation in space robotic hands. In *International Symposium on Artificial Intelligence, Robotics and Automation in Space*, Montréal, Canada (pp. 18-21).

[86] Salisbury, J. K., & Craig, J. J. (1982). Articulated hands: force control and kinematic issues. *The International Journal of Robotics Research*, 1(1), 4-17.

[87] Jacobsen, S., Iversen, E., Knutti, D., Johnson, R., & Biggers, K. (1986, April). Design of the Utah/MIT dextrous hand. In *Robotics and Automation. Proceedings. 1986 IEEE International Conference on* (Vol. 3, pp. 1520-1532). IEEE.

[88] Butterfaß J., Grebenstein, M., Liu, H., & Hirzinger, G. (2001). DLR-Hand II: Next generation of a dextrous robot hand. In *Robotics and Automation, 2001. Proceedings 2001 ICRA. IEEE International Conference on* (Vol. 1, pp. 109-114). IEEE.

[89] Deshpande, A. D., Xu, Z., Weghe, M. J. V., Brown, B. H., Ko, J., Chang, L. Y., Wilkinson, D. D., Bidic, S.M., & Matsuoka, Y. (2013). Mechanisms of the anatomically correct testbed hand. *IEEE/ASME Transactions on Mechatronics*, 18(1), 238-250.

[90] Xu, Z., Kumar, V., Matsuoka, Y., & Todorov, E. (2012, June). Design of an anthropomorphic robotic finger system with biomimetic artificial joints. In *Biomedical Robotics and Biomechanics (BioRob), 2012 4th IEEE RAS & EMBS International Conference on* (pp. 568-574). IEEE.

[91] Xu, Z., Todorov, E., Dellon, B., & Matsuoka, Y. (2011, May). Design and analysis of an artificial finger joint for anthropomorphic robotic hands. In *Robotics and Automation (ICRA), 2011 IEEE International Conference on* (pp. 5096-5102). IEEE.

[92] Townsend, W. (2000). The Barrett Hand grasper - programmably flexible part handling and assembly. *Industrial Robot: An International Journal*, 27(3), 181-188.

[93] Kyberd, P. J., Light, C., Chappell, P. H., Nightingale, J. M., Whatley, D., & Evans, M. (2001). The design of anthropomorphic prosthetic hands: A study of the Southampton hand. *Robotica*, 19(6), 593-600.

[94] Lan, T., Liu, Y. W., Jin, M. H., Fan, S. W., Fang, H. G., Xia, J. J., & Liu, H. (2009, July). DSP&FPGA-based joint impedance controller for DLR/HIT II dexterous robot hand. In *Advanced Intelligent Mechatronics, 2009. AIM 2009. IEEE/ASME International Conference on* (pp. 1594-1599). IEEE.

[95] Yamano, I., & Maeno, T. (2005, April). Five-fingered robot hand using ultrasonic

- motors and elastic elements. In *Robotics and Automation, 2005. ICRA 2005. Proceedings of the 2005 IEEE International Conference on* (pp. 2673-2678). IEEE.
- [96] Shadow. Retrieved from <http://www.shadowrobot.com/products/dexterous-hand/>.
- [97] Jones, L. A., & Lederman, S. J. (2006). *Human Hand Function*. Oxford University Press.
- [98] Napier, J. R. (1956). The prehensile movements of the human hand. *Bone & Joint Journal*, 38(4), 902-913.
- [99] Landsmeer, J. M. F. (1962). Power grip and precision handling. *Annals of the Rheumatic Diseases*, 21(2), 164.
- [100] Buchner, H. J., Hines, M. J., & Hemami, H. (1988). A dynamic model for finger interphalangeal coordination. *Journal of Biomechanics*, 21(6), 459-468.
- [101] Dennerlein, J. T., Diao, E., Mote, C. D., & Rempel, D. M. (1998). Tensions of the flexor digitorum superficialis are higher than a current model predicts. *Journal of Biomechanics*, 31(4), 295-301.
- [102] Sancho-Bru, J. L., Perez-Gonzalez, A., Vergara-Monedero, M., & Giurintano, D. (2001). A 3-D dynamic model of human finger for studying free movements. *Journal of Biomechanics*, 34(11), 1491-1500.
- [103] Buchholz, B., Armstrong, T. J., & Goldstein, S. A. (1992). Anthropometric data for describing the kinematics of the human hand. *Ergonomics*, 35(3), 261-273.
- [104] Pitarch, E. P. (2010). Virtual human hand: autonomous grasping strategy. In *Modelling Simulation and Optimization*. InTech.
- [105] Almecija, S., Moya-Sola, S., & Alba, D. M. (2010). Early origin for human-like precision grasping: a comparative study of pollical distal phalanges in fossil hominins. *PLoS One*, 5(7), e11727.
- [106] Christel, M. I., Kitzel, S., & Niemitz, C. (1998). How precisely do bonobos (*Pan paniscus*) grasp small objects? *International Journal of Primatology*, 19(1), 165-194.
- [107] Feix, T., Bullock, I. M., & Dollar, A. M. (2014). Analysis of human grasping behavior: Correlating tasks, objects and grasps. *IEEE Transactions on Haptics*, 7(4), 430-441.
- [108] Goodfellow, J., O'Connor, J. (1994). *The Knee*, W. Norman Scott Mosby-Year Book, Inc.
- [109] Hamon, A., & Aoustin, Y. (2010, December). Cross four-bar linkage for the knees of a planar bipedal robot. In *Humanoid Robots (Humanoids), 2010 10th IEEE-RAS International Conference on* (pp. 379-384). IEEE.
- [110] Truong, Q. T., Argyoganendro, B. W., & Park, H. C. (2014). Design and

demonstration of insect mimicking foldable artificial wing using four-bar linkage systems. *Journal of Bionic Engineering*, 11(3), 449-458.

[111] Birglen, L., & Gosselin, C. (2004, July). Optimal design of 2-phalanx underactuated fingers. In *Proc. of International Conference on Intelligent Manipulation and Grasping* (pp. 110-116).

[112] Wu, L., Carbone, G., & Ceccarelli, M. (2009). Designing an underactuated mechanism for a 1 active DOF finger operation. *Mechanism and Machine Theory*, 44(2), 336-348.

[113] Moon, Y. M. (2007). Bio-mimetic design of finger mechanism with contact aided compliant mechanism. *Mechanism and Machine Theory*, 42(5), 600-611.

[114] Muller, M. (1996). A novel classification of planar four-bar linkages and its application to the mechanical analysis of animal systems. *Philosophical Transactions of the Royal Society of London B: Biological Sciences*, 351(1340), 689-720.

[115] Patek, S. N., Nowroozi, B. N., Baio, J. E., Caldwell, R. L., & Summers, A. P. (2007). Linkage mechanics and power amplification of the mantis shrimp's strike. *Journal of Experimental Biology*, 210(20), 3677-3688.

[116] Grubich, J. R., & Westneat, M. W. (2006). Four-bar linkage modelling in teleost pharyngeal jaws: computer simulations of bite kinetics. *Journal of anatomy*, 209(1), 79-92.

[117] Eckhardt, H. D. (1998). *Kinematic Design of Machines and Mechanisms*. McGraw-Hill, New York.

[118] Toussaint, G. (2003). Simple proofs of a geometric property of four-bar linkages. *The American Mathematical Monthly*, 110(6), 482.

[119] Norton, R. L. (2012). *Design of Machinery*, 5th ed., McGraw-Hill, New York.

[120] Chase, T. R., & Mirth, J. A. (1993). Circuits and branches of single-degree-of-freedom planar linkages. *Journal of Mechanical Design*, 115(2), 223-230.

[121] Hartenberg, R.S., Denavit, J. (1964). *Kinematic Synthesis of Linkages*. McGraw-Hill, New York.

[122] Mankame, N. D., & Ananthasuresh, G. K. (2002, January). Contact aided compliant mechanisms: Concept and preliminaries. In *ASME 2002 International Design Engineering Technical Conferences and Computers and Information in Engineering Conference* (pp. 109-121). American Society of Mechanical Engineers.

[123] Cannon, J. R., Lusk, C. P., & Howell, L. L. (2005). Compliant rolling-contact element mechanisms. *ASME Paper No. DETC2005-84073*.

[124] Barnes, R. M. (1949). *Motion and Time Study*. Richard D Irwin.

- [125] Khurshid, A., Ghafoor, A., & Malik, M. A. (2011). Robotic grasping and fine manipulation using soft fingertip. In *Advances in Mechatronics*. InTech.
- [126] Durley, R. J. (1903). *Kinematics of Machines: An Elementary Textbook*. J. Wiley.
- [127] J. A. Hrones and G. L. Nelson. (1951). *Analysis of the Four-bar Linkage: Its Application to the Synthesis of Mechanisms*. Technology Press of MIT, Cambridge.
- [128] Mallik, A. K., Ghosh, A., & Dittrich, G. (1994). *Kinematic Analysis and Synthesis of Mechanisms*. CRC Press.
- [129] McCarthy, J. M., & Soh, G. S. (2010). *Geometric Design of Linkages* (Vol. 11). Springer Science & Business Media.
- [130] Radcliffe, C. W. (1994). Four-bar linkage prosthetic knee mechanisms: Kinematics, alignment and prescription criteria. *Prosthetics and Orthotics International*, 18(3), 159-173.
- [131] Gard, S. A., Childress, D. S., & Uellendahl, J. E. (1996). The influence of four-bar linkage knees on prosthetic swing-phase floor clearance. *JPO: Journal of Prosthetics and Orthotics*, 8(2), 34-40.
- [132] Hamon, A., & Aoustin, Y. (2010, December). Cross four-bar linkage for the knees of a planar bipedal robot. In *Humanoid Robots (Humanoids), 2010 10th IEEE-RAS International Conference on* (pp. 379-384). IEEE.
- [133] Birglen, L., & Gosselin, C. M. (2006). Geometric design of three-phalanx underactuated fingers. *Journal of Mechanical Design*, 128(2), 356-364.
- [134] Ansuini, C., Giosa, L., Turella, L., Alto è, G., & Castiello, U. (2008). An object for an action, the same object for other actions: Effects on hand shaping. *Experimental Brain Research*, 185(1), 111-119.
- [135] Wimmer, R., & Boring, S. (2009, February). HandSense: discriminating different ways of grasping and holding a tangible user interface. In *Proceedings of the 3rd International Conference on Tangible and Embedded Interaction* (pp. 359-362). ACM.
- [136] Festo. Retrieved from https://www.festo.com/net/SupportPortal/Files/26915/info_139_en.pdf.
- [137] Gosselin, C. M. (2006). Adaptive robotic mechanical systems: A design paradigm. *Journal of Mechanical Design*, 128(1), 192-198.
- [138] Hirose, S., & Umetani, Y. (1978). The development of soft gripper for the versatile robot hand. *Mechanism and Machine Theory*, 13(3), 351-359.
- [139] Dollar, A. M., & Howe, R. D. (2011). Joint coupling design of underactuated hands for unstructured environments. *The International Journal of Robotics Research*, 30(9), 1157-1169.

- [140] Taylor, R. H., Funda, J., LaRose, D., & Treat, M. (1992, October). A telerobotic system for augmentation of endoscopic surgery. In *Engineering in Medicine and Biology Society, 1992 14th Annual International Conference of the IEEE* (Vol. 3, pp. 1054-1056). IEEE.
- [141] Taylor, R. H., Funda, J., Eldridge, B., Gomory, S., Gruben, K., LaRose, D., Talamini, M., Kavoussi, L., & Anderson, J. (1995). A telerobotic assistant for laparoscopic surgery. *IEEE Engineering in Medicine and Biology Magazine*, 14(3), 279-288.
- [142] Taylor, R., Jensen, P., Whitcomb, L., Barnes, A., Kumar, R., Stoianovici, D., Gupta, P., Wang, Z., Dejuan, E., & Kavoussi, L. (1999). A steady-hand robotic system for microsurgical augmentation. *The International Journal of Robotics Research*, 18(12), 1201-1210.
- [143] Bai, G., Li, D., Wei, S., & Liao, Q. (2014). Kinematics and synthesis of a type of mechanisms with multiple remote centers of motion. *Proceedings of the Institution of Mechanical Engineers, Part C: Journal of Mechanical Engineering Science*, 228(18), 3430-3440.
- [144] Bai, G., Qi, P., Althoefer, K., Li, D., Kong, X., & Dai, J. S. (2015). Kinematic analysis of a mechanism with dual remote centre of motion and its potential application. *ASME Paper No. DETC2015-47118*.
- [145] Laliberté T., Birglen, L., & Gosselin, C. (2002). Underactuation in robotic grasping hands. *Machine Intelligence & Robotic Control*, 4(3), 1-11.
- [146] Birglen, L., Laliberté T., & Gosselin, C. M. (2007). *Underactuated robotic hands* (Vol. 40). Springer.
- [147] Birglen, L., & Gosselin, C. M. (2006). Grasp-state plane analysis of two-phalanx underactuated fingers. *Mechanism and Machine Theory*, 41(7), 807-822.
- [148] Birglen, L. (2011). The kinematic preshaping of triggered self-adaptive linkage-driven robotic fingers. *Mechanical Sciences*, 2(1), 41-49.
- [149] Li, G., Zhang, C., Zhang, W., Sun, Z., & Chen, Q. (2014). Coupled and self-adaptive under-actuated finger with a novel s-coupled and secondly self-adaptive mechanism. *Journal of Mechanisms and Robotics*, 6(4), 041010.
- [150] Amend, J. R., Brown, E., Rodenberg, N., Jaeger, H. M., & Lipson, H. (2012). A positive pressure universal gripper based on the jamming of granular material. *IEEE Transactions on Robotics*, 28(2), 341-350.
- [151] Dai, J. S., & Jones, J. R. (1999). Mobility in metamorphic mechanisms of foldable/erectable kinds. *Journal of Mechanical Design*, 121(3), 375-382.

- [152] Dai, J. S., & Wang, D. (2007). Geometric analysis and synthesis of the metamorphic robotic hand. *Journal of Mechanical Design*, 129(11), 1191-1197.
- [153] Kinzel, E. C., Schmiedeler, J. P., & Pennock, G. R. (2006). Kinematic synthesis for finitely separated positions using geometric constraint programming. *Journal of Mechanical Design*, 128(5), 1070-1079.
- [154] Jensen, J. F., 2005, "Remote Center Positioner," U.S. Patent No.US20050119638.
- [155] Moon, Y. M. (2007). Bio-mimetic design of finger mechanism with contact aided compliant mechanism. *Mechanism and Machine Theory*, 42(5), 600-611.
- [156] Phillips, J. (2007). *Freedom in Machinery* (Vol. 1). Cambridge University Press.
- [157] Birglen, L., & Gosselin, C. M. (2006). Force analysis of connected differential mechanisms: Application to grasping. *The International Journal of Robotics Research*, 25(10), 1033-1046.
- [158] Telegenov, K., Tlegenov, Y., & Shintemirov, A. (2014, November). An underactuated adaptive 3D printed robotic gripper. In *Mecatronics (MECATRONICS)*, 2014 10th France-Japan/8th Europe-Asia Congress on (pp. 110-115). IEEE.
- [159] Hrones, J. A., & Nelson, G. L. (1951). *Analysis of the four-bar linkage: Its application to the synthesis of mechanisms*. Cambridge: Published jointly by the Technology Press of the Massachusetts Institute of Technology, and Wiley, New York.
- [160] Hartenberg, R.S. & J. Denavit (1964) *Kinematic Synthesis of Linkages*, New York: McGraw-Hill, Online Link from Cornell University.
- [161] Prony, R. (1790). *Nouvelle Architecture Hydraulique* (Vol. 1). Didot.
- [162] Kwan, A.S.K. (1991). *A Pantographic Deployable Mast*. Ph.D. Dissertation, Cambridge University.
- [163] You, Z., & Pellegrino, S. (1997). Foldable bar structures. *International Journal of Solids and Structures*, 34(15), 1825-1847.
- [164] Bai, G, Liao, Q., Li, D., & Wei, S. (2013). Synthesis of scaling mechanisms for geometric figures with angulated-straight elements. *Proceedings of the Institution of Mechanical Engineers, Part C: Journal of Mechanical Engineering Science*, 227(12), 2795-2809.
- [165] Jonge, A. E. (1960). The correlation of hinged four-bar straight-line motion devices by means of the roboerts theorem and a new proof of the latter. *Annals of the New York Academy of Sciences*, 84(1), 77-145.